UNIVERSIDAD NACIONAL AUTÓNOMA DE MÉXICO
PROGRAMA DE DOCTORADO EN CIENCIAS BIOMÉDICAS
FACULTAD DE MEDICINA

Impacto de la Separación Materna sobre el Sistema Vasopresinérgico Magnocelular Hipotalámico a Nivel Anatómico, Bioquímico, de Comportamiento y de Conectividad

TESIS
QUE PARA OPTAR POR EL GRADO DE
DOCTORA EN CIENCIAS BIOMÉDICAS

PRESENTA:
ALICIA TRINIDAD NAVA KOPP

TUTORA
DRA. LIMEI ZHANG JI
FACULTAD DE MEDICINA

MIEMBROS DEL COMITÉ TUTOR

GABRIELA MORALÍ DE LA BRENA   JEAN LOUIS CHARLI CASALONGA
CENTRO MEDICO, SIGLO XXI, IMSS   INSTITUTO DE BIOTECNOLOGÍA

CIUDAD UNIVERSITARIA, CD. MX.   ABRIL, 2019

UNIVERSIDAD NACIONAL AUTÓNOMA DE MÉXICO

PROGRAMA DE DOCTORADO EN CIENCIAS BIOMÉDICAS
FACULTAD DE MEDICINA

TESIS DOCTORAL

Impacto de la Separación Materna sobre el Sistema Vasopresinérgico Magnocelular Hipotalámico a Nivel Anatómico, Bioquímico, de Comportamiento y de Conectividad

QUE PARA OBTENER EL GRADO DE
Doctora en Ciencias Biomédicas

Presenta
L.I.B.B. Alicia Trinidad Nava Kopp

Directora de Tesis:
Dra. en C. LIMEI ZHANG JI

Ciudad Universitaria, Ciudad de México, Abril de 2019

A mis abuelos, tíos, primos y sobrinos, por sus incontables bondades y enseñanzas

A mis padres, Christel y Hugo, a quienes debo eterno agradecimiento, un libro completo no alcanza para contar los sacrificios que, con una sonrisa en la cara, han hecho por sus hijos

A mis hermanos:
Hugo, por protegernos siempre y ser el pionero
Beba, por ser la mejor hermana que conozco
Paul, por ser un ejemplo de fuerza y fortaleza
Dolly, a quien algún día, en algún sitio muy bonito, espero conocer
Peter, la enciclopedia humana, por compartirme su pasión por el conocimiento
y Marianito, el hombre más sabio que conozco, por ser mi compadre

A mi esposo e hijos:
Ervell, la mejor mitad de la naranja, mi sostén y mi brújula
Y a los niños más hermosos y dulces del mundo, ellos, los que le dan sentido a la vida: Joseph y Jude

A Dios por los dones aquí mencionados y por los que me faltó enunciar, que francamente no merezco

AD MAJOREM DEI GLORIAM

Miembros del Jurado

Presidente:	Dra. María del Carmen Clapp Jimenez Labora
Secretaria:	Dra. Limei Zhang Ji
Vocal:	Dr. Stefan Mihailescu Lucian
Vocal:	Dra. Teresa Morales Guzmán
Vocal:	Dra. Maria de la Luz Torner Aguilar

ÍNDICE

7.1 Publicaciones

- Prolame ameliorates anxiety and spatial learning and memory impairment induced by ovariectomy in rats. Nissen I, Estrada FS, **Nava-Kopp AT**, Irles C, de-la-Peña-Diaz A, Fernandez-G JM, Govezensky T, Zhang L. Physiol Behav. 2012 May 15;106(2):278-84. doi: 10.1016/j.physbeh.2012.02.019. Epub 2012 Feb 18
- Hypothalamic vasopressin system regulation by maternal separation: its impact on anxiety in rats. Zhang L, Hernández VS, Liu B, Medina MP, **Nava-Kopp AT**, Irles C, Morales M. Neuroscience. 2012 Jul 26;215:135-48. doi: 10.1016/j.neuroscience.2012.03.046. Epub 2012 Apr 20
- Neonatal maternal separation up-regulates protein signalling for cell survival in rat hypothalamus. Irles C, **Nava-Kopp AT**, Morán J, Zhang L. Stress. 2014 May;17(3):275-84. doi: 10.3109/10253890.2014.913017
- A Synaptically Connected Hypothalamic Magnocellular Vasopressin-Locus Coeruleus Neuronal Circuit and Its Plasticity in Response to Emotional and Physiological Stress. Oscar R. Hernández-Perez*, Vito S. Hernandez*, **Alicia Nava-Kopp***, Rafael A. Barrio, Mohsen Seifi, Jerome D. Swinny, Lee E. Eiden and Limei Zhang (*Primeros autores compartidos). *Front. Neurosci.* | doi: 10.3389/fnins.2019.00196

7.2 Presentaciones en congresos

- Nissen I, **Nava-Kopp AT**, Vega-González A, de la Pena A, Fernandez JM & Zhang L. *A 17ß-aminoestrogen (prolame) ameliorates dendritic spine loss in hippocampal pyramidal neurons of young ovariectomized rats*. 40th Annual Meeting of the Society for Neuroscience, San Diego, CA, USA
- Zhang L, Hernández VS, **Nava-Kopp AT** & Irles C. *Maternal separation upregulates hypothalamic vasopressin expression in rat early postnatal and young adult stages: impacts on conditioned anxious state*. 10th FENS Forum of Neuroscience, Barcelona, Spain
- **Nava-Kopp AT**, Zhang L & Irles C. *Maternal separation modulates programmed cell death in rat* hypothalamus. 42nd Annual Meeting of the Society for Neuroscience, New Orleans, LA, USA
- **Nava-Kopp AT**, Irles C & Zhang L. *Anatomical characterization for intra- and extra-hypothalamic kisspeptin projections in neonatal maternal-separated rats: A comparison between genders at different ages*. 43rd Annual Meeting of the Society for Neuroscience, San Diego, CA, USA
- **Nava-Kopp AT**, Irles C, Barrio H & Zhang L. *Effect of neonatal maternal separation and adolescent ethanol exposure on adult preference for ethanol*. 44th Annual Meeting of the Society for Neuroscience, Washington, DC, USA

Resumen

La arginina vasopresina (AVP) es una hormona peptídica muy conservada evolutivamente sintetizada en células neurosecretoras dentro del hipotálamo y liberada desde la hipófisis posterior a la circulación general, cuyo papel en la homeostasis de líquidos y electrolitos ha sido ampliamente estudiada. En los últimos treinta y cinco años ha surgido una segunda identidad neuroanatómica y un nuevo papel fisiológico para la AVP. Es decir, la AVP ahora se considera también como neurotransmisor, liberado de las mismas neuronas que inervan a la neurohipófisis, pero también proyectan a diversas áreas del cerebro, como la amígdala, el hipocampo, la habénula y el *locus coeruleus*.

Por otro lado, la literatura que demuestra que el estrés en la vida temprana (ELS) tiene consecuencias permanentes en el funcionamiento del cerebro sigue en aumento, concretamente en la respuesta al estrés durante toda la vida hasta la edad adulta. Se ha demostrado que estos efectos se deben, al menos en parte, a las alteraciones neuroendócrinas subyacentes que provocan una reactividad excesiva al estrés. Esta tesis se enfoca principalmente en los efectos particulares que la separación materna (MS), un protocolo de ELS, tiene sobre el sistema vasopresinérgico magnocelular hipotalámico.

Este trabajo, hecho en ratas, se puede dividir en tres distintas secciones. Las dos primeras son diferentes aspectos de las alteraciones que se encontró que la MS tiene sobre las neuronas vasopresinérgicas neurosecretoras magnocelulares (AVPMNN) hipotalámicas: **i)** Se demostró que la MS es capaz de aumentar la expresión tanto del péptido como del mRNA de AVP en los núcleos vasopresinérgicos hipotalámicos paraventricular (PVN) y supraóptico (SON), así como también aumentar el volumen de los mismos; **ii)** La MS también demostró aumentar la densidad neuronal en varias regiones del hipotálamo relacionadas con la respuesta al estrés, que es congruente con un aumento en la expresión de proteínas asociadas a la supervivencia celular y una disminución en la expresión de proteínas pro-apoptóticas, que se encontró en lisados de hipotálamo entero; y la última etapa se relaciona con las nuevas proyecciones de las AVPMNN hacia la amígdala, la habénula lateral y el hipocampo halladas por el laboratorio de la Dra. Zhang al mismo tiempo de la realización de este proyecto: **iii)** El *locus coeruleus* (LC) es un núcleo del tallo cerebral, que procesa señales ambientales y las transmite a una amplia gama de núcleos, que ajustan los estados aversivo, apetitivo y de atención de manera apropiada para el entorno en un momento dado. Encontramos que la MS afecta, no solo el estado de las AVPMNNs dentro del propio hipotálamo, sino también sus proyecciones a LC. Los cambios dinámicos en las AVPMNNs y sus proyecciones a LC tienen efectos sutiles pero profundos en el aprendizaje y la memoria, en condiciones adversas, como la deshidratación. Con este trabajo hemos demostrado la importancia de las inervaciones de las AVPMNNs al LC a nivel anatómico, del comportamiento y de circuitos neuronales.

Abstract

Arginine vasopressin (AVP) is a highly evolutionarily conserved peptide hormone elaborated from neurosecretory cells within the hypothalamus, and released from the posterior pituitary into the general circulation, whose function in fluid and electrolyte homeostasis is well established. In the past thirty-five years, a second important neuroanatomical identity and physiological role for AVP has emerged. That is, AVP is also a neurotransmitter, released from the same neurons that supply the neurohypophysis, but also projecting to diverse brain areas including the amygdala, hippocampus, habenula and locus coeruleus.

On the other hand, there is a growing body of literature demonstrating that early life stress has permanent consequences on brain functioning, concretely on stress responsiveness, all through life. These effects have been demonstrated to be due, at least in part, to underlying neuroendocrine alterations which translate into an over reactivity to stress. The focus of this dissertation is the particular effects that maternal separation (MS), a protocol of ELS, has on the vasopressinergic hypothalamic magnocellular system.

This work can be divided into three different stages. The first two are different aspects of the alterations that MS was found to have on the AVP magnocellular neurosecretory neuron (AVPMNN) system, in rats: **i**) MS demonstrated to increase both the peptide and mRNA expression of AVP in the hypothalamic vasopressinergic paraventricular and supraoptic nuclei (PVN and SON, respectively), as well as increasing the volume of these AVP+ nuclei; **ii**) MS also demonstrated to increase neuronal density in several stress-associated regions of the hypothalamus, concomitant with an increase in the expression of survival-associated proteins and a decrease in pro-apoptotic protein expression, found in whole hypothalamus lysates; and the last stage relates to the novel AVPMNN projections to amygdala, lateral habenula, and hippocampus found by Dr. Zhang's lab during the realization of this thesis project**: iii**) The *locus coeruleus* (LC) is a brainstem nucleus that processes environmental cues and transmits to a broad array of core rostral brain nuclei biasing aversive, appetitive, and attentional states towards those most appropriate to the environment at a given time. We found that MS affects not only the status of AVPMNNs in the hypothalamus itself, but also its projections to the LC. The dynamic changes in AVPMNN cells and their projections to the LC have subtle but profound effects on learning and memory, on modulation of learning by exigent states such as dehydration. These correspond to altered activation of neurons in areas of the brain to which both AVPMNNs and LC project. I and my colleagues have demonstrated the importance of AVPMNN inputs to the LC at the anatomical, cell circuit behavioral levels.

Lista de abreviaturas

ABC	complejo avidina-biotina-peroxidasa'
ACTH	adrenocorticotropina (por sus siglas en inglés: *adrenocorticotropic hormone*)
ADH	hormona antidiurética (por sus siglas en inglés: *anti-diuretic hormone*)
AFR	grupo control, criado en bioterio (por sus siglas en inglés: *animal-facility reared*)
AHA	área hipotalámica anterior
Arc	núcleo arcuato hipotalámico
AVP	arginina vasopresina
AVPMNN	neuronas magnocelulares vasopresinérgicas neurosecretoras
cAMP	adenosín monofosfato cíclico
CCTV	circuito cerrado de televisión
cpm	cuentas por minuto (cuentas de desintegración radioactiva)
CRH	hormona liberadora de corticotropina (*corticotropin-releasing hormone*)
CSF	liquido cefalorraquideo (por sus siglas en inglés: *cerebrospinal fluid*)
DEPC	dietilpirocarbonato
ELS	Estrés temprano (early-life stress)
g	unidad de fuerza centrífuga force, 1 g = 9.806 m/s^2
GFAP	proteína acídica glial fibrilar
GPCR	receptor acoplado a proteína G
h	hora del día
HPA	eje hipotálamo-pituitaria-adrenal
hr, hrs	hora(s), unidad de tiempo
HRP	peroxidasa de rábano (por sus siglas en inglés: *horseradish peroxidase*)
IgG	inmunoglobulina G
i.p.	intraperitoneal
kDa	kilodaltones
LC	*locus coeruleus*
min	minuto(s)
MPOc	núcleo medial preóptico región compacta
MPOm	núcleo medial preóptico región medial

mRNA	ácido ribonucleico mensajero
MS	separación materna, procedimiento en general
MS3h	separación materna, 180 min evento aislado
NeuN	proteína Núcleos Neuronales
NDS	suero normal de burro
NHS	suero normal de caballo
NSS	suero normal de cerdo
opt	tracto óptico
PB	solución amortiguadora de fosfatos (*phosphate buffer*)
PCD	muerte celular programada (*programmed cell death*)
PKC	proteína cinasa C
PLC	fosfolipasa C
PND	día post-natal
PVN	núcleo paraventricular hipotalámico
PVNlmd	núcleo paraventricular hipotalámico, división lateral magnocelular
PVNmpd	núcleo paraventricular hipotalámico, división medial parvocelular
s	segundo(s)
SCN	núcleo supraquiasmático
SChDL	núcleo supraquiasmático, división dorsolateral
SHRP	período de hiporesponsividad al estrés (*stress hyporesponsive period*)
SNC	sistema nervioso central
SON	núcleo supraóptico hipotalámico
TBS	*buffer* de Trizma, 0.05 M, pH 7.4 a 25°C, más 0.9% NaCl
TBST	*buffer* de Trizma, 0.05 M, pH 7.4 a 25°C, más 0.9% NaCl y 0.3% Triton X-100
TBT	*buffer* de Trizma más 0.1% de Tween
TH	tirosina hidroxilasa
V1aR	receptor vasopresinérgico 1a
V1bR	receptor vasopresinérgico 1b
WD	privación de agua
3hMS	grupo experimental con separación materna (180 min)
3V	tercer ventrículo

I. INTRODUCCIÓN

1.1 Generalidades

1.1.1 Vasopresina: esctructura, función y receptores

La vasopresina es una hormona peptídica formada por nueve aminoácidos, de los cuales el octavo es arginina en la mayoría de los mamíferos (**du Vigneaud *et al*, 1953**), de ahí que se le conozca también como arginina-vasopresina (AVP), o argipresina. Su función fisiológica primordial es la de concentrar la orina y es por eso que también se le conoce como hormona anti-diurética (ADH). La AVP ejerce esta acción mediante un receptor expresado en las células principales de los túbulos colectores distales, aumentando la reabsorción de agua (**Gottschalk & Mylle, 1959**). La existencia de la AVP se descubrió al infundir extractos hipofisiarios en ranas, lo cual se demostró que ocasionaba un aumento en la presión arterial (**Oliver & Schafer, 1895**). Este efecto se le atribuyó más tarde a la habilidad de la AVP de contraer el músculo vascular (**Somlyo et al, 1965**). La AVP también promueve la agregación de las plaquetas en el plasma sanguíneo (**Haslam & Rosson, 1972**), y a mayores concentraciones, se ha visto que es capaz de alterar el metabolismo hepático, induciendo glucogenólisis (**Hems *et al*, 1975**). Se ha visto un aumento en la concentración plasmática de AVP en respuesta al aumento de osmolalidad sanguínea, o bien a una pérdida de volumen sanguíneo (**Dunn *et al*, 1973**). Todo esto nos indica que la AVP es un efector robusto en la respuesta a retos osmóticos, como la deshidratación y a otras condiciones ambientales que ponen en riesgo al equilibrio electrolítico, tal como la pérdida de sangre. Para mediados de los 1970s la AVP se había establecido firmemente como una hormona, producida en el cerebro, y secretada hacia la circulación desde el lóbulo posterior de la hipófisis para coadyuvar a las funciones cardiovasculares y renales contribuyendo al mantenimiento de la homeostasis.

Al mismo tiempo, en los '70s, un aspecto nuevo de la acción de la AVP comenzó a emerger de distintas observaciones científicas: David de Wied observó que la remoción del lóbulo posterior e intermedio de la hipófisis, en ratas, evitaba que éstas fueran condicionadas en una prueba de evitación, mismo efecto que pudo ser revertido con la administración de extractos hipofisiarios (**de Wied, 1965**) o de vasopresina (**de Wied, 1971**). Tras estos estudios pioneros, siguieron abundantes observaciones científicas que confirmaron que la AVP también cumple un papel en la regulación de la conducta. Se descubrió que la AVP, presente en el núcleo supraquiasmático (SCN), formaba parte del principal circuito encargado de la oscilación circadiana (**Castel *et al*, 1990**); la inactivación de uno de los receptores de AVP (V1a) demostró suprimir la memoria social y disminuir el comportamiento ansioso, en ratas (**Landgraf *et al*, 1995**); se demostró que la administración de AVP es capaz de acelerar el aprendizaje, así como mejorar la memoria, usando un laberinto radial (**Dietrich & Allen, 1997**), entre otros. Los diversos efectos que se observaron que la AVP podían ejercer sobre la conducta, de Wied los atribuyó inicialmente a que, tras ser liberada de la neurohipófisis, la AVP regresaría hacia el cerebro viajando en la circulación sanguínea. Sin embargo, debido a la existencia de la barrera hematoencefálica ésta es una explicación poco plausible; reforzado por el hecho que los

niveles plasmáticos de AVP no se correlacionan con los niveles de AVP en el líquido cefalorraquídeo (CSF), más tarde surgió la idea que la AVP que ejerce efectos sobre el comportamiento -concretamente sobre el cerebro- podría provenir de dentro del cerebro mismo y no de la circulación, tras ser liberada la hormona de la hipófisis. Una posible explicación es la liberación dendrítica del péptido dentro del cerebro difundiendo dentro del sistema nervioso central (SNC) y hacia el CSF para posteriormente ejercer una señalización parácrina; debido a que los neuropéptidos como AVP tienen una vida media relativamente larga, en comparación con los neurotransmisores esta explicación es, cuando menos, posible (**Ludwig & Leng, 2006**).

Conforme apareció la tecnología para afectar la expresión de los receptores vasopresinérgicos tanto en la periferia como en el cerebro, se abrió la posibilidad de estudiar más a fondo los efectos centrales y periféricos de la AVP. Hoy en día se conocen tres receptores para AVP: el **1a**, el **1b** y el **2**. Los tres están acoplados a proteínas G (GPCR) y se expresan diferencialmente a lo largo del cuerpo. La membrana basolateral de las células principales del túbulo colector distal, en el riñón, expresan receptor tipo 2 (V2R) exclusivamente (**Rosenthal *et al*, 1993**). Este receptor está acoplado a una proteína G con subunidad alfa tipo S (αs), lo que quiere decir que tras su activación provoca un aumento intracelular de adenosín monofosfato cíclico (cAMP); esto a su vez provoca la movilización de calcio intracelular, que promueve la fusión de vesículas llenas de acuaporina 2 (AQP2) a la membrana apical de las células del túbulo colector, aumentando la permeabilidad al agua y con esto su reabsorción (**Park & Kwon, 2015**). Por otro lado, la acción de la AVP en el tejido vascular se da gracias al receptor 1a (V1aR), mismo que se expresa también en hígado y pulmones. Y el receptor 1b (V1bR) se encuentra principalmente en los corticotropos de la adenohipófisis. Ambos receptores son GPCRs αq, lo que quiere decir que actúan mediante la activación de fosfolipasa C (PLC) y posterior activación de la proteína cinasa C (PKC) (**Barberis *et al*, 1998**).

1.1.2 Vasopresina: evolución, síntesis y anatomía

Con la excepción del octavo aminoácido de la AVP -una arginina, que en cerdos e hipopótamos es sustituida por una lisina- la hormona está altamente conservada entre mamíferos; en las más de 30 especies que se han estudiado (incluyendo marsupiales y monotremas) se conserva exactamente la misma estructura. La vasotocina, hormona homóloga a AVP en reptiles, anfibios y peces, cuyo gen se considera que dio origen a los dos genes parálogos para AVP y para oxitocina, está presente en las especies de vertebrados más primitivos vivientes: las lampreas, lo cual significaría que este gen no cambió por más de 400 millones de años (**Sawyer, 1967**). Éste es un ejemplo inusual de alta estabilidad evolutiva en un péptido, lo que sugiere que las funciones vitales que ejerce son absolutamente indispensables para la supervivencia de las especies y que cualquier mínima mutación que pudo haber aparecido debió resultar perjudicial.

La AVP es sintetizada como pre-pro-hormona y es escindida durante su transporte axonal a la neurohipófisis, donde se almacenan los productos de este procesamiento proteolítico: la AVP madura, neurofisina y la co-peptina (**Schmale *et al*, 1983**), listas para ser

liberadas hacia el torrente sanguíneo en respuesta a un aumento en la osmolalidad plasmática, o bien a una disminución en la presión sanguínea (**Cunningham & Sawchenko, 1991**). La neurofisina sirve como proteína acarreadora de AVP; mientras que no se ha descubierto ninguna función biológica para la co-peptina, fuera de su participación en el procesamiento de la AVP.

La AVP se sintetiza en varias regiones del cerebro. El sitio principal es el hipotálamo, donde están las neuronas magnocelulares neurosecretoras (AVPMNNs) concentradas en los núcleos paraventricular (PVN) y supraóptico (SON). Sin embargo, además de éstas, el PVN también contiene una población de neuronas menores en tamaño que contienen AVP: las neuronas parvocelulares (de 'parvo' que significa pequeño en griego); estas neuronas pequeñas tienen un soma de aproximadamente 10-20 µm, mientras que las neuronas grandes, o magnocelulares, tienen un cuerpo celular de 20-35 µm. Estas dos poblaciones también tienen funciones fisiológicas distintas, así como orígenes embrionarios distintos. Los axones de las AVPMNNs viajan a través de la capa interna de la eminencia media (ME) hacia la parte posterior de la pituitaria (o neurohipófisis), donde liberan su contenido en respuesta a cambios en osmolaridad o presión sanguíneas; de aquí la AVP viaja a través de la circulación hasta sus tejidos blanco (como el renal o vascular) para ejercer las respuestas adecuadas. Por otro lado las neuronas vasopresinérgicas parvocelulares desembocan en el plexo capilar portal, por donde la AVP liberada viaja a la hipófisis anterior (o adenohipófisis); aquí la AVP estimula la secreción de adenocorticotropina (ACTH) por las células corticotropas (**Armstrong, 2004**). Mientras que las AVPMNNs están presentes en el hipotálamo exclusivamente, se han observado neuronas vasopresinérgicas parvocelulares en otros sitios, como la amígdala y el núcleo del lecho de la estría terminal (BNST; **Buijs *et al*, 1983**).

Por más de 30 años se ha estudiado la diferenciación, migración y el establecimiento de conexiones necesarios para la formación de circuitos con AVPMNNs. El sistema es capaz de responder a estímulos osmóticos desde los últimos días de desarrollo embrionario (E18, E19), aumentando la transcripción de AVP (**Laurent *et al*, 1989**). Sin embargo, las enzimas que procesan a la pre-pro-hormona se expresan más tarde. La secreción de AVP es posible a partir del día posterior al nacimiento, para entonces las neuronas vasopresinérgicas habrán llegado al sitio final que ocuparán por el resto de la vida del animal. (**Wolf et al, 1984**). Sin embargo no se considera un sistema maduro, ya que en esta etapa no se ha alcanzado siquiera el 10% de los niveles de expresión vistos en adultos, además que el número de células continuará aumentando también hasta la pubertad (**Almazan *et al*, 1989**). Aunado a esto, se ha visto que la exposición a glucocorticoides y a la misma AVP es capaz de afectar el desarrollo de este sistema (**Schilling *et al*, 1991; Wotjak *et al*, 1994**); lo que nos indica que el sistema vasopresinérgico es altamente modificable durante la etapa neonatal.

Durante el desarrollo temprano la AVP contribuye a la regulación, proliferación y morfogénesis de sus células y tejidos blanco. En el trabajo de parto promueve la adaptación del feto y contribuye al establecimiento de un nuevo equilibrio de los fluidos corporales, la AVP provoca una redistribución del flujo sanguíneo al nivel del sistema cardiovascular, aumentando

la circulación hacia los órganos vitales y hacia los órganos involucrados en la respuesta al estrés (glándula pituitaria, corazón y glándulas suprarrenales), y al mismo tiempo reduce la circulación hacia otros órganos periféricos (**Ugrumov, 2002**).

1.1.3 Respuesta al estrés y eje HPA

Cuando se presentan eventos estresantes, es decir cambios en el ambiente repentinos y aversivos, potencialmente dañinos, los animales respondemos con un estado de alarma, que provoca cambios inmediatos e inespecíficos del comportamiento (como puede ser el sobresalto) seguidos de cambios específicos de comportamiento, concretamente un estado de lucha o huida (*fight or flight)*. Al mismo tiempo varios parámetros fisiológicos se ajustan, como puede ser un aumento en la presión arterial o taquicardia, que aunados a las respuestas de comportamiento preparan a los animales para afrontar activamente a la amenaza. Estas reacciones de alarma están vinculadas principalmente a un sistema simpato-adrenérgico activo e involucran la activación de los núcleos del tallo cerebral, el nervio vago y las glándulas suprarrenales, lo cual conlleva a la liberación de noradrenalina y adrenalina a la circulación. En contraste, cuando los encuentros aversivos no se pueden sobrellevar mediante la respuesta simpato-adrenérgica, los animales inician estrategias de afrontamiento pasivas que están asociadas principalmente con una liberación de cortisol (en humanos, corticosterona en otras especies, como los roedores). Los cambios hormonales resultantes causan la redistribución adaptativa de energía (aumento de oxigenación y nutrientes al cerebro, gluconeogénesis, lipólisis, inhibición del crecimiento y sistemas reproductivos, contención de respuestas inflamatorias) y comportamiento (aumento de la excitación, vigilancia y cognición, supresión de la alimentación y comportamiento reproductivo). Los eventos aversivos severos, incontrolables y de larga duración pueden conducir a una liberación sostenida de glucocorticoides. Se piensa que esta mala respuesta adaptativa está relacionada causalmente con una variedad de trastornos psiquiátricos humanos, incluidos los trastornos de ansiedad y la depresión (**Engelmann *et al,* 2004**).

La liberación de glucocorticoides es un proceso finamente regulado de forma jerárquica: la liberación de hormona liberadora de corticotropina (CRH) del hipotálamo hacia la pituitaria anterior (o adenohipófisis) estimula a los corticotropos ahí presentes, ocasionando la liberación de adrenocorticotropina (ACTH), que a su vez viaja por la circulación hasta llegar a las glándulas suprarrenales (o adrenales) donde estimula la secreción de cortisol o corticosterona; a esta cascada de hormonas se le conoce como eje hipotálamo-pituitaria-adrenal (HPA). De forma interesante, y como se mencionó antes, la AVP proveniente de las neuronas parvocelulares del PVN, en el hipotálamo, potencian esta cascada, a nivel de la liberación de ACTH en los corticotropos (**Armstrong, 2004**).

1.1.4   El sistema límbico y dos estructuras vinculadas a él: el hipotálamo y *locus coeruleus*

El sistema límbico es un cúmulo de estructuras cerebrales que se encuentran aproximadamente localizadas lateralmente al tálamo, por debajo de la corteza cerebral y por encima del tallo cerebral; entre ellos la amígdala, el hipocampo, el tálamo, hipotálamo, ganglios basales y giro cingulado. Fue en 1878 la primera vez que Paul Broca nombró esta región "el gran lóbulo límbico". Más tarde se designó la terminología para nombrar individualmente las estructuras aquí contenidas y poco a poco se descubrió que esta región está íntimamente ligada a los procesos emocionales y motivacionales, que interactúan con otras regiones del cerebro (**Torrico & Abdijadid, 2019**).

El hipotálamo tiene varios roles en el mantenimiento de la homeostasis, además de estar interconectado con el resto del sistema límbico; concretamente se ha establecido que el hipotálamo forma sinapsis con el núcleo accumbens, área tegmental ventral, hipocampo y amígdala. A esta comunicación entre sistemas se le conoce como la interfaz límbica-motora y es esencial para ciertos comportamientos de supervivencia; tales como la búsqueda de alimento, el escape y miedo a los depredadores y es un claro ejemplo de la iniciación de acción provocada por estructuras límbicas anteriores y ayuda a entender cómo es que el "cerebro emotivo" y el "cerebro cognitivo" trabajan en concierto para iniciar una respuesta (**Mogenson *et al*, 1980**).

El locus coeruleus (LC) inicialmente se describió como un "grupo de neuronas llenas de un pigmento parecido a la melanina localizado en el puente troncoencefálico", también conocido como *nucleus pigmentosus ponti*; se sabe que es una región del tallo cerebral, que consiste de células noradrenérgicas, cuyo nombre viene del latín para "sitio azulado"; este color proviene de los gránulos de melanina derivados de la polimerización de la noradrenalina (**Maeda, 2000**). Este núcleo es un sitio clave para los procesos de la vigilia, sin embargo también se ha involucrado a la respuesta al estrés; y aunque es parte del tallo cerebral, por lo cual no se considera estrictamente parte del sistema límbico, se sabe que inerva regiones del sistema límbico como el hipocampo, hipotálamo y amígdala; en esta última región (que está involucrada en procesos emocionales y de formación de memoria, se ha visto que, por ejemplo, tras estimular el LC eléctricamente *in vivo* se puede observar activación neuronal en la amígdala (**Rodríguez-Ortega *et al*, 2017**).

1.2   Antecedentes directos

1.2.1   Estrés temprano y separación materna

La influencia que el medio ambiente puede tener sobre un individuo neonato ha sido estudiada formalmente por más de 60 años. Seymour Levine observó una correlación entre las condiciones neonatales y la responsividad al estrés en la edad adulta (**Levine, 1957**). Posteriormente, muchos grupos de investigación demostraron que la separación de la madre (o separación materna: MS) tiene consecuencias permanentes sobre la liberación de CRH,

ocasionando una hiperresponsividad a un estresor leve en la edad adulta, en comparación a individuos cuya infancia no fue manipulada (**Plotsky & Meaney, 1993**). También se ha reportado que la MS provoca alteraciones neuroendócrinas (**Ladd *et al*, 2000**), en niveles de neurotrofinas (**Cirulli *et al*, 2003**) e incluso modificaciones epigenéticas (**Murgatroyd *et al*, 2009**), se han visto cambios consistentes en los niveles de CORT, ACTH y CRH, al igual que en la distribución de sus receptores (**Fumagalli *et al*, 2007**); todas éstas son probablemente intentos de adaptación al estrés temprano de la ausencia materna intermitente.

Es relevante para nuestro trabajo señalar que las ratas, así como otros roedores, pasan por un período de hiporresponsividad al estrés (SHRP) entre los días post-natales 3 y 16, durante el cual la secreción de ACTH está disminuida, lo cual implica que los niveles de CORT también sean muy bajos. Es probable que este mecanismo sea uno de neuroprotección, ya que se ha visto que la administración de glucocorticoides exógenos en un período de alta proliferación celular inhibe el crecimiento correcto y la proliferación (**Sapolsky & Meaney, 1986**). Esto indica que el eje HPA no está maduro ni funcionando durante la etapa neonatal. Sin embargo, se ha visto que durante el SHRP la AVP funciona como el secretagogo principal de ACTH, además de tener un efecto supresor sobre la liberación de CORT (**Makara *et al*, 2008**).

Adicionalmente se ha visto que el estrés es capaz de regular la expresión del V1aR en ratas, a las cuales se les había inducido un infarto previamente. El estrés incrementó la expresión del mRNA para V1aR en el diencéfalo y en el tallo cerebral de las ratas con el accidente vascular previamente inducido (**Milik *et al*, 2004**)- El V1bR también es vulnerable a regulación por estrés: la transcripción del gen para V1bR incrementó en una línea celular expuesta a AVP (**Volpi *et al*, 2006**). Por lo tanto los receptores vasopresinérgicos expresados centralmente son regulables dinámicamente por agentes, entre ellos el estrés, que perturban la homeostasis; lo cual nos sugiere que la AVP tiene una función reguladora de la respuesta al estrés a largo plazo, a otro nivel, además de la liberación aguda del péptido.

1.2.2   Supervivencia celular y apoptosis

La etapa neonatal es una de grandes cambios para el cerebro, entre los cuales está la eliminación de células por un proceso natural altamente regulado llamado muerte celular programada (PCD) o apoptosis. Se ha encontrado que este proceso es crucial para la regulación del tamaño de las poblaciones neuronales y el establecimiento apropiado de circuitos neuronales (**Buss *et al*, 2006; Clarke, 1985**). Los niveles más altos de PCD ocurren durante las primeras semanas de vida en el cerebro de la rata en regiones como el tallo cerebral, el neocórtex y el hipotálamo (**White & Barone, 2001**), así como en el hipotálamo murino (**Ahern *et al*, 2013**). Por lo tanto cualquier evento que le ocurra al animal durante este período crítico de desarrollo puede producir alteraciones de largo plazo, que podrían afectar durante el resto de la vida del animal.

Algunas de las proteínas involucradas en la regulación de este proceso son las siguientes: la proteína anti-apoptótica Bcl-2 (*B cell lymphoma 2*) es parte del grupo de supresores de apoptosis mediada por mitocondrias y está encargada de proteger la integridad de la membrana mitocondrial; mientras que Bax (*Bcl-2 associated X protein*) es un efector en la cascada de PCD mediada por factores de necrosis tumoral y es responsable de la liberación del citocromo C de la mitocondria, activando a la caspasa. Por lo tanto la proporción Bcl-2/Bax es un indicador de apoptosis (**Oltvai *et al*, 1993**). Por otro lado, las proteínas cinasas ERK 1/2 (cinasas reguladas por señales extracelulares) y Akt están involucradas en vías de señalización que llevan a supervivencia y proliferación neuronal (**Brunet *et al*, 2001**) y neurogénesis (**Faedo *et al*, 2008**). Bad (*Bcl-2-associated death promoter protein*) es un efector de PCD mediada por el retículo endoplasmático y es una proteína pro-apoptótica que irrumpe la integridad membranal de la mitocondria. Sin embargo, la fosforilación de la serina en Bad, por ERK 1/2 y Akt inactiva a Bad, por lo cual Bad fosforilada (pBad) es un marcador de supervivencia y no muerte celular (**Bonni *et al*, 1999**).

De forma interesante, se ha demostrado que la AVP tiene efectos tróficos en neuronas embrionarias de la médula espinal (**Iwasaki *et al*, 1991**); e incluso es capaz de inhibir la apoptosis inducida por privación de suero en una línea celular hipotalámica (**Chen *et al*, 2009**).

1.2.3   Vasopresina como neuromodulador

Como se mencionó anteriormente, la acción central de la AVP pasó de considerarse como un efecto causado por el retorno de la hormona circulante (liberada en la neurohipófisis) de vuelta hacia el cerebro a través de la circulación; a considerarse que se debía a una difusión desde la liberación dendrítica de las AVPMNNs, señalizando parácrinamente. Sin embargo, una opción menos considerada fue estudiada por nuestro laboratorio y se comprobó que, al menos algunos de los efectos centrales de la AVP se transmiten por una inervación "intencional", donde axones de las AVPMNNs liberan el péptido y hacen sinapsis dentro del cerebro hacia ciertas regiones que subyacen los efectos conductuales conocidos de la AVP: como el hipocampo (**Zhang & Hernández, 2013**), la amígdala (**Hernández *et al*, 2016**) y la habénula (**Zhang et al, 2018**).

II.   **HIPÓTESIS**

2.1   Planteamiento del problema científico

El papel de la vasopresina como una hormona que incrementa la probabilidad de supervivencia en el evento de una pérdida de sangre (o cualquier otro desbalance electrolítico y/o de líquidos) se ha documentado ampliamente y se encuentra bien establecido: la vasopresina enciende una serie de respuestas en distintos órganos y sistemas dentro del cuerpo, ajustando los

parámetros fisiológicos para prevenir que se continúe el daño. Estos efectos no se limitan a tejidos periféricos, ya que también se ha descrito la habilidad de la vasopresina para afectar el funcionamiento cerebral, como en el caso de la memoria y estados emocionales.

La mayoría de los trabajos donde se estudia la vasopresina en el sistema nervioso central y su papel en la respuesta al estrés se han realizado durante, o después de una exposición aguda a AVP y/o a un estímulo estresante. Sin embargo dado que cumple un papel crucial en el procesamiento de condiciones ambientales estresantes durante la infancia, se vio la necesidad de un estudio más profundo de los efectos de la vasopresina sobre el cerebro, en particular durante la etapa perinatal.

Siguiendo este razonamiento, para este proyecto se utilizó un protocolo de estrés temprano que, debido a su naturaleza estresante y privativa de líquidos, implica una secreción constante de vasopresina: la separación materna.

2.2 Hipótesis

Se propone que el estudio de los efectos del estrés en la vida temprana (es decir, la separación materna) sobre el sistema vasopresinérgico magnocelular hipotalámico proporcionará nuevos resultados, que amplían nuestra comprensión de cómo esta hormona modula el comportamiento, la neuroanatomía y los circuitos neuronales para adaptarse a los efectos adversos.

Concretamente, se hipotetiza que i) la separación materna causará cambios significativos sobre el sistema de AVPMNNs, ii) que la MS causaría cambios cuantificables en el comportamiento durante la etapa adulta, y que iii) los cambios en el sistema de AVPMNNs estarían entonces asociados a estos cambios en el comportamiento, de manera causal con plausibilidad anatómica y una correlación bidireccional fuerte.

2.3   Objectivos

2.3.1   Objetivo general

El objetivo del presente estudio es dilucidar los efectos del estrés en la vida temprana, concretamente, de la separación materna, sobre la fisiología (es decir, la función, la citoarquitectura y la conectividad) de las neuronas magnocelulares hipotalámicas vasopresinérgicas y (en la medida en que sea razonablemente posible para el alcance de una tesis de doctorado) los mecanismos subyacentes a éstos.

2.3.2   Objetivos específicos

I   Comprobar si es que la separación materna es capaz de ocasionar cambios significativos a la anatomía y fisiología del sistema vasopresinérgico magnocelular hipotalámico, y si estos cambios se manifiestan en el comportamiento

II   Estudiar más a profundidad los cambios que se pudieran encontraron en el punto anterior y tratar de vislumbrar un mecanismo causal que pudiera explicar, al menos en parte, el origen de estos cambios

III Estudiar la relevancia de estos cambios en un contexto más sistémico y tratar de integrarlos a un modelo donde tarde o temprano se pueda aplicar lo descubierto a problemas de salud pública

III. **MATERIALES Y MÉTODOS**

3.1 Animales

Los experimentos que se presentan en este trabajo se realizaron en ratas Wistar, provistas por el Bioterio de la Facultad de Medicina de la UNAM. Todos los procedimientos realizados se basaron en la Guía para el Cuidado y Uso de Mamíferos en Neurociencias e Investigación Conductual (National Research Council, 2003).

Los animales se albergaron en un cuarto ventilado con la temperatura controlada (20-24°C), se les dio acceso a agua potable y alimento estándar para rata *ad libitum*, se mantuvieron en un ciclo de 12:12 hrs de luz/oscuridad, a menos que se especificara de otra manera. En el caso de cirugías los animales fueron albergados en cajas individualmente con temperatura controlada, administrándoles analgésicos durante el periodo de recuperación.

3.2 Protocolo de separación materna (MS)

El protocolo de separación materna (MS) se realizó de acuerdo con Veenema (**Veenema *et al*, 2006**): ratas Wistar adultas, macho y hembra se obtuvieron de nuestro bioterio y se les permitió copular durante dos días. Las hembras gestantes después de esto fueron albergadas en grupos de tres por caja hasta el día gestacional 17, a partir de ahí se albergaron individualmente en cajas estándar de Plexiglas, en un cuarto con ventilación adecuada y temperatura controlada con acceso a agua potable y alimento estándar para rata *ad libitum*, se mantuvieron en un ciclo de 12:12 hrs de luz/oscuridad (luces encendidas a las 19 h).

El día después del parto (día post-natal 2, PND 2) cada camada fue reducida a 7-8 crías, de las cuales 5-6 fueran machos. Entre los PNDs 2 y 15 las crías fueron separadas de la madre diariamente entre las 9:00 y las 12:00 h. Las crías se transfirieron, tras cubrir las manos del experimentador con aserrín de la misma caja de donde se removió a la cría, a una caja pequeña alfombrada con el mismo aserrín. Se trasladaron entonces a un cuarto contiguo y se introdujeron a una incubadora húmeda con temperatura controlada (29°C ± 1°C). Tras la separación de 3 hrs, las crías se devolvieron a la caja "hogar" seguido de su reunión con su respectiva madre. Al terminar el protocolo de MS las ratas se dejaron sin perturbar hasta el PND 28, cuando se destetaron a las crías y se separaron a las hembras de los machos. El aserrín de las cajas se cambió 2 veces a la semana, minimizando perturbaciones. De aquí en adelante el grupo de animales sometido a este protocolo se refiere como "3hMS" en este trabajo. Los grupos control para estos animales se dejaron con la madre, sin perturbaciones, a excepción de los cambios de aserrín 2 veces a la semana y se les designó como "AFR" (por las siglas en inglés: animal-facility reared).

3.2.1 Privación de agua para evaluar la expresión de AVP en *locus coeruleus*

Se privó de agua a ratas macho de edad PND 75, tanto MS como control, durante las 24 hrs antes de ser perfundidas. La WD24h se hizo para minimizar la variabilidad de la inmunoreacción de AVP basal, incrementando la comparabilidad entre sujetos. Tras la perfusión y fijación, el tejido se procesó para evaluar la inmunoreactividad de AVP, como se describe en detalle en la sección de *Ensayos inmunohistoquímicos*, más adelante.

3.3 Técnicas histológicas

3.3.1 Obtención de tejido

La obtención de tejido cerebral requerido para los distintos experimentos de este trabajo fueron obtenidos, a grandes rasgos, de la siguiente forma, con cambios menores dependiendo de los requerimientos particulares de cada experimento: Las ratas fueron anestesiadas profundamente con pentobarbital sódico (63 mg/kg) administrado por inyección intraperitoneal (i.p.). Después se procedió a diseccionar y perfundir transcardialmente, primero con solución salina isoosmótica (NaCl, 0.9%), con el volumen necesario para lavar toda la sangre del animal, seguido por un volumen de fijador adecuado al tamaño del animal para perfundir durante 15 min, la velocidad de la bomba peristáltica se ajustó dependiendo de la edad y tamaño del animal también. La solución fijadora está compuesta por paraformaldehído 4% diluído en solución amortiguadora de fosfatos (PB, pH 7.4) 0.1M más ácido pícrico saturado a una concentración final de 15% (vol/vol); 0,05% de glutaraldehído se agregó en el caso de tejido que se utilizaría para microscopía electrónica, o bien para hibridización *in situ* (ISH). Todas las soluciones utilizadas para ISH tradicional (es decir no para RNAscope) fueron tratadas con dietilpirocarbonato (DEPC) al 0.1% (vol/vol) con agitación constante por al menos 4 hrs a temperatura ambiente para inactivar ribonucleasas, y posteriormente se inactivaron las trazas remanentes de DEPC en el autoclave. Alternativamente, cuando se requiriera tejido fresco para algún experimento, las ratas se decapitarían inmediatamente después de administrar el anestésico y el cerebro se extraería rápida y cuidadosamente

3.3.2 Tinción con azul de metileno para cuantificación de la densidad celular

Muestras de tejido cerebral de rata obtenidas en el PND 21 se tiñeron con azul de metileno (n=3) de la siguiente manera: los cerebros enteros se removieron y sumergieron en una solución de sacarosa 10% en PB 0.1M por 10 min y después en una al 20% por más de 4 hrs. Posteriormente se seccionaron coronalmente (con un grosor de 12 μm). Una de cada seis rebanadas que contuvieran al hipotálamo se montaron en laminillas previamente tratadas con gelatina y se tiñeron con azul de metileno para su evaluación histológica. Se contó la cantidad

de núcleos teñidos en los siguientes núcleos: arcuato (Arc), paraventricular hipotalámico, división medial parvocelular (PVNmpd), área hipotalámica anterior (AHA), núcleo medial preóptico, región compacta (MPOc), núcleo medial preóptico, región medial (MPOm) y núcleo supraquiasmático división dorsolateral (SChDL). Se seleccionaron estos núcleos hipotalámicos, debido a su asociación en los procesos de acoplamiento al estrés (**Simerly, 2004**).

Estas rebanadas se examinaron bajo microscopía de luz. La densidad celular se evaluó bajo el objetivo 100X en los núcleos hipotalámicos seleccionados para este estudio de acuerdo con The Rat Brain Atlas (**Paxinos & Watson, 2007**), con la ayuda de una cámara lúcida ajustada a 10X. Cuadrados correspondientes a $0.009mm^2$ se imprimieron en papel blanco ajustado al aumento mencionado, al inicio de cada conteo el experimentador empalmó el recuadro proyectado en el tubo de dibujo con la región anatómica correspondiente, se calcò cada neurona teñida para posteriormente contarlas. Se evaluaron entre 3 y 5 cuadros por cada región estudiada. Los dibujos se etiquetaron para proceder a hacer un conteo ciego. Los datos de cada región hipotalámica se promediaron para su posterior análisis estadístico.

3.4 Ensayos inmunohistoquímicos (IHC)

3.4.1 Detección fluorescente de AVP y del proto-oncogén c-Fos

Para determinar si la MS podría ocasionar activación neuronal en las regiones hipotalámicas que contienen neuronas vasopresinérgcas magnocelulares, se sometieron ratas de PND 10 a un sólo procedimiento de separación (MS3h) y se perfundieron 90 min después, junto con sus controles (AFR, n=10), como se describe anteriormente, en la sección de *Obtención de tejido* y se cortaron los cerebros obtenidos con ayuda de un vibratomo a 70 µm de grosor.

Se realizó una inmunofluorescencia contra AVP y c-Fos, un marcador de actividad celular, con anticuerpos primarios de cobayo contra AVP (1:2000) y de conejo contra c-Fos (1:1000), se incubaron toda la noche a 4°C con agitación leve constante. Después se lavaron las rebanadas y posteriormente se incubaron con los anticuerpos secundarios correspondientes: inmunoglobulina G (IgG) de burro contra cobayo conjugado con Cy3 y Alexa Fluor 488 IgG burro anti-conejo (1:1000), en solución amortiguadora de Trizma (pH 7.4 a 25°C, más 0.9% NaCl y Triton X-100 0.3%: TBST) más 1% de suero normal de caballo (NHS), a 4°C por toda la noche. Para finalizar la reacción de inmunofluorescencia, las rebanadas se enjuagaron y se montaron en laminillas, con Vectashield para su posterior análisis en microscopio de epifluorescencia.

Se eligieron campos aleatoriamente dentro de los núcleos hipotalámicos paraventricular (PVN) y supraóptico (SON) con el objetivo 40X y se fotografiaron áreas de $0.22 \ mm^2$, con la ayuda de una cámara digital, para su posterior análisis. Se contó el número total de neuronas vasopresinérgicas (AVP+) marcadas y doble-marcadas (Fos+/AVP+) dentro del PVN y SON.

Los resultados se expresaron como el porcentaje de neuronas doble-marcadas del total de neuronas AVP+.

3.4.2 Marcaje hipotalámico para medición y reconstrucción de núcleos vaopresinérgicos

Se anestesiaron ratas macho de PND 75, tanto separadas (MS3h) como control (AFR); n=4, usando pentobarbital sódico y se perfundieron como se detalla anteriormente, en la sección de *Obtención de tejido*. Los cerebros se removieron rápidamente y se seccionaron con la ayuda de un molde acrílico para cerebro de rata adulta y se enjuagaron con PB 0.1 M. Se obtuvieron rebanadas de 70 µm de grosor inmediatamente, de la sección que contenía al hipotálamo. Después de esto se incubó una de cada dos rebanadas con TBST más 20% de suero normal de cerdo (NSS) para bloquear sitios de unión inespecífica, durante 1 hr a temperatura ambiente, después se incubó con anticuerpo de conejo contra AVP en TBST más 1% de NSS a 4°C por 48 hrs. Las rebanadas se enjuagaron y procedieron a ser incubadas en anticuerpo su secundario, IgG de cerdo contra conejo conjugado con peroxidasa de rábano (HRP), en TBST más 1% de NSS, durante toda la noche a 4°C. Se reveló la reacción utilizando diaminobencidina (DAB, 0.5%) y peróxido de hidrógeno (H_2O_2, 0.01%) como substratos. Después se montaron las rebanadas en laminillas tratadas previamente con gelatina y se dejaron para secar durante un día y se procedió a deshidratarlas en alcohol absoluto (etanol 100%) durante 5 min, se enjuagaron en xileno y se montaron permanentemente con medio de montaje Permount.

Las rebanadas secuenciales inmuno-reaccionadas contra AVP se visualizaron, analizaron y fotografiaron utilizando microscopía de campo claro. Las neuronas AVP+ se agruparon, de acuerdo a Paxinos y Watson (**Paxinos & Watson, 2007**), dentro del PVN y SON.

El cúmulo de neuronas AVP+ dentro de cada grupo se delimitó utilizando Adobe Photoshop y el área ocupada se calculó en milímetros cuadrados (mm^2) con el software Fovea Pro 4.0 para Photoshop. Los volúmenes para cada núcleo/región se determinaron integrando todas las áreas medidas para cada grupo de células, multiplicando esto por 0.7 mm (por el grosor de cada rebanada), por 2 (ya que sólo se inmuno-reaccionaron y midieron una de cada dos rebanadas), por la constante de encogimiento (K). El encogimiento lineal tras los procedimientos histoquímicos se determinó midiendo el diámetro de cerebros frescos a la altura del quiasma óptico inmediatamente después de la perfusión (Lf) y midiendo el diámetro en las mismas coordenadas de las rebanadas montadas permanentemente (Ld). Y de aquí se obtuvo K=Lf/Ld.

Para visualizar en qué dirección se aumentó el tamaño del PVN se hizo una reconstrucción digital representativa tridimensional del PVN, basándonos en coordenadas anatómicas obtenidas de fotografías digitales de la siguiente manera. Se seleccionó un par de secuencias de rebanadas inmuno-reaccionadas contra AVP para la reconstrucción del PVN, las

neuronas AVP+ dentro del PVN se marcaron utilizando ImageJ, dentro de la fotomicrografías. Las neuronas magnocelulares y parvocelulares se caracterizaron de acuerdo a su eje largo, se consideró neurona magnocelular aquellas con un eje mayor a 20 µm (**Armstrong, 2004**). Para cada neurona marcada se obtuvieron coordenadas (x, y) para su localización bidimensional (de ImageJ) y la coordenada (z) se determinó por el lugar dentro de la secuencia que ocupara la rebanada. Se dibujó un esquema tridimensional utilizando un programa escrito en python.

3.4.3 Marcaje contra NeuN y GFAP para la evaluación de la densidad celular

Se obtuvieron cerebros completos al PND 36, como se detalla en *Obtención de tejido* anteriormente (n=3), y se enjuagaron con PB 0.1 M. Después se obtuvieron rebanadas coronalmente de 50 µm de grosor, donde estuviera el hipotálamo (Bregma 0.24mm a 2.64 mm, **Paxinos & Watson, 2007**) con la ayuda de un vibratomo. Una de cada seis rebanadas se transfirió a TBST y se bloqueó para minimizar marcaje inespecífico incubando las rebanadas en suero normal de burro (NDS, 10% en TBST) por 1 hr a temperatura ambiente, con agitación leve.

Dos series enteras se incubaron entonces cada una con alguno de los dos anticuerpos primarios, monoclonales de ratón, ya sea contra Núcleos Neuronales (NeuN) o bien contra proteína acídica glial fibrilar (GFAP) ambos a 1:1000, en TBST más NDS 1% a 4°C, toda la noche. Después de enjuagar, se incubaron con anticuerpo biotinilado de burro contra ratón (1:500) en TBST más NDS 1% toda la noche. Tras enjuagar varias veces con TBST, las rebanadas se incubaron entonces con complejo avidina-biotina-peroxidasa (ABC), durante 1 hr a temperatura ambiente. Se detectó la peroxidasa utilizando DAB (0.05%) y H_2O_2 (0.01% v/v) como sustrato. Las rebanadas posteriormente se montaron en laminillas previamente tratadas con gelatina y se dejaron a secar a temperatura ambiente durante un día, después de esto se deshidrataron sumergiendo en alcohol absoluto por 5 min, enjuagando en xileno y montando permanentemente con Permount.

Las células inmuno-positivas para NeuN se contaron en las siguientes regiones hipotalámicas: Arc, PVNmpd, AHA, MPO, SCN y en el núcleo preóptico periventricular (PePO). Todas estas regiones relevantes en el acoplamiento al estrés (**Simerly, 2004**). Debido a que GFAP mostró un patrón de expresión muy heterogéneo, la densidad de las células marcadas con este marcador astrocítico no pudo ser cuantificada.

3.4.4 Ensayos IHC para el estudio de la conectividad hipotalámica hacia *locus coeruleus* (LC)

Ratas macho fueron profundamente anestesiadas y perfundidas, como se describe anteriormente en este trabajo. Los cerebros se removieron inmediatamente, seccionados y

enjuagados con PB 0.1 M hasta que la solución se viera clara, sin fijador. Los cerebros se rebanaron, utilizando un vibratomo, a un grosor de 70 μm.

Para las IHC que se observarían por microscopía de luz, el marcaje inespecífico se bloqueó en las rebanadas que contuvieran *locus coeruleus* (LC) con NDS 20%, en TBST, por 1 hr a temperatura ambiente. Las secciones se incubaron con los siguientes anticuerpos primarios: generado en conejo contra AVP, de ratón contra tirosina hidroxilasa (TH, 1:3000) y de cobayo contra vGLUT2 (1:3000) toda la noche. Al siguiente día las rebanadas se enjuagaron con TBST por 30 min y se incubaron con una combinación de anticuerpos secundarios adecuados: Alexa Fluor 488, Alexa Fluor 594 y Cy5, por 2 hrs. Las rebanadas se enjuagaron en TBST y montaron en laminillas, dejadas a secar brevemente y se cubrieron con cubreobjetos y medio de montaje Vectashield.

Para el análisis de AVP en LC de animales 3hMS y AFR, el área ocupada por la señal se calculó en 10 campos visuales de la siguiente manera: Se obtuvieron todas las imágenes bajo condiciones idénticas, usando ImageJ, se convirtieron todas las imágenes a escala de grises. Se determinaron umbrales manualmente hasta obtener que el área tomada en cuenta cubriera la mayoría del área ocupada por fibras marcadas y con filtraje máximo para el marcaje de fondo. Las imágenes se convirtieron a formato binario y las áreas dentro del umbral fueron medidas.

Para el marcaje con doble peroxidasa-cromógeno y posterior microscopía electrónica de transmisión, las rebanadas que contuvieran el LC fueron crio-protegidas con sacarosa 10% y luego 20% en PB 0.1 M (en agitación leve constante, hasta que las rebanadas se sumergieran). Entonces se incrementó la permeabilidad de las membranas del tejido congelando y descongelando las rebanadas rápidamente, co nitrógeno líquido. Las rebanadas se enjuagaron con PB 0.1 M y se bloqueó el marcaje inespecífico con NDS 20% en *buffer* de Trizma con 0.9% de NaCl (TBS), por 1 hr a temperatura ambiente.

Después las rebanadas fueron incubadas con anticuerpo de conejo contra AVP y de borrego contra TH en TBS más NDS 1% por 48 hrs a 4°C con agitación leve. Tras enjuagar en TBS se procedió a incubar con el primero de los anticuerpos secundarios, IgG de cerdo contra conejo conjugada con HRP (1:100) en TBS con NDS 1%, toda la noche a 4°C. Las rebanadas se enjuagaron y la primera reacción se finalizó usando DAB como cromógeno y H_2O_2, 0.01% como substrato. El producto de la reacción se intensificó con níquel en algunas rebanadas. Posteriormente las rebanadas se incubaron con el segundo anticuerpo secundario, generado en cabra contra borrego y biotinilado, y después se incubó con un kit ABC estándar de Vectastain. La inmuno-reacción para TH se visualizó utilizando un kit de peroxidasa de Vector-VIP (morado muy intenso o *very intense purple*). Este procedimiento deja un producto de la reacción que al microscopio de luz se ve de color morado y en microscopía electrónica tiene una apariencia granular. Las rebanadas fueron post-fijadas con tetróxido de osmio en 0.1 M PB por 1 hr, y deshidratadas utilizando una serie de alcoholes graduados (incluyendo 45 min en acetato de uranilo 1% en etanol 70%), después se transfirieron a óxido de propileno, seguido

de una resina epóxica (Durcupan ACM). Las rebanadas después se incrustaron planas en laminillas de cristal y la resina se polimerizó a 60ºC por 2 días. Tras remover el cubreobjetos, las regiones con LC, identificadas por inmuno-reactividad positiva para TH, se rebanaron y re-incrustaron en cápsulas de Durcupan. Rebanadas ultra-delgadas (de 70 nm) secuenciales se obtuvieron con un ultramicrotomo, y se recolectaron en redes sencillas cubiertas de Butiral y se examinaron en un microscopio electrónico de transmisión Philips CM100. Micrografías digitales electrónicas se obtuvieron con una cámara digital 3.4.

3.4.5 Evaluación de c-Fos en el LC, hipocampo y corteza prefrontal

Para evaluar la actividad neuronal en LC, hipocampo y corteza prefrontal, el producto del proto-oncogén c-Fos se estudió; ya que éste se observa mejor en una ventana de entre 60 y 120 min tras la activación de una neurona (**Kovacs, 1998**), nosotros perfundimos a las ratas 90 min después de la prueba vespertina (AT, del laberinto acuático de Morris). Para la IHC, una de cada tres rebanadas que contuvieran los núcleos cerebrales de nuestro interés fueron bloqueadas con NDS 10% en TBST por 1 hr a temperatura ambiente, después se incubaron con anticuerpo primario de conejo contra c-Fos, en TBST más NDS 1%, a 4ºC con agitación leve. Después se enjuagaron las rebanadas 3 veces, 10 min cada vez, con TBST y se incubaron con anticuerpo secundario biotinilado de cabra contra conejo. Finalmente, las rebanadas se incubaron con ABC por 1 hr a temperatura ambiente. Se detectó la presencia de peroxidasa utilizando DAB (0.05%). Las rebanadas se enjuagaron y se montaron permanentemente con Permount. Se contó la cantidad de núcleos Fos+ en cada $0.0346mm^2$ (el área del campo de visión con el objetivo 100X), utilizando un microscopio Nikon Eclipse 50i.

3.5 Hibridización *in situ* (ISH)

Los efectos de la MS en el RNA mensajero (mRNA) de AVP en el hipotálamo fueron evaluados en condiciones basales al PND 21 (n=6) y PND 63 (n=8), de ratas provenientes de cuatro camadas distintas (cuatro AFR y cuatro 3hMS). La obtención de tejido se hizo como está descrito anteriormente, con la distinción que los cerebros fueron post-fijados en paraformaldehído 1% (en PB 0.1 M) tras la perfusión y mantenidos a 4ºC hasta su procesamiento. Dos días antes de cortar los cerebros, éstos se transfirieron a una solución de sacarosa 18% en PB libre de ribonucleasas, con azida de sodio (NaN_3). La solución se volvió a cambiar un día antes del corte y de nuevo se transfirieron a solución de sacarosa fresca 1 hr antes del corte.

Utilizando un criostato Leica, se hicieron criosecciones coronales secuenciales (de 12 µm de grosor) del hipotálamo completo (desde la comisura anterior hasta la coordenada donde el hipocampo ventral aparece en la dimensión rostrocaudal). Las rebanadas se recolectaron en el inserto de vidrio Leica y posteriormente se transfirieron a placas de cultivo celular de 24 pozos en PB 0.1 M. Se procesaron una de cada seis rebanadas para ISH, como está descrito

en la literatura (**Morales & Bloom, 1997**), utilizando sondas con ribonucleótido marcado [35]S- y ^{33}P-UTP. El plásmido pT7T3D-PacI, conteniendo DNA complementario (cDNA) para AVP de rata (602 pares de bases), se linearizó con EcoRI y después transcrita *in vitro* con RNA polimerasa T3 para obtener la sonda antisentido complementaria de RNA. El diseño se verificó por secuenciación. La radioactividad se ajustó a 107 cpm por ml de *buffer* de hibridización. Las rebanadas se montaron en laminillas y secadas al aire libre. Las laminillas se expusieron primero a un *film* autoradiográfico, el cual se analizó en un Phosphorimager, las laminillas se sumergieron posteriormente en una emulsión de plata y se expusieron por 4 semanas antes de revelarlas. Las laminillas también se contratiñeron con azul de metileno.

La abundancia relativa del mRNA de AVP se midió de dos maneras. (A) La expresión de mRNA para AVP en hipotálamo entero: una de cada seis rebanadas secuenciales de cada rata, fue evaluada por cuantificación densitométrica en imágenes digitales de los autoradiogramas obtenidos con la ayuda de un Phosphorimager. (B) La abundancia relativa de mRNA de AVP en PVN, SON y SCN: 3-4 rebanadas, pareadas por coordenada antero-posterior, que contuvieran cada una de estos núcleos, en las laminillas contrateñidas se fotografiaron y las áreas con precipitación de plata se midieron digitalmente. En ambos casos se utilizó el software Fovea Pro 4.0 para Adobe Photoshop. Los datos se expresan como porcentaje de los controles.

3.5.1 RNAscope, una nueva técnica de ISH

Las ratas para RNAscope fueron profundamente anestesiadas y decapitadas utilizando una guillotina para animales pequeños. Los cerebros se removieron y congelados rápidamente utilizando polvo de hielo seco. El tejido fresco congelado se rebanó usando un criostato (a un grosor de 12 µm) y se montaron las rebanadas en laminillas cargadas positivamente. Las sondas de RNA para ISH utilizadas en este estudio fueron diseñados y provistos por Advanced Cell Diagnostics para reconocer los genes de TH, receptores V1a (Avpr1) y V1b (Avpr3). Se siguieron todos los pasos para esta técnica de acuerdo al protocolo RNAscope® 2.5 HD Duplex Assay para rebanadas congeladas de tejido fresco.

3.6 Pruebas conductuales

3.6.1 Laberinto elevado en cruz (EPM)

El EPM se basa en el conflicto entre la naturaleza de los roedores de explorar entornos nuevos contra el miedo de estar en pasillos abiertos y elevados (**Pellow & File, 1986**). Lo utilizamos en PND 65 para evaluar el estado de estrés agudo no condicionado. El laberinto, hecho de madera, consiste de una plataforma en forma de cruz elevada 50 cm del piso con dos brazos cerrados (50 cm x 10 cm x 40 cm) y dos brazos abiertos (50 cm x 10 cm), con una orilla sobresaliente de 0.5 cm, conectados por un cuadro central de 10 cm x 10 cm. La orilla sobresaliente está ahí para prevenir que la rata se cayera accidentalmente, sin comprometer

las características elementales de la prueba. El laberinto se iluminó con una luz roja tenue y se observó utilizando un circuito cerrado de televisión (CCTV). El laberinto se limpió con agua y un detergente neutro y se secó antes de cada prueba.

Antes del EPM 10 ratas macho de cada grupo (10 MS y 10 AFR), fueron escogidas aleatoriamente, una de cada camada, se expusieron a una caja de campo abierto durante 5 min, los 3 días antes de la prueba, Esta medida se tomó para aumentar la probabilidad de entrar a los brazos abiertos, incrementando la sensibilidad de la prueba (**Zhang *et al*, 2010**). Ratas de ambos grupos se sometieron a la prueba durante su periodo de actividad temprano. La prueba comienza poniendo al sujeto en el centro del laberinto viendo hacia un brazo abierto y se deja para explorar durante 5 min. El tiempo pasado en brazos abiertos, expresado como el porcentaje del tiempo total (300s), fue analizado como parámetro de un estado de estrés no condicionado (exploración contra evitación).

3.6.2 Prueba del conflicto de Vogel (VCT)

La prueba de conflicto de Vogel (VCT) involucra dos etapas: i) la privación de agua (WD) durante 48 hrs y privación de alimento durante las últimas 24; y ii) el conflicto en sí. Las ratas pueden tolerar WD de hasta 72 hrs, con una pérdida de peso dentro de un rango aceptable (aproximadamente 11%) y sin pérdida aparente del vigor físico. Al terminar las 48 hrs de WD, las ratas sedientas fueron expuestas a un choque eléctrico leve e intermitente mediante una botella de agua. Este procedimiento incorpora un elemento de conflicto, donde el sujeto experimenta tendencias opuestas concomitantemente: el deseo de beber para saciar la sed contra el miedo a un estímulo aversivo. Cuando el miedo supera el deseo de saciar la sed, siendo que no existe un verdadero peligro, esto es un indicador de un estado de alta ansiedad condicionada. Por lo tanto el VCT se usó para evaluar el estado de ansiedad condicionada, como se ha descrito en el pasado (**Zhang *et al*, 2010**).

A diferencia del EPM, donde los parámetros fisiológicos basales no están alterados, en el VCT el sistema vaopresinérgico está regulado a la alta, por la WD. De ahí que el VCT resultó un paradigma interesante para evaluar el impacto de un sistema vasopresinérgico posiblemente alterado dentro la ansiedad. Un día después del EPM, los mismos sujetos experimentales fueron habituados, manteniéndolos en la cámara del conflicto descrita a continuación, sin aplicar corriente, durante 4 días consecutivos por 30 min (a partir del PND 70). La cámara para el conflicto consiste en una caja de Plexiglas (20 cm x 30 cm x 20 cm) con un piso metálico, una tapa de reja metálica, una botella con un bebedero de acero inoxidable, un generador de corriente eléctrica constante con un indicador para contar el número de choques y una cámara de video. Durante la prueba se utilizó una solución de dextrosa 10% disuelta en agua (solución hipertónica). Los electrodos para administrar el choque eléctrico se posicionaron entre el bebedero y el piso (metálicos). El bebedero se aisló para evitar que tocara la tapa. Distintas intensidades de corriente (0.1–0.3 mA en intervalos de 0.02 mA) se probaron previamente para determinar la óptima para la prueba (datos no publicados). Estas pruebas se

hicieron con ratas distintas. Se encontró que 0.22 mA es la corriente óptima, donde los animales podían beber la solución con una molestia mínima. Al finalizar las 48 hrs de WD la prueba se comenzó en un cuarto distinto con una cámara sensible a baja iluminación para monitorear y ganar la prueba. La prueba se realizó durante la etapa de oscuridad de las ratas y el cuarto donde se hizo se iluminó tan solo con una luz roja tenue. Al comenzar la prueba cada animal se puso en la cámara y se le permitió tomar durante 25 s sin corriente eléctrica. Después de esto, se aplicó una corriente de 0.22 mA con un ciclo de trabajo del 50%, de 5s alternadamente entre el piso y el bebedero. Se registró el número de choques eléctrico recibidos (n=10).

3.6.3 Laberinto acuático de Morris (MWM)

El laberinto acuático de Morris (MWM) evalúa el aprendizaje espacial y la retención de memoria. El montaje experimental que usamos consistió de una alberca circular (diámetro: 156 cm, altura: 80 cm) llena de agua hasta una altura de 30 CM, con una temperatura controlada (de 25°C ± 1°C) con referencias visuales puestas en las paredes de la alberca. Se determinaron cuatro cuadrantes virtuales como I, II, III y IV. Se colocó una plataforma (de 12 cm) sumergida 1 cm bajo la superficie del agua, que serviría como plataforma de salida. Las pruebas fueron grabadas usando una luz roja tenue. Este montaje experimental ha demostrado ser útil para evaluar aprendizaje espacial y retención de memoria en el pasado (**Zhang *et al*, 2008**).

En particular, para los experimentos de conectividad de LC, los animales estuvieron en un ciclo luz/oscuridad de 12:12 hrs, las luces se encendían a las 7:00 am, hora que se determinó como tiempo 0 del *zeitgeber*, o tiempo circadiano 0 (CT0). Las ratas se dividieron en 2 grupos: control con agua y alimento *ad libitum* y el grupo con WD de 24 hrs (WD24h). La prueba se realizó durante el periodo de inactividad de las ratas, para evitar la alta expresión espontánea de c-Fos en el LC que se ve en el periodo temprano de actividad. Se hicieron dos evaluaciones: la prueba "matutina" (MT: realizada entre CT3 y CT5) y la "vespertina" (AT: entre CT8 y CT10). Antes de la MT se hizo una habituación pre-prueba, que consistió en poner a los sujetos en la alberca por 2 min para permitir que se habituaran al agua. Las ratas son nadadores natas, así que esta medida reduce el estrés derivado posiblemente de la inmersión al agua en cada ensayo de la prueba, además de familiarizarse al entorno.

La MT del MWM comenzó con la plataforma de salida colocada en el cuadrante II. Cada sujeto se colocó cuidadosamente dentro de la alberca en el cuadrante I. El tiempo transcurrido entre este evento y la llegada del sujeto a la plataforma se registró. En el primer ensayo se les permitió a los sujetos explorar la alberca durante 60 s, después el experimentador las guió a la plataforma, permitiendo que treparan la plataforma solas y que observaran la ubicación de la plataforma con respecto a su entorno, por 5 s. Se hicieron 6 ensayos por sujeto, con intervalos de 5 min entre cada uno. Las ratas se devolvieron al cuarto de descanso con agua y alimento *ad libitum* por 3 hrs. Después comenzó la AT a las CT8 repitiendo el mismo procedimiento,

modificando solamente la ubicación de la plataforma de salida al cuadrante I y el cuadrante donde se depositó a los sujetos al III.

3.7 Medición de AVP plasmática durante privación de agua

Cien ratas macho en PND 75 tomadas de 20 camadas distintas (10 AFR y 10 3hMS) contribuyeron al muestreo de sangre. Para poder caracterizar la concentración plasmática de AVP durante la WD, se obtuvieron muestras sanguíneas de la punta de la cola de las ratas en cinco ocasiones a lo largo del periodo de privación: antes de comenzarlo (Basal), después de las primeras 6 hrs de privación de agua (6h WD), tras 12 hrs (12h WD), tras 24 hrs (24h WD) y después de 48 hrs (48h WD). Cada camada proveyó solamente una muestra en cada punto temporal. Durante el muestreo los animales fueron inmovilizados en un tubo de contención. Para minimizar el efecto estresante ejercido por este proceso, las ratas se introdujeron al mismo tubo (estándar para ratas) durante 30 min los 3 días previos a la prueba. Al momento adecuado 500 µl de sangre se obtuvieron de cada rata correspondiente intacta y se recolectó la muestra dentro de un microtubo refrigerado con 0.5 mg de EDTA en las paredes del tubo (50 µl de solución de EDTA 1% se agregó previamente a cada tubo, el cual se agitó y refrigeró hasta que se secara la solución. Las muestras se centrifugaron inmediatamente a 1600 g por 15 min a 4°C. El sobrenadante plasmático (200 µl por tubo) fue transferido a un tubo nuevo y conservado a -70°C hasta que se llevó a cabo la ELISA. Se utilizó el kit Arg8-vasopressin EIA. Se siguieron las recomendaciones del fabricante del kit de ELISA para cuantificar AVP. Cada muestra se analizó por duplicado.

3.8 Inmunoensayo tipo Western (WB)

En los PNDs 1, 3, 6, 9, 12, 15, 21 y 43, ratas macho (n=6 para cada edad; no se utilizaron hermanos dentro del mismo PND en ningún caso) fueron decapitadas rápidamente. El tejido fresco se removió y fue diseccionado rápidamente en solución salina (0.9%) helada. Los cerebros se seccionaron a partir del quiasma óptico hasta 1-3 mm posteriores, dependiendo del PND (Bregma 0 a 3mm en PND 43, basados en **The Rat Brain Atlas; Paxinos & Watson, 2007**) y cubos de aproximadamente 1–27 mm^3 (dependiendo del PND) de diencéfalo ventral fueron obtenidos bajo un microscopio estereoscópico con herramientas de microdisección. Cada muestra obtenida de cada hipotálamo (tejido evaluado por cada individuo) se homogenizó en *buffer* de lisis helado compuesto de 130 mM NaCl, 20 mM Tris–HCl (pH 7.4), 1% Triton X-100, una mezcla de inhibidores de proteasas y de fosfatasas (0.01 M NaH_2PO_4, 0.05 M NaF, 0.002 M Na_3VO_4). Los lisados fueron centrifugados a 18,210 g (a 4° C) por 15 min y los sobrenadantes se recolectaron para determinar su concentración de proteína posteriormente utilizando un kit para el método de Bradford. La misma cantidad de proteína (30 mg) de cada muestra fue utilizada en cada ensayo. Las proteínas se separaron por SDS-PAGE 10% o 15% y se transfirieron a una membrana de nitrocelulosa.

Las membranas se bloquearon por 1 hr a temperatura ambiente en el *buffer* de bloqueo *Starting block T20*, después se incubaron en los anticuerpos primarios correspondientes (especificados más adelante) a 4ºC toda la noche. Los anticuerpos se probaron previamente en lisados de cerebro para determinar las concentraciones de trabajo. Tras enjuagar seis veces con *buffer* de Trizma con Tween 0.1% (TBT), las membranas fueron incubadas con IgG de ratón o bien de conejo acopladas a HRP (1:40,000) por 1 hr a temperatura ambiente. Las membranas se volvieron a enjuagar seis veces con TBT y después se sometieron a detección de señal, utilizando kits para detección Supersignal ECL o SuperSignal West Dura Western en *hiperfilm* ECL. Un anticuerpo de β-actina acoplado a HRP fue utilizado para control de carga. Los niveles de expresión de las proteínas (intensidad de inmunoreactividad) fueron interpretados por análisis densitométrico de las bandas en el *hiperfilm*, utilizando ImageJ.

3.8.1   Especificaciones de los anticuerpos

Los siguientes anticuerpos de conejo se obtuvieron de Cell Signaling Technology: caspasa 3 escindida (activa; Asp175, 1:1000) reconoce el fragmento grande de la caspasa 3 activa como una doble banda de 17/19 kDa en WB y no hay reactividad cruzada con la forma completa de caspasa 3 (inactiva) ni con ninguna otra caspasa. El anticuerpo para fosfo-ERK (pERK, 1:1000) reconoce bandas en 42/44 kDa sólo cuando se presenta la doble fosforilación de ERK1 (pThr202/pThr204) y la fosforilación simple en Thr202 de ERK2. El anticuerpo para fosfo-Akt detecta Akt sólo en cuando éste está fosforilado (pThr308, 1:1000) como una banda de 60 kDa y no ocasiona reactividad cruzada con residuos fosforilados de JNK/SAPK o p38 MAP cinasa. El anticuerpo para Bcl-2 (1:1000) reconoce una sola banda de 25 kDa y no muestra reactividad cruzada con ningún otro miembro de la familia de Bcl-2. El anticuerpo para fosfo-Bad detecta exclusivamente a Bad fosforilado en la Ser113 (1:1000) como una sola banda de 23 kDa y no detecta a otros miembros de la misma familia. Los anticuerpos para ERK1/2 y Bad (ambos usados a una concentración de 1:1000) detectan a ERK1/2 y Bad respectivamente. El anticuerpo de ratón monoclonal contra Bax (B9, 1:1000) detecta a Bax como una sola banda de 21 kDa.

3.9 Marcaje retrógrado con Fluoro-gold (FG)

La inyección de FG se hizo de acuerdo a protocolos previamente descritos (**Morales & Wang 2002, Zhang & Hernández 2013**). Un total de 20 ratas Wistar macho de 300g se utilizaron para este experimento. Las ratas se anestesiaron con xilacina (20 mg/ml) y ketamina (100 mg/ml) en una proporción 1:1, a una dosis de 1 ml/kg de peso corporal administrada i.p. Ratas anestesiadas profundamente se posicionaron en un aparato estereotáxico y el trazador retrógrado Fluoro-Gold se disolvió en *buffer* de cacodilato 0.1M (pH 7.5) y se administró iontoforéticamente a través de una micropipeta de cristal (con un diámetro interno de aproximadamente 20µm, con pulsos de corriente de 0.1 µA, a 0.2 Hz, con un ciclo de trabajo del 50%), en las siguientes coordenadas: Bregma -9.48mm, lateral 1.20 mm and dorso-ventral

7.30 mm. La micropipeta se dejó en el sitio durante 10 min para evitar el reflujo del trazador de vuelta hacia la trayectoria de la micropipeta. Tras recuperarse de la anestesia, se les administró ketorolaco 0.4 mg/kg i.p. y ceftriaxona 50 mg/kg i.p. como agentes analgésico/antiinflamatorio y antibiótico, respectivamente. Una semana tras la inyección de FG las ratas fueron perfundidas y los cerebros se rebanaron coronalmente. Los sitios de inyección fueron evaluados y los criterios de inclusión fueron los siguientes: 1) que el centro de la inyección se encontrara dentro de un radio de 300µm alrededor del LC y 2) que no hubiera filtración visible de FG hacia el líquido cefalorraquídeo (CSF), evidenciado por una señal difusa y bilateral. Los casos que cumplieran con estos criterios se procesaron para ICH contra TH en las rebanadas a la altura del tallo cerebral y contra AVP en las rebanadas de hipotálamo anterior.

3.10 Análisis estadístico

Los resultados se expresaron como el promedio ± el error estándar. Las diferencias estadísticas se evaluaron utilizando pruebas t de Student y análisis de varianza (ANOVA) de una, dos y tres colas; dependiendo en el experimento y posterior evaluación con pruebas de Bonferrioni. Para la mayoría de los experimentos se utilizó Prisma (GraphPad), para la ANOVA de tres colas utilizada para evaluar los resultados del MWM se utilizó Stata 11. Las diferencias se consideraron estadísticamente significativas con $*p<0.05$; $**p<0.01$ and $***p<0.01$.

Para WB, antes de hacer el análisis estadístico, se evaluaron todas las variables dependientes para determinar datos atípicos univariados y normalidad (**Verma *et al*, 2013**). Todas las variables se encontraron dentro de un rango aceptable, y por lo tanto se realizaron ANOVAs de dos colas para evaluar los efectos principales (tratamiento y edad) con comparación múltiple de Bonferrioni.

RESULTADOS

4.1 Efectos de la separación materna en el sistema vasopresinérgico hipotalámico

4.1.1 Expresión de Fos y AVP en los núcleos paraventricular y supraóptico hipotalámicos tras un evento de MS

Un solo evento de separación materna (de 3 hrs: MS3h) fue capaz de aumentar la expresión del protooncogén de expresión rápida c-Fos (un marcador de activación neuronal), tanto en el PVN ($F_{(3, 36)}=179.6$, $p<0.0001$), como en el SON ($F_{(3, 36)}=154.3$, $p<0.0001$); realizado el PND 10, 90 min después de la separación materna (MS).

Como era de esperarse, hubieron algunos núcleos inmunorreactivos contra c-Fos (Fos+) en la población AVP+ del PVN y SON en condiciones basales. Sin embargo, después de la MS3h, la mayoría de estas neuronas resultó Fos+ (Fig. 1A' y B'). Sin embargo no se observaron diferencias significativas entre AFR y MS3h, utilizando una ANOVA de una cola.
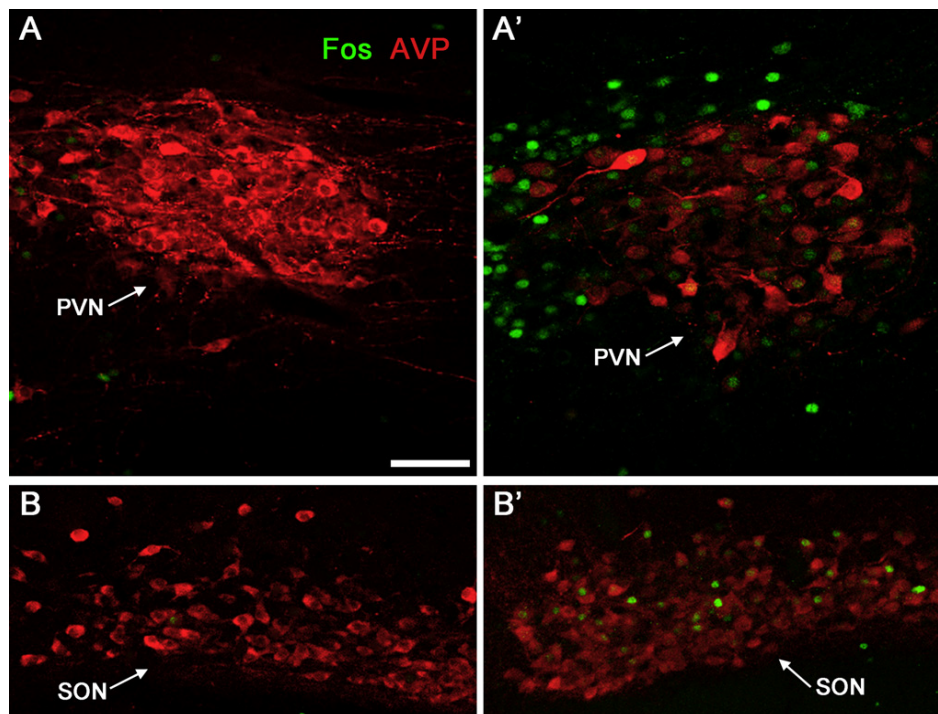
Figura 1. Un sólo evento de separación materna (MS) es capaz de provocar activación neuronal en los núcleos hipotalámicos, evidenciado por la expresión de c-Fos
Se observa el protooncogén c-Fos, un marcador de activación neuronal, en las fotomicrografías de fluorescencia (en verde). Las ratas usadas para este experimento no fueron perturbadas (AFR, A y B) o bien fueron sujetas a un sólo evento de MS (MS3h, Fig. 1 A' y B') al PND 10. El procedimiento de MS provocó que una población neuronal en el PVN y SON, parte esta población era vasopresinérgica (AVP+ en rojo). (Barra de escala: 100 µm)

4.1.2 Efectos de la MS en la expresión de mRNA de AVP en regiones hipotalámicas, a dos edades distintas

Figura 2. La MS aumentó la cantidad de mRNA para AVP presente en el PVN y SON de ratas en PND 21

Los paneles azules muestran las autorradiografías expuestas toda la noche de una ISH hecha al PND 21 para detectar mRNA de AVP en el hipotálamo de animales AFR y 3hMS (A y A' respectivamente). Se observa que en el grupo MS hubo un aumento en el número de secciones conteniendo mRNA de AVP, lo cual nos indica un tamaño rostro-caudal incrementado. Las fotomicrografías del medio, tomadas tras sumergir las mismas laminillas en una emulsión de plata para detectar radioactividad (Ilford K.5) durante 4 semanas en la oscuridad a 4°C, muestran un aumento en la expresión de mRNA para AVP en el PVN y SON de animales 3hMS (b') comparados con el control (B), mientras que no se observaron diferencias significativas en el núcleo supraquiasmático (SCN, C y C'). La densidad óptica de la autorradiografía para la serie entera de rebanadas coronales fue medida y convertida en un histograma (D). Barras de escala: A y A': 10 mm; B,B',C y C': 200 µm

Los animales 3hMS mostraron un incremento pronunciado en la abundancia relativa de mRNA de AVP en el hipotálamo entero, al utilizar ribosondas antisentido, comparado con AFR al PND 21 (Fig. 2 A and A'). La cuantificación densitométrica de las imágenes obtenidas de la autorradiografía de la ISH reveló un aumento del 147±7.6% en los animales 3hMS, comparado con los controles (100±1.1%), (t=12.75, df=4, p=0.0002) (Fig. 2 D). La abundancia relativa del mRNA de AVP en PVN y SON de los animales MS aumentó significativamente: 139.8± 13.5% (t=3.63, df=22, p=0.0013) y 122.6±9.6% (t=2.356, df=22, p=0.0274), comparado a los controles (100±3.5% y 100±4.7%) respectivamente (Fig. 2 B, B' y D). SCN mostró un 109±10% (3hMS) contra 100±8.4% (AFR) (Fig. 2 C, C' y D). El análisis estadístico con la t de Student no encontró diferencias significativas para el SCN (t=0.6718, df=22, p=0.5084).
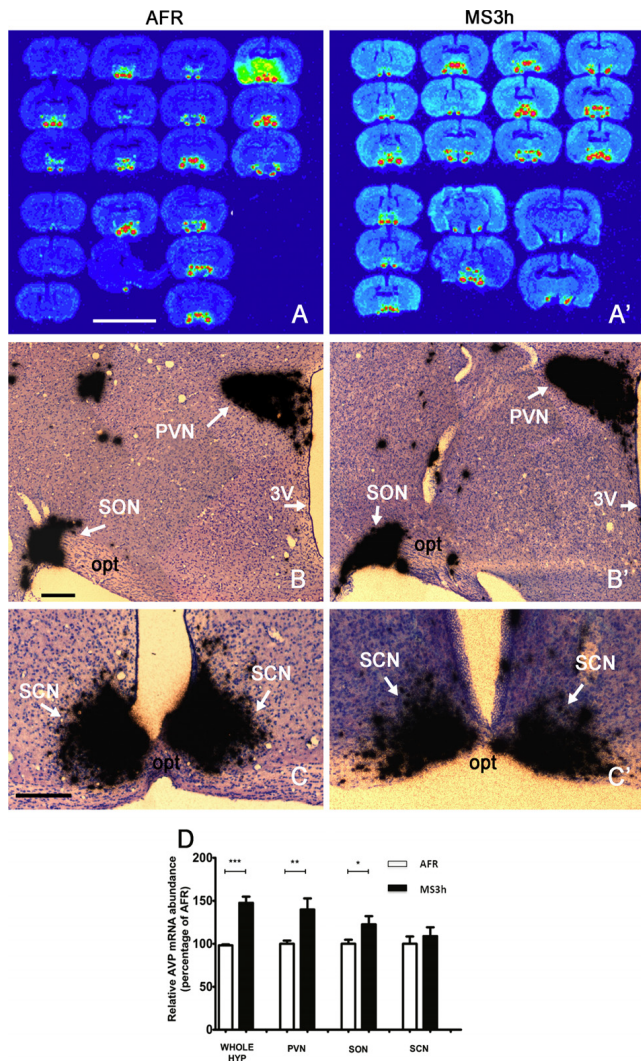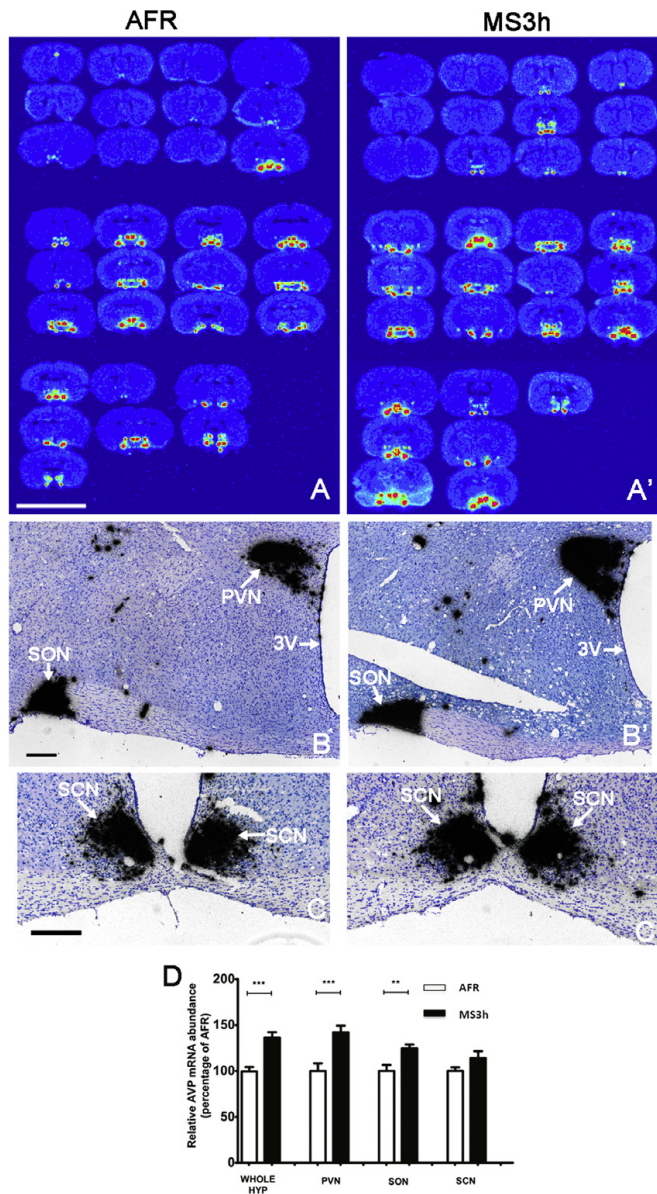
Figura 3. La MS aumentó la cantidad de mRNA para AVP presente en el PVN y SON de ratas en PND 63

Los paneles azules muestran las autorradiografías expuestas toda la noche de una ISH hecha al PND 63 para detectar mRNA de AVP en el hipotálamo de animales AFR y 3hMS (A y A' respectivamente). Se observa que en el grupo MS hubo un aumento en el número de secciones conteniendo mRNA de AVP, lo cual nos indica un tamaño rostro-caudal incrementado. Las fotomicrografías del medio, tomadas tras sumergir las mismas laminillas en una emulsión de plata para detectar radioactividad (Ilford K.5) durante 4 semanas en la oscuridad a 4°C, muestran un aumento en la expresión de mRNA para AVP en el PVN y SON de animales 3hMS (b') comparados con el control (B), mientras que no se observaron diferencias significativas en el núcleo supraquiasmático (SCN, C y C'). La densidad óptica de la autorradiografía para la serie entera de rebanadas coronales fue medida y convertida en un histograma (D). Barras de escala: A y A': 10 mm; B,B',C y C': 200 μm

Al PND 63, la expresión relativa de mRNA de AVP en los 3hMS se incrementó significativamente en el hipotálamo entero: 136.3±5.9% comparado con los AFR (100±4.8%); t=8.108, df=6, p=0.0002, (Fig. 3 A, A' y D). La abundancia relativa del mRNA de AVP en PVN y SON de los animales MS aumentó significativamente: 142.8±7.3% (t=3.813, df=22, p=0.001) y 124.5±4.4% (t=3.109, df=22, p=0.0051), comparado a los controles (100±8.2% and 100±6.5%) respectivamente (Fig. 3 B, B' y D). SCN mostró un 114.2±7.4% (3hMS) contra 100±3.8% (AFR) (Fig. 3 C, C' y D). El análisis estadístico con la t de Student no encontró diferencias significativas para el SCN (t=1.685, df=22, p=0.10).

4.1.3 Análisis del volumen de los núcleos vasopresinérgicos hipotalámicos
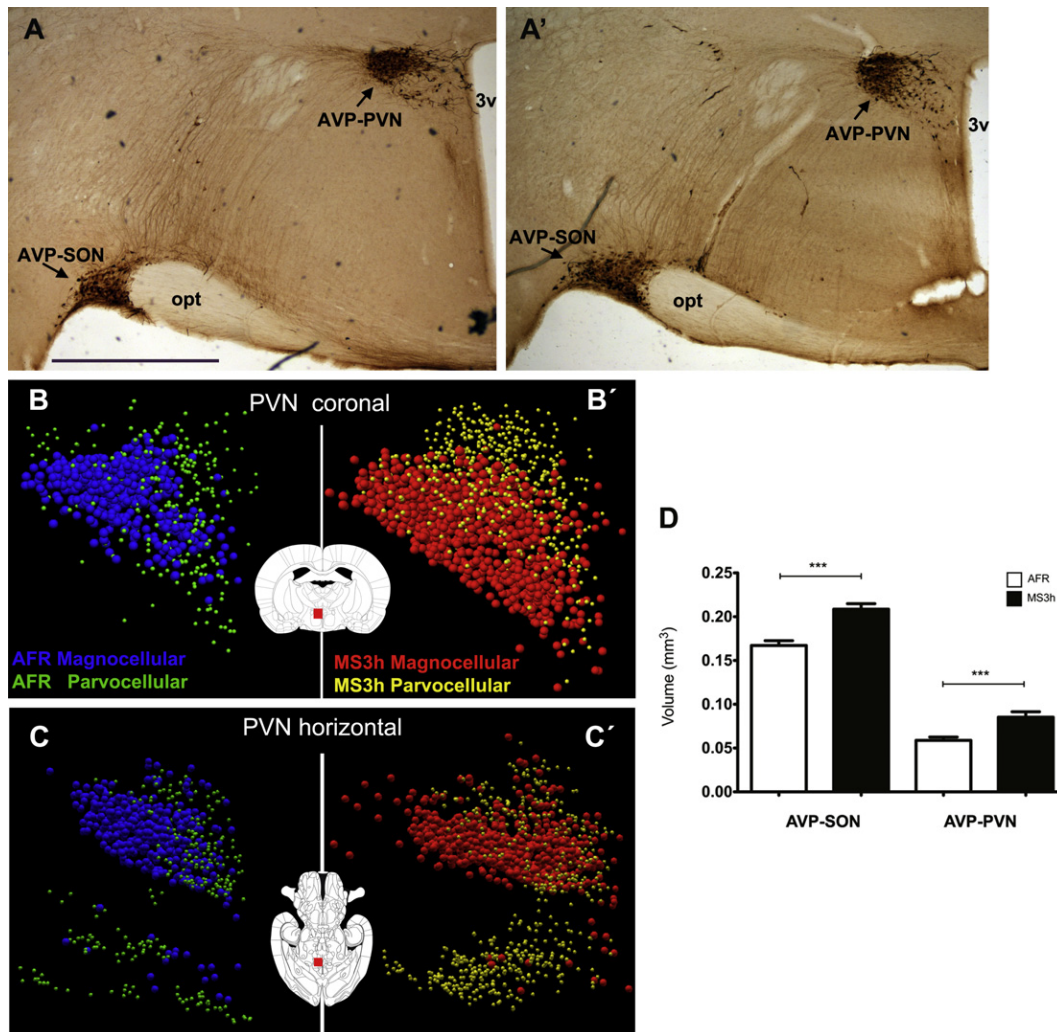
Figura 4. La MS aumentó el volumen de los núcleos PVN y SON AVP+

A y A ': fotomicrografías representativas que muestran tinción inmunohistoquímica para vasopresina en cortes coronales hipotalámicos que muestran las áreas agrandadas ocupadas por neuronas de vasopresina en los núcleos paraventricular (PVN) y supraóptico (SON) de 3hMS (A') en comparación con AFR (A). B, B ', C, C': muestran las vistas coronal (B y B ') y horizontal (C y C') de la reconstrucción 3D por computadora de PVN: las neuronas magnocelulares AVP + están en azul para AFR y en rojo para 3hMS y Las neuronas parvocelulares están en verde para AFR y en amarillo para 3hMS. D: El histograma muestra la media SEM de las medidas de extensión de volumen AVP + en las regiones SON y PVN. Barra de escala = 1 mm

La MS aumentó significativamente el volumen de los núcleos AVP-SON y AVP-PVN evaluados en PND 75 (Fig. 4). El volumen medio de AVP-SON MS3h fue de 0.2086 mm3 ± 0.0064 mm3 frente a 0.1671 mm3 ± 0.0055 mm3 del grupo AFR (t = 4.883, df = 14, p <0.001). En AVP-PVN,

el 3hMS tuvo un volumen de 0.0853 mm3 ± 0.0062 mm3 frente a 0.0588 mm3 ± 0.0038 mm3 en el grupo AFR (Fig. 4D; t = 4.75, df = 14, p <0.001). En ratas 3hMS se observó un aumento en el número de neuronas que expresan AVP en la porción medial del PVN (datos no mostrados). También hubo un aumento en la extensión del núcleo en las dimensiones rostro-caudal y medio-lateral. (Fig. 4B, B 'y C, C').

4.1.4 Efectos de la MS sobre la conducta ansiosa

Los estados ansiosos no condicionados y condicionados se evaluaron mediante dos pruebas de comportamiento bien validadas, la prueba EPM y el APV. EPM prueba el estado de exploración frente a evitación, colocando a la rata en un entorno no condicionado con el brazo cerrado que representa seguridad y el brazo abierto elevado que denota novedad, aunque es arriesgado.

El tiempo disminuido en los brazos abiertos y el número reducido de entradas implican un mayor estado de ansiedad incondicionado. Las ratas MS3h pasaron lapsos de tiempo similares en los brazos abiertos (86.2 s ± 6.96 s) en comparación con las ratas AFR (80.7 s ± 5.50 s) (t = 0.6198, df = 18, p = 0.5432) (Fig. 5A). Posteriormente, las ratas se sometieron a WD, como un estresor osmótico, durante 48 h. Posteriormente, las ratas sedientas se sometieron a la prueba de conflicto en la que tuvieron que decidir entre beber agua (recompensa) y posiblemente recibir una descarga eléctrica leve (castigo) o, más bien, mantenerse alejadas de la botella de agua (evasión). Las ratas MS3h mostraron una reducción significativa en el número de choques recibidos durante los 5 minutos de la prueba (11.60 ± 2.56) en comparación con el AFR (91.4 ± 7.58) (t = 10.04, df = 18, p <0.0001) (Fig. 5B) , lo que indica un estado de ansiedad superior desencadenado por este desafío osmótico. Los valores se expresan como media ± SEM.
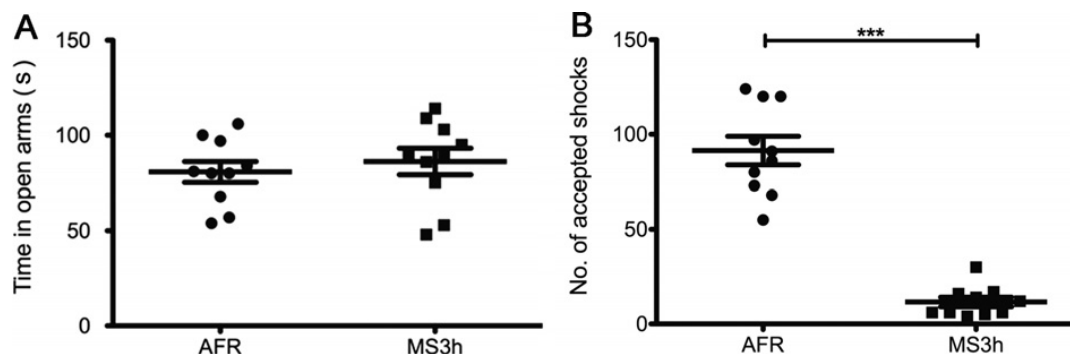
Figura 5. No se vieron diferencias en el EPM, mientras que en el VCT, los animales MS demostraron un aumento en su estado de ansiedad condicionada, comparados con AFR En el EPM, los animales 3hMS no demostraron un cambio estadísticamente significativo, en comparación con los controles, en su estado de ansiedad aguda no condicionada (A). Sin embargo, los animales sujetos a MS demostraron estar en un estado de ansiedad condicionada mucho mayor que los controles, en el VCT (B)

4.1.5 La MS alteró los niveles de AVP tras la WD

La concentración plasmática de AVP del grupo MS a las 12 hrs de WD mostró un aumento significativo (16.14 ± 1.15 pg/ml), en comparación al grupo AFR (12.23 ± 1.12 pg/ml) (p<0.05). Una ANOVA de dos vías mostró efectos significativos para los distintos puntos temporales (F4, 72=46.7, p<0.0001) y para los distintos tratamientos (F1, 72=14.35, p=0.0013).
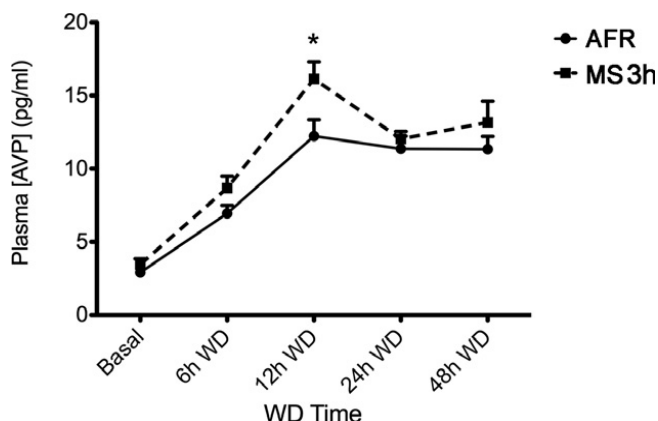
Figura 6. La MS aumentó la concentración plasmática de AVP en respuesta a la WD
Los animales MS demostraron una respuesta exacerbada en respuesta a la WD, se puede ver una diferencia significativa en la concentración plasmática de AVP a las 12 hrs de WD

4.2   Efectos de la MS en la supervivencia celular/apoptosis en el hipotálamo

4.2.1 Aumento de la densidad celular y el número de células NeuN+ en algunas regiones hipotalámicas

MS aumentó la densidad celular y el número de células que expresan NeuN en las regiones hipotalámicas de crías de rata. La densidad celular total de varias regiones hipotalámicas en PND 21 se evaluó utilizando secciones teñidas con azul de metileno. Las ratas MS mostraron densidades significativamente más altas de núcleos celulares teñidos con azul de metileno que las ratas AFR para todos los núcleos hipotalámicos estudiados (Figura 7, panel A). El resultado promedio de los conteos, expresado como número de células por área contada (de 0.009 mm^2) se reporta, para cada región, a continuación: MS 72.7 ± 2.7 versus AFR 53.7 ± 2 en el MPOc (t (4) = 5.59, p <0.01); MS 69.7 ± 2 versus AFR 59.3 ± 1.4 en el MPOm (t (4) = 4.14, p <0.05); MS 43.3 ± 0.9 versus AFR 36 ± 1.2 en el PePO (t (4) = 5.05, p <0.01); MS 58.3 ± 0.7 versus AFR 46.3 ± 1.2 en el PVNmpd (t (4) = 8.73, p <0.005); MS 70.3 ± 3.4 versus AFR 54.3 ± 1.8 en el SChDL (t (4) = 4.19, p <0.05); MS 55.3 ± 0.9 versus AFR 45.3 ± 0.9 en el AHA (t (4) = 8.02, p <0.01) y MS 87 ± 2.9 versus AFR 72.7 ± 3 en el Arc (t (4) = 3.47, p <0.05; Figura 7, panel A).

La inmunohistoquímica para NeuN (Figura 7, paneles C – E ') y GFAP (Figura 7, paneles F – H) se utilizó para distinguir los efectos sobre las poblaciones neuronales y gliales.

El número medio de células inmunopositivas con NeuN aumentó en ratas con MS en comparación con ratas con AFR en las siguientes regiones: MS 43.3 ± 2.4 versus AFR 30.7 ± 2 (t (4) = 4.028, p <0.05) en la MPOm; MS 33.7 ± 0.3 contra AFR 25.9 ± 1.5 células (t (4) = 5.211, p <0.01) en el PVNmpd; MS 40 ± 1.2 versus AFR 28.3 ± 1.8 (t (4) = 5.534, p <0.01) en el AHA y MS 65.3 ± 1.9 versus AFR 51 ± 1.2 (t (4) = 6.557, p <0.01) en el hipotálamo ventromedial núcleo (Figura 7, panel B). En particular, algunos núcleos hipotalámicos, con alta densidad celular en la misma etapa de desarrollo, no expresaron NeuN. Estos núcleos incluían los núcleos de PVN magnocelular, supraóptico y supraquiasmático.
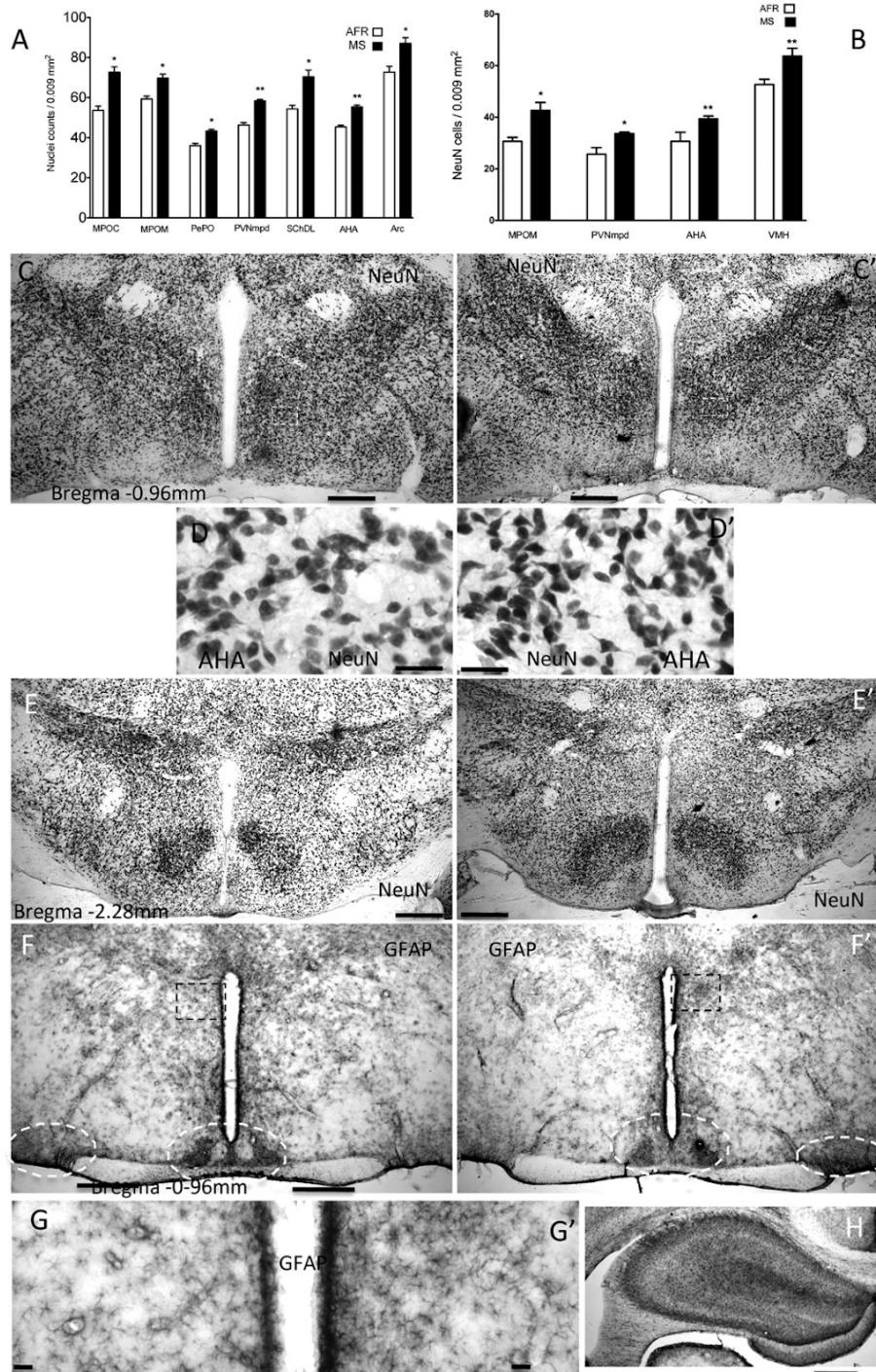
Figura 7. La MS aumentó la densidad celular y el número de células NeuN+ en el hipotálamo de ratas jóvenes

La MS aumentó la densidad celular en todos las regiones hipotalámicas que estudiamos; (A) número de núcleos observados por campo visual al PND 21 usando tinción con azul de metileno; (B) número de células NeuN+ al PND 36. (C-E') Fotomicrografías representativas mostrando un aumento de células NeuN+ en los animales MS (C', D' y E') en comparación con los controles (C,D y E). (F-H) Fotomicrografías mostrando que el marcaje de GFAP resultó muy heterogéneo para poder hacer alguna cuantificación.

Respecto a la expresión de GFAP, a diferencia del hipocampo donde los astrocitos inmunopositivos GFAP ya estaban distribuidos en un patrón de matriz ordenada en PND 36 (Figura 1H), los astrocitos inmunopositivos GFAP hipotalámicos mostraron un patrón altamente heterogéneo (Figura 7, paneles F y F ') Lo cual no nos permitió obtener datos cuantitativos para cada núcleo. No obstante, se observó un claro aumento en el etiquetado de GFAP en algunas regiones, como los núcleos periventricular (Figura 7, G a G ') y supraquiasmático (Figura 7, F a F').

4.2.2 Efectos de la MS en la expresión de proteínas asociadas a la supervivencia celular y apoptosis

Figura 8. La MS alteró la expresión de caspasa 3 activa (escindida) en el hipotálamo de ratas jóvenes
(a) WBs representativos de la reacción contra caspasa 3 y β-actina en lisados hipotalámicos de animales AFR y MS, a distintas edades. (b) El análisis densitométrico de estos inmunoblots muestran una caída repentina en la expresión de caspasa 3 activa al PND 15 en animales MS; cada punto temporal indica la proporción de caspasa 3 contra la expresión relativa de proteína total, como porcentaje de PND 1

Analizamos el patrón de expresión de varias proteínas clave implicadas en la muerte celular o la supervivencia celular durante el desarrollo temprano y la adultez temprana, en extractos hipotalámicos completos obtenidos de ratas AFR y MS, por electrotransferencia o Western. Las vías de muerte extrínseca e intrínseca culminan en la activación de la caspasa 3 (por escisión de la pro-enzima). Por lo tanto, utilizamos la detección de caspasa 3 activada para identificar eventos de muerte celular programada (PCD). Se observó un patrón similar de expresión de caspasa 3 activa entre ratas MS y AFR en los puntos temporales 3, 6, 9 y 12 de la PND (Figura 8a). Sin embargo, en PND 15, las ratas MS presentaron una reducción significativa de 9,4

veces en la expresión, en comparación con ratas AFR (p <0,05; Figura 8b; Tabla 1). Por PND 20 y en adultos jóvenes, ambos grupos de tratamiento mostraron niveles reducidos de caspasa 3 activa (escindida) en comparación con PND 1 (Figura 8b). El análisis de ANOVA de dos vías versus la edad reveló que la edad afectó significativamente el patrón temporal de la expresión de la caspasa 3 activada en los grupos de tratamiento (p <0,03, Tabla 1). Estos resultados revelan un patrón temporal desplazado de la activación de caspasa 3 en la MS en comparación con las ratas AFR.
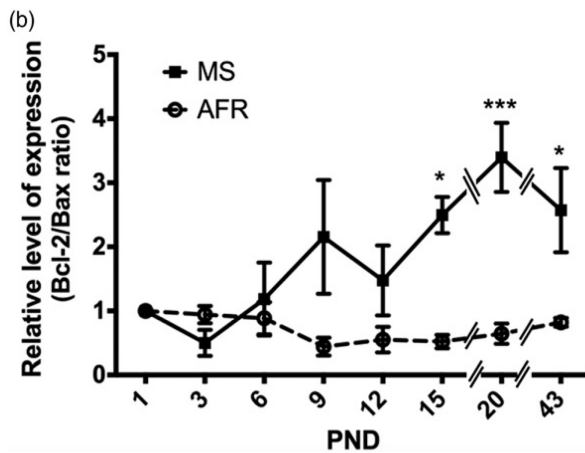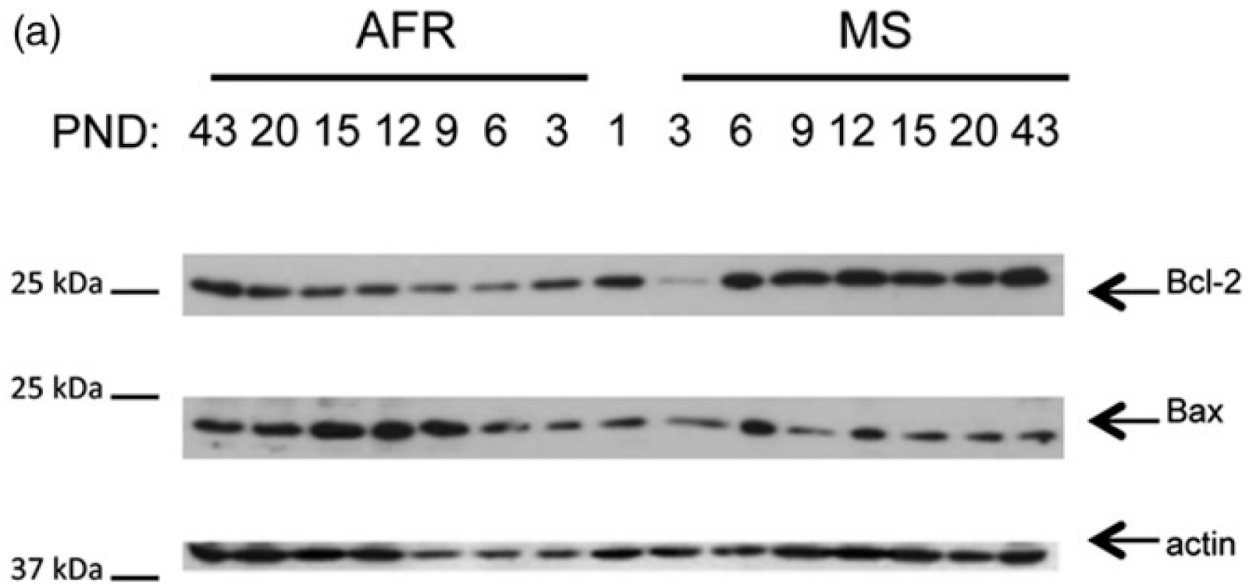
Figura 9. La MS alteró la proporción de expresión de Bcl-2 contra Bax en el hipotálamo de ratas jóvenes

(a) WBs representativos de la reacción contra Bcl-2, Bax y β-actina en lisados hipotalámicos de animales MS y AFR, a distintas edades (b) El análisis densitométrico de los inmunoblots para Bcl-2 y Bax muestran una curva suprimida en animales MS; cada punto temporal indica la proporción de las expresiones relativas de Bcl-2 contra Bax, como porcentaje de PND 1

Se analizó la inmunorreactividad anti-apoptótica Bcl-2 y pro-apoptótica Bax en diferentes puntos de tiempo postnatales como bandas únicas a 26 y 23 kDa, respectivamente (Figura 9a). La proporción de Bcl-2 / Bax disminuyó de PND 9 a PND 20 en ratas AFR, en contraste con los niveles crecientes en ratas MS (Figura 9b). Un ANOVA indicó que el procedimiento de MS, la edad y una interacción entre el tratamiento y la edad, afectaron significativamente la relación Bcl-2 / Bax (p <0,001, p <0,05 y p <0,01, respectivamente; Tabla 1). Los efectos de la separación materna sobre la proporción de Bcl-2 / Bax dependieron de la

edad del neonato y mostraron un patrón de expresión cuantitativo distintivo. Específicamente, las ratas MS mostraron un aumento significativo de 4.5, 5.3 y 3.3 veces la expresión de la relación Bcl-2 / Bax en PND 15, 20 y 43, respectivamente (p <0.05, p <0.001 y p <0.05, respectivamente; Figura 9b; Tabla 1).

La inmunorreactividad de ERK1/2 activa (ERK1/2 fosforilada) para ratas AFR y MS se detectó como bandas únicas a 42/44 kDa de proteínas ERK1 / 2 fosforiladas (Figura 10a). El nivel de ERK1 / 2 activado disminuyó a medida que aumentaba la edad neonatal en ratas AFR, en contraste con los niveles más altos encontrados en ratas con MS en todos los PND estudiados, y en PND 20 ambos grupos de tratamiento (control vs. MS) presentaron una expresión disminuida (Figura 10b). El análisis cuantitativo mostró que la interacción entre la MS y el tratamiento versus la edad afectó significativamente la activación de ERK1 / 2 (p <0,0001 y p <0,05, respectivamente, Tabla 1), con un aumento significativo de 4,5, 6 y 5,2 veces la expresión en PND 15, PND 20 y 43, respectivamente, en ratas MS en comparación con ratas AFR (p <0.01, p <0.05 y p <0.01; Figura 10b; Tabla 1). Estos resultados demuestran que las diferencias entre los grupos de tratamiento (control vs MS) no se debieron a un patrón de activación temporal desplazado, sino a un nivel prolongado y mayor de activación de ERK1/2.
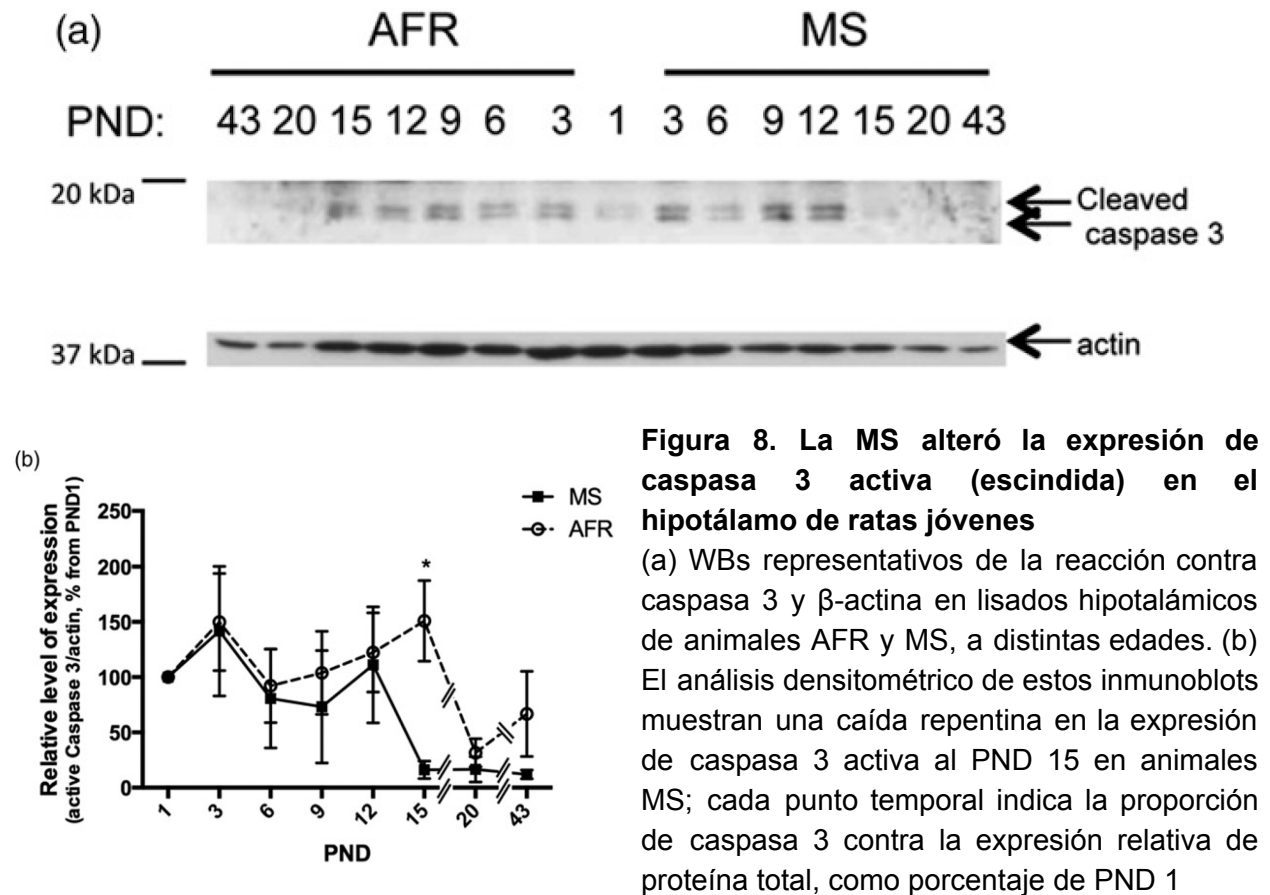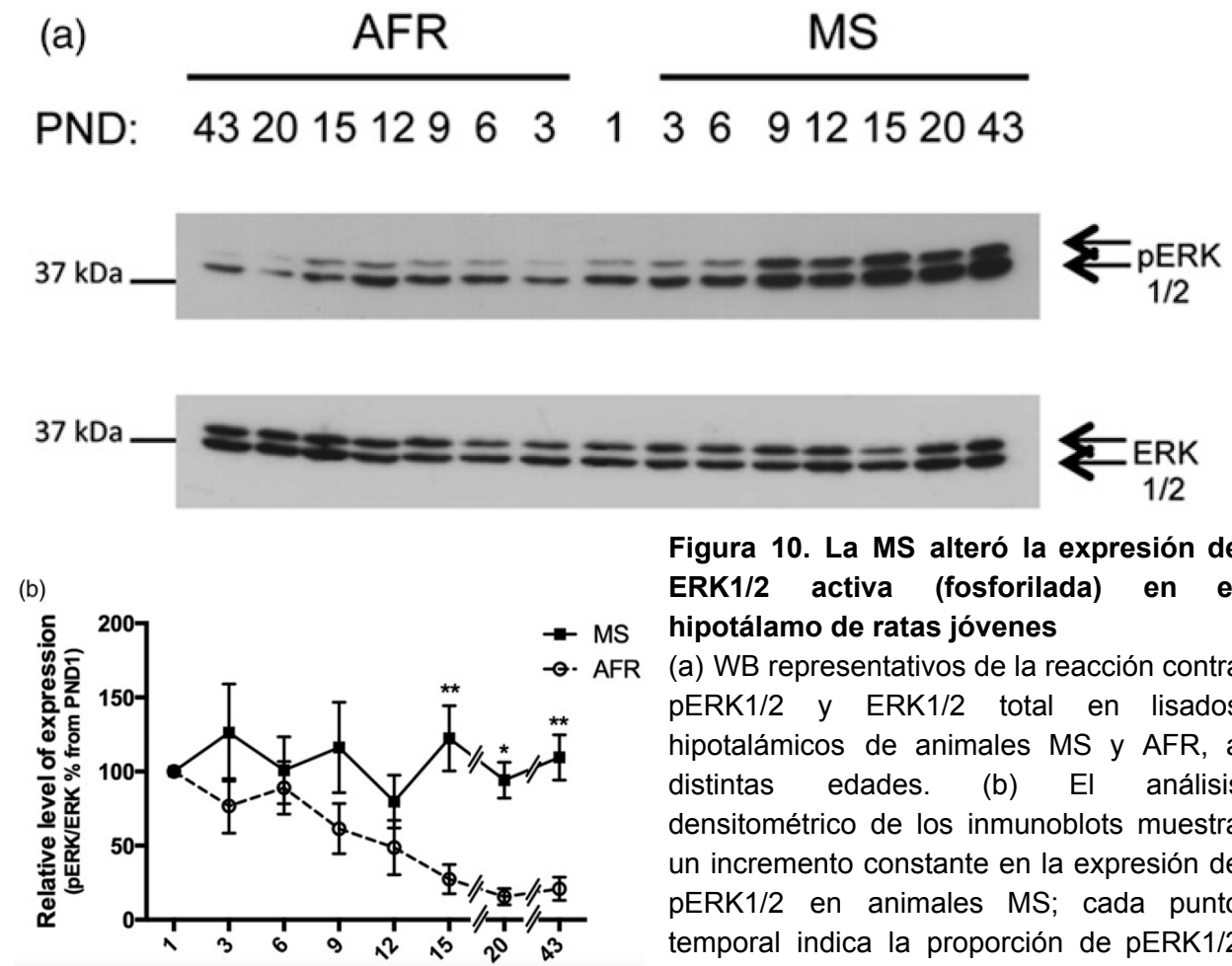

Figura 10. La MS alteró la expresión de ERK1/2 activa (fosforilada) en el hipotálamo de ratas jóvenes

(a) WB representativos de la reacción contra pERK1/2 y ERK1/2 total en lisados hipotalámicos de animales MS y AFR, a distintas edades. (b) El análisis densitométrico de los inmunoblots muestra un incremento constante en la expresión de pERK1/2 en animales MS; cada punto temporal indica la proporción de pERK1/2 dentro de ERK1/2 total, como porcentaje de

PND 1

A continuación, examinamos el nivel de Akt activada (Akt fosforilada) de ratas AFR y MS (banda única a 60 kDa, Figura 5a). Ambos grupos de tratamiento (control vs. MS) mostraron niveles similares de Akt; sin embargo, las ratas MS presentaron un aumento significativo de 5 y 5,9 veces en PND 20 y PND 43 en contraste con las ratas AFR ($p < 0.0001$ y $p < 0.001$; Figura 5b; Tabla 1). El análisis cuantitativo reveló que la interacción entre la MS, la edad y el tratamiento afectó significativamente los niveles de Akt activados ($p < 0.001$; Tabla 1).
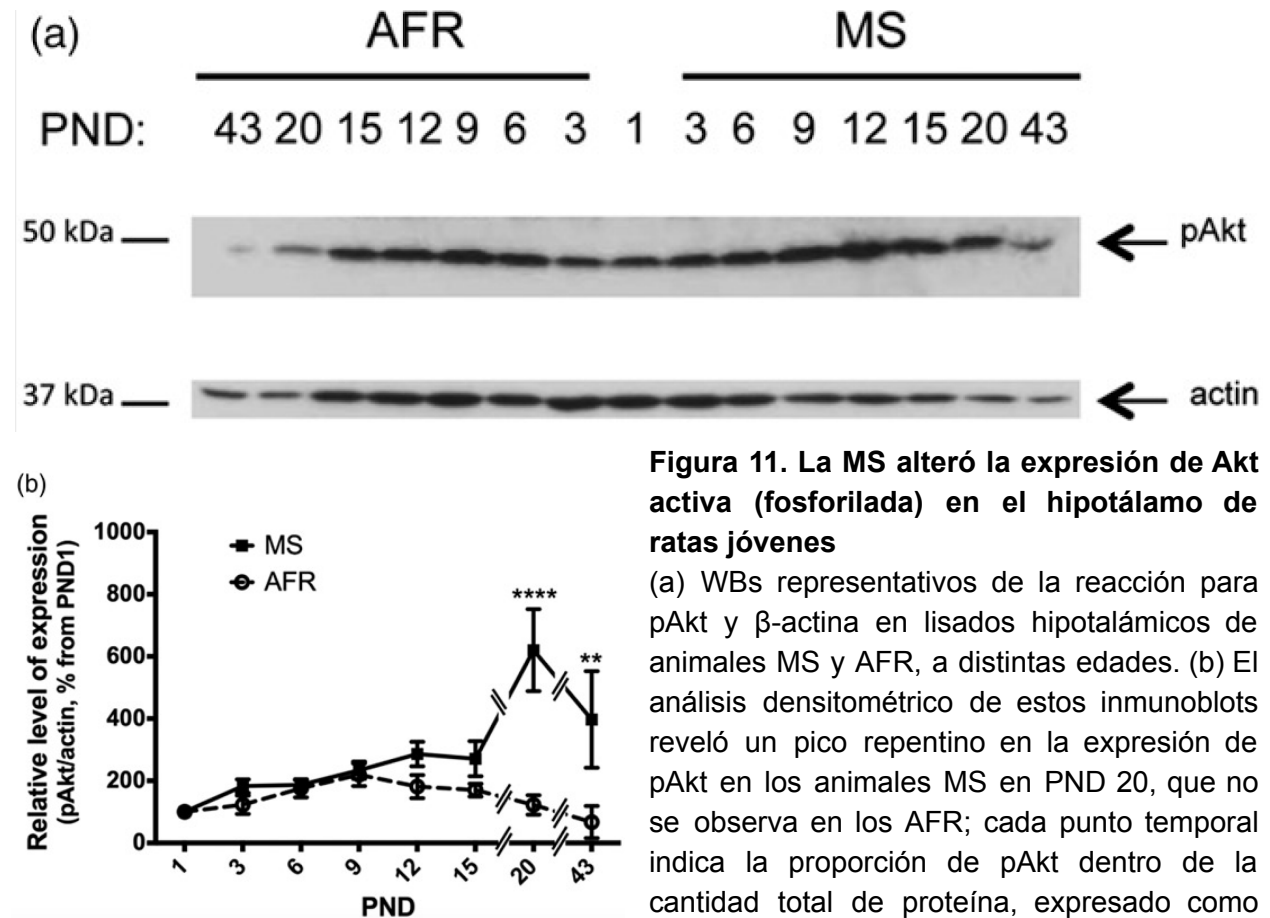
Figura 11. La MS alteró la expresión de Akt activa (fosforilada) en el hipotálamo de ratas jóvenes

(a) WBs representativos de la reacción para pAkt y β-actina en lisados hipotalámicos de animales MS y AFR, a distintas edades. (b) El análisis densitométrico de estos inmunoblots reveló un pico repentino en la expresión de pAkt en los animales MS en PND 20, que no se observa en los AFR; cada punto temporal indica la proporción de pAkt dentro de la cantidad total de proteína, expresado como porcentaje del PND 1

Finalmente, se analizaron los niveles de Bad anti-apoptótico (pBad, fosforilado en Ser112, banda única a 25 kDa; Figura 12a). ANOVA reveló que el tratamiento y la edad afectaron significativamente los niveles de pBad, con una interacción (edad vs. tratamiento) ($p < 0.001$, $p < 0.0001$ y $p < 0.05$, respectivamente; Tabla 1). La Figura 6 (b) muestra niveles más altos de pBad durante las edades neonatales con un pico alrededor de PND 15 en ratas AFR, mientras que este pico se alcanzó en un día posterior al nacimiento (PND 20) con un aumento significativo de 2,4 veces en ratas con MS ($p < 0.001$; Tabla 1). Además, también se observó una diferencia significativa en los niveles de pBad en PND 43 ($p < 0.05$; Tabla 1).

(a)

AFR   MS

PND: 43 20 15 12 9   6   3   1   3   6   9   12 15 20 43

25 kDa — ← pBad

25 kDa — ← Bad

(b)
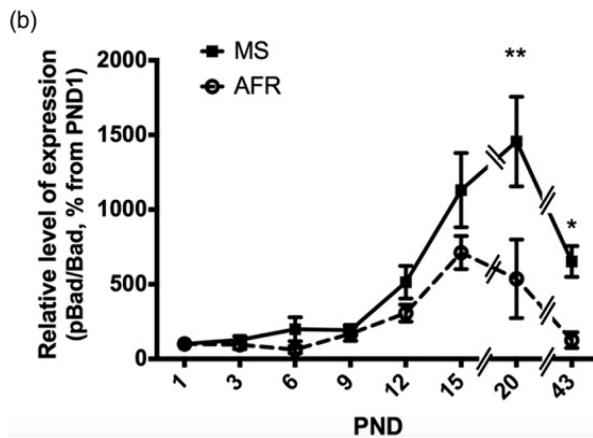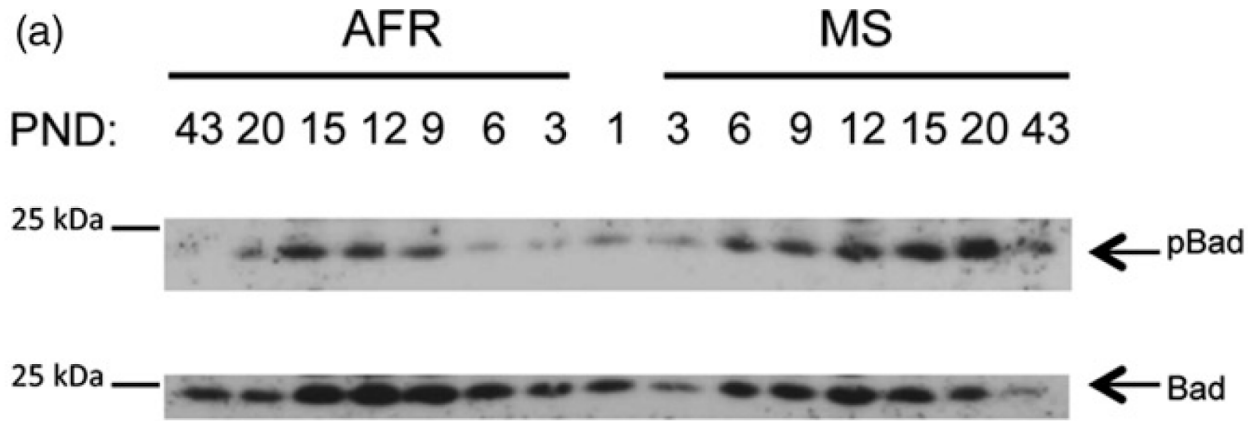
Figura 12. La MS alteró la expresión de la cinasa Bad inactiva (fosforilada) en el hipotálamo de ratas jóvenes

(a) WBs representativos de pBad y Bad total en lisados hipotalámicos de animales MS y AFR, a distintas edades. (b) El análisis densitométrico de estos inmunoblots mostró una curva reducida por la MS; cada punto temporal indica la proporción de pBad contra Bad total, expresado como porcentaje del PND 1

Table 1. Summary of statistical analysis of relative protein expression from MS and AFR.

	Active (cleaved) caspase 3	Bcl-2/Bax ratio	Active (phosphorylated) pERK1/2	Active (phosphorylated) pAkt	Inactive (phosphorylated) pBad
Treatment $F(1, 80)$	$F = 3.743$ $p = 0.0570$	$F = 12.08$ $p = 0.0009$	$F = 34.51$ $p < 0.0001$	$F = 29.63$ $p < 0.0001$	$F = 13.41$ $p = 0.0006$
Age $F(7, 80)$	$F = 2.382$ $p = 0.03$	$F = 2.421$ $p = 0.0296$	$F = 2.112$ $p = 0.0527$	$F = 5.270$ $p < 0.0001$	$F = 11.68$ $p < 0.0001$
Interaction $F(7, 80)$	$F = 0.9011$ $p = 0.5105$	$F = 3.857$ $p = 0.0016$	$F = 2.160$ $p = 0.0477$	$F = 6.269$ $p < 0.0001$	$F = 2.195$ $p = 0.0483$

Levels of protein analyzed by Western blot at PND 1, 3, 6, 9, 12, 15, 20 and 43 ($n = 6$ rats per group per age). Two-way ANOVA. Caspase 3, cysteinyl aspartic protease 3; Bcl-2, B-cell lymphoma 2; Bax, Bcl-2 associated X protein; ERK , extracellulr signal regulated kinase 1/2; Akt, protein kinase identified in the Akt virus or protein kinase B; Bad, Bcl-2 associated death promoter protein.

4.3   Evidencia de inervación AVP+ hipotalámica hacia *locus coeruleus* (LC)

4.3.1 Conectividad sináptica entre axones AVP+ y neuronas del LC

En el ratón, se han informado escasos axones AVP + en la región ocupada por LC, utilizando un microscopio de luz de etiquetado único (Rood y De Vries, 2011). Más

recientemente, se ha demostrado que los axones AVP + en la LC de ratón se encuentran en una posición cercana a las proteínas marcadoras sinápticas inhibitorias y excitadoras (**Campos-Lira *et al*, 2018**). Sin embargo, no está claro si existe la misma asociación de AVP con maquinaria sináptica molecular en otras especies, como en ratas, y si la señal está ubicada dentro de uniones sinápticas, o en compartimientos vecinos. Por lo tanto, comenzamos examinando la asociación de los perfiles AVP + con dichas firmas moleculares de transmisión sináptica, en LC de rata utilizando microscopía óptica (LM).

Usando anticuerpos AVP ampliamente validados (anti-AVP de conejo y ratón, generosos regalos de Ruud Buijs y Harold Gainer, respectivamente, detectamos fibras AVP + dispersas en la LC que se unieron estrechamente a tirosina hidroxilasa (TH) dendritas perfiladas inmunoreactivas (Fig. 13 A) y somata (Fig. 13 B). A diferencia de lo informado anteriormente (Aston-Jones & Waterhouse 2016), no se detectaron cuerpos celulares AVP + en la LC. Esto sugiere que no hubo una fuente local de AVP dentro de la LC y estos axones AVP + se originan de otras regiones cerebrales. Las varices AVP + también fueron inmunopositivas para el transportador vesicular de glutamato 2 (VGLUT2) (Fig. 13 B), una proteína expresada exclusivamente en los terminales de los axones glutamatérgicos. Esto sugiere que los axones AVP + podrían formar sinapsis excitatorias con las neuronas LC.

Para confirmar esto, realizamos la inmunotinción de cromógeno peroxidasa doble y TEM, utilizando V-VIP y DAB como cromógenos (consulte la sección M&M para obtener más información). Vale la pena señalar que en las preparaciones EM, el producto de reacción VIP es de aspecto granular y fácilmente distinguible del producto de reacción difusa de DAB (Fig. 13 D). La visualización del producto de reacción DAB a nivel LM reveló varios perfiles AVP + (Fig. 13 C puntas de flecha). También fue evidente una gran varicosidad similar al cuerpo de AVP + Herring, que es una característica anatómica de los axones magnocelulares que contienen AVP (Fig. 13, paneles C y E, asteriscos blancos). Dentro de este campo de visión, se pueden ver dos botones AVP + estrechamente unidos a una dendrita TH + (Fig. 13 C, área en caja). El examen de las secciones de MS en serie tomadas del área en caja reveló que uno de estos botones AVP + formaba una sinapsis asimétrica (tipo I gris) con una dendrita TH + (Fig. 13 C, inserción). El botón presináptico contenía abundante precipitado de DAB y vesículas centrales densas marcadas (dcv, AVP +, punta de flecha verde), características de los terminales de axones que contienen neuropéptidos. En conjunto, esto demuestra que el AVP está contenido en un conjunto de aferentes de LC, que hacen conexiones sinápticas excitadoras con perfiles noradrenérgicos de la LC.
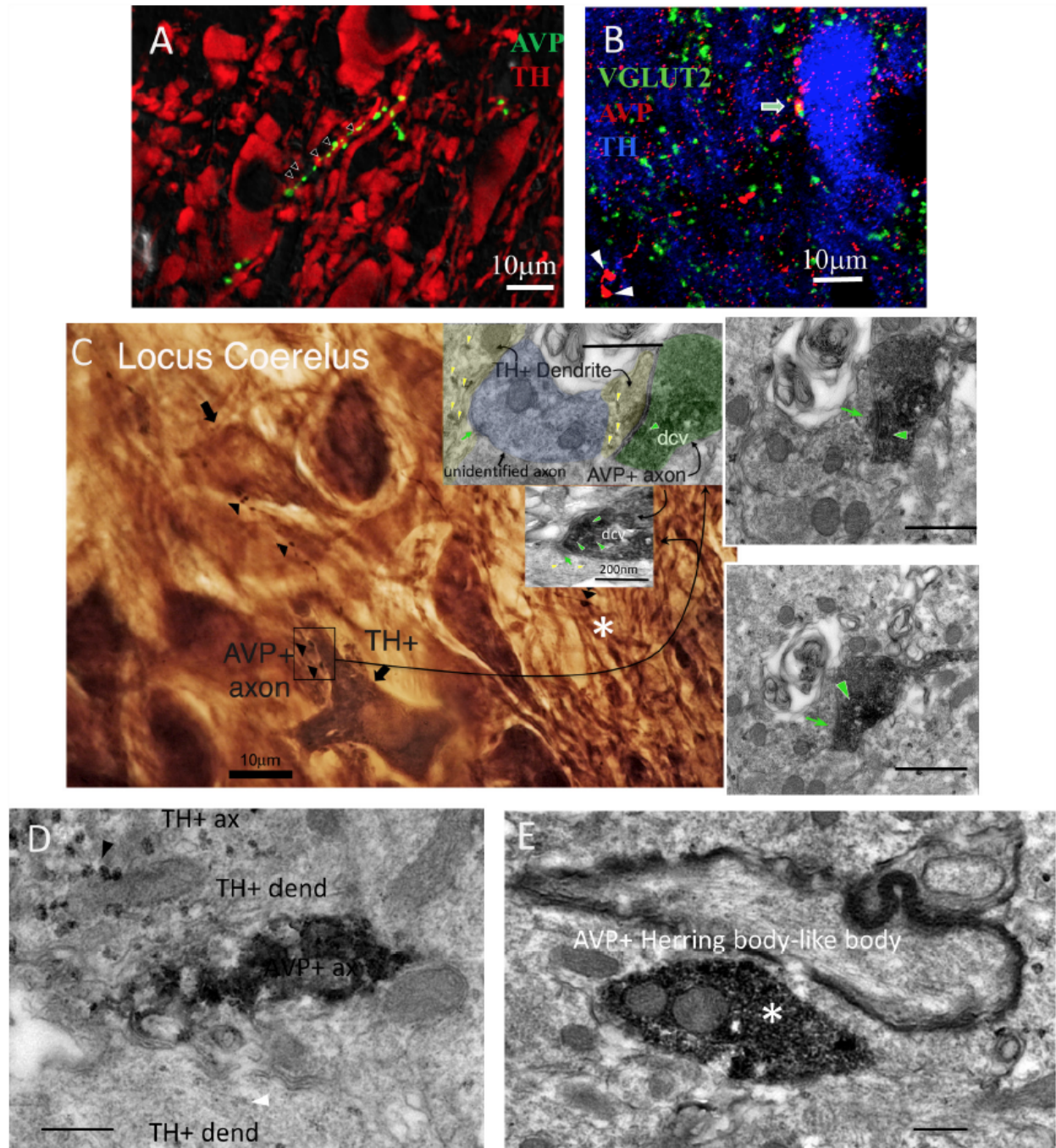
Figura 13. Fibras inmuno-reactivas para AVP–VGLUT2 (AVP+/VGLUT2+) establecen sinapsis Gray tipo I (asimétricas) hacía dendritas TH+ dentro del LC

(A, B) Fotomicrografías confocales mostrando fibras AVP+que están haciendo contacto con dendritas TH+ (A) y la co-localización de segmentos AVP+/VGLUT2+ (B, donde hay dos varicosidades parecidas a cuerpos de Herring indicadas por puntas de flecha). (A) La reacción contra AVP se realizó utilizando un anticuerpo obsequiado por el Dr. Gainer y fue tomada a 0.5 AU (unidades de Airy, utilizando un sistema confocales Leica SP5), el grosor de la sección

óptica fue de aproximadamente 0.596 μm. Esto ayuda a mejorar la resolución óptica para visualizar los puntos de contacto en tejido con señal muy fuerte. El panel B corresponde a LC de ratón utilizando un anticuerpo distinto y tomado con 1 AU (el grosor de la sección óptica de aproximadamente 0.892 μm). (C) Fotomicrografías tomadas pre-incrustación, de una inmunoreacción de la superficie de la cápsula de resina recortada (la "pirámide" osmicada perdiendo el color morado bajo LM), mostrando LC, preparada para EM, usando marcaje de doble peroxidasa-cromógeno DAB/VIP. Las fibras AVP+ evidentemente hacen contacto con segmentos dendríticos TH+, indicados por puntas de flecha negras. Los recuadros son micrografías de TEM de muestras secuenciales de la región indicada con un rectángulo en C. La imagen muestra un axón AVP+ con una terminal (mostrada en cuatro rebanadas contiguas) que contiene vesículas de núcleo denso (dcv, indicadas por puntas de flecha verdes), estableciendo una sinapsis Gray tipo I con una dendrita TH+ (TH se ve como un marcaje granular producido por el reactivo ViP a nivel de MS, puntas de flecha amarillas). Las densidades post-sinápticas (PSD), un rasgo en TEM de sinapsis Gray to I, lo que generalmente es una señal de sinapsis glutamatérgica, están indicadas por flechas verdes. (D) Micrografía de TEM mostrando un segmento de la misma neurona AVP+ (marcaje con DAB-níquel) cursando en paralelo con dos dendritas TH+ (marcaje con VIP). Se puede observar que el marcaje con VIP en dendritas (puntas de flecha blancas) es más tenue que el mismo para el segmento axonal (puntas de flecha negras). (E) Un cuerpo similar a los cuerpos de Herring (una varicosidad axonal grande), un rasgo anatómico de las AVPMNNs (B: puntas de flecha blancas, C y E: asteriscos blancos) examinados bajo EM. Barras de escala: 400 nm, donde no se determina de otra forma

4.3.2 Neuronas noradrenérgicas del LC coexpresan mRNA para receptores V1a y V1b

Usando inmunohistoquímica en ratones, se encontraron V1a y V1b, pero no receptores V2 en la LC (**Campos-Lira *et al*, 2018**). Mientras que el V1b fue expresado por neuronas LC noradrenérgicas y no noradrenérgicas, el V1a fue expresado exclusivamente por neuronas LC adrenérgicas. Utilizamos una técnica de hibridación in situ doble de alta resolución (RNAscope® 2.5 HD Duplex Assay) para evaluar el perfil comparativo de la expresión del receptor AVP en la rata LC. Las neuronas LC adrenérgicas, identificadas por la señal de ARNm para la señal coexpresada de TH para los receptores V1a (Fig. 14 A) y V1b (Fig. 14 B). Esto indica que el AVP, liberado en las sinapsis excitadoras, utiliza los receptores V1a y V1b para la señalización postsináptica dentro de las neuronas LC.

TH- V1b- negative in DRN   TH+ V1b negative in LC
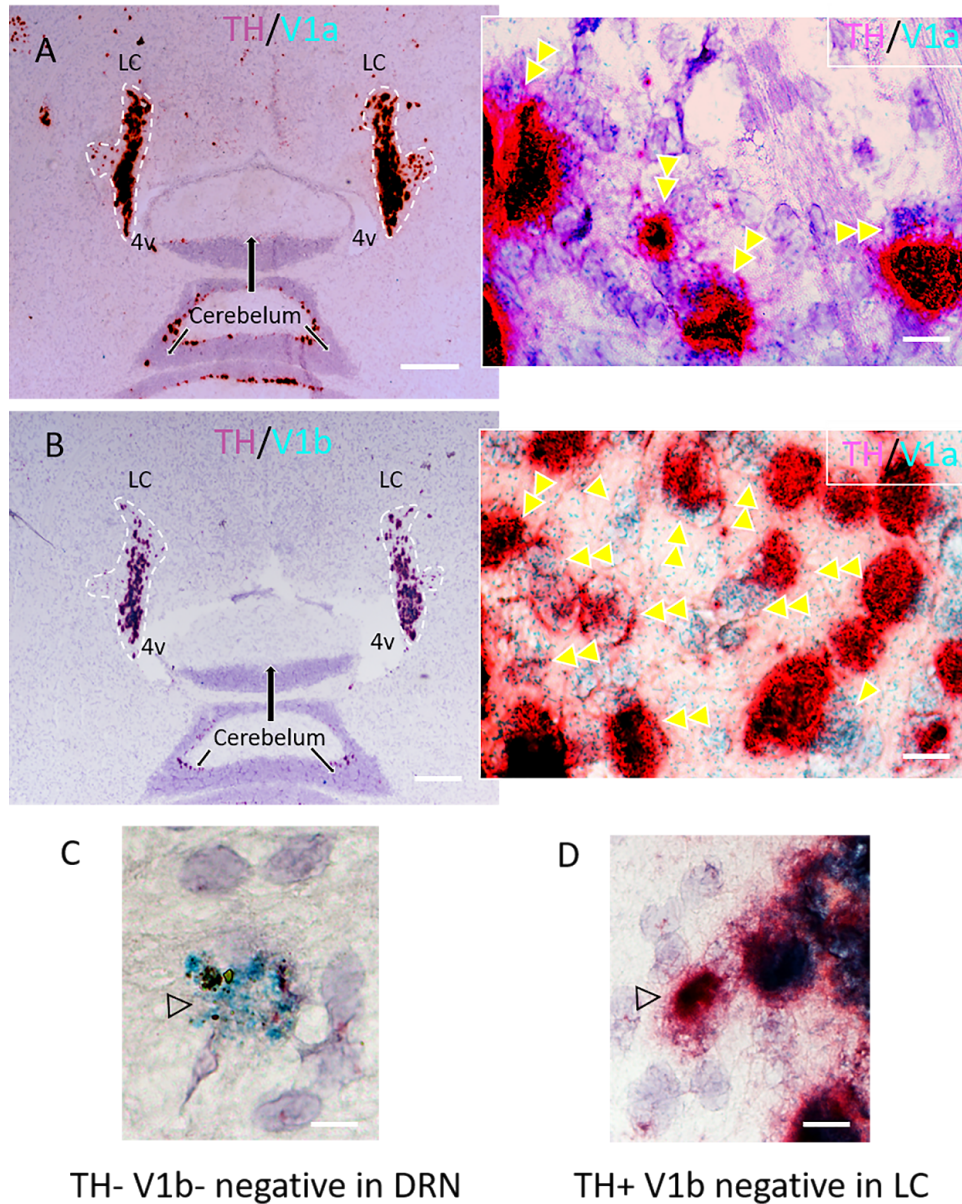
Figura 14. Confirmación de la expresión de mRNA de los receptores V1a y V1b mRNA en neuronas noradrenérgicas de LC, utilizando una técnica de ISH de alta sensibilidad

(A, B)Secciones horizontales de LC de rata mostrando la co-localización (dobles puntas de flecha) de V1aR/TH (A) y V1bR/TH (B). La señal para mRNA de TH fue amplificada usando las sondas relacionadas al canal 2 de RNAscope y el cromógeno Fast Red que funciona por fosfatasa alcalina (AP), dando como resultado una señal roja fácilmente detectable y las señales para V1aR y V1bR fueron amplificadas usando las sondas relacionadas al canal 1 de RNAscope y el cromógeno verde que funciona por HRP, dando una señal verde punteada. (C, D) Controles mostrando el marcaje de V1bR solamente en el núcleo dorsal del raphe y TH solamente en LC, respectivamente. Barras de escala, A,B: 0.5 mm; el resto: 10 μm

4.3.3 Axones AVP+ en el LC se originan de las neuronas vasopresinérgicas magnocelulares neurosecretoras (AVPMNN) de los núcleos paraventricular (PVN) y supraòptico (SON)

Nuestro análisis LM reveló que la rata LC está desprovista de AVP + somata. Esto indica que todos los axones AVP + se originan en regiones más allá de la LC. La presentación de los axones LC AVP + como perfiles de gran diámetro, con frecuentes varicosidades y estructuras similares a las del cuerpo de Herring que expresan conjuntamente la proteína marcadora sináptica glutamatérgica VGLUT2 es típica de las AVPMNN hipotalámicas, lo que hace que esta región del cerebro sea la fuente probable de estos acontecimientos.

Para evaluar esta hipótesis, el trazador retrógrado de fluorogold (FG) se inyectó estereotáxicamente en la LC, y la señal transportada se evaluó en las regiones objetivo. Se confirmó que un total de 4 animales tenían inyecciones de FG dentro del núcleo de la LC, confirmados con TH IHC (Fig. 15 A). La inspección de la inmunofluorescencia de AVP junto con la señal de FG, en las regiones del hipotálamo anterior confirmó la coexpresión de AVP-FG en los núcleos paraventricular hipotalámico (PVN) y supraóptico (SON) (Fig. 15, C-H). Esto confirma que AVPMNNs proporciona inervación inmunopositiva AVP a las neuronas LC-NE.
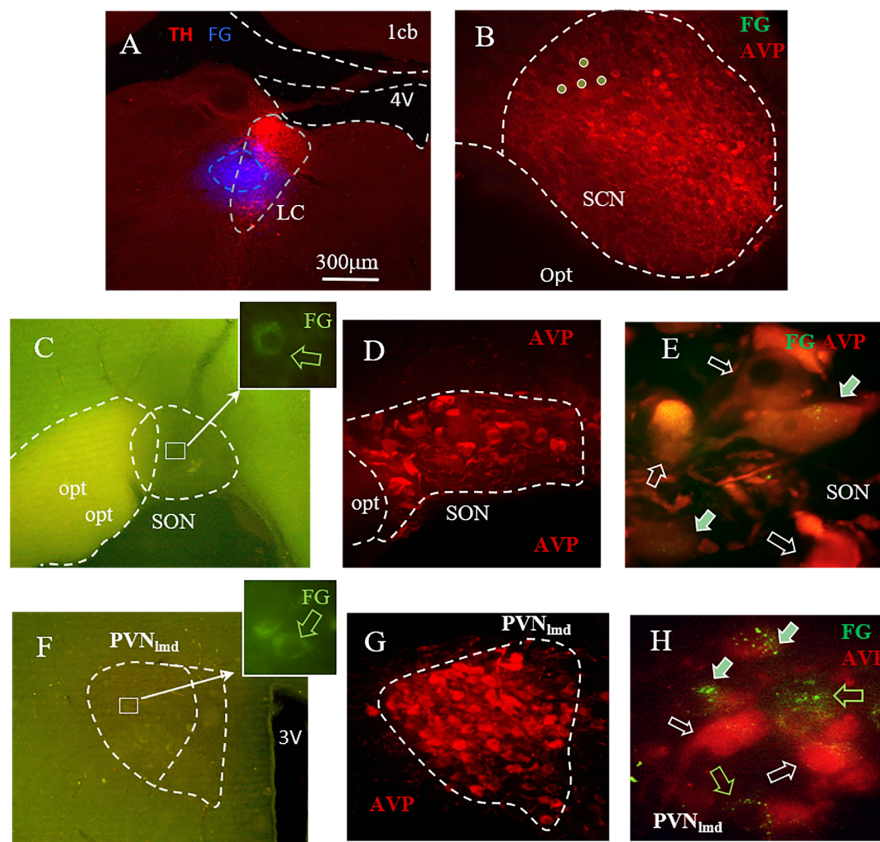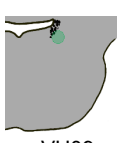
Figura 15. El marcador retrógrado Fluoro-Gold identificó al SON y PVN como la fuente de las aferencias vasopresinérgicas en LC (continúa)

(A) Corte coronal del tegmento pontino, Bregma –9.84 mm; en rojo TH+ delimita a LC, en azul se ve el sitio de inyección de FG (con aproximadamente 300 µm de diámetro). (B) Dentro del núcleo supraquiasmático (SCN) no se observaron núcleos marcados con FG. Sin embargo, en el SON (C-E) y PVN, división medial parvocelular (PVNlmd, F-H) entre el 20% y el 60% de neuronas AVP+ resultaron marcadas (C, F). Las fotomicrografías de rebanadas coronales de hipotálamo recién cortadas en el vibratomo muestran el marcaje esporádico de neuronas magnocelulares con FG (patrón de marcaje lisosomal perinuclear). Se observó co-marcaje de FG y AVP (flechas llenas) en una población de neuronas del SON (D, E) y el PVNlmd (G, H). Flechas blancas huecas indican células AVP+ sin FG y flechas verdes huecas indican las neuronas FG+ sin AVP. Barras de escala: 20 µm para E y H; el resto 300 µm

La Tabla 2 describe el análisis semi-cuantitativo de los 4 casos que cumplieron con los criterios de inclusión. Es interesante observar que no se encontraron neuronas doble-marcadas (AVP+/FG+) en el SCN.

Tabla 2.Registro experimental y descripción anatómica para el marcaje retrógrado con Fluorogold (FG)*

Subject's Pons at Breg. -9.84mm	Main hypoth. AVP+ Regions	Ipsi-lateral	Contra-lateral	Observation	Subject's Pons at Breg. -9.84mm	Main hypoth. AVP+ Regions	Ipsi-lateral	Contra-lateral	Observation
VH07	PVN	+	+		OH02	PVN	+++	+++	
	SON	++	++			SON	+++	+++	
	SCN	-	-	++ in AVP- cell in dorso-lateral portion		SCN	-	-	++ in AVP- cell in dorso-lateral portion
Subject's Pons at Breg. -9.84mm	Main hypoth. AVP+ Regions	Ipsi-lateral	Contra-lateral	Observation	Subject's Pons at Breg. -9.84mm	Main hypoth. AVP+ Regions	Ipsi-lateral	Contra-lateral	Observation
VH09	PVN	+	+		OH05	PVN	+++	++	
	SON	++	++			SON	+++	++	
	SCN	-	-	++ in AVP- cell in dorso-lateral portion		SCN	-	-	++ in AVP- cell in dorso-lateral portion

* Se utilizaron 20 ratas jóvenes para este estudio. Dieciséis de los sitios de inyección no cumplieron con los criterios de inclusión y por lo tanto no se utilizaron. Número de neuronas Fluorogold+/AVP+ por cada 0.2 mm^2: +, 1–5; ++, 6–10; +++, >10. "VH" y "OH" son las iniciales de los experimentadores y el número adyacente denota el número de animal

4.3.4 El estrés temprano aumenta la expresión de AVP en el LC, en la etapa adulta
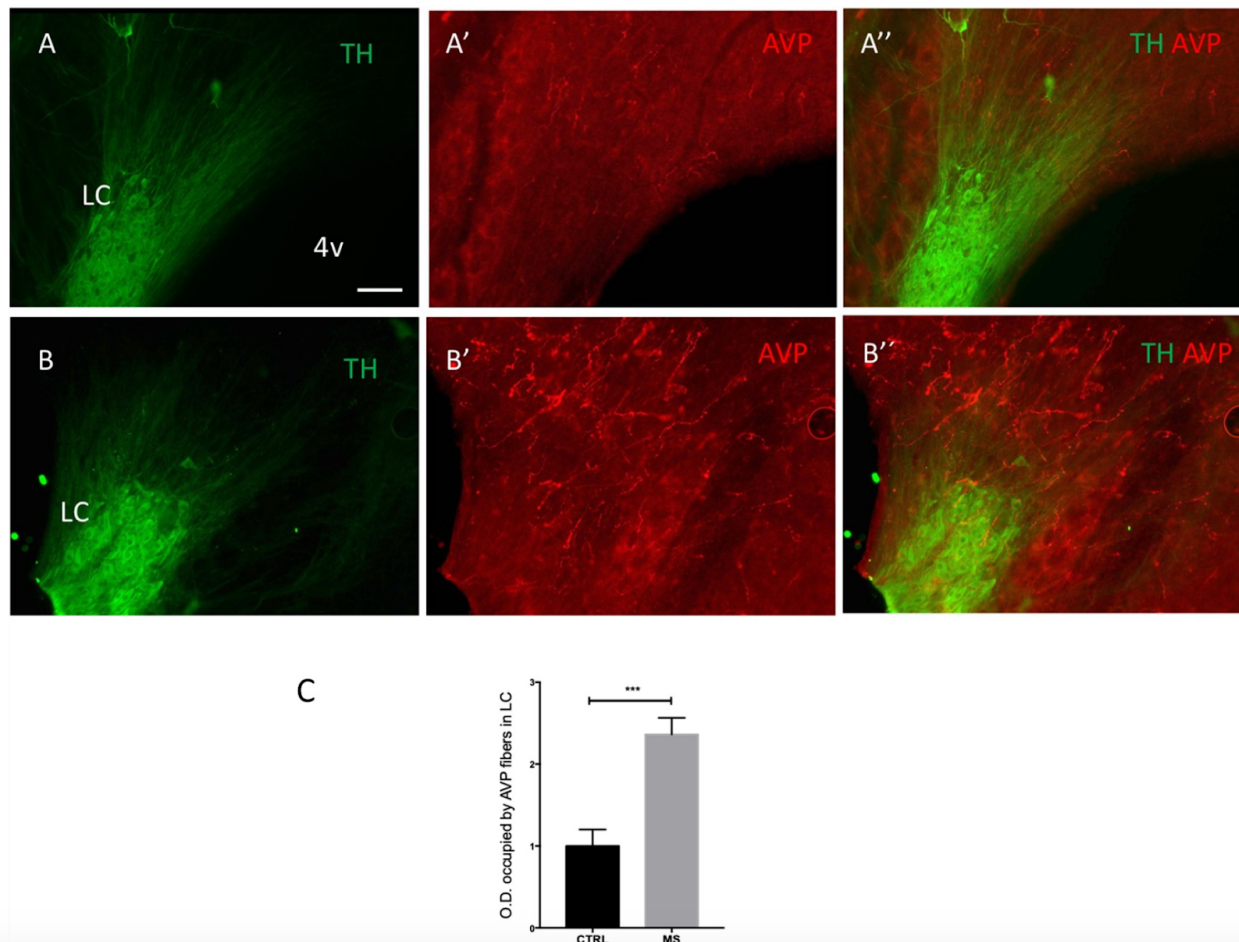
Figura 16. La MS aumenta la inmunoreactividad para AVP en LC (continúa)

Fotomicrografías de cortes horizontales de cerebro de rata (dorso-ventral 7.30 mm) muestran inmunoreactividad para TH y AVP en LC de animales control (As) y MS (Bs). Todos las cortes fueron procesados y fotografiados en condiciones idénticas. (C) Cuantificación de inmunorreacción contra AVP, las columnas representan los promedios de la densidad óptica y las barras el error estándar; (n = 5); p < 0.001. Barra de escala: 100 μm

En ratones, el estrés agudo altera significativamente la expresión de AVP y receptores vasopresinérgicos en LC (**Campos-Lira *et al*. 2018**). Por lo tanto, surge la pregunta de si tal plasticidad inducida por el estrés en el sistema LC AVP es duradera después de la exposición al estrés crónico. Un tipo de estrés que induce una plasticidad molecular, fisiológica y estructural de larga duración en diferentes regiones del cerebro, incluida la LC, es el estrés en la vida temprana (ELS, **Swinny *et al*, 2010**). Dados los datos anteriores que indican que los axones LC AVP se originan, en parte, en un centro que es integral a la respuesta al estrés, es decir, el PVN, evaluamos si el ELS anterior altera el perfil de expresión de los axones AVP + en la LC, utilizando la separación materna como Un modelo de ELS. Como se informó

anteriormente en otras regiones del cerebro (**Zhang *et al*, 2012**; **Hernandez *et al*, 2016**), la MS produjo un aumento notable en la intensidad de la inmunorreactividad de AVP en la LC, en la edad adulta (Fig. 16 A ', B'). La cuantificación de la intensidad de inmunofluorescencia AVP reveló un aumento significativo en las muestras de MS (Fig. 16 C), $p < 0.001$, prueba t de Student no pareada; n=5 animales.

4.3.5 La privación de agua de 24 hrs (WD24h) mejoró el desempeño en el MWM, junto con un incremento en la actividad neuronal de LC, hipocampo y corteza prefrontal, observado por la expresión de Fos

Para responder nuestra pregunta si la regulación a la alta sub-crónica del sistema AVPMNN ejerce efectos moduladores en la activación de las neuronas LC-NE y las subsiguientes regiones de proyección, que podrían reflejarse en sus modificaciones de comportamiento, diseñamos un experimento para evaluar el aprendizaje espacial y la retención de memoria en ratas con deprivación de agua (WD) utilizando el laberinto acuático de Morris (MWM). A partir de las 12 h de privación de agua, la concentración de AVP en plasma en ratas alcanza su nivel máximo y continúa durante las siguientes 12 h (**Zhang *et al*, 2010**). Por lo tanto, este modelo fisiológico podría regular el AVP aferente a la LC.

Como se muestra en la Figura 17 A, en la prueba de la mañana, el grupo de WD ya mostró una mejora sutil del aprendizaje espacial con un curso de aprendizaje más suave y una reducción significativa del tiempo para alcanzar la plataforma de escape en la segunda prueba en comparación con el control (Fig. 17 A). Esta mejora se confirma aún más en la sesión de la tarde con una reducción significativa en el tiempo para alcanzar la plataforma de escape en el segundo y tercer ensayos en comparación con el control (Fig. 17 B). Se observó un fenómeno interesante en el primer ensayo de la prueba de la tarde, en el que los sujetos de WD pasaron más tiempo nadando en el cuadrante II donde se había ubicado la plataforma de escape en la prueba de la mañana, mientras que las ratas de control no mostraron esta preferencia (Fig. 17 C vs. Fig. 17 D).

La expresión de c-Fos, un marcador de plasticidad neuronal, evaluada 90 min después del punto final de MWM, reveló un aumento significativo en la LC, así como en la capa de células granulares (gcl) de la circunvolución dentada (DG) de Hipocampo dorsal y corteza prefrontal. El panel E de la Fig. 17 muestra un número mayor de núcleos Fos + en todas las regiones evaluadas comparando el control con ratas WD24h, es decir, LC: 9.62 ± 0.9 vs 13.14 ± 1.2, $p < 0.05$; DG: 6.0 ± 0.7 vs 11.62 ± 1.3, $p < 0.001$ y PFC: 12.45 ± 0.5 vs 19.73 ± 1.5, $P < 0.001$. Vale la pena señalar que las dos últimas regiones reciben abundantes inervaciones de NE por parte de LC (**Schwarz *et al*, 2015**) pero no se han informado inervaciones directas de AVP (Rood y De Vries 2011, Zhang y Hernandez 2013). Por lo tanto, es coherente interpretar que estos incrementos en la expresión de c-Fos son secundarios a la potenciación de LC-NE aferente a esas regiones.

A Morning test (MT)

Ctrl. Morning △ — WD Morning ◇

B Afternoon test (AT)

Ctrl. Afternoon △ — WD Afternoon ◇

C 1st trial in MT

D 1st trial in AT
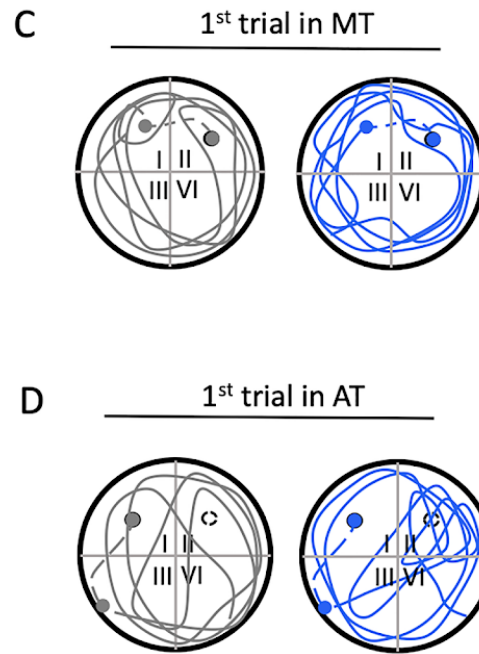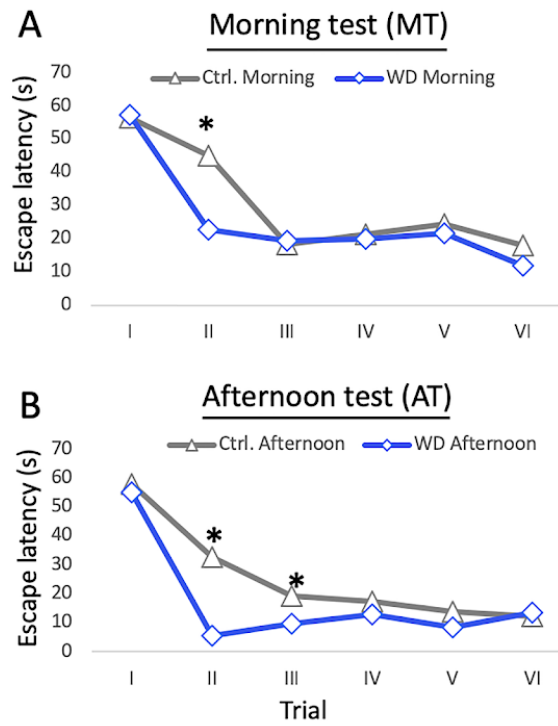
E Fos expression after 90 min of "afternoon" test

LC at sagittal plane Lat. 1.40mm

DG at coronal plane -3.30mm

PrL at coronal plane Bregma 2.70mm

Fos expression at 90 min post-AT

CTRL / WD24
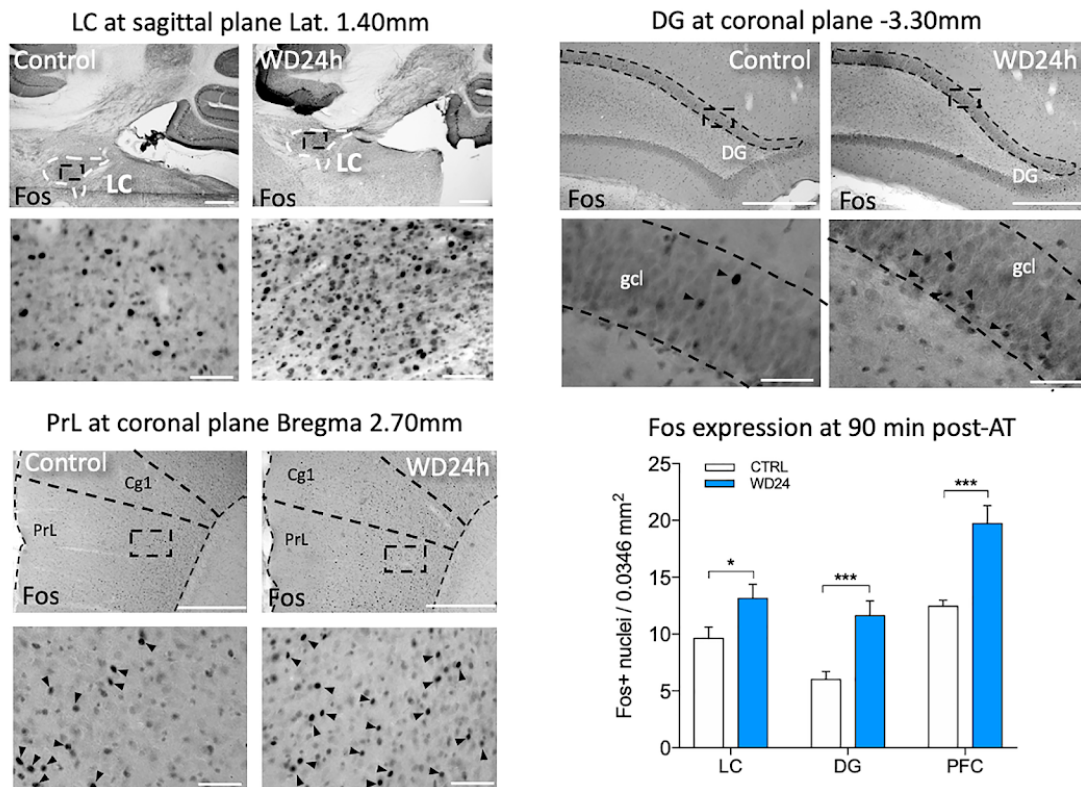
Figura 17. El MWM demostró que la WD24h aceleró el aprendizaje espacial y la retención de memoria, así como también incrementó la actividad neuronal en LC, el hipocampo y la corteza prefrontal: regiones vinculadas a la memoria de trabajo

(A) La prueba matutina (MT) mostró que las ratas sujetas a WD24h aprendieron a localizar la plataforma sumergida (en el cuadrante II) más rápido que las ratas control, evidenciado por una reducción en la latencia para llegar a la plataforma en el segundo ensayo. (B) La prueba vespertina (AT) confirmó la observación de la prueba anterior, donde las ratas sometidas a WD24h mostraron una reducción en el tiempo que tardaron en llegar a la plataforma de salida en el segundo y tercer ensayo, en comparación al control. (C) No se observaron diferencias en la estrategia de nado, como se puede apreciar en un trazo de la trayectoria seguida en el primer ensayo de la MT. (D) Se observó una diferencia en la estrategia distinta de nado en la AT, las ratas sometidas a WD24h pasaron una cantidad significativamente mayor de tiempo en el cuadrante donde la plataforma se había encontrado en la prueba anterior (MT, cuadrante II). En los paneles C y D los círculos llenos simbolizan la plataforma de salida, los círculos vacíos representan el lugar ocupado por la plataforma anteriormente, el círculo punteado marca el lugar donde las ratas se encontraron al finalizar los 60 s de exploración, la línea punteada muestra la trayectoria por la que el experimentador guió a las ratas hacia la plataforma. (E) Fotomicrografías y gráficas de barras mostrando un aumento en el número de núcleos Fos+ en LC, en la capa de células granulosas del giro dentado (DG) y en la corteza prefrontal, en particular, la corteza prelímbica (PrL, capa 5) 90 min después de la AT. Las imágenes de inmunofluorescencia muestran cortes sagitales del LC de sujetos expuestos a WD24h ilustrativas del aumento en activación de LC-NE (flechas negras) tras la MWM. Barra de escala: 500 µm para las fotomicrografías de bajo aumento y 50 µm para las de alto; $p < 0.05$; $p < 0.001$

V. **DISCUSIÓN**

Al comienzo de mis estudios, planteé como hipótesis que i) la separación materna (MS) causaría cambios significativos sobre el sistema de AVPMNNs, ii) que la MS causaría cambios cuantificables en el comportamiento durante la etapa adulta, y que iii) los cambios en el sistema de AVPMNNs estarían entonces asociados a estos cambios en el comportamiento, de manera causal con plausibilidad anatómica y una correlación bidireccional fuerte.

En esta sección de la tesis examino la evidencia que obtuvimos para cada una de estas hipótesis específicas. Finalmente determino si acaso logramos avanzar en cada una de ellas con datos específicos, y cómo los resultados obtenidos pueden afectar la investigación en esta área en un futuro, llegando a una explicación mecanística completa y clara de cómo las AVPMNNs modulan el aprendizaje, memoria, estados afectivos y comportamientos aversivos y apetentes específicos que jerarquizan tendencias homeostáticas y alostáticas para promover la supervivencia:

Nuestro primer estudio ("El impacto de la MS en las AVPMNNs y sobre el comportamiento-ansiedad") examinó los efectos del estrés en la vida temprana, la separación materna, sobre la celularidad, la activación de c-Fos, la expresión de mRNA para AVP y la morfología y el tamaño de las células hipotalámicas. La MS ocasionó un aumento en la cantidad de péptido y mRNA de AVP, además de aparentemente incrementar el tamaño de los núcleos vasopresinérgicos hipotalámicos paraventricular (PVN) y supraóptico (SON) en ratas.

Los resultados de este trabajo se pueden interpretar como un intento de adaptación a un ambiente temprano adverso; donde la ausencia materna, que conlleva a un estado de deshidratación moderada, ya que las crías no pueden amamantarse durante 3 horas, provoca una liberación anormalmente alta de AVP. Esto es particularmente relevante ya que, como se mencionó en la introducción la AVP es capaz de tener efectos tróficos, además que se sabe que el hipotálamo, en particular los núcleos vasopresinérgicos expresan V1bR (**Vaccari *et al*, 1998**). Luego entonces, el aumento de neuronas en el PVN y el SON que expresan AVP podría explicarse por una señalización autócrina temprana que promueve ya sea la proliferación, o bien (como se propone en el trabajo siguiente) la supervivencia celular de neuronas en el hipotálamo. Los cambios citoarquitectónicos ocasionados por la MS se reflejan también en el comportamiento, lo cual nos hace reflexionar sobre la fragilidad de la etapa neonatal temprana y su importancia en el desarrollo del individuo maduro.

En el trabajo siguiente ("La MS incrementó la expresión de proteínas para la supervivencia celular") examinamos los cambios en las vías de transducción de señales y la expresión de proteínas pro y antiapoptóticas, que podrían proporcionar una visión mecanística de cómo en la etapa neonatal ocurre cierta plasticidad celular, a manera de un aumento en la densidad celular hipotalámica, en respuesta a la separación materna, cambios que permanecen hasta la edad adulta.

Este trabajo nos provee de una posible explicación mecanística para el fenómeno observado en el trabajo anterior, donde se reporta una regulación a la alta del sistema AVPMNN. Los resultados de los experimentos de medición de la densidad celular hipotalámica y evaluación de la expresión de proteínas pro- y anti-apoptóticas sugieren que el procedimiento de MS (posiblemente a través de un aumento en la liberación de AVP) desplaza el equilibrio de las proteínas involucradas en el proceso de muerte celular programada hacia un nuevo equilibrio donde ocurre la supervivencia de un mayor número de neuronas, en varias regiones del hipotálamo; interesantemente todas estas regiones están involucradas en la respuesta al estrés. Este último detalle también nos sugiere que los cambios generados por el estrés de la MS son intentos de adaptación a un ambiente adverso, preparando al individuo para una vida estresante.

Nuestro último estudio fue derivado de otros trabajos realizados en nuestro laboratorio (en amígdala, habénula y amígdala). El hallazgo más sorprendente de estos estudios fue el descubrimiento de conexiones sinápticas reales entre AVPMNNs y células diana en la amígdala, el hipocampo y la habénula lateral. Elegimos examinar si existen proyecciones similares hacia el *locus coeruleus* (LC), una región también involucrada en la respuesta al estrés. Encontramos que las AVPMNNs también se conectan sinápticamente al LC. No sólo eso, sino que muy probablemente mediante estas inervaciones, la regulación a la alta del sistema vasopresinérgico produce cambios en el comportamiento concomitante con una mayor activación de LC y otras regiones inervadas por él; además la MS aumentó la inmunoreactividad de AVP en LC.

Estos resultados involucran una parte mucho más dinámica del sistema de AVPMNNs, su papel dentro de los circuitos cerebrales que se encargan, entre otras cosas, de procesar los estímulos ambientales y generar una respuesta fisiológica, ya sea endócrina o bien de comportamiento. El control endócrino y conductual por circuitos cerebrales vasopresinérgicos parece estar ligado anatómicamente a través de proyecciones duales hacia la pituitaria y hacia núcleos cerebrales encargados de regular el comportamiento, concretamente en el caso de este artículo el LC.

VI. BIBLIOGRAFÍA

- Ahern TH, Krug S, Carr AV, Murray EK, Fitzpatrick E, Bengston L, McCutcheon J. *Cell death atlas of the postnatal mouse ventral forebrain and hypothalamus*, 2013: effects of age and sex. Journal of Comparative Neurology
- Almazan G, Lefebvre DL & Zingg HH. *Ontogeny of hypothalamic vasopressin, oxytocin and somatostatin gene expression*, 1989. Developmental Brain Research
- Armstrong WE. *Chapter 15: Hypothalamic Supraoptic and Paraventricular Nuclei*, 2004. In: Paxinos G, editor. The rat nervous system
- Aston-Jones G & Waterhouse B. *Locus Coeruleus: From Global Projection System to Adaptive Regulation of Behavior*, 2016. Brain research
- Barberis C, Mouillac B & Durroux T. *Structural bases of vasopressin/oxytocin receptor function*, 1998. Journal of Endocrinology
- Bonni A, Brunet A, West AE, Datta SR, Takasu MA, Greenberg ME. *Cell survival promoted by the Ras-MAPK signaling pathway by transcription-dependent and -independent mechanisms*, 1999. Science
- Brunet A, Datta SR, Greenberg ME. *Transcription-dependent and -independent control of neuronal survival by the PI3K-Akt signaling pathway*, 2001. Current Opinions in Neurobiology
- Buijs RM, de Vries GJ, van Leeuwen FW & Swaab DF. *Vasopressin and Oxytocin : Distribution and Putative Functions in the Brain*, 1983. Progress in Brain Research
- Buss RR, Sun W & Oppenheim RW. *Adaptive roles of programmed cell death during nervous system development*, 2006. Annual Reviews in Neuroscience
- Campos-Lira E, Kelly L, Seifi M, Jackson T, Giesecke T, Mutig K, Koshimizu T, Hernandez VS, Zhang L & Swinny JD. *Dynamic Modulation of Mouse Locus Coeruleus Neurons by Vasopressin 1a and 1b Receptors*, 2018, Frontiers in Neuroscience
- Castel N, Feinstein S, Cohen S & Harari N. *Vasopressinergic Innervation of the Mouse - Suprachiasmatic Nucleus: An Immuno-Electron Microscopic Analysis*, 1990. The Journal of Comparative Neurology
- Chen J, Liu Y, Soh JW & Aguilera G. *Antiapoptotic effects of vasopressin in the neuronal cell line H32 involve protein kinase C alpha and beta*, 2009. J Neurochem
- Cirulli F, Berry A & Alleva E. *Early disruption of the mother– infant relationship: effects on brain plasticity and implications for psychopathology*, 2003. Neuroscience & Biobehavioral Reviews
- Clarke PG. *Neuronal death during development in the isthmooptic nucleus of the chick: sustaining role of afferents from the tectum*, 1985. Journal of Comparative Neurology
- Cunningham ET & Sawchenko PE. *Reflex control of magnocellular vasopressin and oxytocin secretion*, 1991. Trends in Neurosciences
- de Wied. *The influence of the posterior and intermediate lobe of the pituitary and pituitary peptides on the maintenance of a conditioned avoidance response in rats*, 1965. International Journal of Neuropharmacology
- de Wied. *Long Term Effect of Vasopressin on the Maintenance of a Conditioned Avoidance Response in Rats*, 1971. Nature

- Dietrich A & Allen JD. *Vasopressin and memory II. Lesions to the hippocampus block the memory enhancing effects of AVP4–9 in the radial maze*, 1997 Allen Behavioral Brain Research

- du Vigneaud V, Lawler HC & Popenoe EA. *Enzymatic cleavage of glycinamide from vasopressin and a proposed structure for this pressor-antidiuretic hormone of the posterior pituitary*, 1953. Journal of the American Chemical Society

- Dunn FL, Brennan TJ, Nelson AE & Robertson GL. *The Role of Blood Osmolality and Volume in Regulating Vasopressin Secretion in the Rat*, 1973. The Journal of Clinical Investigation

- Engelmann M, Landgraf R & Wotjak CT. *The hypothalamic–neurohypophysial system regulates the hypothalamic–pituitary–adrenal axis under stress: An old concept revisited*, 2004. Frontiers in Neuroendocrinology

- Faedo A, Tomassy GS, Ruan Y, Teichmann H, Krauss S, Pleasure SJ, Tsai SY. *COUP-TFI coordinates cortical patterning, neurogenesis, and laminar fate and modulates MAPK/ERK, AKT, and beta-catenin signaling*, 2008. Cerebral Cortex

- Fumagalli F, Molteni R, Racagni G Riva MA. *Stress during development: Impact on neuroplasticity and relevance to psychopathology*, 2007. Progress in Neurobiology

- Gottschalk CW & Mylle M. *Micropuncture study of the mammalian urinary concentrating mechanism: evidence for the countercurrent hypothesis*, 1959. The American Journal of Physiology

- Haslam RJ & Rosson GM. *Aggregation of human blood platelets by vasopressin*, 1972. American Journal of Physiology

- Hems DA, Whitton PD and Ma GY. *Metabolic actions of vasopressin, glucagon and adrenalin in the intact rat*, 1975. Acta biochimica et biophysica

- Hernández VS, Hernández OR, Perez de la MOra M, Gömora MJ, Fuxe K, Eiden L & Zhang L. *Hypothalamic Vasopressinergic Projections Innervate Central Amygdala GABAergic Neurons: Implications for Anxiety and Stress Coping*, 2016. Frontiers in Neural Circuits

- Iwasaki Y, Kinoshita M, Ikeda K, Shiojima T, Kurihara T & Appel SH. *Trophic effect of angiotensin II, vasopressin and other peptides on the cultured ventral spinal cord of rat embryo*, 1991. Journal of the Neurological Sciences

- Kovacs KJ. *c-Fos as a transcription factor: a stressful (re)view from a functional map*, 1998. Neurochem International

- Ladd C, Huot RL, Thrivikraman KV, Nemeroe CB, Meaney MJ & Plotsky PM. *Chapter 7: Long-term behavioral and neuroendocrine adaptations to adverse early experience*, 2000. In: Mayer EA & Saper CB. Progress in Brain Research

- Landgraf R, Gertsberger R, Montkowski A, Probst JC, Wotjak CT, Holsboer F & Engelmann M. *V1 Vasopressin Receptor Antisense Oligodeoxynucleotide into Septum Reduces Vasopressin Binding, Social Discrimination Abilities, and Anxiety-Related Behavior in Rats*, 1995. The Journal of Neuroscience

- Laurent FM, Hindelang C, Klein MJ, Stoeckel ME & Felix JM. *Expression of the oxytocin and vasopressin genes in the rat hypothalamus during development: an in situ hybridization study*, 1989. Developmental Brain Research

- Ludwig M & Leng G. *Dendritic peptide release and peptide-dependent behaviours*, 2006. Nature Reviews. Neuroscience
- Maeda T. *The locus coeruleus: history*, 2000. Journal of Chemical Neuroanatomy
- Makara G, Varga J, Barna I, Pinter O, Klausz B & Zelena D. *The Vasopressin-Deficient Brattleboro Rat: Lessons for the Hypothalamo–Pituitary–Adrenal Axis Regulation*, 2012. Cellular and Molecular Neurobiology
- Milik E, Szczepanska-Sadowska E, Dobruch J, Cudnoch-Jedrzejewska A, Maslinski W. *Altered expression of V1a receptors mRNA in the brain and kidney after myocardial infarction and chronic stress*, 2014. Neuropeptides
- Mogenson GJ, Jones DL & Yim CY. *From motivation to action: funtional interface between the limbic system and the motor system*, 1980. Progress in Neuorbiology
- Morales M & Bloom FE. *The 5-HT3 receptor is present in different subpopulations of GABAergic neurons in the rat telencephalon*, 1997. The Journal of Neuroscience
- Morales M & Wang SD. *Differential Composition of 5-Hydroxytryptamine3 Receptors Synthesized in the Rat CNS and Peripheral Nervous System*, 2002. The Journal of Neuroscience
- Murgatroyd C, Patchev AV, Wu Y, Micale V, Bockmuhl Y, Fischer D, Holsboer F, Wotjak CT, Almeida OFX & Spengler D. *Dynamic DNA methylation programs persistent adverse effects of early-life stress*, 2009. Nature Neuroscience
- National Research Council, 2003. Guidelines for the Care and Use of Mammals in Neuroscience and Behavioral Research
- Oliver G & Schafer EA. *On the physiological action of extracts of pituitary body and certain other glandular organs*. 1895, The Journal of Physiology
- Oltvai ZN, Milliman CL, Korsmeyer SJ. *Bcl-2 heterodimerizes in vivo with a conserved homolog, Bax, that accelerates programmed cell death*, 1993. Cell
- Park EJ & Kwon TH. *A Minireview on Vasopressin-regulated Aquaporin-2 in Kidney Collecting Duct Cells*, 2015. Electrolyte & blood pressure
- Paxinos G & Watson C. *The rat brain in stereotaxic coordinates*, 2007, 6th edition. Elsevier
- Pellow S & File SE. *Anxiolytic and anxiogenic drug effects on exploratory activity in an elevated plus-maze: a novel test of anxiety in the rat*, 1986. Pharmacology, Biochemistry and Behavior
- Plotsky PM & Meaney MJ. *Early, postnatal experience alters hypothalamic corticotropin-releasing factor (CRF) mRNA, median eminence CRF content and stress-induced release in adult rats*, 1993. Molecular Brain Research
- Rodríguez-Ortega E, Cañadas F, Carvajal F & Cardona D. *In vivo stimulation of locus coeruleus: effects on amygdala subnuclei*, 2017. Acta Neurobiologiae Experimentalis
- Rood D & de Vries GJ. *Vasopressin Innervation of the Mouse (Mus musculus) Brain and Spinal Cord*. 2011, The Journal of Comparative Neurology
- Rosenthal W, Antaramian A, Gilbert S & Birnbaumer M. *A V2 vasopressin receptor unable to stimulate adenylyl cyclase*, 1993. The Journal of Biological Chemistry

- Sapolsky RM & Meaney MJ. *Maturation of the Adrenocortical Stress Response: Neuroendocrine Control Mechanisms and the Stress Hyporesponsive Period*, 1986. Brain Research Reviews

- Sawyer WH. *Evolution of Antidiuretic Hormones and Their Functions*, 1967. The American Journal of Medicine

- Schilling K, Schmale H, Oeding P & Pilgrim Ch. *Regulation of vasopressin expression in cultured diencephalic neurons by glucocorticoids*, 1991. Neuroendocrinology

- Schmale H, Heinsohn S & Richter D. *Structural organization of the rat gene for the arginine vasopressin-neurophysin precursor*, 1983. The EMBO Journal

- Schwarz, LA & Luo. *Organization of the locus coeruleus norepinephrine system*, 2015. Current Biology

- Simerly RB. *Chapter 17: Anatomical substrates of hypothalamic integration*, 2004. In: Paxinos G, editor. The rat nervous system

- Somlyo, AV, Sandberg RL & Somlyo AP. *Pharmacologically heterogeneous smooth muscle cell distribution in blood vessels*, 1965.The Journal of Pharmacology and Experimental Therapeutics

- Swinny JD, O'Farrell E, Bingham BC, Piel DA, Valentino RJ & Beck SG. *Neonatal rearing conditions distinctly shape locus coeruleus neuronal activity, dendritic arborization, and sensitivity to corticotrophin-releasing factor*. 2010, International Journal of Neuropsychopharmacology

- Torrico TJ & Abdijadid S. *Neuroanatomy, Limbic System*, 2019. StatPearls

- Turner RA, Pierce JG & du Vigneaud V. *The purification and the amino acid content of vasopressin preparations*, 1951. The Journal of Biological Chemistry

- Ugrumov MV. *Magnocellular vasopressin system in ontogenesis: development and regulation*, 2002. Microscopy Research and Technique

- Vaccari C, Lolait SJ & Ostrowski NL. *Comparative Distribution of Vasopressin V1b and Oxytocin Receptor Messenger Ribonucleic Acids in Brain*, 1998. Endocrinology

- Veenema AH, Blume A, Niederle D, Buwalda B & Neumann ID. *Effects of early life stress on adult male aggression and hypothalamic vasopressin and serotonin*, 2006. European Journal of Neuroscience

- Verma SP, Cruz-Huicochea R, Díaz-González L. *Univariate data analysis system: deciphering mean compositions of island and continental arc magmas, and influence of the underlying crust*, 2013. Int Geology Reviews

- Volpi S, Rabadan-Diehl C, Cawley N & Aguilera G. *Transcriptional regulation of the pituitary vasopressin V1b receptor involves a GAGA binding protein*, 2002. The Journal of Biological Chemistry

- White LD, Barone Jr S. *Qualitative and quantitative estimates of apoptosis from birth to senescence in the rat brain*, 2001. Cell Death and Differentiation

- Wolf G, Kiessig R & Landgraf R. *Levels of vasopressin and oxytocin in neurohypophysis and plasma of the postnatally developing rat and the influence of hypothyroidism on rat fetuses*, 1984. Experimental and Clinical Endocrinology

- Wotjak CT, Ludwig M & Landgraf R. *Vasopressin facilitates its own release within the rat supraoptic nucleus in vivo*, 1994. Neuroendocrinology

- Zhang L, Hernandez VS, Medina-Pizarro M, Valle-Leija P, Vega-González A & Morales T. *Maternal Hyperthyroidism in Rats Impairs Stress Coping of Adult Offspring*, 2008. Journal of Neuroscience Research
- Zhang L, Medina MP, Hernandez VS, Estrada FS & Vega-González A. *Vasopressinergic network abnormalities potentiate conditioned anxious state of rats subjected to maternal hyperthiroidism*, 2010. Neuroscience
- Zhang L & Hernández VS. *Synaptic innervation to rat hippocampus by vasopressin-immuno-positive fibres from the hypothalamic supraoptic and paraventricular nuclei*, 2013. Neuroscience
- Zhang L, Hernández VS, Swinny JD , Verma AK, Giesecke T, Emery AC, Mutig K, Garcia-Segura LM & Eiden LE. *A GABAergic cell type in the lateral habenula links hypothalamic homeostatic and midbrain motivation circuits with sex steroid signaling*, 2018. Translational Psychiatry

VII. **APÉNDICE**

Publicaciones científicas

derivadas de mis estudios de doctorado

Prolame ameliorates anxiety and spatial learning and memory impairment induced by ovariectomy in rats

Nissen I, Estrada FS, **Nava-Kopp AT**, Irles C, de-la-Peña-Diaz A,
Fernandez-G JM, Govezensky T, Zhang L.

Mis contribuciones:

- Concepción del estudio: ++
- Participación en los experimentos:
    - Procedimientos quirúrgicos   +++
    - Inmunohistoquímica   +++
    - Evaluación conductual de la ansiedad   +++
    - Evaluación del aprendizaje espacial   +++
- Análisis estadístico   +++
- Discusión de los resultados y comentarios al manuscrito: +++
- Escritura del artículo: +

(-): Ninguna contribución; (+): Contribución menor; (++): Contribución importante; (+++); Contribución crucial

Prolame ameliorates anxiety and spatial learning and memory impairment induced by ovariectomy in rats

Itzel Nissen [a,1], Felipe S. Estrada [a,1], Alicia T. Nava-Kopp [a], Claudine Irles [a], Aurora de-la-Peña-Diaz [b], Juan M. Fernandez-G [c], Tzipe Govezensky [d], Limei Zhang [a,*]

[a] Departamento de Fisiología, Universidad Nacional Autónoma de México (UNAM), Av. Universidad 3000, Mexico City, 04510, Mexico
[b] Departamento de Farmacología, Facultad de Medicina, Universidad Nacional Autónoma de México (UNAM), Av. Universidad 3000, Mexico City, 04510, Mexico
[c] Instituto de Química, Universidad Nacional Autónoma de México (UNAM), Av. Universidad 3000, Mexico City, 04510, Mexico
[d] Instituto de Investigaciones Biomedicas, Universidad Nacional Autónoma de México (UNAM), Av. Universidad 3000, Mexico City, 04510, Mexico

ARTICLE INFO

ABSTRACT

N-(3-hydroxy-1, 3, 5 (10) estratrien-17beta-yl)-3-hydroxypropylamine (17β aminoestrogen, prolame) is a steroidal compound with weak estrogen-related trophic-proliferative effects in uterus. Contrasting with 17β-estradiol (E2) pro-coagulant effects, this compound has high anticoagulant and antiplatelet effects. It has been extensively demonstrated that E2 plays important roles in brain function. However, prolame's influence on central nervous system has not been documented. In this study, we evaluated the effects of prolame replacement in young ovariectomized rats on spatial learning and memory and anxiety, correlating pyramidal cell dendritic spine density changes and neuronal nitric oxide synthase (nNOS) expression in the hippocampus. Ovariectomized young rats were treated with prolame for 4 weeks. Three other groups were used as physiological, pathological, and pharmacological references as follow: gonadally intact cycling females, ovariectomized, and ovariectomized with 17β-estradiol treatment respectively, for the same time period. Experiment 1 investigated the behavioral effects of prolame on anxiety and spatial learning using elevated plus maze (EPM) and Morris water maze (MWM) paradigms respectively. Experiment 2 studied the dendritic spine density and neuronal nitric oxide synthase expression in the hippocampus of the 4 experimental groups. Similar to estradiol, prolame reversed the anxiogenic effects of ovariectomy, evaluated by EPM, and enhanced MWM performance to the level of gonadally intact subjects. Hippocampi from prolame-treated rats exhibited enhanced nNOS immunoreactivity and its relocation in dendritic compartments, as well as recovery of dendritic spine density loss in pyramidal neurons. Hence, prolame may provide an alternative option for ameliorating neurological symptoms caused by surgical menopause.

1. Introduction

Estrogens regulate a host of physiological processes, but most important among those that affect reproduction and basic physiological functions are mammary gland development, reproductive success, hypothalamus–hypophyseal functions, bone integrity, cardiovascular protection, and immune response [1]. Two forms of the nuclear estrogen receptor (ER) are found in mammalian species. These two receptor subtypes are products of different genes and are designated ER α (ERα) and ER β (ERβ). Both monomeric forms of each receptor subtype are approximately 60 kDa, and both subtypes bind 17β-estradiol (E2) with high affinity, but differ in DNA-binding affinity [2]. The ERα and ERβ can be co-expressed in some target tissues, but they also exhibit different tissue or cell expression patterns. A small amount (around

3%) of ERs are found to be located in the plasma membrane [3] and treatment with E2 stimulates a phosphoinositide cascade as well as activation of adenylate cyclase, suggesting that the ERs are coupled to $G\alpha_q$ and $G\alpha_s$ [3,4].

On the other hand, while estrogen's effects on mammal's peripheral physiology have been extensively explored and characterized, our knowledge on estrogen's influence on central nervous system (CNS) and its consequences on cognition and behavior are still fragmentary and are currently being intensively studied. E2 exerts potent and wide-ranging effects on the morphology and function in different regions of the CNS [5]. Brain targets for E2 effects on anxiety and depression include the hippocampus and amygdala. Administration of E2, compared to vehicle, subcutaneously or directly into the hippocampus or amygdala of ovariectomized rats decreases anxiety and depressive behaviors [6,7].

Estrogen deficiency due to natural or surgical menopause is associated with cognitive and emotional impairment [8]. Hormone replacement therapy (HRT) has proven to be effective in preventing and reversing

---

some of these conditions, including neurological impairments such as spatial memory and learning deficiencies [9], development of anxiety-like behavior [7], and (at microscopical level) the loss of synaptic and dendritic spine density [10]. However, the increased risk of breast cancer [11] and venous thromboembolism [12,13] produced by conventional estrogenic treatment remains a major drawback and a strong motive to find new therapeutic strategies. This need has been underscored in the Women's Health Initiative (WHI) [14].

The monoamino-estrogen N-(3-hydroxy-1, 3, 5 (10) estratrien-17beta-yl)-3-hydroxypropylamine (*prolame*) belongs to the group of 17β-aminoestrogens-estradiol analogs, such as prodiame, buame, and pentolame [15]. These estrogen derivatives posses a modification of the steroid nucleus in the C-17-amino-side chain position (with an increased length in the amino-alcohol side chain). Since it was initially synthesized in 1985 [16] this steroidal compound has been shown to have low estrogen-related trophic-proliferative effects in uterus [17] [18] and prolonged anticoagulant/antiplatelet effects [17,19,20]. These results seem to be linked to an increased nitric oxide (NO) production by platelets and endothelial cells [21]. It has been reported that this amino-estrogen compound activates ER-dependent reporter gene expression, preferentially mediated through the ERα, whereas less activation occurred through the ERβ [17]. However, the effects of this amino-estrogen on the CNS have not been properly evaluated, except for a recent paper where Lemini and Canchola [22] reported that prolame promotes sexual behavior in ovariectomized young female rats. Ovariectomy, surgical removal of the ovaries, is a common animal model for studying postmenopausal changes in adult female rats due to ovarian hormone loss [7,23]. This procedure has been utilized mainly to assess E2 behavioral effects. Ovariectomy increases anxiety and depressive-like behaviors and impairs spatial learning and memory. Subcutaneous administration of E2 can reverse these effects in several tasks [8,24–27].

It has been shown that NO mediates neuronal signaling and processes involving synaptic plasticity, such as long-term potentiation (LTP), widely considered one of the major cellular mechanisms underlying learning and memory [28–30]. NO is able to facilitate synaptic transmission in the hippocampus, contributing to LTP [31,32]. NO formation, by neuronal NO synthase (nNOS), has been shown to depend on the estrogen mediated association of nNOS with NMDA receptors, which enhances nNOS activation in preoptic neurons [33]. Estrogen increases spine density via activation of NMDA receptors [6], and triggers nNOS expression (for a review see [34]), inducing the activation of NO signaling, which may contribute to learning and memory.

In this study, we hypothesized that chronic prolame administration enhances the production of nNOS, which reverses the detrimental effects on dendritic spine density produced by chronic loss of estrogen levels in the brain, diminishing anxiety and spatial learning and memory deficiency caused by ovariectomy. Our control/reference groups included: gonadally intact cycling female rats, ovariectomized rats without any treatment, and ovariectomized rats with E2 treatment.

2. Materials and methods

2.1. Prolame synthesis

The detailed process for prolame synthesis was described elsewhere [35]. Briefly, a toluene solution of 3-hydroxypropylamine and estrone was refluxed for 12 h with a Dean–Stark trap and then vacuum concentrated. The obtained solid product was dissolved in methanol, and reacted with sodium borohydride. The obtained product was filtered, washed with water and recrystallized from methanol–water. Estrone, 3-hydroxypropylamine, toluene, methanol and sodium borohydride were purchased from Sigma-Aldrich Chemical Co (St. Louis MO, USA). The structural formula of prolame is depicted in Fig. 1.
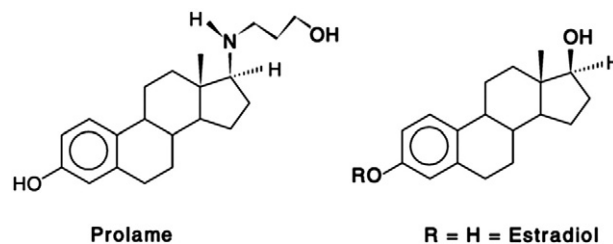

Fig. 1. Structural formula of N-(3-hydroxy-1, 3, 5(10) estratrien-17β-yl)-3-hydroxypropylamine, *prolame,* (A) in comparison to 17β-estradiol (B).

2.2. Animals

Wistar rats from the Faculty of Medicine, UNAM animal facility were used in this study. All animal procedures were approved by the local ethical committee (*Comisión de Investigación y Ética de la Facultad de Medicina*, UNAM, ID 044-2011), in accordance with the principles exposed in the Handbook for the Use of Animals in Neuroscience Research (Society for Neuroscience. Washington, D.D.1991). Animals were housed in an artificial 12-h light schedule (light on at 20:00) in a room with temperature between 20 °C and 24 °C with adequate ventilation and given access to standard rat chow and water *ad libitum*.

Forty-eight female rats were used in this study. Animals were assigned to the following groups: gonadally intact cycling (GI, $n = 12$), ovariectomized (Ovx, $n = 12$), ovariectomized plus estradiol treatment (OvxE, $n = 12$) and ovariectomized plus prolame treatment (OvxP, $n = 12$). The GI, Ovx, and OvxE groups served as the physiological, pathological and pharmacological reference groups. Rats were bilaterally ovariectomized according to procedures described elsewhere [36], except for GI group, which only received sham surgery. These procedures were performed at postnatal day 90 (PND90) under *i.p.* ketamine (90 mg/kg) and xylazine (10 mg/kg) anesthesia.

2.3. Prolame and E2 treatment

Daily subcutaneous injections of E2 (Sigma-Aldrich Co, E8875, 50μg/kg) and a molar equivalent dose of prolame (60 μg/kg) were applied for a month to the OvxE and OvxP groups respectively, starting 4 weeks after the surgery. The dose of E2 was determined according to previous studies [37]. Treatments were applied for a month to the OvxE and OvxP groups respectively, starting 4 weeks after the surgery. The drugs were diluted (10%) in vehicle containing glycerol and distilled water 1:1. GI and Ovx groups received vehicle only. It is worth mentioning that we used a model of 4-week delay between Ovx and hormone replacement, which was determined for the purposes of this study. This delay is within the 2 to 8 week window in which acute estrogen replacement has previously shown to influence behavior effectively [38].

2.4. Experiment 1—effects of prolame treatment on anxiety-like behavior and spatial memory performance

The behavioral tests were conducted after 1 month of treatment, during animal activity period (light-off period).

2.4.1. Elevated plus maze test (EPM)
EPM was used to assess the unconditioned acute anxious state and the procedure was described elsewhere [39]. Briefly, the plus maze was made from wood with conventional dimensions. The only relevant modification is that the open arms were surrounded by an upwards-protruding edge of 0.5 cm. This latter measure prevents the rat from falling accidentally without jeopardizing the elemental features of the setting. The EPM was lit with dim red light and monitored by closed-circuit television (CCTV). The maze was cleaned with neutral detergent and water and dried before each rat was tested.

Prior to the test, rats of each experimental group were habituated by handling and placing them in an open field box (50 cm × 50 cm × 50 cm, made from wood) for the previous three days and immediately before the EPM, 5 min per session. This procedure is based on previous observations from our group that gentle handling and pre-exposure to a novel environment before testing in the EPM increases the motor activity and the likelihood of entering to the open arms of the maze [39]. This procedure was also reported previously in the literature [40]. At the beginning of the test, rats were placed on the center of the maze heading to an open arm and then left for free exploratory activity during 5 min. The total time spent on the open arms (with all limbs placed out of the central square) was the operational definition of unconditioned anxiety (exploration vs. avoidance). The percent of the 5-min test time spent in the open arms was the dependent variable used for statistical analysis.

2.4.2. Morris water maze test (MWM)

The MWM [41] was conducted the day after the EPM. A black circular pool (156 cm diameter, 80 cm high) filled with 30 cm height of water (25 °C ± 1 °C) was used for this cognitive test. Some visual cues were placed on the pool wall. A circular black escape platform (12 cm diameter) was submerged 1 cm below the water surface. Rats were habituated to the MWM by 5 training trials performed one day before the test. These training trials followed the same protocol mentioned below, except for a different location of the platform. On the day of the test, rats were allowed to swim up to 60 sec in order to find the new location of the escape platform. If the experimental subjects had not found the platform when the allowed time-lapse was over, they were guided to it. Once on the platform, rats were permitted to stay for 5 seconds to let them observe the location of the platform. Eight acquisition trials were performed for every rat, with a 5-min interval between each one. The time latency for reaching the platform was measured.

2.5. Experiment 2—effects of prolame treatment on the number and morphology of nNOS expressing cells and dendritic spine densities of projection neurons in the hippocampus

After performing the MWM, five rats from each group were randomly chosen for histological studies, excepting the GI group in which the selection was based on observation from vaginal smears - only rats in the proestrous stage were chosen. It is worth pointing out that the proestrus in female rats represents the highest estrogen blood levels found during estral cycle [42] [43]. We chose this criterion to make an equivalent comparison with the other two treatment groups and also to minimize the intragroupal variability of measured histological parameters, which according to the literature [44,45], depend critically on the intracerebral estrogen levels. Vaginal smears obtained with cotton swabs were stained using Papanicolau staining procedure. The presence of nucleated epithelial cells in the vaginal smear was used as a criterion for proestrus determination [46].

For perfusion–fixation, rats were anesthetized with an overdose of sodium pentobarbital (Sedalpharma, México, Mexico, 63 mg/kg b. w., i.p.) and transcardially perfused with 0.9% saline, followed by ice-cold fixative containing 4% paraformaldehyde dissolved in 0.1 M phosphate buffer (PB, pH 7.4), for 15 min. Brains were removed, thoroughly rinsed in PB and blocked sagitally in two halves, for both nNOS immunohistochemistry and Golgi–Cox impregnation.

One half of each rat brain was used for nNOS immunohistochemistry. The brain tissue containing dorsal hippocampus was coronally sliced using a Leica vibratome (VT1000). The thickness of the section was 50 μm. One out of every 4 sections from Bregma −2.40 mm to −4.00 mm [47] (8 sections per rat) were processed for nNOS free-floating immunoreaction. Sections were first blocked with 20% normal horse serum (NHS) in Tris-buffered (0.05 M, pH 7.4) saline (0.9%) plus 0.3% of Triton X-100 (Tris-buffered saline with Triton, TBST) for 1 h at room temperature and then immunoreacted with mouse anti-nNOS (1:1000, Sigma-Aldrich Co. in TBST with 1% NHS). Sections were incubated overnight at 4 °C with gentle shaking. After corresponding washings (3 × 10'), sections were further incubated with secondary antibody donkey anti-mouse Alexa fluor 488 (1:1000, Invitrogen, Life Technologies, Carlsbad, California, USA, in TBST with 1% NHS), at 4 °C overnight. Sections were then thoroughly rinsed and mounted with Vectashield (Vector Laboratories, Inc, Burlingame, CA, USA).

For cell counting, eight slices from each rat were taken at 150 μm interval. Two independent researchers who were blind to the experimental conditions carried out cell counting. Principal neurons located in CA1, CA3 and dentate gyrus (DG), immunoreactive to nNOS were counted using a modified method from [48,49]. Nikon ECLIPSE 50i fluorescence microscope at 40× objective with B-2A longpass emission filter was used. Counting of nNOS + cells was performed under microscope, inside a length of 540 μm (corresponded to the diameter of the 40× objective field) of the cell body layer, i.e. pyramidal layer for CA1 and CA3, and granule cell layer for DG. Neurons were differentiated from glial cells by the morphological characteristics of pyramidal and granule cells. Due to the cellular heterogeneity of the hippocampal subregions, counting fields were not chosen randomly but 2 fields per each subregion (i.e. CA1, CA2/3 and DG) per section, namely, from the CA1-CA2 border, two consecutive fields to CA1 direction for "CA1" counting and two consecutive fields to CA2/3 direction for "CA2/3" counting. For DG granule cell layer only the supra-pyramidal segment in the hilar region was chosen for counting. This criterion was set to minimize the possible errors due to the anatomo-functional heterogeneity of studied region.

The remaining halves of the rat brain tissue underwent Golgi–Cox stain protocol to assess dendritic spine densities of hippocampus projection neurons. The detailed procedure was described elsewhere [50]. Briefly, the central one-third parts of the forebrain, along antero-posterior axis, were cut to form blocks of approximately 10 mm between the rostral and caudal edges. Tissues were rinsed briefly in PB and then immersed in sequenced impregnation solutions following the fabricant's indications (FD Rapid GolgiStain kit, FD NeuroTechnologies, Ellicott City, MD, USA) for 2 weeks in the dark. Sections of 150 μm were sliced using a vibratome and mounted on gelatine-coated glass slides. These sections were dried naturally at room temperature in the dark for at least two days and then stained with a staining solution included in the kit mentioned above. Samples were followed by dehydration and processed for permanent mounting with Permount (Electron Microscopy Sciences, PA, USA) mounting medium.

Spine densities were counted on the primary basilar branches, classified as left/right basilar and primary, secondary and tertiary apical dendritic branches from CA1 and CA2/3 pyramidal neurons at 100x light microscope and traced with the help of a drawing tube. Six randomly chosen segments of 10 μm length per each subject/hippocampal subregion/dendritic branches were analyzed, $n = 30$, i.e., 5 subjects × 6 segments in each classified dendritic branch.

2.6. Statistical analysis

Quantitative results were expressed as mean ± standard error of mean (SEM). Multiple pair-comparisons were performed using Tukey's test after ordinary one-way analysis of variance (ANOVA), except for the MWM data where repeated measures ANOVA was performed, using 'trials' as the within-subject factor and 'treatment' as between-subject factor, followed by Tukey's test. Post-hoc differences were considered statistically significant at a value $p < 0.05$ (*$p < 0.05$, **$p < 0.01$, ***$p < 0.001$). The analysis was done using SPSS release 9.0 software.

3. Results

3.1. Experiment 1. Prolame reversed anxiety-like behavior exhibited during EPM

After 1 month of treatment, EPM was used to assess anxiety-like behavior. Fig. 2 depicts the EPM performance of the 4 tested groups, expressed as percentage of time spent in the open arms during the 5-min test. A one-way ANOVA showed that the time spent on the open arms differed significantly between the treatment groups, $F(3, 44) = 5.174$, $p = 0.0036$. Furthermore, post-hoc Tukey's multiple comparison test showed that gonadally intact cycling (GI) (29.13 ± 3.45) and prolame-treated (OvxP) rats (33.91 ± 2.87) spent significantly more time in the open arms than ovariectomized (Ovx) rats (16.64 ± 2.86). All other comparisons were not significant.

3.2. Prolame treated subjects exhibited enhanced spatial learning and memory during MWM

Following the EPM, the rats underwent MWM habituation test as described in Materials and methods. All groups acquired the platform location, as supported by decreased latency to locate the platform (or decreased swimming time to the platform) across the 8 trails (Fig. 3). There was no apparent difference regarding swimming speed. Repeated measurements analysis showed statistical differences among trials (multivariate tests $F(7, 38) = 27.75$, $p < 0.0001$), among treatments $(F(3, 44) = 4.95$, $p = 0.005$), but no interaction between trial and treatment (multivariate tests $F(7, 40) = 1.651$, $p = 0.485$). Post-hoc Tukey's analysis showed that trials from 3 to 8 were statistically different $(p < 0.05)$ from the first trial, in this trials GI, OvxE and OvxP rats found the platform faster than Ovx rats. (For Ovx vs GI $p = 0.017$; for Ovx vs OvxE $p = 0.051$ and for Ovx vs GI $p = 0.008$).

3.3. Prolame-treated subjects exhibited enhanced nNOS immunoreactivity and dendritic relocation in the hippocampus

Neurons from CA1, CA2/CA3 and the DG cell body layers expressing nNOS were counted in the dorsal hippocampus (Fig. 4A). A one way ANOVA showed a significant effect of treatment on CA1 $(F(3,316) = 148.9$, $p < 0.0001)$, CA2/CA3 $(F(3,316) = 65.96$, $p < 0.0001)$ and DG $(F(3,316) = 41.89$, $p < 0.0001)$. Post-hoc analyses showed a reduction in the number of neurons that express nNOS in Ovx compared to GI in all areas $(p < 0.001)$. However nNOS expression was restored in both OvxE and OvxP $(p < 0.001)$ (Fig. 4A, right panel).
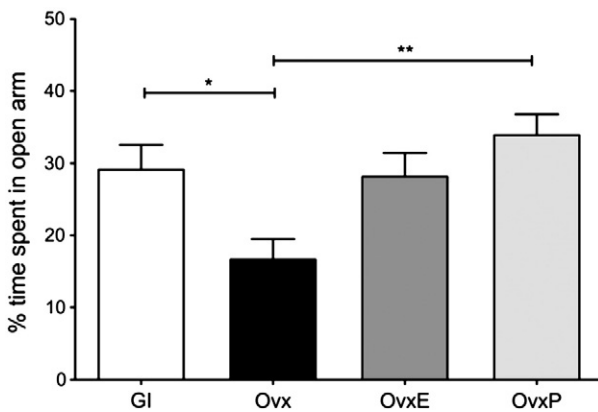

Fig. 2. Prolame and estradiol treatments reversed anxiety-like behavior exhibited during Elevated plus maze (EPM) test. GI: gonadally intact, Ovx: ovariectomized, OvxE: ovariectomized with estradiol (E2), OvxP: ovariectomized with prolame. Values represent mean ± SEM of the percentage of time that animals spent in the open arms during the 5-min test. (*$p < 0.05$, **$p < 0.01$, $n = 12$).
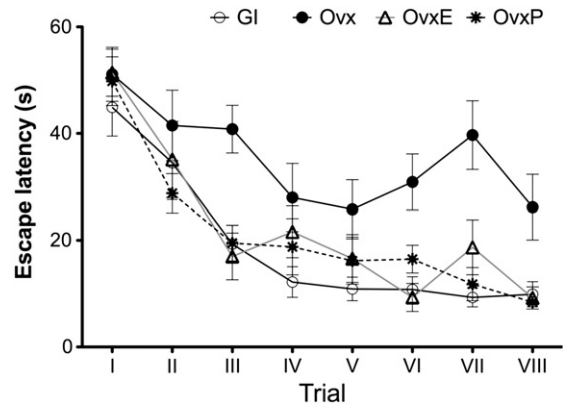

Fig. 3. Prolame treated subjects exhibited enhanced spatial learning and memory during Morris water maze test (MWM). GI: Gonadally Intact, Ovx: ovariectomized, OvxE: ovariectomized with estradiol, OvxP: ovariectomized with prolame. Values represent mean ± SEM of escape latencies along eight trials. Post-hoc Tukey's analysis showed that trials from 3 to 8 were statistically different $(p < 0.05)$ from the first trial, in these trials GI, OvxE and OvxP rats found the platform faster than Ovx rats. (For Ovx vs GI $p = 0.017$; for Ovx vs OvxE $p = 0.051$ and for Ovx vs GI $p = 0.008$), $n = 12$.

Fig. 4B depicts nNOS immunoreactivity in the DG. Compared with the GI group, ovarian hormone loss not only diminished nNOS positive cell number, but also changed its expression pattern: the presence of nNOS in the main dendritic shaft seen in the GI group (Fig. 4B insert of "GI") had disappeared in the Ovx group (Fig. 4B insert of "Ovx"). Treatment either with estradiol or prolame restored this expression pattern after 1 month (Fig. 4B, insert of "OvxE" and "OvxP").

3.4. Prolame-treated subjects exhibited dendritic spine density recovery of pyramidal neurons

A one-way ANOVA showed a significant effect of treatment on dendritic spine density of pyramidal cells in CA1, on the right basilar branch $(F(3,116) = 19.38$, $p < 0.0001)$, left basilar branch $(F(3,116) = 23.53$, $p < 0.0001)$, secondary apical branch $(F(3,116) = 48.89$, $p < 0.0001)$ and tertiary apical branch $(F(3,116) = 62.90$, $p < 0.0001)$.

CA2/3 also showed differences on the right basilar branch $(F(3,116) = 24.23$, $p < 0.0001)$, left basilar branch $(F(3,116) = 63.66$, $p < 0.0001)$, secondary apical branch $(F(3,116) = 17.63$, $p < 0.0001)$ and tertiary apical branch $(F(3,116) = 239$, $p < 0.0001)$.

Post-hoc analyses showed higher dendritic spine density in GI (right and left basilar, secondary and tertiary), and OvxE (right basilar, left basilar, secondary and tertiary) in comparison with Ovx. Prolame reversed dendritic spine loss in OvxP, in particular in the left basilar, secondary and tertiary branches (Fig. 5A) of CA1 and the right basilar, left basilar, secondary and tertiary branches (Fig. 5B) of CA2/3.

4. Discussion

The present study demonstrated for the first time that prolame, which has previously showed to have weak estrogenic effects, 22- to 36-fold less potent than estradiol in uterus [18], can reverse anxiogenesis and impaired spatial learning and memory produced by ovarian hormone loss in ovariectomized young rats. Furthermore, prolame was able to increase nNOS expression and recover the dendritic location of this enzyme in the hippocampus in a similar way as E2. Moreover, the reduction of dendritic spines in the principal neurons due to the loss of ovarian hormones was also restored after prolame treatment, matching the levels of GI and E2 treated rats.

Estrogens have many effects in the central nervous system, including effects on anxiety and depression behavior. Results of the EPM experiments confirmed previous reports in which the loss of ovarian function caused by surgical removal of ovaries, causes anxiety-like behavior [51].
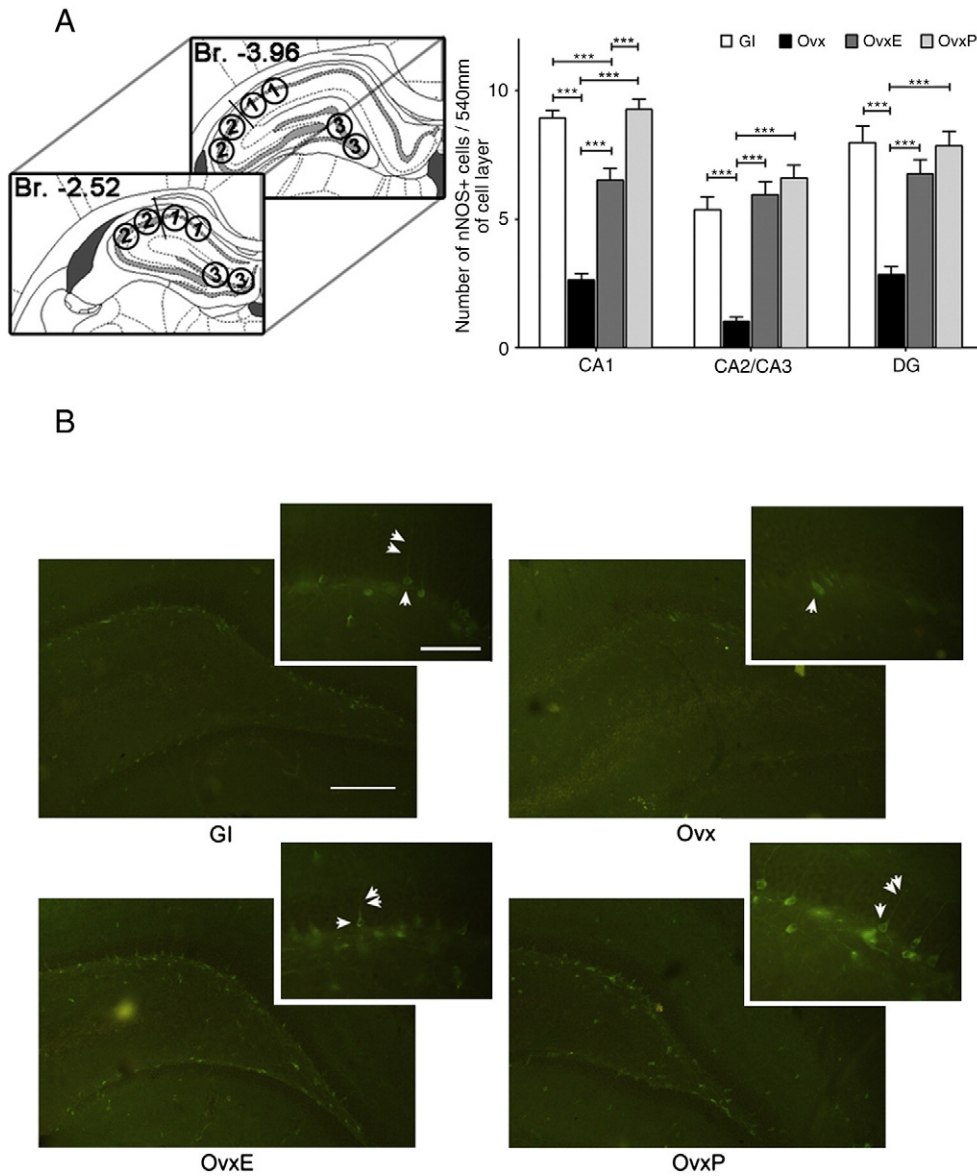
Fig. 4. Prolame-treated subjects exhibited enhanced nNOS immunoreactivity and nNOS expression relocation in the hippocampus from GI, Ovx, OvxE and OvxP groups. (A) Number of cells expressing nNOS immunoreactivity in the DG, CA1 and CA2/3 regions of the pyramidal cell layer of the hippocampus (right panel). In the inserted brain plate, the measurement sites are indicated using black circles. "1," "2" and "3" indicate CA1, CA2/3 and DG measured regions respectively (left panel). Values represent the mean $\pm$ SEM of nNOS + IR cell counts per 540 μm length of pyramidal cell layer for CA1 and CA2/3 and granule cell layer for the DG (***$p < 0.001$, $n = 80$). (B) Representative photomicrographs of examples showing nNOS immunoreactivity in the DG of the four groups (scale bars: 250 μm for low magnification photos and 100 μm for inserts). Double arrows indicate neuronal dendrites and single arrows denote soma.

Furthermore, prolame treatment reversed anxiety-like behavior, matching the effects of estradiol on EPM. Estrogenic signaling on anxiety may depend upon many factors. Administration of E2, compared to vehicle, subcutaneously or directly into the hippocampus or amygdala of ovariectomized rats decreases anxiety and depressive behavior (for a review see [7]). Administration of an ER antagonist to the hippocampus, but not to the amygdala, increases anxiety and depression behavior of naturally receptive female rats [7]. Results from this study support previous findings and suggests that prolame could reverse the anxiogenic effects caused by ovarian hormone loss.

In the MWM, our data confirmed a recent report [52], which showed that ovarian hormone loss due to ovariectomy in rat impairs MWM performance, revealed by escape latency. Results from our study showed that the Ovx group had significant increases in escape latencies at least three trials compared with all three other groups, i.e. GI, OvxE and OvxP. There were no significant differences at any time point among the latter ones, demonstrating that prolame

effectively repaired the detrimental effect of ovariectomy on this spatial learning and memory assessment, so as E2 treatment. Interestingly, this recent report [52] also showed that the use of nitric oxide synthase (NOS) inhibitor, N(G)-nitro-L-arginine methyl ester (L-NAME) abolished the estradiol-mediated restoration of spatial learning and memory in ovariectomized rats evaluated in MWM. This result indicated an interaction of NO and E2 in this specific brain function. Our results concerning nNOS expression in hippocampus showed a significant loss of nNOS positive cells in the pyramidal and granular cell layers of the Ovx group, in which nNOS expression was exclusively found in the cell bodies. Treatment with both E2 and prolame reversed these detrimental effects, which is consistent with the improvement of MWM performance. These data, together with the results published by Azizi-Malekabadi et al., suggest that the modifications in nNOS expression and MWM performance produced by prolame could have a causal relationship. Concerning the distinct sub-cellular localization of nNOS, the expression of this enzyme in the Ovx
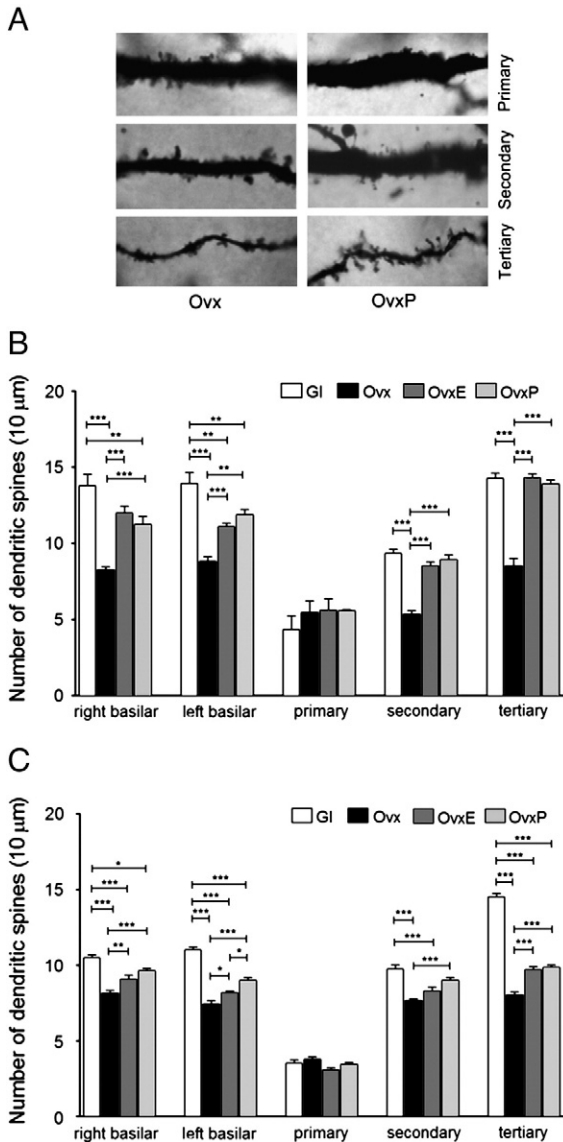
Fig. 5. Golgi–Cox impregnation revealed recovery of dendritic spine density loss in hippocampal pyramidal neurons of prolame treated rats. (A) Photomicrographs of examples showing dendritic spine loss in the Ovx and recovery in OvxP. Histogram represents the analysis of dendritic spine density found in 10 μm segments of pyramidal neurons in CA1 (B) and CA2/3 (C) in the hippocampus. "Right basilar" and "left basilar" refer to the counting from the basilar dendritic branches, "primary," "secondary" and "tertiary" refer to the counting from the apical dendrites. Values are expressed as mean ± SEM. (*$p < 0.05$, **$p < 0.01$, ***$p < 0.001$, $n = 30$).

(PI3K)/Akt signaling pathways, mainly by nuclear- and membrane-mediated ERs [54–56]. Indeed, Akt activation has been observed in multiple brain areas and has been associated with spine formation. Additionally, Akt pathway plays a well-known role in cell survival, and has also been implicated in estrogen's neuroprotective actions (for a review see [6]). Akt has a number of downstream targets including the anti-apoptotic member Bcl-2 and endothelial NOS, among others. Recently, the GABA A receptor has been shown to be a substrate of Akt. Phosphorylation of GABA A receptor by Akt increases its cell surface expression, further linking ER-mediated PI3K/Akt signaling with regulation of synaptic plasticity.

Interestingly prolame, which has been demonstrated to have weak estrogenic effects compared to E2 [18], had similar effects on the parameters measured in this report. Indeed, *in vitro* experiments have shown that prolame is less able to: 1) displace E2 bound to cytosolic ER and 2) activate ER dependent reporter gene CAT expression in comparison with estradiol [17], although it is possible that the degree of inhibition observed may represent an underestimation, due to the *in-vitro*-experiment limitations. Nevertheless, decreased ER activation results in diminished ER protein expression in the hippocampus [57]. As a result, we would have expected a reduced prolame responsiveness, but this was not the case. One option may be that prolame structure may alter its interaction with ERs, changing its binding to promoter sites and activating transcription of important estrogen responsive genes as efficiently as E2. Another possibility could be that the negative regulation of the genomic and non-genomic mechanisms induced by this amino-estrogen is reduced in comparison to E2, promoting an enhanced responsiveness. A third possibility could be that prolame effects may be more dependent on non-genomic mechanisms, using multiple membrane-associated ERs or novel G-protein-coupled E2 receptors, such as the GPR30, that responds to estrogen with kinase activation as well as transcriptional responses [58–60]. To elucidate the mechanisms underlying prolame's influence in CNS further molecular biology studies are required.

5. Conclusion

Prolame treatment of ovariectomized rats has important effects on the central nervous system, as shown in this study. The behavioral effects include restoring spatial learning and memory and ameliorating high anxiety caused by ovariectomy in young rats. At anatomical neuropharmacology level, we showed an enhanced expression of nNOS and restoration of dendritic spine density in the principal neurons of the hippocampal formation.

References

[1] Stormshak F, Bishop CV. Board-invited review: estrogen and progesterone signaling: genomic and nongenomic actions in domestic ruminants. J Anim Sci 2008;86: 299–315.
[2] Cowley SM, Hoare S, Mosselman S, Parker MG. Estrogen receptors alpha and beta form heterodimers on DNA. J Biol Chem 1997;272:19858–62.
[3] Razandi M, Pedram A, Greene GL, Levin ER. Cell membrane and nuclear estrogen receptors (ERs) originate from a single transcript: studies of ERalpha and ERbeta expressed in Chinese hamster ovary cells. Mol Endocrinol 1999;13:307–19.
[4] Razandi M, Pedram A, Merchenthaler I, Greene GL, Levin ER. Plasma membrane estrogen receptors exist and functions as dimers. Mol Endocrinol 2004;18: 2854–65.

group was restricted to the soma, in contrast with a strong signal in soma and apical dendrites in OvxE and OvxP. The enzyme nNOS has been found in dendritic spines and interacts with several proteins. The distribution we observed closely resembled that of Dreyer et al. [53], where NOS interacting protein (NOSIP) modulates nNOS subcellular localization by interacting with nNOS. A non-nuclear localization of NOSIP was found after NMDA receptor-evoked activity of neurons, while silencing neuronal activity favors a nuclear localization [53]. Taken together, these results indicate that prolame and E2 treatments normalize nNOS subcellular localization, probably promoting NMDA receptor-evoked activity of hippocampal neurons, thus regulating NO production.

Analysis of the results obtained by quantification of dendritic spine density showed that prolame and E2 reversed dendritic spine loss in the hippocampus. This may be explained by the fact that estrogens, and probably prolame too, can activate phosphatidylinositol-3-OH kinase

[5] Maggi A, Ciana P, Belcredito S, Vegeto E. Estrogens in the nervous system: mechanisms and nonreproductive functions. Annu Rev Physiol 2004;66:291–313.

[6] Spencer JL, Waters EM, Romeo RD, Wood GE, Milner TA, McEwen BS. Uncovering the mechanisms of estrogen effects on hippocampal function. Front Neuroendocrinol 2008;29:219–37.

[7] Walf AA, Frye CA. A review and update of mechanisms of estrogen in the hippocampus and amygdala for anxiety and depression behavior. Neuropsychopharmacology 2006;31:1097–111.

[8] Walf AA, Paris JJ, Frye CA. Chronic estradiol replacement to aged female rats reduces anxiety-like and depression-like behavior and enhances cognitive performance. Psychoneuroendocrinology 2009;34:909–16.

[9] Talboom JS, Williams BJ, Baxley ER, West SG, Bimonte-Nelson HA. Higher levels of estradiol replacement correlate with better spatial memory in surgically menopausal young and middle-aged rats. Neurobiol Learn Mem 2008;90:155–63.

[10] Woolley CS, McEwen BS. Estradiol mediates fluctuation in hippocampal synapse density during the estrous cycle in the adult rat. J Neurosci 1992;12:2549–54.

[11] Stahlberg C, Pedersen AT, Lynge E, Andersen ZJ, Keiding N, Hundrup YA, et al. Increased risk of breast cancer following different regimens of hormone replacement therapy frequently used in Europe. Int J Cancer 2004;109:721–7.

[12] Daly E, Vessey MP, Hawkins MM, Carson JL, Gough P, Marsh S. Risk of venous thromboembolism in users of hormone replacement therapy. Lancet 1996;348: 977–80.

[13] Rosendaal FR, Helmerhorst FM, Vandenbroucke JP. Female hormones and thrombosis. Arterioscler Thromb Vasc Biol 2002;22:201–10.

[14] Coker LH, Espeland MA, Rapp SR, Legault C, Resnick SM, Hogan P, et al. Postmenopausal hormone therapy and cognitive outcomes: the Women's Health Initiative Memory Study (WHIMS). J Steroid Biochem Mol Biol 2010;118:304–10.

[15] Mandoki JJ, Rubio-Poo C, Lemini C, De la Pena A, Fernandez JM, Garcia-Mondragon J, et al. The effects of five new 17 beta-amino-estrogens, buame, endiame, etolame, picae, and procame on blood clotting time. Proc West Pharmacol Soc 1991;34: 99–106.

[16] Fernandez JM, Rubio-Arroyo MF, Soriano-Garcia M, Toscano RA, Perez-Cesar MC. Synthesis and molecular structure of prolame, N-(3-hydroxy-1,3,5(10)-estratrien-17 beta-yl)-3-hydroxypropylamine; an amino-estrogen with prolonged anticoagulant and brief estrogenic effects. Steroids 1985;45:151–7.

[17] Jaimez R, Cooney A, Jackson K, Lemus AE, Lemini C, Cardenas M, et al. In vivo estrogen bioactivities and in vitro estrogen receptor binding and transcriptional activities of anticoagulant synthetic 17beta-aminoestrogens. J Steroid Biochem Mol Biol 2000;73:59–66.

[18] Lemini C, Franco Y, Avila ME, Jaimez R. Estrogenic effects of 17 beta-aminoestrogens assessed in uteri of rats and mice. Eur J Pharmacol 2005;510: 235–9.

[19] Lemini C, Rubio-Poo C, Silva G, Garcia-Mondragon J, Zavala E, Mendoza-Patino N, et al. Anticoagulant and estrogenic effects of two new 17 beta-aminoestrogens, buto-lame [17 beta-(4-hydroxy-1-butylamino)-1,3,5(10)-estratrien-3-ol] and pentolame [17 beta-(5-hydroxy-1-pentylamino)-1,3,5(10)-estratrien-3-ol]. Steroids 1993;58: 457–61.

[20] De la Pena A, Banos G, Izaguirre R, Mandoki JJ, Fernandez JM. Comparative effect of synthetic aminoestrogens with estradiol on platelet aggregation. Steroids 1993;58:407–9.

[21] Gonzalez G, Alvarado-Vasquez N, Fernandez GJ, Cruz-Robles D, Del Valle L, Pinzon E, et al. The antithrombotic effect of the aminoestrogen prolame (N-(3-hydroxy-1,3,5(10)-estratrien-17B-YL)-3-hydroxypropylamine) is linked to an increase in nitric oxide production by platelets and endothelial cells. Atherosclerosis 2010;208: 62–8.

[22] Lemini C, Canchola E. Effects of 17beta-aminoestrogens on the sexual behavior of female rats. Physiol Behav 2009;96:662–6.

[23] Daniel JM, Hulst JL, Berbling JL. Estradiol replacement enhances working memory in middle-aged rats when initiated immediately after ovariectomy but not after a long-term period of ovarian hormone deprivation. Endocrinology 2006;147: 607–14.

[24] Bernardi M, Vergoni AV, Sandrini M, Tagliavini S, Bertolini A. Influence of ovariectomy, estradiol and progesterone on the behavior of mice in an experimental model of depression. Physiol Behav 1989;45:1067–8.

[25] Estrada-Camarena E, Fernandez-Guasti A, Lopez-Rubalcava C. Antidepressant-like effect of different estrogenic compounds in the forced swimming test. Neuropsychopharmacology 2003;28:830–8.

[26] Frye CA, Walf AA. Estrogen and/or progesterone administered systemically or to the amygdala can have anxiety-, fear-, and pain-reducing effects in ovariectomized rats. Behav Neurosci 2004;118:306–13.

[27] Rachman IM, Unnerstall JR, Pfaff DW, Cohen RS. Estrogen alters behavior and forebrain c-fos expression in ovariectomized rats subjected to the forced swim test. Proc Natl Acad Sci U S A 1998;95:13941–6.

[28] Hawkins RD, Son H, Arancio O. Nitric oxide as a retrograde messenger during long-term potentiation in hippocampus. Prog Brain Res 1998;118:155–72.

[29] Zorumski CF, Izumi Y. Modulation of LTP induction by NMDA receptor activation and nitric oxide release. Prog Brain Res 1998;118:173–82.

[30] Bon CL, Garthwaite J. On the role of nitric oxide in hippocampal long-term potentiation. J Neurosci 2003;23:1941–8.

[31] O'Dell TJ, Hawkins RD, Kandel ER, Arancio O. Tests of the roles of two diffusible substances in long-term potentiation: evidence for nitric oxide as a possible early retrograde messenger. Proc Natl Acad Sci U S A 1991;88:11285–9.

[32] Schuman EM, Madison DV. A requirement for the intercellular messenger nitric oxide in long-term potentiation. Science 1991;254:1503–6.

[33] d'Anglemont de Tassigny X, Campagne C, Steculorum S, Prevot V. Estradiol induces physical association of neuronal nitric oxide synthase with NMDA receptor and promotes nitric oxide formation via estrogen receptor activation in primary neuronal cultures. J Neurochem 2009;109:214–24.

[34] Panzica GC, Viglietti-Panzica C, Sica M, Gotti S, Martini M, Pinos H, et al. Effects of gonadal hormones on central nitric oxide producing systems. Neuroscience 2006;138:987–95.

[35] Férnandez-G. JM. Synthesis and molecular structure of Prolame, N-(3-hydroxy-1,3,5(10)-estratrien-17b-yl)-3-hydroxypropylamine; an amino-estrogen with prolonged anticuagulant and brief estrogenic effects. Steroids 1985;45:151–7.

[36] Waynforth, H. B., Flecknell, P. A. Experimental and Surgical Technique in the Rat. Second Edition ed. San Diego, California: Academic Press; 1992.

[37] Burdette JE, Liu J, Lantvit D, Lim E, Booth N, Bhat KP, et al. Trifolium pratense (red clover) exhibits estrogenic effects in vivo in ovariectomized Sprague–Dawley rats. J Nutr 2002;132:27–30.

[38] McLaughlin KJ, Baran SE, Wright RL, Conrad CD. Chronic stress enhances spatial memory in ovariectomized female rats despite CA3 dendritic retraction: possible involvement of CA1 neurons. Neuroscience 2005;135:1045–54.

[39] Zhang L, Medina MP, Hernandez VS, Estrada FS, Vega-Gonzalez A. Vasopressinergic network abnormalities potentiate conditioned anxious state of rats subjected to maternal hyperthyroidism. Neuroscience 2010;168:416–28.

[40] Walf AA, Frye CA. The use of the elevated plus maze as an assay of anxiety-related behavior in rodents. Nat Protoc 2007;2:322–8.

[41] Morris R. Developments of a water-maze procedure for studying spatial learning in the rat. J Neurosci Methods 1984;11:47–60.

[42] Becker JB, Arnold AP, Berkley KJ, Blaustein JD, Eckel LA, Hampson E, et al. Strategies and methods for research on sex differences in brain and behavior. Endocrinology 2005;146:1650–73.

[43] Woolley CS. Acute effects of estrogen on neuronal physiology. Annu Rev Pharmacol Toxicol 2007;47:657–80.

[44] Grohe C, Kann S, Fink L, Djoufack PC, Paehr M, van Eickels M, et al. 17 Beta-estradiol regulates nNOS and eNOS activity in the hippocampus. Neuroreport 2004;15:89–93.

[45] Woolley CS, Gould E, Frankfurt M, McEwen BS. Naturally occurring fluctuation in dendritic spine density on adult hippocampal pyramidal neurons. J Neurosci 1990;10:4035–9.

[46] Marcondes FK, Bianchi FJ, Tanno AP. Determination of the estrous cycle phases of rats: some helpful considerations. Braz J Biol 2002;62:609–14.

[47] Paxinos g., W. C. The Rat Brain in Stereotaxic Coordinates. Fourth ed. ed. San Diego, California. USA: Academic Press; 1998.

[48] Yan BC, Choi JH, Yoo KY, Lee CH, Hwang IK, You SG, et al. Leptin's neuroprotective action in experimental transient ischemic damage of the gerbil hippocampus is linked to altered leptin receptor immunoreactivity. J Neurol Sci 2011;303:100–8.

[49] Koshimura K, Murakami Y, Tanaka J, Yamamoto M, Kato Y. Effect of tetrahydrobiopterin on nitric oxide synthase-containing cells in the rat hippocampus. Neurosci Res 2004;50: 161–7.

[50] Zhang L, Guadarrama L, Corona-Morales AA, Vega-Gonzalez A, Rocha L, Escobar A. Rats subjected to extended L-tryptophan restriction during early postnatal stage exhibit anxious-depressive features and structural changes. J Neuropathol Exp Neurol 2006;65:562–70.

[51] Koss WA, Gehlert DR, Shekhar A. Different effects of subchronic doses of 17-beta estradiol in two ethologically based models of anxiety utilizing female rats. Horm Behav 2004;46:158–64.

[52] Azizi-Malekabadi H, Hosseini M, Saffarzadeh F, Karami R, Khodabandehloo F. Chronic treatment with the nitric oxide synthase inhibitor, L-NAME, attenuates estradiol-mediated improvement of learning and memory in ovariectomized rats. Clinics (Sao Paulo) 2011;66:673–9.

[53] Dreyer J, Schleicher M, Tappe A, Schilling K, Kuner T, Kusumawidijaja G, et al. Nitric oxide synthase (NOS)-interacting protein interacts with neuronal NOS and regulates its distribution and activity. J Neurosci 2004;24:10454–65.

[54] Belcher SM, Zsarnovszky A. Estrogenic actions in the brain: estrogen, phytoestrogens, and rapid intracellular signaling mechanisms. J Pharmacol Exp Ther 2001;299: 408–14.

[55] Mendez P, Azcoitia I, Garcia-Segura LM. Estrogen receptor alpha forms estrogen-dependent multimolecular complexes with insulin-like growth factor receptor and phosphatidylinositol 3-kinase in the adult rat brain. Brain Res Mol Brain Res 2003;112:170–6.

[56] Malyala A, Kelly MJ, Ronnekleiv OK. Estrogen modulation of hypothalamic neurons: activation of multiple signaling pathways and gene expression changes. Steroids 2005;70:397–406.

[57] Prange-Kiel J, Wehrenberg U, Jarry H, Rune GM. Para/autocrine regulation of estrogen receptors in hippocampal neurons. Hippocampus 2003;13:226–34.

[58] Ronnekleiv OK, Malyala A, Kelly MJ. Membrane-initiated signaling of estrogen in the brain. Semin Reprod Med 2007;25:165–77.

[59] Vasudevan N, Pfaff DW. Non-genomic actions of estrogens and their interaction with genomic actions in the brain. Front Neuroendocrinol 2008;29:238–57.

[60] Prossnitz ER, Arterburn JB, Smith HO, Oprea TI, Sklar LA, Hathaway HJ. Estrogen signaling through the transmembrane G protein-coupled receptor GPR30. Annu Rev Physiol 2008;70:165–90.

Hypothalamic vasopressin system regulation by maternal separation: its impact on anxiety in rats

Zhang L, Hernández VS, Liu B, Medina MP,
Nava-Kopp AT, Irles C, Morales M

Mis contribuciones:

- Concepción del estudio: ++
- Participación en los experimentos:
    - Separación materna: +++
    - Inmunohistoquímica +++
    - Hibridización *in situ:* -
    - Medición de los núcleos PVN y SON: +++
    - Reconstrucción tridimensional: -
    - Evaluación de la ansiedad: +++
    - Medición de la AVP plasmática: +++
    - Evaluación del aprendizaje espacial: +++
- Análisis estadístico: +++
- Discusión de los resultados y comentarios al manuscrito: +++
- Escritura del artículo: +

(-): Ninguna contribución; (+): Contribución menor; (++): Contribución importante; (+++); Contribución crucial

HYPOTHALAMIC VASOPRESSIN SYSTEM REGULATION BY MATERNAL SEPARATION: ITS IMPACT ON ANXIETY IN RATS

L. ZHANG, [a]*[†] V. S. HERNÁNDEZ, [a][†] B. LIU, [b]
M. P. MEDINA, [a] A. T. NAVA-KOPP, [a] C. IRLES [a] AND
M. MORALES [b]*

[a] *Departamento de Fisiología, Facultad de Medicina, Universidad Nacional Autónoma de México, Mexico City 04510, Mexico*

[b] *Intramural Research Program, Neuronal Network Section, National Institute on Drug Abuse, Biomedical Research Center, Baltimore, MD 21224, USA*

Abstract—Maternal separation (MS) has been used to model the causal relationship between early life stress and the later stress-over-reactivity and affective disorders. Arginine vasopressin (AVP) is among several factors reported to be abnormal. The role of AVP on anxiety is still unclear. In order to further investigate this causal relationship and its possible role in anxiogenesis, male rat pups were separated from their dams for 3 h daily (3hMS) from post-natal day (PND) 2 to PND15. Fos expression in AVP+ neurons in the hypothalamic paraventricular (PVN) and supraoptic nuclei (SON) triggered by 3hMS, and AVP-mRNA expression, were examined at PND10 and PND21 respectively, whereas AVP-mRNA expression, PVN and SON volumes and plasma AVP concentration were assessed in adulthood. Elevated plus maze test (EPM) and Vogel conflict test (VCT) were also performed to evaluate unconditioned and conditioned anxious states at PND70–75. At PND10, a single 3hMS event increased Fos expression in AVP+ neurons fourfold in PVN and six to twelvefold in SON. AVP-mRNA was over-expressed in whole hypothalamus, PVN and SON between 122% and 147% at PND21 and PND63. Volumes of AVP-PVN and AVP-SON measured at PND75 had marked increases as well as AVP plasma concentration at 12 h of water deprivation (WD). MS rats demonstrated a high conditioned anxious state under VCT paradigm whereas no difference was found under EPM. These data demonstrate direct relationships between enhanced AVP neuronal activation and a potentiated vasopressin system, and this latter one with high conditioned anxiety in MS male rats. © 2012 IBRO. Published by Elsevier Ltd. All rights reserved.

*Corresponding authors. Address: Departamento de Fisiología, Facultad de Medicina, UNAM, Av. Universidad 3000, Col. Universidad Nacional Autónoma de México, México 04510, D.F., Mexico. Tel/fax: +52-55-56232348 (L. Zhang), tel: +1-443-740-2717; fax: +1-443-740-2817 (M. Morales).
E-mail addresses: limei@unam.mx (L. Zhang), MMORALES@intra.nida.nih.gov (M. Morales).
[†] Authors contributed equally to this study.

Key words: maternal separation, arginine vasopressin, paraventricular nucleus, supraoptic nucleus, Vogel conflict test, elevated plus maze.

INTRODUCTION

Seymour Levine's group first reported the effects of early life experience on emotionality and stress-responsiveness in adult rats half a century ago (Levine, 1957; Levine et al., 1957). Following this discovery, rodent maternal separation (MS) models have been widely used to investigate the effects of early postnatal adversity at adulthood. Plotsky, Meaney and others had developed a relatively standardized handling/MS model for manipulating early postnatal interaction between mother rats and their pups (Plotsky and Meaney, 1993; Wigger and Neumann, 1999; Lehmann and Feldon, 2000; Cirulli et al., 2003). The most widely studied paradigm consists of periods of daily separation (usually 3 h) performed from post-natal day (PND) 2 to PND14 (Fumagalli et al., 2007). While it is a generally accepted idea that MS permanently changes the offspring's neuroendocrine and behavioral stress reactivity, the factors that promote the sustained effects of early-life stress have not yet been fully elucidated (Wigger and Neumann, 1999; Lehmann and Feldon, 2000; Cirulli et al., 2003).

It has been shown that protracted periods (3 h or more) of separation from the dam may increase the hypothalamus–pituitary-adrenal axis (HPA) activity in pups, and may also increase the stress reactivity during adulthood (Anisman et al., 1998). Our classical understanding of the HPA axis comprises that the release of corticotropin-releasing factor (CRF) and vasopressin (VP) from the paraventricular nucleus (PVN) of the hypothalamus elicits pituitary adrenocorticotropin hormone (ACTH) secretion, which in turn, provokes release of the adrenal glucocorticoids. In addition to a considerable amount of reports describing CRF-ACTH-glucocorticoids secretion and their receptor abnormalities observed in the MS rodent model (Kuhn and Schanberg, 1998; Kalinichev et al., 2002; Fumagalli et al., 2007; Korosi and Baram, 2009), VP system has been reported to undergo developmental changes from the perinatal period through adulthood and MS was shown to disrupt this age-dependent changes. It is interesting to observe that there is a controversy about levels of AVP in MS rodent models, which were found either increased (Murgatroyd et al., 2009; Veenema and Neumann, 2009), decreased (Desbonnet et al., 2008) or unchanged (Oreland et al., 2010) in the hypothalamus, whereas no information about the possible

physiological mechanism(s) underlying this abnormality, regulated by neonatal recurrent MS, is available.

Vasopressin (VP, also widely known as antidiuretic hormone, ADH) is nonapeptide synthesized mainly in magnocellular neurons in the supraoptic nucleus (SON) and PVN of the hypothalamus. Its foremost physiological functions are the regulation of water-electrolyte metabolism, hepatic glucose metabolism, and cardiovascular function in adults (Hatton, 1990). However, together with another nonapeptide, oxytocin, VP is an important generator of behavioral diversity (Goodson, 2008) and provides an integrational neural substrate for the dynamic modulation of behaviors by endocrine and sensory stimuli (Goodson and Bass, 2001).

During ontogenesis, VP contributes to the regulation of proliferation and morphogenesis of the target cells and organs (brain, pituitary, kidney and liver) (Boer, 1987). VP system is known to be activated around birth when VP contributes to the establishment of a new equilibrium in the body fluids and the adaptation of the fetuses to the stress of the labor (Oosterbaan et al., 1985). Following birth, VP induces a redistribution of the blood flow via the cardiovascular system in order to increase blood volume in the vital organs and those responsible for stress reaction (brain, pituitary gland, heart, adrenals), while reducing the blood flow in other peripheral organs (Pohjavuori and Fyhrquist, 1980). Afterward, the physiological role of VP extends to the regulation of the cardiovascular system, water re-absorption in kidney (Dlouha et al., 1982; Siga and Horster, 1991) and glucogenolysis in liver (Ostrowski et al., 1993). Although the physiological mechanism(s) underlying the observed modification of vasopressin system by MS is currently unknown, a recent surprising report from Makara's group demonstrated that AVP was the predominant secretagogue during the perinatal period in a maternal deprivation model using VP producing (AVP+/−) and deficient (AVP−/−) Brattleboro rat pups. Both maternal deprivation and ether inhalation induced remarkable ACTH elevation only in AVP+/− pups, supporting the role of VP in HPA axis regulation. However, corticosterone (CORT) elevations were even more pronounced in AVP−/− pups, suggesting the possibility of an ACTH-independent CORT-secretion regulation (Makara et al., 2008).

AVP's promoting role on anxiogenesis is also not widely accepted yet, although there have been several reports in the literature suggesting that AVP system is critically involved in anxiogenesis (Landgraf and Wigger, 2002; Zhang et al., 2010). On the other hand, the role of MS on anxiogenesis is currently a matter of debate. Several studies have shown that MS promotes an increase in anxiety-like behavior in different anxiety tests (Huot et al., 2002; Wigger et al., 2004; Aisa et al., 2007) while others have found no differences (de Jongh et al., 2005; Slotten et al., 2006; Hulshof et al., 2011; Lajud et al., 2011).

Therefore, the specific aims of the present study were, in the first place, to investigate whether the 3hMS paradigm was capable to modify the neuronal activation of the magnocellular AVP system using the immediate early gene product Fos as a marker of AVP neuron activation and plasticity (Pirnik and Kiss, 2005) and, in the second place, to evaluate both short- and long-term effects of MS on AVP messenger RNA (mRNA) expression by using in situ hybridization (ISH) with AVP riboprobe and quantitative analysis at PND21 and PND63. It is worth mentioning that due to a discrepancy in the literature regarding the AVP-mRNA expression evaluated in adulthood of MS offspring (Desbonnet et al., 2008; Murgatroyd et al., 2009; Veenema and Neumann, 2009; Oreland et al., 2010), and the lack of evidences in the neonatal periods, we used AVP-riboprobe-ISH method, which allows observing much stronger hybridization signals due to its greater sensitivity and better signal-to-noise ratios (Herman et al., 1991; Marks et al., 1992; Grino and Zamora, 1998; Young et al., 2006). Moreover, riboprobes form more stable hybrids than oligo-probes. Further, the volumes of the magnocellular regions expressing vasopressin (AVP-SON and AVP-PVN) were morphometrically and quantitatively characterized at PND75. Finally, the hypothesis that the persistent enhancement of hypothalamic magnocellular vasopressin system should generate in rats a high anxious state, when the AVP system was selectively up-regulated, was assessed using the Vogel conflict test (VCT) for conditioned anxiety and comparing with elevated plus maze (EPM) test for unconditioned anxiety. Plasma AVP concentration during water deprivation (WD) was also measured.

EXPERIMENTAL PROCEDURES

Animals and MS procedure

Wistar rats reared from the local animal facility were used in this study. All animal procedures were approved by the local bioethical and research committees, with the approval ID 138-2009, in accordance with the principles exposed in the National Institute of Health Guide for the Care and Use of Laboratory Animals (NIH Publications No. 80-23) revised 1996.

MS (3 h daily, 3hMS) procedure was performed according to Veenema et al. previously described (Veenema et al., 2006). Briefly, female and male adult rats were mated for 2 days. During the last week of the gestation, female rats were single-housed in standard rat Plexiglas cages and maintained under standard laboratory conditions with 12:12 light–dark cycle (light on 0700), temperature maintained at 22 ± 2 °C, food and water ad libitum. On the day after parturition, PND2, each litter was culled to 7–8 pups, in which 5–6 were males. During the period from PND2–PND15, the pups were separated daily between 900 h and 1200 h from their dams. Pups were removed and transferred by hands previously coated with fine bedding-powder from the same cage of each litter. They were moved to an adjacent room and placed individually into a small box filled with bedding, and then put into a humid incubator with temperature maintained at 29 ± 1 °C. After the 3 h separation period, the pups were returned to the home-cage followed by reunion with their respective dam. Non-separated litters (animal facility-reared pups, AFR) were left undisturbed except for changes of the bedding twice a week and served as control groups for this study.

Experimental design

Four experiments were performed in 2 postnatal stages, neonatal and young adulthood. Experiment 1 evaluated the immediate

early gene product Fos expression in the PVN and the SON at PND10, 90 min after MS for 3 h (3hMS). Experiment 2 assessed the effects of MS on AVP messenger RNA expression in the hypothalamus at both PND21 and PND63 under basal conditions. In experiment 3, hypothalamic AVP nuclei volumes at PND75, under basal conditions, were quantitatively assessed. In experiment 4, long-term effects of MS on young adult rat unconditioned and conditioned anxious states were investigated using elevated plus maze test (EPM) and VCT, respectively. Due to the physiological up-regulation of the vasopressinergic system by the osmotic stressor in VCT (48 h of WD), plasma AVP concentration changing patterns, during the WD, were evaluated.

A total of 162 male rats were used in this study. For experiment 1, 20 PND10 rats were taken from five AFR and five MS litters. For experiment 2, 14 male rats were taken from four AFR and four MS3h litters, ($n = 3$ for PND21 ISH and $n = 4$ for PND63 ISH). For experiment 3, eight male rats were chosen from four AFR and four MS3h litters. Finally, for experiment 4, 120 rats from 20 litters (10 AFR and 10 MS3h) were used ($n = 10$/group for behavioral tests and $n = 10$/group for each time-point of plasma AVP concentration measurement). No siblings were used in the same experiment or same time-point for plasma AVP measurement.

Experiment 1 Evaluation of the immediate early gene product Fos expression in the hypothalamic PVN and the SON at PND10, 90 min after acute 3hMS: Fos/AVP double labeling and total Fos+ nuclei quantification

In order to test whether a single 3hMS procedure affects neuronal activation in the hypothalamic magnocellular regions containing vasopressinergic neurons, rats from both AFR and MS3h were perfused at PND10. Two treatments were applied: (1) no 3hMS procedure before perfusion-fixation and (2) 3hMS applied 90 min before perfusion-fixation. Twenty pups from ten litters (five AFR and five MS3h) were used in this experiment. Rats were deeply anaesthetized with an overdose of sodium pentobarbital (63 mg/kg, Sedalpharma, México) and then perfused with 10 ml of 0.9% saline followed by 20 ml of cold fixative containing 4% of paraformaldehyde in 0.1 M sodium phosphate buffer (PB, pH 7.4) plus 15% v/v of saturated picric acid and 0.05% of glutaraldehyde for 15 min. AVP/Fos immunofluorescence reaction was performed with guinea pig anti-AVP (T-5048, 1:2000, Peninsula Laboratories) and rabbit anti-Fos (SC52, 1:1000, Santa Cruz Biotechnology, Santa Cruz, CA) as primary antibodies, incubated overnight at 4 °C with gentle shaking. After several washings, sections were further incubated with Alexa Fluor 488 donkey anti-rabbit IgG (1:1000, Molecular Probes Inc. Eugene, OR) and Cy3 conjugated donkey anti-guinea pig IgG (1:1000, Jackson ImmunoResearch Laboratories, Inc., Baltimore, PA) as secondary antibodies, in TBST plus 1% of normal horse serum (NHS), at 4 °C overnight. At the end of the immunofluorescence reaction, sections were rinsed and mounted with Vectashield (Vector Laboratories, Inc., Burlingame, CA) and analyzed by epi-fluorescence microscopy using a Nikon 50i with a N-2B long-pass emission filter. Fields in the PVN and SON regions were randomly chosen with 40× objective, corresponding areas of 0.22 mm^2 and photomicrographs were taken using a digital camera. Total number of AVP+ neurons and the number of Fos+/AVP+ neurons from the PVN and SON (3 matched sections per rat, $n = 15$) were counted. Percentages of double-labeled neurons in total AVP+ neurons were calculated.

Experiment 2: Assessment of MS effects on AVP messenger RNA expression in the hypothalamus in both postnatal stages under basal conditions

Experiment 2 comprises two sets of rats taken from eight litters (four AFR and four MS3h): set 1, six PND21 male rats and set 2, eight PND63 male rats.

Rats were deeply anesthetized with sodium pentobarbital (Sedalpharma, México, 63 mg/kg b. w., i. p.) and perfused via ascendent aorta with 0.9% saline followed by cold fixative containing 4% of paraformaldehyde in 0.1 M phosphate buffer (PB), pH 7.4. Brains were post-fixed with 1% paraformaldehyde in PB and kept at 4 °C until use. All solutions used had been diethyl pyrocarbonate (DEPC)-treated (0.1% v/v with gentle stir for at least 4 h at room temperature) to inactivate any residual RNase and then autoclaved to inactivate the traces of DEPC.

Two days before the start of sectioning, the brains were moved to 18% sucrose in RNase free PB + NaN$_3$. Another change was done one day before the sectioning and a third change with fresh sucrose solution was done 1 h before the sectioning.

Serial coronal cryosectioning (12 μm) of whole hypothalamus (from anterior commissure to the level where ventral hippocampus appears in the rostrocaudal dimension) was made using a Leica CM1950 cryostat (Leica Microsystem, Wetzlar, 35578, Germany). Sections were collected on Leica glass insert and then transferred to a 24-well tissue culture plate with PB.

ISH was performed in 1 in 6 coronal sections as previously described (Morales and Bloom, 1997) using ^{35}S- and ^{33}P-UTP-labeled ribonucleotide probes. The pT7T3D-PacI plasmid (accession number: AI072073, clone ID: 1786383 Thermo Scientific) containing rat arginine vasopressin (AVP) cDNA (602 bp, Accession number: NM_016992) was linearized with EcoRI and then transcribed in vitro with T3 RNA polymerase to yield antisense complementary RNA probe. The construct was verified by sequencing. The radioactivity was adjusted to 10^7 cpm per ml hybridization buffer. Sections were mounted on coated slides, air-dried. Slides were first exposed to autoradiography film and analyzed on a phosphorimager (Fuji BAS5000, Tokyo, Japan) and then dipped in nuclear track emulsion (Eastman Kodak, Rochester, NY), and exposed for 4 weeks prior to development. Slides were counterstained with Methylene Blue for histological examination.

Data analysis. The relative abundance of AVP mRNA was measured in two fashions: (A) for whole hypothalamus AVP mRNA expression, all 1 in 6 serial sections from each rat were measured by densitometric quantification on phosphorimager digital images of autoradiograms. (B) For PVN, SON and SCN relative AVP mRNA abundances, 3–4 sections which were matched in the antero-posterior coordinates and containing each of the above-mentioned regions were digitally photographed from the counterstained slides and the silver grain precipitation areas in the studied regions were digitally measured. Fovea Pro 4.0 (Reindeer Graphics, Asheville, NC, USA) plug-in for Adobe Photoshop was used for both measurements. Data in the figures are presented as mean ± SEM values and expressed as % of the controls.

Experiment 3: Hypothalamic AVP nuclei volume quantitative assessment at PND75 under basal conditions

Perfusion-fixation and immunohistochemistry. Eight male rats at PND75 taken from eight litters (four AFR and four MS3h) were deeply anaesthetized with sodium pentobarbital (Sedalpharma México, Mexico, 63 mg/kg b. w., i. p.) and perfused via the ascending aorta with 0.9% saline followed by cold fixative containing 4% of paraformaldehyde in 0.1 M sodium phosphate buffer (PB, pH 7.4) plus 15% v/v of saturated picric acid for 15 min. Brains were removed, blocked with the help of an acrylic adult rat brain matrix (Prod No. 15062, Ted Pella, Inc, CA, USA), then thoroughly rinsed with PB. Vibratome coronal sections of 70 μm of hypothalamus (spanning from Bregma −0.24 mm to −2.64 mm, (Paxinos and Watson, 2007)) were made immediately after perfusion to enhance the

immunoreaction (in a free floating manner). Alternative sections were then blocked with Tris buffered saline Triton X100 0.3% (TBST), plus 20% normal swine serum (NSS) for 1 h at room temperature and then incubated with rabbit anti-AVP (T-4563, 1:2000, Península Laboratories, San Carlos CA, 94070) in TBST + 1% NSS at 4 °C over two nights. Finishing this lapse, sections were rinsed and proceeded for secondary antibody incubation with swine anti-rabbit IgG with horseradish peroxidase conjugated (P021702, 1:100, Dako, Denmark) in TBST + 1% NSS over night at 4 °C. This immunoreaction was developed using 3,3′-diaminobenzidine (DAB, Electron Microscopy Sciences, Hatfield, PA 19440) at 0.5% and hydrogen peroxide (H_2O_2, 0.01%) as substrates. Sections were mounted in gelatin-coated slides and allowed to dry for one day. Then were further dehydrated by passing through 100% ethanol for 5 min, then rinsed with xylene and mounted with Permount mounting medium (Fisher Scientific).

Hypothalamic vasopressinergic nuclei volume measurement. Sequenced AVP immunoreacted sections were viewed, analyzed and digitally photographed in bright-field using a Nikon Eclipse 50i microscope with a $4\times$ objective lens and a Nikon DS digital camera. AVP positive nuclei in the hypothalamic region were grouped according to Paxinos and Watson (2007) in the PVN and SON nuclei. The cluster AVP+ neuron area inside each group was delimited using Adobe Photoshop and the area in square millimeters (mm^2) was calculated with the Fovea Pro 4.0 (Reindeer Graphics, Asheville, NC, USA) plug-in for Photoshop. Volumes of each nucleus/region were determined by integrating all areas inside one group, then multiplying by 0.07 mm (the thickness of the section), times 2 (only the alternative sections were AVP-immunoreacted and measured) and times linear shrinkage constant (K). Linear shrinkage after the histochemical procedure was determined measuring the fresh brain diameters at optic chiasm immediately after perfusion (L_f) and the dehydrated coronal section widths at the same coordinates after the permanent mounting (L_d). Hence, $K = L_f/L_d$.

Representative 3-dimensional reconstruction of PVN. In order to visualize the directionality of the enlargement of PVN, a representative 3D digital reconstruction of PVN was made based on anatomical coordinates determined on digital photomicrographs. Briefly, one pair of AVP immunoreacted serial sections was chosen for 3D reconstruction of PVN. AVP+ neurons inside the PVN were labeled using ImageJ (NIH, MD, USA) on sequential digital photomicrographs. Magnocellular and parvocellular neurons were justified according to their long axes (magnocells were assigned to those with long axes more than 20 μm, (Armstrong, 2004)). For each of the marked neurons, coordinates (x, y) corresponding the 2D location (obtained from ImageJ, NIH, MD, USA) and z coordinate corresponding to the slide sequential position were obtained. Three-D plot was drawn using a computing program written in python (Python Software Foundation).

Experiment 4: MS effects on unconditioned and conditioned anxious states and neuroendocrine reactivity

Anxiety-related behavior could be measured with a variety of tests. For the purpose of this study, which was to assess the behavioral influence of the vasopressinergic system reorganization, elevated plus maze (EPM) and VCT were chosen due to their particular characteristics.

EPM. EPM is based on the conflict between the rodent nature of exploration to new environments vs. the fear of being on open and elevated alleys (Pellow and File, 1986). Hence, it was used at PND65 to assess the unconditioned acute anxious state as

described previously (Zhang et al., 2010). Briefly, the maze was made of wood, consisting of a plus-shaped platform elevated 50 cm above the floor with two closed arms (50 cm × 10 cm × 40cm) and two open arms (50 cm × 10 cm) surrounded by an upward-protruding edge of 0.5 cm connecting to the central square of 10 cmx10cm. This latter measure prevents the rat from falling accidentally, without jeopardizing the elemental features of the setting, hence enhances the efficacy of the test. The EPM was lit with dim red light and monitored by CCTV. The maze was cleaned with water containing a neutral detergent and dried before each trial.

Prior to the EPM test, 10 MS3h and 10 AFR randomly chosen rats, one per litter were exposed to a standard open-field box for 5 min during three consecutive days before and immediately previous to the EPM test. This procedure was made to increase the likelihood of entering the open arms of the maze, thus increasing the sensitivity of the test (Walf and Frye, 2007; Zhang et al., 2010). Rats from each experimental group underwent the EPM test during their early activity period. The test starts by placing the rat in the center of the maze heading to an open arm and then left for free exploratory activity for 5 min. The time spent on the open arms, as percentage of total time (300 s) was analyzed as a measure of unconditioned acute anxious state (exploration vs. avoidance).

VCT. VCT (Vogel et al., 1971; File et al., 2004) involves two main steps: WD for 48 h and food deprivation for the latter 24 h, and the conflict test proper. WD as long as 72 h, is well tolerated by rats with weight loss in an acceptable range (approximately 11%) and no apparent loss of physical vigor (Rowland, 2007). Completing the WD period, thirsty rats were exposed to a mild and intermittent electrical shock via a water bottle. This procedure incorporates an element of conflict whereby the subject experiences opposing and concomitant tendencies of desire of drinking for reward and of fear of a potentially aversive stimulus. An indicator of a high conditioned anxious state is when fear prevails in this conflict, where no genuine risk is present (Millan and Brocco, 2003). Hence, VCT was used to assess the conditioned acute anxious state as described previously (Zhang et al., 2010). In contrast to the EPM where the basal physiological parameters are mainly unaltered, in VCT, the vasopressinergic system is known to be up-regulated due to the WD. Hence, VCT provided an interesting paradigm to evaluate the role of a putatively altered AVP system on anxiety.

One day after the EPM test, the same experimental subjects were habituated by staying in the conflict chamber described below, without current application for 30 min each day per 4 consecutive days (started at PND70). The conflict chamber consisted in a clear Plexiglas cage (20 cm × 30 cm × 20 cm) with a metal floor and lattice lid, a water bottle with stainless steel drinking spout, a constant current shock generator with an indicator for counting the number of shocks and a video camera. During the test, a 10% dextrose-water solution (hypertonic solution) was used. The shocker leads were attached between the metal drinking spout and the grid floor. The drinking spout was isolated to avoid contact with the lid of the cage. Different shock levels (0.1–0.3 mA in steps of 0.02 mA) were assessed previously to determine the appropriate current to be used during the test (unpublished data). This was done with a different set of Wistar rats. A current of 0.22 mA was found to be optimal (i.e. it allowed animals to drink the solution with minimal discomfort).

Concluding the 48 h of WD period, the test started in a separate room and a video camera sensitive to low illumination was used for monitoring and recording the test. The test was performed during the dark period and the test-room was illuminated solely with a dim red light. At the beginning of the test, each animal was put in the test chamber and was allowed to drink for 25 s without electrical current applied. After this period, a current of 0.22 mA with a 50% duty cycle of 5 s was applied between the metal drinking spout and the floor alternately during 5 min. The number of shocks received was recorded. Ten rats of each group undertook this test.

Plasma AVP concentration measurement during WD. A hundred male rats at PND75 taken from 20 litters (10 AFR and 10 MS3h) contributed to the blood sampling. In order to characterize the plasma AVP concentration during the WD, blood samples were obtained from rat tail-tips at five time-points: before WD as basal point (Basal), after 6 h of WD (6 h WD), after 12 h of WD (12 h WD), after 24 h of WD (24 h WD) and after 48 h of WD (48 h WD). Each litter provided one and only one sample at each time-point. During the blood sampling, experimental subjects were immobilized using a restraint tube. In order to minimize the stressful effect exerted by this procedure, rats were placed in the same restraint tube (standard for rats) for 30 min during the 3 previous days of the test. At the corresponding time-point, 500 µl of blood samples from each of the respective intact rats was collected into chilled microtubes containing 0.5 mg of EDTA on the wall (50 µl of EDTA solution of 10 mg/ml was added to each tube, agitated and then dried inside a fridge). Samples were immediately centrifuged at $1600 \times g$ for 15 min at 4 °C. Plasma supernatant (200 µl per tube) was transferred to a new tube and stored at −70 °C until the ELISA test was performed. The Arg8-Vasopressin EIA Kit (Cat. 900-017, Assay Designs, Inc., Ann Arbor, Michigan 48108, USA) was used. The experimental procedure was the one recommended by the manufacturer of the ELISA vasopressin estimation kit. Each sample was analyzed in duplicate.

Statistical analysis

Quantitative results were expressed as mean ± SEM. The software package Prism (GraphPad Software, San Diego, CA, USA) was used. AVP mRNA expression was analyzed between AFR and MS for each brain region with an unpaired Student's *t*-test. Group normality was validated using D'Agostino & Pearson omnibus normality test. Groups were tested for differences by analysis of variance (ANOVA) followed by the Bonferroni test. Significance was accepted at $p < 0.05$. ($^*p < 0.05$, $^{**}p < 0.01$, and $^{***}p < 0.001$, vs. the control group).

RESULTS

Experiment 1: Fos expression in vasopressinergic magnocellular nuclei PVN and SON after 3hMS compared with basal conditions

An acute 3hMS significantly increased the expression of the immediate early gene product Fos (a generic marker of neuronal activation) in both SON ($F_{(3, 36)} = 154.3$, $p < 0.0001$) and PVN ($F_{(3, 36)} = 179.6$, $p < 0.0001$) in AFR and MS3h at the PND10, 90 min after the 3hMS. As expected, there were few Fos+ nuclei in the AVP+ populations in PVN and SON under basal conditions (Table. 1, treatment 1, and Fig. 1A, B). However, after the 3hMS (Table. 1, treatment 2) the majority of this neuronal population was expressing Fos (Table. 1 and Fig. 1A′, B′). However, one way ANOVA failed to reveal any differences between AFR and MS3h groups under both experimental conditions.

Experiment 2: Effects of MS on AVP mRNA expression in hypothalamic regions in both postnatal stages

By using AVP antisense riboprobes and compared to AFR group at PND21, MS3h group showed a marked increase in the relative AVP mRNA abundance in the whole hypothalamus (Fig. 2A and A′). Densitometric quantification of phosphorimager digital images of the 1/6 serial, 12 µm-thickness-coronal-section's autoradiograph

revealed an increase to 147 ± 7.6% compared to AFR (100 ± 1.1%), ($t = 12.75$, df = 4, $p = 0.0002$) (Fig. 2D). The relative abundance of AVP-mRNA in the PVN and SON of MS3h was significantly increased: 139.8 ± 13.5% ($t = 3.63$, df = 22, $p = 0.0013$) and 122.6 ± 9.6% ($t = 2.356$, df = 22, $p = 0.0274$) compared to AFR (100 ± 3.5% and 100 ± 4.7%) respectively (Fig. 2B, B′ and D). SCN had 109 ± 10% (MS3h) vs. 100 ± 8.4% (AFR) (Fig. 2C, C′ and D). Statistic analysis with Student's *t*-test failed to reveal a significant difference for SCN ($t = 0.6718$, df = 22, $p = 0.5084$).

At PND63, the relative expression level of AVP mRNA in the whole hypothalamus was significantly increased: 136.3 ± 5.9% compared to AFR (100 ± 4.8%); $t = 8.108$, df = 6, $p = 0.0002$, (Fig. 3A, A′ and D). The relative abundance of AVP mRNA in the PVN and SON of MS3h was 142.8 ± 7.3% ($t = 3.813$, df = 22, $p = 0.001$) and 124.5 ± 4.4% ($t = 3.109$, df = 22, $p = 0.0051$) compared to AFR (100 ± 8.2% and 100 ± 6.5%) respectively (Fig. 3B, B′ and D). SCN had 114.2 ± 7.4% (MS3h) vs. 100 ± 3.8% (AFR) (Fig. 3C, C′ and D). Statistic analysis with Student's *t*-test revealed no significant differences for this latter one ($t = 1.685$, df = 22, $p = 0.10$).

Experiment 3: Volume analysis of AVP+ PVN, SON and SCN at PND75

MS significantly increased the volume of AVP-SON and AVP-PVN nuclei evaluated at PND75 (Fig. 4). The mean volume of AVP-SON MS3h was 0.2086 mm³ ± 0.0064 mm³ vs. 0.1671 mm³ ± 0.0055 mm³ of AFR group ($t = 4.883$, df = 14, $p < 0.001$). In AVP-PVN the MS3h had a volume of 0.0853 mm³ ± 0.0062 mm³ vs. 0.0588 mm³ ± 0.0038 mm³ in AFR group (Fig. 4D; $t = 4.75$, df = 14, $p < 0.001$).

In MS3h rats an increase was observed in the number of neurons expressing AVP in the medial portion of the PVN (data not shown). There was also an increase in the extension of the nucleus in the rostro-caudal and medio-lateral dimensions. (Fig. 4B, B′ and C, C′).

Experiment 4: Anxiety-like behavioral effects of MS measured at PND75

Unconditioned and conditioned anxious states were assessed using two well-validated behavioral tests, the EPM test and the VCT. EPM tests the exploration vs. avoidance state placing the rat in an unconditioned environment with the closed arm representing safety and the open-elevated arm denoting novelty, though risky. Diminished time spent in the open arms and reduced number of entries imply a higher unconditioned anxious state. The MS3h rats spent similar time lapses in the open arms (86.2 s ± 6.96 s) as compared to AFR rats (80.7 s ± 5.50 s) ($t = 0.6198$, df = 18, $p = 0.5432$) (Fig. 5A). Subsequently, rats were subjected to WD, as an osmotic stressor, for 48 h. Afterward, thirsty rats underwent the conflict test in which they had to decide between drinking water (reward) and possibly receiving a mild electrical shock (punishment) or rather stay apart from the waterspout (avoidance). MS3h rats showed a
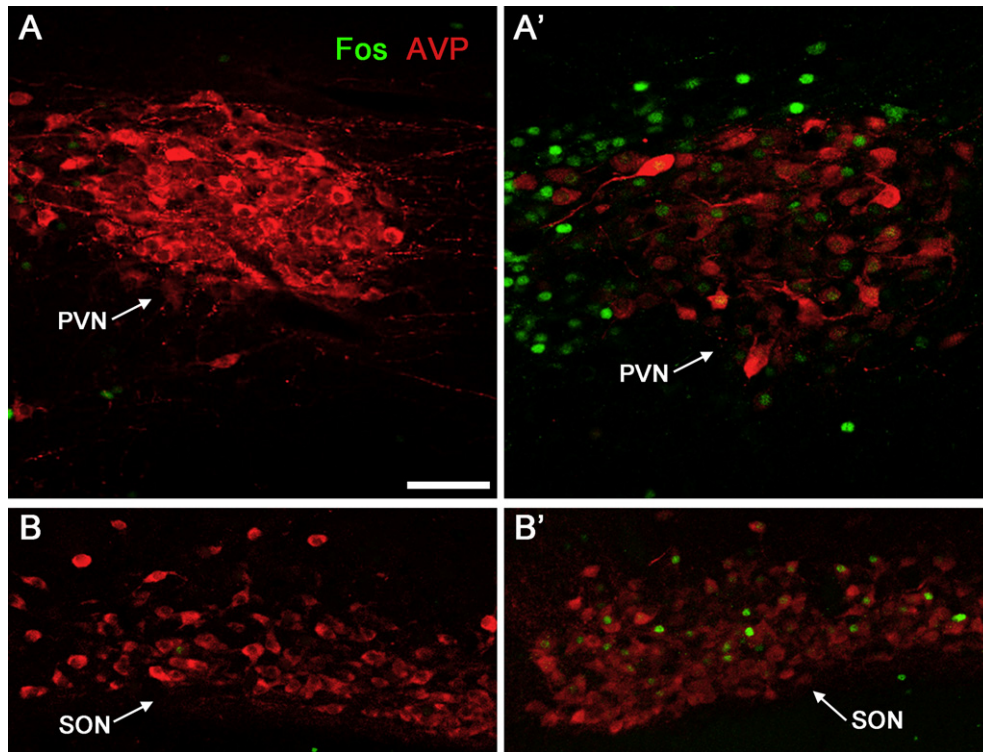
Fig. 1. Fos expression (green) in AVP containing neurons (red) of PVN and SON observed after a single acute 3hMS procedure at PND10. Panel A and B: photomicrographs of PVN and SON under basal conditions. Panels A′ and B′: same regions 90 min after an acute 3hMS. Scale bar = 100 μm.

significant reduction in the number of shocks received during the 5 min of the test (11.60 ± 2.56) compared to AFR (91.4 ± 7.58) ($t = 10.04$, df = 18, $p < 0.0001$) (Fig. 5B), which indicates a higher anxious state triggered by this osmotic challenge. Values are expressed as mean $\pm$ SEM.

Experiment 4: Altered plasma AVP concentration dynamics during WD

The plasma AVP concentration of MS3h group at 12 h WD had a significant increase (16.14 ± 1.15 pg/ml) compared to AFR group (12.23 ± 1.12 pg/ml) ($p < 0.05$). Two-way ANOVA indicated significant effects for time ($F_{4, 72} = 46.7$, $p < 0.0001$) and treatment ($F_{1, 72} = 14.35$, $p = 0.0013$) (Fig. 6).

DISCUSSION

The results of the present study can be summarized as follows: first, at PND10, a single 3hMS event increased Fos expression in AVP + neurons, fourfold in PVN and 6- to 12-fold in SON, regardless of the previous 3hMS exposure. Second, AVP mRNA, revealed by an ISH method using a vasopressin riboprobe, was over-expressed in whole hypothalamus, PVN and SON at both rat neonatal stage and adulthood, which indicate that the MS produces an immediate up-regulation of the vaso-pressin system and a persistent re-organization of this system. The enlarged volumes of PVN and SON mea-sured at PND75 were coherent with the ISH data. Third,

we provide evidence for a functional relationship between MS/AVP abnormalities and the shift toward a high anx-ious state when the potentiated AVP magnocellular sys-tem was up-regulated by WD, demonstrated also by plasma AVP values.

Fos activation triggered by a single 3hMS event and its relationship with AVP mRNA and volume analysis

The PVN and SON of the hypothalamus are major inte-grative sites for autonomic function by maintaining

Table 1. Fos + /AVP + neuron percentage in total AVP + neurons in hypothalamic paraventricular nucleus (PVN) and supraoptic nucleus (SON) at PND10

Region	Group	Treatment 1 (%)	Treatment 2 (%)	
PVN	AFR	12.6 ± 0.40	56.83 ± 2.46	$p < 0.001$
	MS3h	15.49 ± 1.28 ns	63.7 ± 2.87 ns	$p < 0.001$
SON	AFR	9.87 ± 2.27	58.08 ± 2.85	$p < 0.001$
	MS3h	5.02 ± 0.89 ns	63.71 ± 2.87 ns	$p < 0.001$

ns: not statistically significant, one-way ANOVA.
AFR: animal facility-reared rat group.
MS3h: maternal separation 3 h daily group.
Treatment 1: no maternal separation was performed before perfusion/fixation for Fos/AVP immunoreaction.
Treatment 2: Maternal separation 3 h applied in both groups, 90 min before the perfusion/fixation.
Values represent mean $\pm$ SEM of percentages of Fos + /AVP + in total AVP neurons in the PVN and SON.
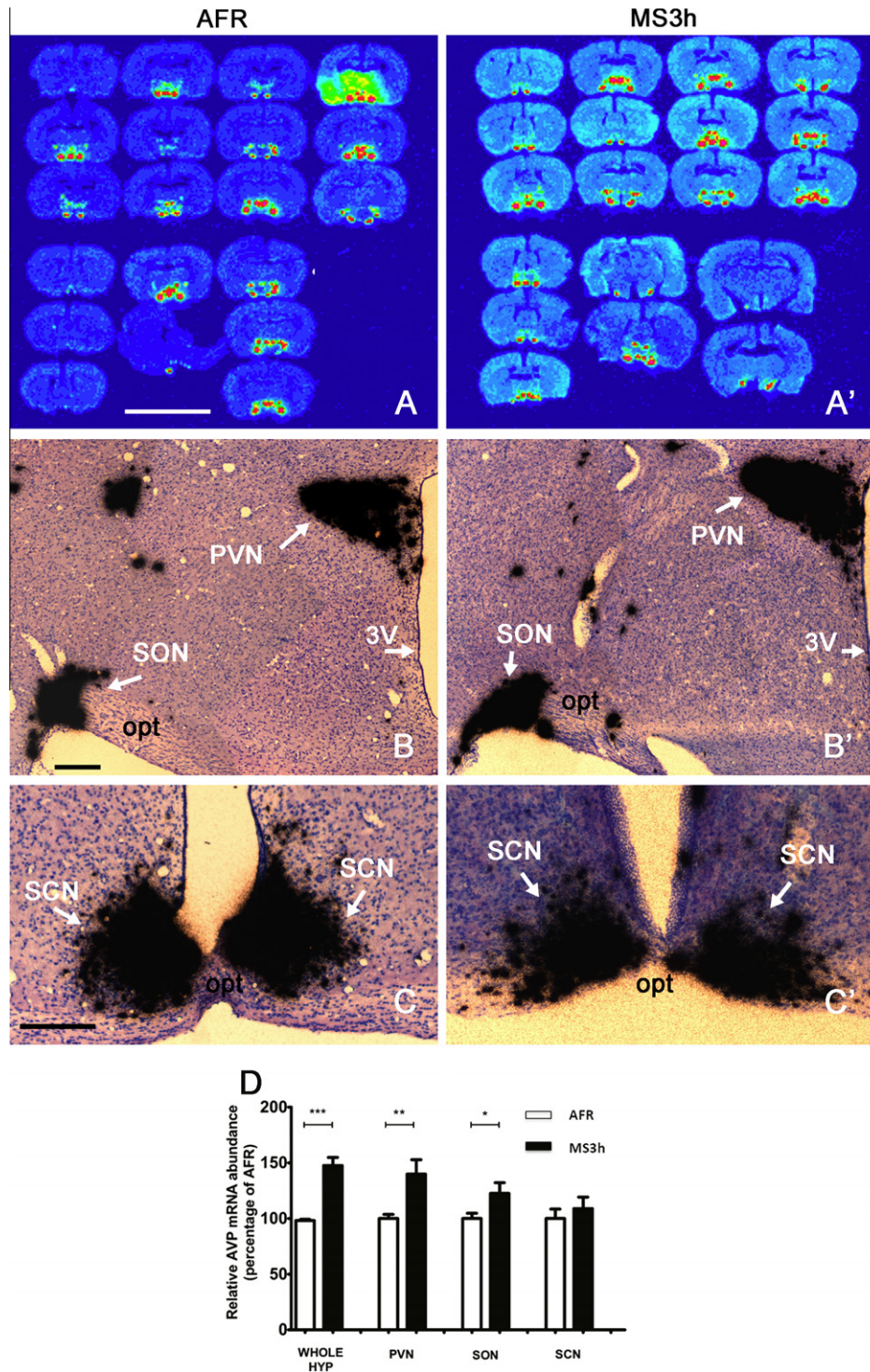
Fig. 2. Effects of maternal separation on AVP mRNA expression in hypothalamus at PND21. Panels A and A′: representative (1/6) coronal section series of whole hypothalamus from animal facility-reared (AFR) and maternal separation 3h (MS3h) groups respectively. Sections were hybridized with antisense radioactive AVP riboprobe. Autoradiographs with overnight-exposure were read by phosphorimager. Note that in MS3h group there was an evident increase of section numbers that contained AVP mRNA, which indicated a rostro-caudal enlargement of the expressing regions. Panels B, B′, C and C′: representative bright-field photomicrographs of sections from Ilford K.5 nuclear tract emulsion dipped slides exposed in the dark at 4 °C for 4 weeks showing, B and B′, increased areas in hypothalamic paraventricular nucleus (PVN) and supraoptic nucleus (SON). C and C′, suprachiasmatic nucleus (SCN) had no significant difference compared to AFR. Sections were counterstained with Methylene Blue. 3V: third ventricle; opt: optic tract. Scale bars for A, and A′ = 10 mm, and for B, B′, C and C′ = 200 μm. Panel D: the relative abundance of AVP mRNA in selective areas. "WHOLE HYP" (whole hypothalamus), optical density of the autoradiographs of whole series of coronal sections, was related to the AVP mRNA abundance in three dimensions. PVN, SON and SCN data were obtained by 2-dimension measurement of representative coronal sections. Data are as mean ± SEM, as % of averaged AFR. ***$p < 0.001$, **$p < 0.01$, *$p < 0.05$.
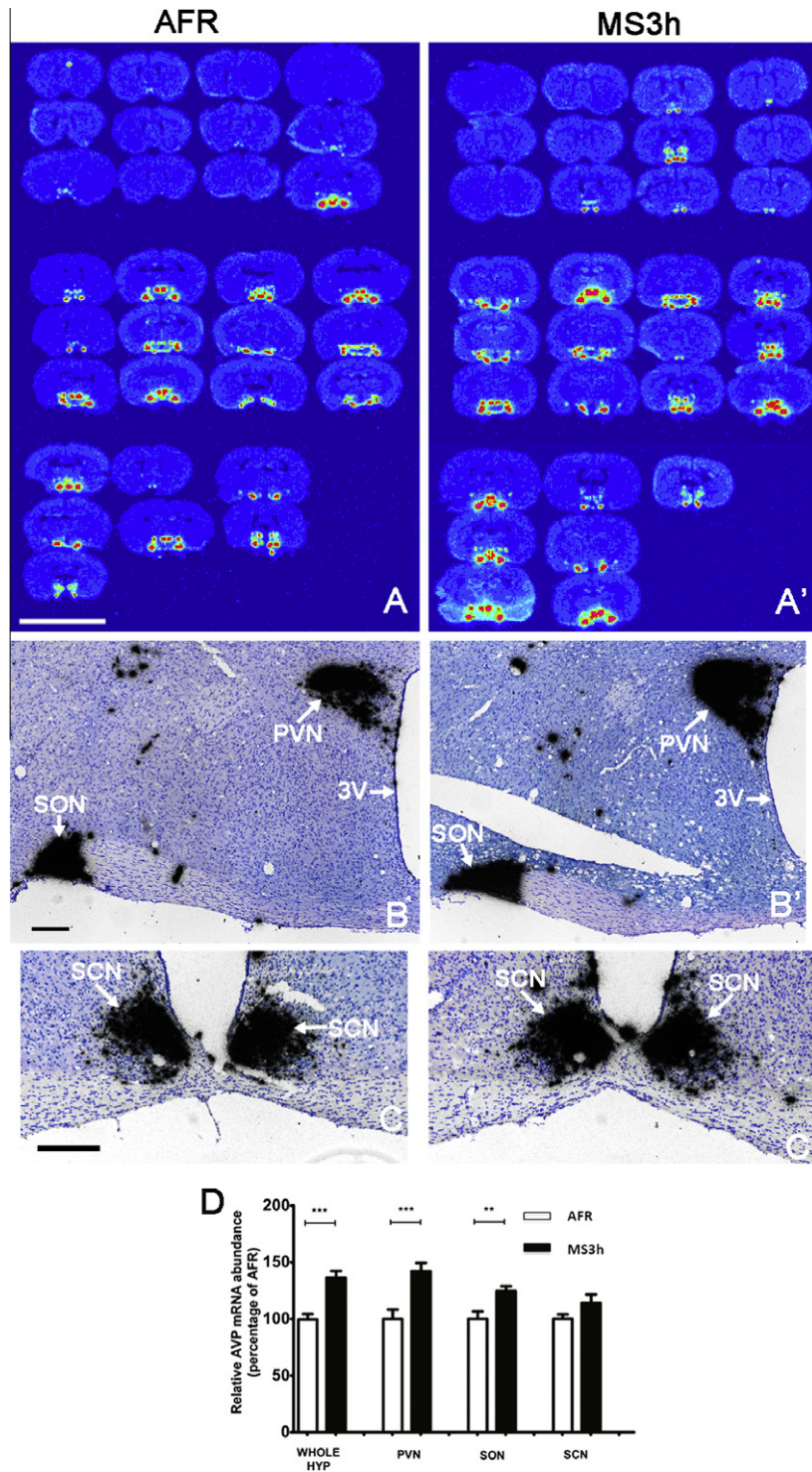
Fig. 3. Effects of MS3h on AVP mRNA expression in hypothalamus at PND63. Panels A and A′: representative (1/6) coronal section series of whole hypothalamus from animal facility-reared (AFR) and maternal separation 3 h (MS3h) groups respectively. Sections were hybridized with antisense radioactive AVP riboprobe. Overnight-exposure autoradiographs were read by phosphorimager. Note that in MS3h group there was an evident increase of section numbers that contained AVP mRNA, which indicated a rostro-caudal enlargement of the expressing regions. Panels B, B′, C and C′: representative bright-field photomicrographs sections from Ilford K.5 nuclear tract emulsion dipped slides exposed in the dark at 4 °C for 4 weeks showing, B and B′, increased areas in hypothalamic paraventricular nucleus (PVN) and supraoptic nucleus (SON). C and C′, suprachiasmatic nucleus (SCN) had no significant difference compared to AFR. Sections were counterstained with Methylene Blue. 3V: third ventricle; opt: optic tract. Scale bars for A, and A′ = 10 mm, and for B, B′, C and C′ = 200 μm. Panel D: the relative abundance of AVP mRNA in selective areas. "WHOLE HYP" (whole hypothalamus), optical density of the autoradiographs of whole series of coronal sections, was related to the AVP mRNA abundance in three dimensions. PVN, SON and SCN data were obtained by 2-dimension measurement of representative coronal sections. Data are as mean ± SEM, as % of averaged AFR. ***$p < 0.001$, **$p < 0.01$.
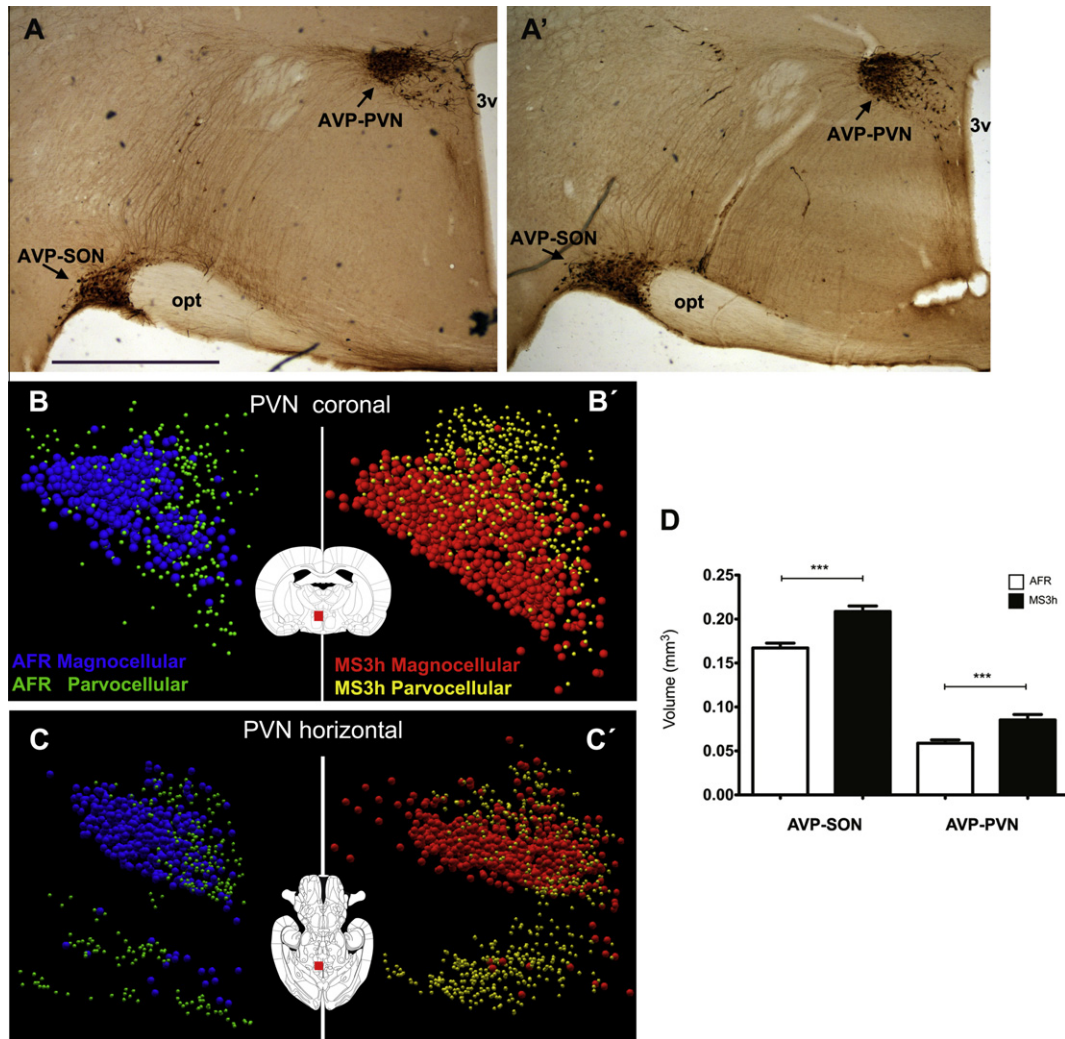
Fig. 4. Effects of MS3h on the extension of AVP+ neurons inside the PVN and SON at PND75. A and A′: representative photomicrographs showing immunohistochemical staining for vasopressin on hypothalamic coronal sections showing the enlarged areas occupied by vasopressin neurons in paraventricular (PVN) and supraoptic (SON) nuclei of MS3h (A′) compared to AFR (A). B, B′, C, C′: showing the coronal (B and B′) and horizontal (C and C′) views of the 3D computer reconstruction of PVN: AVP+ magnocellular neurons are in blue for AFR and in red for MS3h and parvocellular neurons are in green for AFR and in yellow for MS3h. D. Histogram shows the mean ± SEM of the AVP+ volume extension measurements in SON and PVN regions. 3v, third ventricle, opt, optic tract. ***$p < 0.001$. Scale bar = 1 mm.
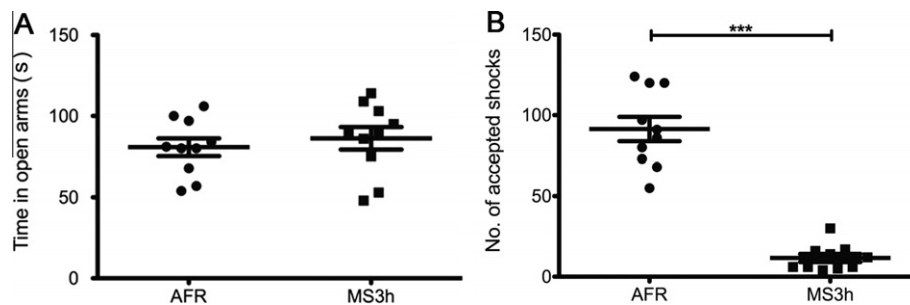
Fig. 5. MS3h subjects showed differential anxious states compared to AFR under unconditioned and conditioned behavioral tests for anxiety assessment. Panel A: Elevated plus maze test performed before water deprivation to evaluate the unconditioned anxiety related behavior revealed by the time spent in the open arms (total test time was 300 s). During this test, the experimental subjects showed similar behavior compared to control subjects. Panel B: Vogel conflict test (VCT). This test assessed conditioned anxious state posterior to a lapse of 48 h of water deprivation. During the test, a 0.22-mA current with a 50% duty cycle (5 s) was applied to the VCT apparatus during 300 s. The operational parameter we tested was the number of shocks the rats received. ***$p < 0.001$.
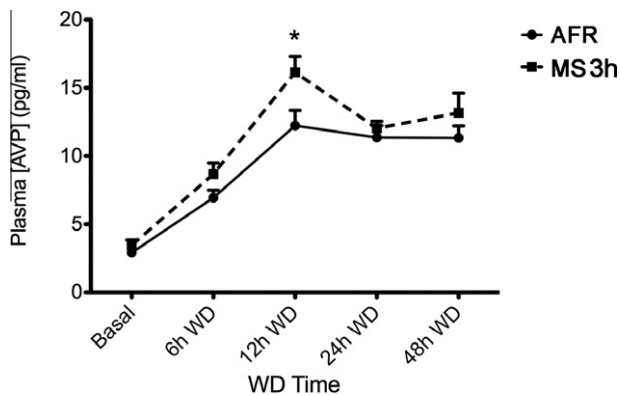
Fig. 6. Time evolution curve of the plasma AVP concentration (mean ± SEM) in function of water deprivation (WD) progression. $^{*}p < 0.05$.

homeostasis. Neuroanatomic and electrophysiologic evidences indicate that SON and magnocellular division of PVN are reciprocally connected to areas of the central nervous systems (CNS), besides their massive projections to neurolobe of the pituitary gland (Inyushkin et al., 2009; Kc and Dick, 2010). Using Fos mapping for AVP neuronal activation we revealed significant increases in Fos response to a single 3hMS event in both AFR and MS3h at PND10 (Table 1 and Fig. 1). No significant difference was observed between the two experimental groups in terms of percentage of activation of AVP neurons in PVN and SON. This no-difference was also observed under basal conditions (Table 1). These data indicated that the activation was mainly due to the 3hMS procedure and not due to the individual past MS experience. Although it is impossible to rule out a slight variation of plasma osmolarity during the 3hMS in newborn rats, this massive activation in magnocellular AVP containing regions suggested a broader physiological role of AVP during the early-life. It is known that AVP on its own is able to induce ACTH secretion from rat pituitary cells but only in large, supra-physiological concentrations (Antoni, 1993). Therefore, in adult rats it is accepted that CRF is the main secretagogue, while AVP modifies its effects. This seemed not the case during early-life. In two markedly different early-life stress models (maternal deprivation 24 h and repeated ether inhalation), Makara and collaborators reported strong evidence for a dominant regulating role of AVP on HPA axis during neonatal period. In the absence of AVP (AVP−/− Brattleboro rats) there was no measurable ACTH elevation in 10-day-old rat pups. However, both procedures provoked CORT elevations significantly superior to AVP+/− Brattleboro rats, which suggested an ACTH-independent CORT-secretion regulation during neonatal stage, probably related to AVP (Makara et al., 2008). In a recent study, Lajud and collaborators found a dual phenomenon regarding CORT elevation as a consequence of 3hMS using the same MS rat model. At the PND3, the MS group's elevation was significantly higher than the one from AFR, but surprisingly this phenomenon was reversed at PND12 (which correlated to PND13 of this study where the day of birth was assigned as PND1 instead of PND0 as in Lajud's study) (Lajud

et al., 2011), i.e. the MS group's elevation was significantly lower than the one from AFR. It is thus tempting to speculate that the hyper-activation of AVP system during the MS in early postnatal stage represents a homeostatic mechanism to balance the hyper-activated HPA axis and may contribute to the so called "stress hyporesponsive period or SHRP" (Sapolsky and Meaney, 1986; Lajud et al., 2011).

Enhanced Fos expression in AVP containing magnocellular neurons during MS periods implicated an abnormally higher neuronal activity during early post-natal development. During development, neurons establish specific synaptic connections to produce highly organized functional neuronal networks. While the general map of neuronal connections is encoded by genes, spontaneous and sensory-driven activities are thought to be equally important for CNS development (Khazipov and Buzsáky, 2010). Considerable evidence indicates that early electrical activity controls a number of developmental processes including neuronal differentiation, migration, synaptogenesis and synaptic plasticity (for a review see (Ben-Ari, 2001). Moreover, during normal development of the nervous system of most species, large numbers of immature neuronal and glial cells are lost by a process of programed cell death (PCD). For rats, the postnatal massive process of PCD occurs from PND1 to PND14 (White and Barone, 2001), the period that overlaps with MS. It is well know that neuronal activity plays an important role in modulating neuronal survival (Oppenheim et al., 2010). Hence, our data regarding an immediate and persistent over-expression of AVP mRNA in whole hypothalamus and in particular, in the PVN and SON, and enlarged PVN and SON observed in adulthood are in accordance with the Fos results.

Several transcription factors and intracellular signaling pathways modulate AVP gene regulation. The role of the Fos/Jun proteins in AVP gene regulation is still unclear. However, the rat AVP promoter contains a functional activation protein 1 (AP1) transcription element that consists of hetero- or homodimers of Fos proteins, including c-Fos, and Jun proteins that bind to AP1 (Yoshida et al., 2006). Several studies have shown that Fos/Jun proteins are rapidly expressed in AVP-positive neurons in response to multiple stimuli, such as hypertonic saline challenge, coordinating with the activation of AVP gene expression (Sharp et al., 1991; Shiromani et al., 1995). Our data showed a rapid expression of c-Fos protein in AVP neurons in response to an acute 3hMS. These evidences, together with our results suggest that the expression of Fos/Jun proteins may be one of the possible mechanisms mediating the rapid transcriptional induction of AVP gene.

Recently, the increased expression of AVP mRNA, and protein, in PVN of MS mice was shown to be accompanied by hypomethylation of an AVP key regulatory region (Murgatroyd et al., 2009). One of the proteins responsible for regulating DNA methylation is methyl CpG-binding protein 2 (MeCP2), its binding represses DNA transcription. In a hypothalamic cell line, neuronal depolarization by K+ was shown to trigger Ca2+-dependent phosphorylation of MeCP2 by Ca2+-calmodulin kinase II (CAMKII), causing dissociation of MeCP2 from the AVP

promoter and an increase in AVP transcription. Furthermore, MeCP2 and CAMKII phosphorylation levels were found increased in AVP-positive neurons from PND10 MS mice. The authors put forward that MeCP2 phosphorylation, via CAMKII activity, is critical for the repressive role of MeCP2 at the AVP enhancer of MS mice (Murgatroyd et al., 2009).

Methodological considerations

It is worth pointing out that we provided, for the first time, quantitative and morphometric assessments of AVP mRNA in PVN and SON at both neonatal stage and young adulthood. Our data are in discrepancy with some data found in the literature where observations of no-differences under basal condition in SON and PVN were reported (Veenema et al., 2006; Veenema and Neumann, 2009). In our study, we used an AVP riboprobe for ISH for whole hypothalamus, PVN and SON, analyzed through both densitometric and morphological measurements of silver grain precipitation areas on histological slides with Methylene Blue counterstaining. This method allowed observing much more anatomical details with much stronger hybridization signals due to its greater sensitivity and better signal-to-noise ratios. Moreover, riboprobes form more stable hybrids than oligo-probes. Hence we could analyze the histological slide under bright-field microscope and digitally measure the hybridized areas in the respective regions (PVN, SON and SCN). Veenema and collaborator's data were obtained using oligonucleotide probe-ISH (Veenema et al., 2006; Veenema and Neumann, 2009) with lower sensitivity compared with this riboprobe-ISH method.

Regarding the volume assessment of the AVP containing neurons inside PVN and SON (AVP-PVN and AVP-SON), we found a remarkable increase in the volumes of both magnocellular nuclei at rat young adult stage (PND75). This observation is in accordance with data from Veenema and Neumann (2009) but in discrepancy with results from another study in which a decreased AVP+ cell density in the PVN was found in MS adult rats (Desbonnet et al., 2008). We consider that this could be due to methodological discrepancies. Our experience indicates that AVP immunoreaction depends strongly on the histological procedures. A series of factors increases the AVP immunoreaction, such as a relatively short perfusion/fixation period (15 min approximately) with fixative containing 4% paraformaldehyde fixative and 15% v/v picric acid, followed by same day slicing of freshly fixed brain block by vibratome and thorough rinsing of the sections to remove the fixative. These actions enhanced AVP immunoreaction while post-fixation and freeze–thaw procedures dampen the AVP immunoreaction (data not shown).

Functional considerations

We assessed anxiety-like behavior in this MS3h animal model in rat young adulthood. We used two well-validated behavioral models. The EPM assesses internal conflict between voluntary approach and withdrawal tendencies that is related to unconditioned anxiety. We did not observe any significant difference regarding the unconditioned anxious state between MS3h and AFR rats. This observation supports data published by Lajud et al. (2011). The Vogel thirsty rat conflict test (VCT) assesses conditioned anxiety-behavior under WD conditions (Millan and Brocco, 2003), which involve intrinsically the activation of AVP magnocellular system due to the WD procedure which represents an osmotic stressor. Following the WD, AVP is greatly released in the blood circulation, which was found significantly increased in the MS3h at 12 h. During the last step of the VCT, MS3h rats exhibited a significantly higher anxiety-related behavior than AFR rats. Although the intra-cerebral AVP release under VCT experimental conditions was not measured in this study, this parameter is likely to be increased, according to previous evidence such as intra-PVN release of AVP during stress coping (Engelmann et al., 2004; Leng and Ludwig, 2008). The possible release mechanisms include dendritic release by exocytosis in the PVN and lateral hypothalamus, as previously demonstrated by Pow and Morris at electron microscopy level (Pow and Morris, 1989). Since the high anxious behavior was only detected with VCT, once osmotic stressor was applied and not with the EPM test, it is rational to consider that the main cause of the expressed high anxious state was due to the major physiological mechanism to cope with this *stressor*, i.e. vasopressinergic system activation. Experimental evidences have shown that intra-PVN administration of an AVP V1 receptor antagonist resulted in a decrease of anxiety-related behavior of the high anxiety bred rats (Engelmann et al., 2004) and increased AVP release within PVN, measured by microdialysis, was observed during anxious situations (Wotjak et al., 1996). These data support the assumption that higher contents of released AVP within PVN serve as a physiological substrate for anxiogenesis, which is in concordance with the results from this study. It is worth mentioning that the pain sensitivity was assessed using a warm water tail withdrawal test in a separate study and the observations indicated that under basal condition this parameter remained unchanged compared to AFR subjects (unpublished data).

There has been broad literature exploring the physiological and anatomical substrates underlying the fear response observed during the VCT (conditioned anxiety-like behavior, (Millan and Brocco, 2003)). It is well known that the amygdala plays an important role in anxiety and fear behavior, integrating emotionally relevant sensory information and encoding the aversive affect of fearful stimuli. Subsystems of the amygdalar complex are known to mediate different aspects of anxiety-related behaviors, as observed in the elevated plus-maze or in the VCT (Graeff et al., 1993; Killcross et al., 1997).

Previous evidence has shown that VCT triggers the expression of c-fos specifically within the central nucleus of the amygdala (Moller et al., 1994). In addition, lesions only to the central nucleus (CeA), but not to the basolateral nucleus (BLA), extraordinarily increased the punished component of the VCT (Moller et al., 1997). Also, lesions to the CeA were observed to produce anxiolytic effects only during the VCT, but not in other anxiety tests

(Kopchia et al., 1992). In this line, CeA has been reported to be mainly involved in the encoding of the anxiety-like behavior when subjects are confronted with an aversive stimulus, i.e. punished drinking (Pesold and Treit, 1995), while BLA has clearly shown a role in unconditioned or basal innate fear as measured by EPM (Green and Vale, 1992; Pesold and Treit, 1995). In this study, behavioral experiments clearly demonstrate a marked divergence between unconditioned (EPM) and conditioned (VCT) anxiety-like behaviors induced by MS, as a significant increase was only observed in the MS3h rats after an aversive stimulus was applied. Based on this divergence, CeA is probably playing a crucial role in the increased anxiety-like behavior observed during the VCT in the MS3h subjects.

AVP is a key component in the regulation of stress response and complex behaviors, such as anxiety, social cognition and fear conditioning (Meyer-Lindenberg et al., 2011). Hypothalamus, specifically PVN and SON nuclei, has been recognized as the principal source of extra- and intra-cerebral AVP projections (Buijs, 1978). More-over, AVP receptors are distributed throughout the central nervous system, finding a significant expression of V1b subtype in the adenohypophysis and within limbic struc-tures (Lolait et al., 1995). In addition, the anxiogenic effect of AVP has been demonstrated in broad different studies (Landgraf and Neumann, 2004; Zhang et al., 2010; Mak et al., 2011). Likewise, a recent report has found that the systemic administration of a non-peptide V1b antago-nist (SSR149415) is able to produce anxiolytic effects in classical (EPM, VCT) and atypical rat models of anxiety, suggesting a crucial role of AVP V1b receptor in the production of anxiogenic states (Griebel et al., 2002).

A number of previous studies have suggested that the amygdala is an important target of AVP to exert its stress-responsive and anxiogenic action. Amygdaloid nuclei present extensive AVP innervation with fibers coming from hypothalamic sources (Buijs, 1978; Sofroniew, 1980), and recent immunohistochemical studies have demonstrated the presence of V1b receptors throughout the entire amygdalar complex: central, medial and baso-lateral divisions (Hernando et al., 2001; Stemmelin et al., 2005). Activation of amygdalar AVP receptors has been shown to enhance fear and anxiety-like behaviors, as well as aggressiveness, stress levels and the consolidation of fear memory (Bielsky and Young, 2004) (Landgraf and Wigger, 2002). At the cellular level, it has been demonstrated that AVP increases the probability of provoking postsynaptic action potentials in specific populations of neurons within the CeA. This latter finding suggests that the endogenous balance between the acti-vation of the vasopressinergic system and the expression of AVP receptors, paralleled with oxytocin system, may set and tune the levels for the activation of the fear response and anxiety behavior (Huber et al., 2005). In this context, it has been reported that AVP levels within the extracellular fluid of the amygdala increase after WD (Epstein et al., 1983), and during stressful behavioral situations (i.e. FST, (Ebner et al., 2002)). In our study, higher concentration of plasmatic AVP after WD and potentiation of the vasopressinergic system is

demonstrated. This hyper-active AVP system observed in the MS animals could be releasing higher levels of AVP within CeA, increasing the excitability of the network after the application of the osmotic stress in the VCT, thus tuning the endogenous balance of the network toward activation of fear and anxiety responses, with the second-ary functional effect of reduced avoidance latency at the conflict test.

CONCLUSION

In the present study, we could demonstrate for the first time a direct relationship between a potentiated vasopres-sin system induced by MS, evidenced by the enlarged AVP-SON and AVP-PVN volumes and abnormal high level of AVP-mRNA expression and significant increase of AVP release under WD, and the high conditioned anxiety revealed by VCT. The present data not only extended the previous knowledge that MS potentiates the vasopressin systems in adulthood, but they also clearly showed that a single 3hMS event was capable of activating the majority of the AVP neurons inside the SON and PVN, showed by Fos expression analysis. Hence, the data provided a physiological substrate for the observed AVP up-regulation by MS.

DECLARATION FOR AUTHOR'S CONTRIBUTIONS

Conceived and designed the experiments: L.Z., V.S.H. Performed the experiments: L.Z., V.S.H., B.L., M.P.M., A.N.K., C.I. Analyzed the data: L.Z., V.S.H., M.P.M., A.N.K., C.I., M.M. Contributed reagents/materials/analy-sis tools: L.Z., M.M. Wrote the paper: L.Z., V.S.H., C.I., M.P.M. Revised the manuscript critically for important intellectual content: all authors.

REFERENCES

Aisa B, Tordera R, Lasheras B, Del Rio J, Ramirez MJ (2007) Cognitive impairment associated to HPA axis hyperactivity after maternal separation in rats. Psychoneuroendocrinology 32:256–266.

Anisman H, Zaharia MD, Meaney MJ, Merali Z (1998) Do early-life events permanently alter behavioral and hormonal responses to stressors? Int J Dev Neurosci 16:149–164.

Antoni FA (1993) Vasopressinergic control of pituitary adrenocorticotropin secretion comes of age. Front Neuroendocrinol 14:76–122.

Armstrong W (2004) Hipothalamic supraoptic and paraventricular nuclei. In: Paxinos G, editor. The rat nervous system. Elsevier. p. 369–387.

Ben-Ari Y (2001) Developing networks play a similar melody. Trends Neurosci 24:353–360.

Bielsky IF, Young LJ (2004) Oxytocin, vasopressin, and social recognition in mammals. Peptides 25:1565–1574.

Boer GJ (1987) Development of vasopressin system and their functions. In: Gash DM, Boer GJ, editors. Vasopressin: principles and properties. New York: Plenum Press. p. 117–174.

Buijs RM (1978) Intra- and extrahypothalamic vasopressin and oxytocin pathways in the rat. Pathways to the limbic system, medulla oblongata and spinal cord. Cell Tissue Res 192:423–435.

Cirulli F, Berry A, Alleva E (2003) Early disruption of the mother-infant relationship: effects on brain plasticity and implications for psychopathology. Neurosci Biobehav Rev 27:73–82.

de Jongh R, Geyer MA, Olivier B, Groenink L (2005) The effects of sex and neonatal maternal separation on fear-potentiated and light-enhanced startle. Behav Brain Res 161:190–196.

Desbonnet L, Garrett L, Daly E, McDermott KW, Dinan TG (2008) Sexually dimorphic effects of maternal separation stress on corticotrophin-releasing factor and vasopressin systems in the adult rat brain. Int J Dev Neurosci 26:259–268.

Dlouha H, Krecek J, Zicha J (1982) Postnatal development and diabetes insipidus in Brattleboro rats. Ann N Y Acad Sci 394:10–20.

Ebner K, Wotjak CT, Landgraf R, Engelmann M (2002) Forced swimming triggers vasopressin release within the amygdala to modulate stress-coping strategies in rats. Eur J Neurosci 15:384–388.

Engelmann M, Landgraf R, Wotjak CT (2004) The hypothalamic-neurohypophysial system regulates the hypothalamic-pituitary-adrenal axis under stress: an old concept revisited. Front Neuroendocrinol 25:132–149.

Epstein Y, Castel M, Glick SM, Sivan N, Ravid R (1983) Changes in hypothalamic and extra-hypothalamic vasopressin content of water-deprived rats. Cell Tissue Res 233:99–111.

File SE, Lippa AS, Beer B, Lippa MT (2004) Animal tests of anxiety. In: Crawley JN, et al., editors. Current protocols in neuroscience (editorial board) (Chapter 8:Unit 8.3).

Fumagalli F, Molteni R, Racagni G, Riva MA (2007) Stress during development: impact on neuroplasticity and relevance to psychopathology. Prog Neurobiol 81:197–217.

Goodson JL (2008) Nonapeptides and the evolutionary patterning of sociality. Prog Brain Res 170:3–15.

Goodson JL, Bass AH (2001) Social behavior functions and related anatomical characteristics of vasotocin/vasopressin systems in vertebrates. Brain Res Brain Res Rev 35:246–265.

Graeff FG, Silveira MC, Nogueira RL, Audi EA, Oliveira RM (1993) Role of the amygdala and periaqueductal gray in anxiety and panic. Behav Brain Res 58:123–131.

Green S, Vale AL (1992) Role of amygdaloid nuclei in the anxiolytic effects of benzodiazepines in rats. Behav Pharmacol 3:261–264.

Griebel G, Simiand J, Serradeil-Le Gal C, Wagnon J, Pascal M, Scatton B, Maffrand JP, Soubrie P (2002) Anxiolytic- and antidepressant-like effects of the non-peptide vasopressin V1b receptor antagonist, SSR149415, suggest an innovative approach for the treatment of stress-related disorders. Proc Natl Acad Sci U S A 99:6370–6375.

Grino M, Zamora AJ (1998) An in situ hybridization histochemistry technique allowing simultaneous visualization by the use of confocal microscopy of three cellular mRNA species in individual neurons. J Histochem Cytochem 46:753–759.

Hatton GI (1990) Emerging concepts of structure-function dynamics in adult brain: the hypothalamo-neurohypophysial system. Prog Neurobiol 34:437–504.

Herman JP, Schafer MK, Watson SJ, Sherman TG (1991) In situ hybridization analysis of arginine vasopressin gene transcription using intron-specific probes. Mol Endocrinol 5:1447–1456.

Hernando F, Schoots O, Lolait SJ, Burbach JP (2001) Immunohistochemical localization of the vasopressin V1b receptor in the rat brain and pituitary gland: anatomical support for its involvement in the central effects of vasopressin. Endocrinology 142:1659–1668.

Huber D, Veinante P, Stoop R (2005) Vasopressin and oxytocin excite distinct neuronal populations in the central amygdala. Science 308:245–248.

Hulshof HJ, Novati A, Sgoifo A, Luiten PG, den Boer JA, Meerlo P (2011) Maternal separation decreases adult hippocampal cell proliferation and impairs cognitive performance but has little effect on stress sensitivity and anxiety in adult Wistar rats. Behav Brain Res 216:552–560.

Huot RL, Plotsky PM, Lenox RH, McNamara RK (2002) Neonatal maternal separation reduces hippocampal mossy fiber density in adult Long Evans rats. Brain Res 950:52–63.

Inyushkin AN, Orlans HO, Dyball RE (2009) Secretory cells of the supraoptic nucleus have central as well as neurohypophysial projections. J Anat 215:425–434.

Kalinichev M, Easterling KW, Plotsky PM, Holtzman SG (2002) Long-lasting changes in stress-induced corticosterone response and anxiety-like behaviors as a consequence of neonatal maternal separation in Long-Evans rats. Pharmacol Biochem Behav 73:131–140.

Kc P, Dick TE (2010) Modulation of cardiorespiratory function mediated by the paraventricular nucleus. Respir Physiol Neurobiol 174:55–64.

Khazipov R, Buzsáky G (2010) Early patterns of electrical activity in the developing cortex. In: Blumberg MS, Freeman JH, Robinson SR, editors. Oxford handbook of developmental behavioral neuroscience. Oxford: Oxford University Press. p. 161–180.

Killcross S, Robbins TW, Everitt BJ (1997) Different types of fear-conditioned behaviour mediated by separate nuclei within amygdala. Nature 388:377–380.

Kopchia KL, Altman HJ, Commissaris RL (1992) Effects of lesions of the central nucleus of the amygdala on anxiety-like behaviors in the rat. Pharmacol Biochem Behav 43:453–461.

Korosi A, Baram TZ (2009) The pathways from mother's love to baby's future. Front Behav Neurosci 3:27.

Kuhn CM, Schanberg SM (1998) Responses to maternal separation: mechanisms and mediators. Int J Dev Neurosci 16:261–270.

Lajud N, Roque A, Cajero M, Gutierrez-Ospina G, Torner L (2011) Periodic maternal separation decreases hippocampal neurogenesis without affecting basal corticosterone during the stress hyporesponsive period, but alters HPA axis and coping behavior in adulthood. Psychoneuroendocrinology.

Landgraf R, Neumann ID (2004) Vasopressin and oxytocin release within the brain: a dynamic concept of multiple and variable modes of neuropeptide communication. Front Neuroendocrinol 25:150–176.

Landgraf R, Wigger A (2002) High vs low anxiety-related behavior rats: an animal model of extremes in trait anxiety. Behav Genet 32:301–314.

Lehmann J, Feldon J (2000) Long-term biobehavioral effects of maternal separation in the rat: consistent or confusing? Rev Neurosci 11:383–408.

Leng G, Ludwig M (2008) Neurotransmitters and peptides: whispered secrets and public announcements. J Physiol 586:5625–5632.

Levine S (1957) Infantile experience and resistance to physiological stress. Science 126:405.

Levine S, Alpert M, Lewis GW (1957) Infantile experience and the maturation of the pituitary adrenal axis. Science 126:1347.

Lolait SJ, O'Carroll AM, Brownstein MJ (1995) Molecular biology of vasopressin receptors. Ann N Y Acad Sci 771:273–292.

Mak P, Broussard C, Vacy K, Broadbear JH (2011) Modulation of anxiety behavior in the elevated plus maze using peptidic oxytocin and vasopressin receptor ligands in the rat. J Psychopharmacol.

Makara GB, Domokos A, Mergl Z, Csabai K, Barna I, Zelena D (2008) Gender-specific regulation of the hypothalamo-pituitary-adrenal axis and the role of vasopressin during the neonatal period. Ann N Y Acad Sci 1148:439–445.

Marks DL, Wiemann JN, Burton KA, Lent KL, Clifton DK, Steiner RA (1992) Simultaneous visualization of two cellular mRNA species in individual neurons by use of a new double in situ hybridization method. Mol Cell Neurosci 3:395–405.

Meyer-Lindenberg A, Domes G, Kirsch P, Heinrichs M (2011) Oxytocin and vasopressin in the human brain: social neuropeptides for translational medicine. Nat Rev Neurosci 12:524–538.

Millan MJ, Brocco M (2003) The Vogel conflict test: procedural aspects, gamma-aminobutyric acid, glutamate and monoamines. Eur J Pharmacol 463:67–96.

Moller C, Bing O, Heilig M (1994) c-fos expression in the amygdala: in vivo antisense modulation and role in anxiety. Cell Mol Neurobiol 14:415–423.

Moller C, Wiklund L, Sommer W, Thorsell A, Heilig M (1997) Decreased experimental anxiety and voluntary ethanol consumption in rats following central but not basolateral amygdala lesions. Brain Res 760:94–101.

Morales M, Bloom FE (1997) The 5-HT3 receptor is present in different subpopulations of GABAergic neurons in the rat telencephalon. J Neurosci 17:3157–3167.

Murgatroyd C, Patchev AV, Wu Y, Micale V, Bockmuhl Y, Fischer D, Holsboer F, Wotjak CT, Almeida OF, Spengler D (2009) Dynamic DNA methylation programs persistent adverse effects of early-life stress. Nat Neurosci 12:1559–1566.

Oosterbaan HP, Swaab DF, Boer GJ (1985) Oxytocin and vasopressin in the rat do not readily pass from the mother to the amniotic fluid in late pregnancy. J Dev Physiol 7:55–62.

Oppenheim RW, Milligan C, Sun W (2010) Programmed cell death during nervous system development: mechanisms, regulation, function, and implications for neurobehavioral ontogeny. In: Blumberg MS, Freeman JH, Robinson SR, editors. Oxford handbook of developmental behavioral neuroscience. Oxford: Oxford University Press. p. 76–180.

Oreland S, Gustafsson-Ericson L, Nylander I (2010) Short- and long-term consequences of different early environmental conditions on central immunoreactive oxytocin and arginine vasopressin levels in male rats. Neuropeptides 44:391–398.

Ostrowski NL, Young 3rd WS, Knepper MA, Lolait SJ (1993) Expression of vasopressin V1a and V2 receptor messenger ribonucleic acid in the liver and kidney of embryonic, developing, and adult rats. Endocrinology 133:1849–1859.

Paxinos G, Watson C (2007) The rat brain in stereotaxic coordinates. San Diego, California, USA: Academic Press.

Pellow S, File SE (1986) Anxiolytic and anxiogenic drug effects on exploratory activity in an elevated plus-maze: a novel test of anxiety in the rat. Pharmacol Biochem Behav 24:525–529.

Pesold C, Treit D (1995) The central and basolateral amygdala differentially mediate the anxiolytic effects of benzodiazepines. Brain Res 671:213–221.

Pirnik Z, Kiss A (2005) Fos expression variances in mouse hypothalamus upon physical and osmotic stimuli: co-staining with vasopressin, oxytocin, and tyrosine hydroxylase. Brain Res Bull 65:423–431.

Plotsky PM, Meaney MJ (1993) Early, postnatal experience alters hypothalamic corticotropin-releasing factor. CRF) mRNA, median eminence CRF content and stress-induced release in adult rats. Brain Res Mol Brain Res 18:195–200.

Pohjavuori M, Fyhrquist F (1980) Hemodynamic significance of vasopressin in the newborn infant. J Pediatr 97:462–465.

Pow DV, Morris JF (1989) Dendrites of hypothalamic magnocellular neurons release neurohypophysial peptides by exocytosis. Neuroscience 32:435–439.

Rowland NE (2007) Food or fluid restriction in common laboratory animals: balancing welfare considerations with scientific inquiry. Comp Med 57:149–160.

Sapolsky RM, Meaney MJ (1986) Maturation of the adrenocortical stress response: neuroendocrine control mechanisms and the stress hyporesponsive period. Brain Res 396:64–76.

Sharp FR, Sagar SM, Hicks K, Lowenstein D, Hisanaga K (1991) c-fos mRNA, Fos, and Fos-related antigen induction by hypertonic saline and stress. J Neurosci 11:2321–2331.

Shiromani PJ, Magner M, Winston S, Charness ME (1995) Time course of phosphorylated CREB and Fos-like immunoreactivity in the hypothalamic supraoptic nucleus after salt loading. Brain Res Mol Brain Res 29:163–171.

Siga E, Horster MF (1991) Regulation of osmotic water permeability during differentiation of inner medullary collecting duct. Am J Physiol 260:F710–F716.

Slotten HA, Kalinichev M, Hagan JJ, Marsden CA, Fone KC (2006) Long-lasting changes in behavioural and neuroendocrine indices in the rat following neonatal maternal separation: gender-dependent effects. Brain Res 1097:123–132.

Sofroniew MV (1980) Projections from vasopressin, oxytocin, and neurophysin neurons to neural targets in the rat and human. J Histochem Cytochem 28:475–478.

Stemmelin J, Lukovic L, Salome N, Griebel G (2005) Evidence that the lateral septum is involved in the antidepressant-like effects of the vasopressin V1b receptor antagonist, SSR149415. Neuropsychopharmacology 30:35–42.

Veenema AH, Blume A, Niederle D, Buwalda B, Neumann ID (2006) Effects of early life stress on adult male aggression and hypothalamic vasopressin and serotonin. Eur J Neurosci 24:1711–1720.

Veenema AH, Neumann ID (2009) Maternal separation enhances offensive play-fighting, basal corticosterone and hypothalamic vasopressin mRNA expression in juvenile male rats. Psychoneuroendocrinology 34:463–467.

Vogel JR, Beer B, Clody DE (1971) A simple and reliable conflict procedure for testing anti-anxiety agents. Psychopharmacologia 21:1–7.

Walf AA, Frye CA (2007) The use of the elevated plus maze as an assay of anxiety-related behavior in rodents. Nat Protoc 2:322–328.

White LD, Barone Jr S (2001) Qualitative and quantitative estimates of apoptosis from birth to senescence in the rat brain. Cell Death Differ 8:345–356.

Wigger A, Neumann ID (1999) Periodic maternal deprivation induces gender-dependent alterations in behavioral and neuroendocrine responses to emotional stress in adult rats. Physiol Behav 66:293–302.

Wigger A, Sanchez MM, Mathys KC, Ebner K, Frank E, Liu D, Kresse A, Neumann ID, Holsboer F, Plotsky PM, Landgraf R (2004) Alterations in central neuropeptide expression, release, and receptor binding in rats bred for high anxiety: critical role of vasopressin. Neuropsychopharmacology 29:1–14.

Wotjak CT, Kubota M, Liebsch G, Montkowski A, Holsboer F, Neumann I, Landgraf R (1996) Release of vasopressin within the rat paraventricular nucleus in response to emotional stress: a novel mechanism of regulating adrenocorticotropic hormone secretion? J Neurosci 16:7725–7732.

Yoshida M, Iwasaki Y, Asai M, Takayasu S, Taguchi T, Itoi K, Hashimoto K, Oiso Y (2006) Identification of a functional AP1 element in the rat vasopressin gene promoter. Endocrinology 147:2850–2863.

Young WS, Li J, Wersinger SR, Palkovits M (2006) The vasopressin 1b receptor is prominent in the hippocampal area CA2 where it is unaffected by restraint stress or adrenalectomy. Neuroscience 143:1031–1039.

Zhang L, Medina MP, Hernandez VS, Estrada FS, Vega-Gonzalez A (2010) Vasopressinergic network abnormalities potentiate conditioned anxious state of rats subjected to maternal hyperthyroidism. Neuroscience 168:416–428.

Neonatal maternal separation up-regulates protein signalling for cell survival in rat hypothalamus

Claudine Irles, **Alicia T. Nava-Kopp**, Julio Morán, and Limei Zhang

Mis contribuciones:

- Concepción del estudio: +++
- Participación en los experimentos:
    - o Separación materna   +++
    - o Inmunohistoquímica   +++
    - o Western blots   +++
    - o Análisis estadístico   ++
- Discusión de los resultados y comentarios al manuscrito: +++
- Escritura del artículo: +

(-): Ninguna contribución; (+): Contribución menor; (++): Contribución importante; (+++); Contribución crucial

STRESS
The International Journal on the Biology of Stress

informa
healthcare

ORIGINAL RESEARCH REPORT

Neonatal maternal separation up-regulates protein signalling for cell survival in rat hypothalamus

Claudine Irles[1], Alicia T. Nava-Kopp[1], Julio Morán[2], and Limei Zhang[1]

[1]Departamento de Fisiología, Facultad de Medicina and [2]Departamento de Neurodesarrollo y Fisiología, División de Neurociencias, Instituto de Fisiología Celular, Universidad Nacional Autónoma de México, México, D.F., Mexico

Abstract

We have previously reported that in response to early life stress, such as maternal hyperthyroidism and maternal separation (MS), the rat hypothalamic vasopressinergic system becomes up-regulated, showing enlarged nuclear volume and cell number, with stress hyperresponsivity and high anxiety during adulthood. The detailed signaling pathways involving cell death/survival, modified by adverse experiences in this developmental window remains unknown. Here, we report the effects of MS on cellular density and time-dependent fluctuations of the expression of pro- and anti-apoptotic factors during the development of the hypothalamus. Neonatal male rats were exposed to 3 h-daily MS from postnatal days 2 to 15 (PND 2–15). Cellular density was assessed in the hypothalamus at PND 21 using methylene blue staining, and neuronal nuclear specific protein and glial fibrillary acidic protein immunostaining at PND 36. Expression of factors related to apoptosis and cell survival in the hypothalamus was examined at PND 1, 3, 6, 9, 12, 15, 20 and 43 by Western blot. Rats subjected to MS exhibited greater cell-density and increased neuronal density in all hypothalamic regions assessed. The time course of protein expression in the postnatal brain showed: (1) decreased expression of active caspase 3; (2) increased Bcl-2/Bax ratio; (3) increased activation of ERK1/2, Akt and inactivation of Bad; PND 15 and PND 20 were the most prominent time-points. These data indicate that MS can induce hypothalamic structural reorganization by promoting survival, suppressing cell death pathways, increasing cellular density which may alter the contribution of these modified regions to homeostasis.

Introduction

Major developmental processes occur postnatally in the brain. Deletion of cells, through a natural highly regulated process of programmed cell death (PCD, particularly apoptosis), has been found to be crucial for the regulation of neural population size and the establishment of appropriate neural networks (Buss et al., 2006; Clarke, 1985; Oppenheim, 1991). The highest levels of PCD occur during the first postnatal weeks in rat brain regions such as the brainstem, neocortex and hippocampus (White & Barone, 2001), as well as in mouse hypothalamus (Ahern et al., 2013). Therefore, experiences occurring throughout this critical developmental window may produce enduring effects, which can impact on behavior in adult life.

We have previously reported that in response to early life stress, such as maternal hyperthyroidism (Zhang et al., 2008, 2010) and neonatal maternal separation (MS) (Hernandez et al., 2012; Zhang et al., 2012), the rat hypothalamic

vasopressin system becomes up-regulated, showing enlarged volume of the hypothalamic paraventricular and supraoptic vasopressin nuclei and increased cell number, with an increased sensitivity to acute stressors or anxiogenic conditions in adulthood. However, the detailed signaling pathways involving cell death/survival, modified by the adverse experience in this developmental window remain unknown.

MS is a well-validated rodent model used to assess the effect of early postnatal stress on cognition and emotionality in adulthood (Meaney et al., 1985; Plotsky & Meaney, 1993; Veenema, 2009; Zhang et al., 2012). It is well established that the neonatal stage is particularly susceptible to MS, during which neuroendocrine responses (Ladd et al., 2000; Levine, 1994; Plotsky & Meaney, 1993), neurotrophin levels (Cirulli et al., 2003) and epigenetic patterns (Murgatroyd et al., 2009) of the animal undergo modifications. Because the peak of PCD in normal brain development occurs during the early postnatal period (Oppenheim, 1991; White & Barone, 2001), it seemed important to evaluate the expression of pro- and anti-apoptotic proteins and their ratios as a consequence of MS.

The protein caspase 3 (cysteinyl aspartic protease) is responsible for the irreversible proteolysis of cellular components and is thus considered a key enzyme in both the intrinsic (mitochondrial) and extrinsic pathways, leading to

Correspondence: Dr. Limei Zhang and Dr. Claudine Irles, Departamento de Fisiología, Facultad de Medicina, Universidad Nacional Autónoma de México, Av. Universidad 3000, Col. Universidad Nacional Autónoma de México, México 04510, D.F., Mexico. Tel/Fax: +52 5556232348. E-mail: limei@unam.mx (L. Zhang); cloirles@gmail.com (C. Irles)

RIGHTSLINK

apoptosis during brain development (Hengartner, 2000; Kuida et al., 1996; Porter & Janicke, 1999). The anti-apoptotic Bcl-2 protein (B cell lymphoma *2*, a group-II mitochondria mediated cell death suppressor) protects the integrity of the mitochondrial membrane inhibiting apoptosis while pro-apoptotic Bax (Bcl-2 associated X protein, a group-I tumor necrosis factor family mediated cell death effector) is responsible for the release of cytochrome *c* from the mitochondria, causing caspase activation. Thus, the Bcl-2/Bax ratio is an apoptosis indicator (Oltvai et al., 1993). In contrast, the protein kinases ERK1/2 (extracellular signal-regulated kinases 1 and 2) and Akt (protein kinase identified in the AKT virus or protein kinase B) are implicated in pathways leading to neuronal survival/proliferation (Brunet et al., 2001; Davies, 2003; Hetman & Gozdz, 2004; Oppenheim et al., 2010) and neurogenesis (Faedo et al., 2008). Bad (Bcl-2-associated death promoter protein, group-III endoplasmic reticulum mediated cell death effector) is a pro-apoptotic protein since it disrupts mitochondrial membrane integrity. However, serine phosphorylation by ERK1/2 and Akt inactivates Bad, and consequently phosphorylated Bad has an anti-apoptotic effect (Bonni et al., 1999; Fang et al., 1999; Zha et al., 1996).

In the present study, we hypothesized that MS, as an adverse stressor for the neonatal pups, up-regulates hypothalamic activity during an early postnatal window, leading to abnormal cell survival, as a result of the premature activation of the stress coping mechanisms. As a first step to test our hypothesis, we designed the following strategy: (1) to determine the effects of MS on the rat hypothalamic cell-density and (2) to find out whether this stress can modify certain pro- and anti-apoptotic protein expression during the development of the postnatal hypothalamus and in young adults.

Methods

Animals

All animal procedures were approved by the local bioethical and research committees, with approval ID CIEFM-085-2013, in accordance with the ''Principles of laboratory animal care'' detailed in the National Institute of Health Guide for the Care and Use of Laboratory Animals (NIH Publications No. 80-23) revised 1996. Wistar male rats from 24 litters (12 for MS and 12 for animal facility reared rats, AFR, groups) were used in this study. The rats were provided by the local animal facility. Rats were maintained on a 12:12 light–dark cycle (light-on at 07:00 h), in a room with controlled temperature (20–24 °C) and adequate ventilation and given access to standard rat chow and water *ad libitum*.

MS procedure

MS was performed as described previously (Veenema et al., 2006; Zhang et al., 2012). Briefly, to establish pregnancy adult female and male rats were caged together for 2 d and these dates were assigned as ''gestation-day'' (±1 d). Females were then caged in groups of 3 until gestational day 17 when they started to be single-housed in standard rat Plexiglas cages and maintained under standard laboratory conditions as

above. On the day after parturition, PND 2, each litter was culled to 8 pups, of which 5–6 were male. During PND 2 to PND 15, pups were separated daily between 09:00 and 12:00 h from their mothers. Pups were removed from the home cage of each litter by the experimenter whose hands were coated by fine bedding-material corresponding to each cage before transfer. The litter was moved to an adjacent room and placed individually into small boxes filled with bedding, and then put into a humid incubator with temperature maintained at 29 ± 1 °C. After the 3 h-separation period, the pups were returned to the home-cage followed by reunion with their respective mother. Non-separated litters (AFR) were left undisturbed, except for changing the bedding material twice a week, and served as control groups for this study. Pups were weaned from their mother on PND 21 and then housed in standard rat Plexiglas cages and maintained under standard laboratory conditions. Pups were weighed daily from PND 2 to PND 15.

Tissue processing for cell density assessment

Brains for methylene blue staining were taken from rats perfused-fixed on PND 21 ($n = 3$), and for neuronal specific nuclear protein (NeuN) immuno-labeled cell quantification brains were from rats perfused-fixed on PND 36 ($n = 3$). Briefly, male rats were deeply anesthetized with sodium pentobarbital (63 mg/kg, b.w., i.p. injection, Sedalpharma, Mexico City, Mexico) and perfused via the ascending aorta using gravity-fed system, first with 0.9% saline till the liquid from the scissor-opened right atrium getting clear and the liver becoming pale (about 10 ml, 2 min) and followed by ice-cold fixative containing 4% paraformaldehyde (Sigma-Aldrich, St Louis, MO) in 0.1 M sodium phosphate buffer (PB, pH 7.4) plus 15% v/v of saturated picric acid for 15 min (about 150 ml of fixative for young rats).

Histological procedures for total cell-density assessment using methylene blue

Whole brains were removed, cryoprotected (sucrose solution in PB, 10% for 10 min and 20% for more than 4 h) and coronally cryosectioned (12 μm thickness). One out of every six free-floating sections containing hypothalamus were mounted on gelatine-treated glass slides and stained with methylene blue for histological examination. Methylene blue stained nuclei in the arcuate hypothalamic nucleus (Arc), paraventricular nucleus, medial parvocellular division (PVNmpd), anterior hypothalamic area (AHA), medial preoptic nucleus compact (MPOc), medial preoptic nucleus medial (MPOm) and suprachiasmatic nucleus, dorsolateral division (SChDL) were counted. We selected these hypothalamic nuclei because of their proposed relationship with stress coping (Simerly, 1995).

Immunohistochemical procedures for NeuN- and GFAP-expressing cell density assessment

Antibodies

The monoclonal antibodies against neuronal nuclei (NeuN, Chemicon Millipore, Temecula, CA; Cat. No. MAB377,

1 mg/ml stock solution) and against glial fibrillary acidic protein (GFAP, Biocare Medical, Concord, CA, Control Number: 901-065-021513) were raised in mouse, and characterized previously (Estrada et al., 2009, 2012; McLendon & Bigner, 1994, respectively). Biotinylated donkey-anti-mouse antibody was used as second antibody (715-066-150, Jackson ImmunoResearch Laboratories Inc., Pennsylvania, PA, 1:500).

Immunohistochemical procedures

Whole brains were removed and thoroughly rinsed with PB. Vibratome-cut free-floating 50 μm coronal sections containing hypothalamus (spanning from Bregma −0.24 mm to −2.64 mm, Paxinos & Watson, 2009) were obtained. One in every six sections was then immersed in Trizma buffer (pH 7.4 at 25 °C), 0.9% NaCl and Triton X-100 0.3% (TBST). To block unspecific labeling, sections were first incubated in TBST plus 10% normal donkey serum (NDS, Jackson Immunoresearch, West Grove, PA) for 1 h at room temperature. Then, sections were incubated with mouse anti-GFAP (1:1000) or mouse anti-NeuN (1:1000) in TBST + 1% NDS at 4 °C over night. After rinsing, sections were incubated with biotinylated donkey-anti-mouse antibody (1:1000) in TBST + 1% NDS over night. After rinsing several times with TBST, sections were then incubated in avidin–biotin–peroxidase complex (Elite ABC kit PK-6100, Vector Laboratories, Peterborough, UK) for 1 h at room temperature. Peroxidase was detected using 3,3′-diaminobenzidine (0.05%, Electron Microscopy Sciences, Hatfield, PA) as a chromogen and hydrogen peroxide (0.01% v/v) as a substrate. Sections were mounted on gelatin-coated slides and allowed to dry for a day, at room temperature. Then they were further dehydrated by soaking in ethanol 100% for 5 min and rinsing with xylene and mounted with Permount mounting medium (Thermo Fischer Scientific, Waltham, MA).

Western blot

Antibody specifications

The following rabbit antibodies were obtained from Cell Signaling Technology (Danvers, MA): cleaved (active) caspase 3 antibody (Asp175, #9661, 1:1000) recognizes the large fragment of activated caspase 3 as a 17/19 kDa doublet on Western blots and does not cross-react with full-length (inactive) caspase n3 or other caspases (Ahern et al., 2013; Sammeta & McClintock, 2010). Phospho-ERK antibody (pThr202/pThr204, #4376, 1:1000) recognizes single bands at 42/44 kDa only when dually phosphorylated at Thr202 and Tyr204 of ERK1 (Thr185 and Tyr187 of Erk2), and singly phosphorylated at Thr202 of ERK2 (Fado et al., 2013; Gonzalez-Perez et al., 2013). Phospho-Akt antibody (pThr308, #4056, 1:1000) detects Akt phosphorylated at Thr308 as a single band at 60 kDa and does not cross-react with the corresponding phosphorylated residues of either JNK/SAPK or p38 MAP kinase (Gonzalez-Perez et al., 2013). Bcl-2 (#2870, 1:1000) antibody recognizes a single band at 25 kDa and does not cross-react with other Bcl-2 family members (Montes-Rodríguez et al., 2009). phospho-Bad (pSer112, #5284, 1:1000) detects Bad only when phosphorylated at Ser113 as a single band at 23 kDa and does not detect

related family members (Chen et al., 2009). ERK1/2 (#4695P, 1:1000) and Bad (#9292S, 1:1000) antibodies recognize total ERK1/2 and Bad proteins, respectively. Mouse monoclonal antibody for Bax (B9, #sc-7480, 1:1000, Santa Cruz Biotechnology, Santa Cruz, CA) detects Bax as a single band at 21 kDa (Montes-Rodríguez et al., 2009).

Western blot procedure

At postnatal days (PND) 1, 3, 6, 9, 12, 15, 21 and 43, male rats ($n = 6$ at each time-point; no siblings were used for any single time-point) were killed by rapid decapitation. Fresh brain tissue was removed quickly and dissected on ice-cooled saline (0.9%) solution. Brains were coronally blocked from optic chiasm to posterior 1–3 mm, depending on the PND (Bregma 0 to −3 mm for PND 43, according to *The Rat Brain Atlas*; Paxinos & Watson, 2009) and cubes of approximately 1–27 mm^3 (depending on the PND) of ventral diencephalon were obtained under a stereoscopic microscope using microdissection tools. Each sample derived from a single hypothalamus (tissue individually assayed) was homogenized in ice-cooled lysis buffer containing 130 mM NaCl, 20 mM Tris–HCl (pH 7.4), 1% Triton X-100, protease inhibitor cocktail (Sigma-Aldrich) and phosphatase inhibitors (0.01 M NaH$_2$PO$_4$, 0.05 M NaF, 0.002 M Na$_3$VO$_4$). The lysates were centrifuged at 18,210 g (4 °C) for 15 min and the supernatants were collected for protein concentration assessment using a Bradford assay kit (Biorad, Hercules, CA). The same amount of total protein (30 μg) was assayed for each immunoblot. Proteins were separated on 10% or 15% SDS–PAGE and transferred onto nitrocellulose membranes (Amersham Pharmacia Biotech, Arlington Heights, IL). Membranes were blocked for 1 h at room temperature in Starting block T20 blocking buffer (Pierce, Rockford, IL). They were then incubated with the primary antibodies listed in the section above at 4 °C overnight. Antibodies were previously tested with a total brain lysate in order to obtain the working concentration. After rinsing six times in Trizma buffer + Tween 0.1%, membranes were incubated with anti-mouse or anti-rabbit horseradish peroxidase-coupled IgG (#115-035-003 and #111-035-003, respectively, 1:40,000, Jackson Immunoresearch) for 1 h at room temperature. Membranes were rinsed again six times with TBST, and then subjected to detection by Supersignal ECL (Pierce) or SuperSignal West Dura Western blotting kits (Pierce) on hyperfilm ECL (Amersham Pharmacia Biotech). Beta-actin horseradish peroxidase conjugated (#47778, C4, 1:5000, Santa Cruz) was used as an internal control for equal protein loading. Protein levels (intensity of immunoreactivity) were interpreted by densitometric analysis using a computer-assisted densitometry program NIH ImageJ 1.31 (National Institutes of Health, Bethesda, MD) on bands of the hyperfilm.

Cell density quantification and statistical analysis

One out of every six methylene blue stained sections containing hypothalamus were examined under light micro-scope. Cellular density was assessed under the 100× object-ive in the hypothalamic nuclei selected for this study

according to *The Rat Brain Atlas* (Paxinos & Watson, 2009) with help of a drawing tube set at $10\times$. A square corresponding to $0.009\,mm^2$ at the above magnification was printed on white papers. At the beginning of each assessment, the experimenter overlapped the square image projected from the drawing tube to the visual field with the anatomical region to be assessed. Stained cells inside one square were draw. Three to five square-fields were assessed per each nucleus. The drawings were coded for subsequent blind counting. Data from the hypothalamic nucleus were averaged for statistic analysis. NeuN positive cells in the following hypothalamic regions were counted: Arc, PVNmpd, AHA, MPO, SCh and PePO, which are regions relevant for stress coping (Simerly, 1995). Due to the heterogeneous pattern of expression of GFAP, the density of the cells expressing this astrocyte marker was not quantified.

All data are presented as mean ± standard error of the mean (±SEM). For cell density assessment, statistical significance ($p < 0.05$) was determined using Student's *t*-test. For Western blots, prior to running any statistical analyses, all dependent variables were assessed for univariate outliers and normality (Verma et al., 2013). All variables were within an acceptable range. Therefore two-way analysis of variance (ANOVA) of main effects (*treatment* and *age*) with *post hoc* Bonferroni multiple comparisons was used. Statistical analyses were performed using *GraphPad Prism* 5 (Prism Software Corporation, Irvine, CA).

Results

MS increased cell density and NeuN-expressing cell number in hypothalamic regions of rat pups

Total cellular density of several hypothalamic regions on PND 21 was evaluated using methylene blue-stained sections. MS rats exhibited significantly higher densities of methylene blue-stained cellular nuclei than AFR rats for all the hypothalamic nuclei studied (Figure 1, panel A). The mean counts for each region were as follows: MS 72.7 ± 2.7 versus AFR 53.7 ± 2 in the MPOc ($t(4) = 5.59$, $p < 0.01$); MS 69.7 ± 2 versus AFR 59.3 ± 1.4 in the MPOm ($t(4) = 4.14$, $p < 0.05$); MS 43.3 ± 0.9 versus AFR 36 ± 1.2 in the PePO ($t(4) = 5.05$, $p < 0.01$); MS 58.3 ± 0.7 versus AFR 46.3 ± 1.2 in the PVNmpd ($t(4) = 8.73$, $p < 0.005$); MS 70.3 ± 3.4 versus AFR 54.3 ± 1.8 in the SChDL ($t(4) = 4.19$, $p < 0.05$); MS 55.3 ± 0.9 versus AFR 45.3 ± 0.9 in the AHA ($t(4) = 8.02$, $p < 0.01$) and MS 87 ± 2.9 versus AFR 72.7 ± 3 in the Arc ($t(4) = 3.47$, $p < 0.05$; Figure 1, panel A). Immunohistochemistry for NeuN (Figure 1, panels C–E′) and GFAP (Figure 1, panels F–H) was used to distinguish effects on neuronal and glial populations. The mean number of NeuN-immunopositive cells was increased in MS rats compared to AFR rats in the following regions studied: MS 43.3 ± 2.4 versus AFR 30.7 ± 2 ($t(4) = 4.028$, $p < 0.05$) in the MPOm; MS 33.7 ± 0.3 versus AFR 25.9 ± 1.5 cells ($t(4) = 5.211$, $p < 0.01$) in the PVNmpd; MS 40 ± 1.2 versus AFR 28.3 ± 1.8 ($t(4) = 5.534$, $p < 0.01$) in the AHA and MS 65.3 ± 1.9 versus AFR 51 ± 1.2 ($t(4) = 6.557$, $p < 0.01$) in the ventromedial hypothalamic nucleus (Figure 1, panel B). Notably, some hypothalamic nuclei, with high cellular density at the same developing stage, did not express NeuN.

These nuclei included the magnocellular PVN, supraoptic and suprachiasmatic nuclei.

Regarding GFAP expression, unlike the hippocampus where the GFAP immunopositive astrocytes were already distributed in an ordered-matrix pattern at PND 36 (Figure 1H), the hypothalamic GFAP immunopositive astrocytes showed a highly heterogeneous pattern (Figure 1, panels F and F′), which did not allow us to obtain quantitative data for each nucleus. Nonetheless, a clear increase in GFAP labeling was observed in some regions, such as the periventricular (Figure 1, G vs. G′) and suprachiasmatic nuclei (Figure F vs. F′).

MS effects on death or cell-survival related proteins in the developing and adolescent hypothalamus

We analyzed by Western blot the expression pattern of several key proteins implicated in death or cell survival during early development and young adulthood, in whole hypothalamic extracts obtained from AFR and MS rats. The extrinsic and intrinsic death pathways culminate in the activation of caspase 3 (by cleavage of the pro-enzyme). Thus we used the detection of activated caspase 3 to identify PCD events. A similar pattern of active caspase 3 (cleaved caspase 3) expression between MS and AFR rats was observed at the 3, 6, 9 and 12 PND time-points (Figure 2a). However, at PND 15 the MS rats presented a significant 9.4-fold reduction in expression – compared to AFR rats ($p < 0.05$; Figure 2b; Table 1). By PND 20 and in young adults both treatment groups showed decreased levels of active caspase 3 (cleaved) compared to PND 1 (Figure 2b). Two-way ANOVA analysis *treatment* versus *age* revealed that *age* (PND) significantly affected the temporal pattern of activated caspase 3 expression in the treatment groups ($p < 0.03$, Table 1). These results reveal a displaced temporal pattern of caspase 3 activation in MS compared to AFR rats.

Anti-apoptotic Bcl-2 and pro-apoptotic Bax immunoreactivity was analyzed at different postnatal time points as single bands at 26 and 23 kDa, respectively (Figure 3a). The ratio of Bcl-2/Bax decreased from PND 9 to PND 20 in AFR rats, in contrast to increasing levels in MS rats (Figure 3b). ANOVA indicated that MS procedure, age as well as an interaction between *treatment* and *age*, all significantly affected the Bcl-2/Bax ratio ($p < 0.001$, $p < 0.05$ and $p < 0.01$, respectively; Table 1). The effects of MS on the Bcl-2/Bax ratio depended on the age of the neonate and showed a distinctive quantitative pattern of expression. Specifically, MS rats showed a significant 4.5-, 5.3- and 3.3-fold increased expression of the Bcl-2/Bax ratio at PND 15, 20 and 43, respectively ($p < 0.05$, $p < 0.001$ and $p < 0.05$, respectively; Figure 3b; Table 1).

Activated ERK1/2 (phosphorylated ERK1/2) immunoreactivity for AFR and MS rats was detected as single bands at 42/44 kDa of phosphorylated ERK1/2 proteins (Figure 4a). The level of activated ERK1/2 decreased with neonatal age in AFR rats, in contrast to higher levels found in MS rats throughout all PNDs studied, and by PND 20 both treatment-groups (control vs. MS) presented a diminished expression (Figure 4b). Quantitative analysis showed that MS and *treatment* versus *age* interaction significantly affected
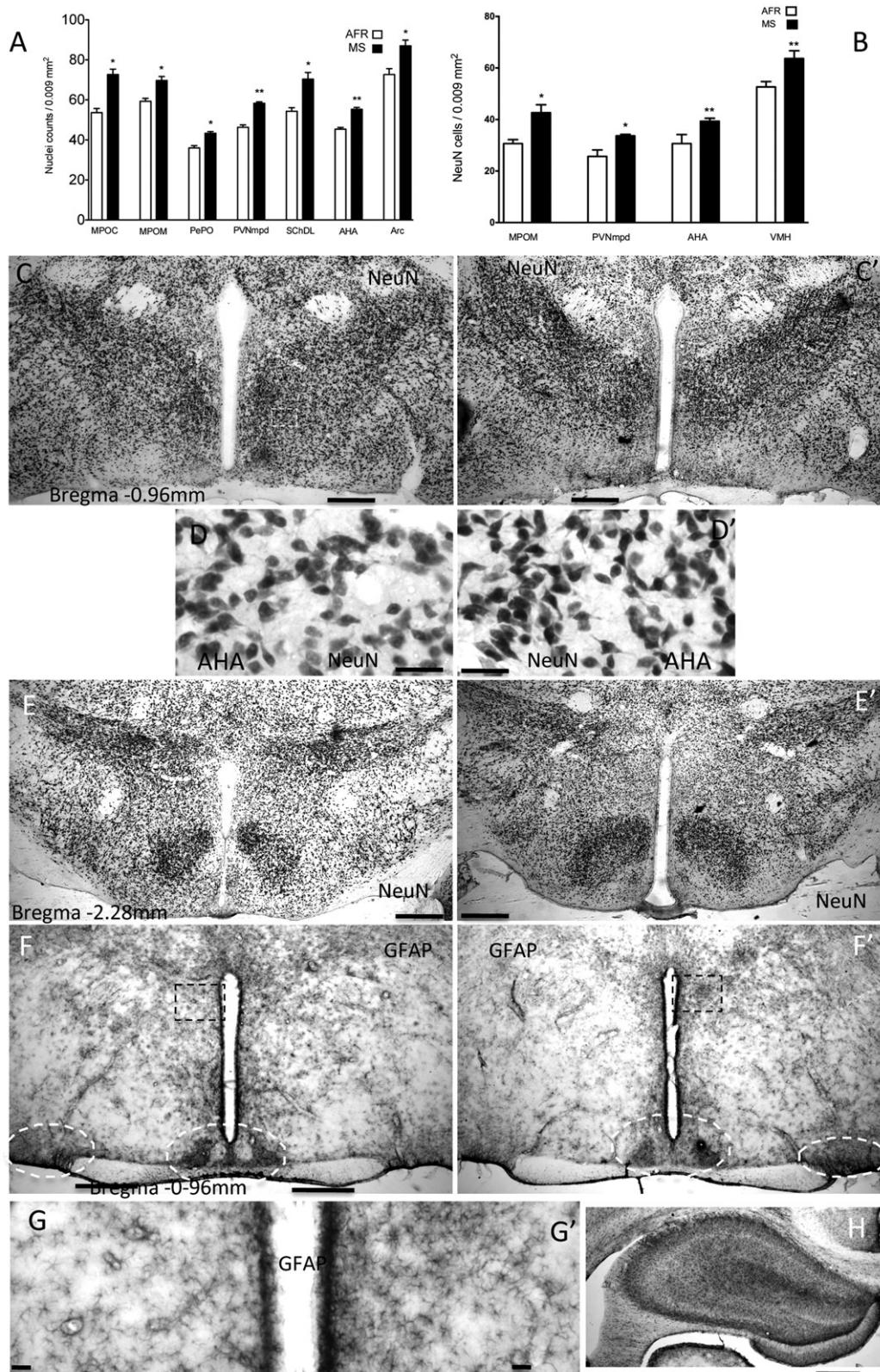
Figure 1. Maternal separation influence on hypothalamic cell density of male offspring on postnatal day (PND) 21 and PND 36. Histograms showing (A) nuclear counts (methylene blue staining on PND 21) and (B) neuronal specific nuclear protein(NeuN) immunostaining on PND 36 in the respective hypothalamic nuclei. Data represent mean ± SEM. $n = 3$. *$p < 0.05$, **$p < 0.01$. (Student *t*-test). MS: maternal separation; AFR: animal facility reared control. MPOc: medial preoptic nucleus compact division; MPOm: medial preoptic nucleus medial division; PePO: periventricular preoptic nucleus; PVNmpd: paraventricular nucleus medial parvocellular division; SChdl: suprachiasmatic nucleus dorsolateral division; AHA: anterior hypothalamic area; Arc: arcuate hypothalamic nucleus; VMH: ventromedial hypothalamic nucleus. Panels C–G′: representative photomicrographs (AFR: left column; MS: right column) showing C and C′ NeuN immunostaining of coronal preoptic/anterior hypothalamus around Bregma −0.96 mm with higher magnification of dashed rectangles showed in D and D′. (E and E′) Coronal sections around tuberal hypothalamus, Bregma −2.28 mm. Note the difference of cell density and the span of the nuclear regions on PND 36. Glial fibrillary acidic protein (GFAP) staining for astrocytes shows uneven immunostaining patterns (F and F′). However, some regions showed increased astrocytic densities in the MS sections, e.g. regions marked by dashed ovals corresponding to supraoptic and suprachiasmatic nuclei and periventricular regions (dashed rectangles showed in higher magnification in panels G and G′). In contrast to hypothalamus, the hippocampus on PND 36 exhibits an ordered GFAP+ astrocyte distribution (panel H). Scale bars: 500 μm for panels C, C′, E, E′, F, F′ and H; 50 μm for other panels.

activation of ERK1/2 ($p < 0.0001$ and $p < 0.05$, respectively, Table 1), with a significant 4.5-, 6- and 5.2-fold increased expression at PND 15, PND 20 and 43, respectively, in MS rats compared to AFR rats ($p < 0.01$, $p < 0.05$ and $p < 0.01$; Figure 4b; Table 1). These results demonstrate that the differences between the treatment-groups (control vs MS) were not due to a displaced temporal pattern of activation but rather to a prolonged and higher level of ERK1/2 activation.

We next examined the level of activated Akt (phosphorylated Akt) from AFR and MS rats (single band at 60 kDa, Figure 5a). Both treatment-groups (control vs. MS) showed similar levels of Akt; however, MS rats presented a significant

5- and 5.9-fold increase at PND 20 and PND 43 in contrast to AFR rats ($p < 0.0001$ and $p < 0.001$; Figure 5b; Table 1). Quantitative analysis revealed that MS, age and *treatment-age* interaction significantly affected activated Akt levels ($p < 0.001$; Table 1).

Finally, the levels of anti-apoptotic Bad (phosphorylated Bad, *pBad*, at Ser[112], single band at 25 kDa; Figure 6a) were analyzed. ANOVA revealed that *treatment* and *age*
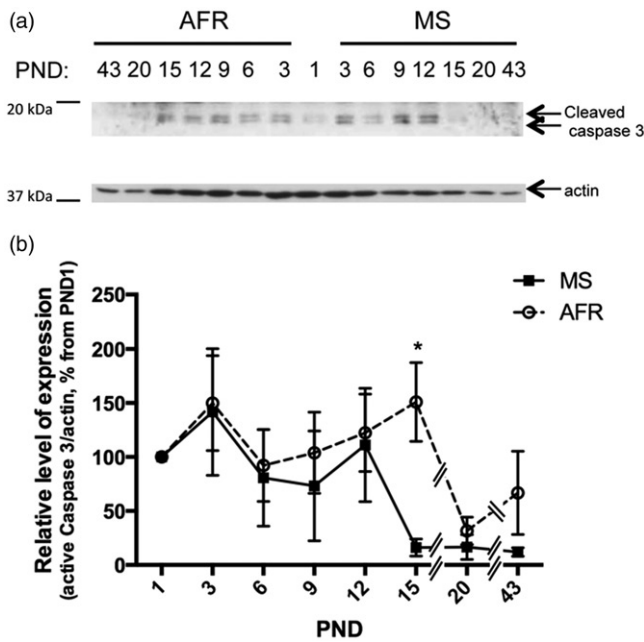

Figure 2. Effect of MS on the expression of pro-apoptotic active (cleaved) caspase 3 protein in early postnatal and young adult rat hypothalamus. Time course of expression of active caspase 3 (cleaved caspase 3) levels in animal facility reared (AFR) and maternally separated (MS) rats. PND: postnatal day. (a) Representative Western blots illustrating immunoreactivity for active caspase 3 and β-actin from dissected hypothalamus. (b) Densitometric analysis of active caspase 3 immunoblots. Each age point (PND) indicates the ratio of the active protein to the total protein expressed as the relative level of expression, estimated as a percentage of PND 1 values. Data are mean ± SEM. Open circles correspond to AFR and black boxes to MS rats. Statistical analyses by factorial ANOVA was used to determine the effects of MS treatment, age and treatment × age on protein levels (Table 1). *$p < 0.05$ versus AFR group ($n = 6$ rats per group per day).
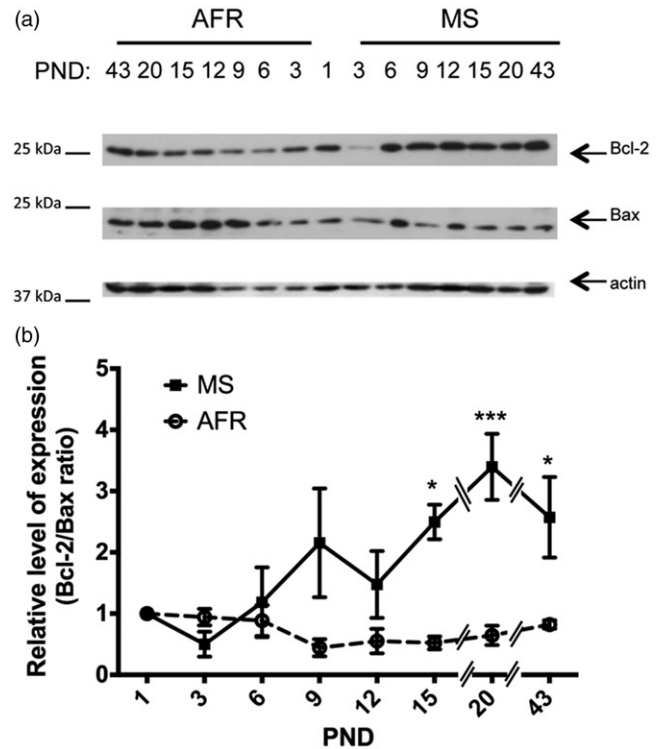
Figure 3. Effect of MS on the ratio of expression of anti-apoptotic Bcl-2 and pro-apoptotic Bax proteins in early postnatal and young adult rat hypothalamus. Time course of expression of the ratio between Bcl2 and Bax in animal facility reared (AFR) and maternally separated (MS) rats. PND: postnatal day. (a) Representative Western blots illustrating immunoreactivity for Bcl-2, Bax and β-actin proteins from dissected hypothalamus. (b) Densitometric analysis of Bcl-2 and Bax immunoblots. Each age point indicates the ratio of the relative level of expression of Bcl-2 and Bax. Data are mean ± SEM. Open circles correspond to AFR and black boxes to MS rats. Statistical analyses by factorial ANOVA was used to determine the effects of MS treatment, age and treatment × age on protein levels (Table 1): *$p < 0.05$ and ***$p < 0.001$ versus AFR group ($n = 6$ rats per group per day).

Table 1. Summary of statistical analysis of relative protein expression from MS and AFR.

	Active (cleaved) caspase 3	Bcl-2/Bax ratio	Active (phosphorylated) pERK1/2	Active (phosphorylated) pAkt	Inactive (phosphorylated) pBad
Treatment $F_{(1, 80)}$	$F = 3.743$ $p = 0.0570$	$F = 12.08$ $p = 0.0009$	$F = 34.51$ $p < 0.0001$	$F = 29.63$ $p < 0.0001$	$F = 13.41$ $p = 0.0006$
Age $F_{(7, 80)}$	$F = 2.382$ $p = 0.03$	$F = 2.421$ $p = 0.0296$	$F = 2.112$ $p = 0.0527$	$F = 5.270$ $p < 0.0001$	$F = 11.68$ $p < 0.0001$
Interaction $F_{(7, 80)}$	$F = 0.9011$ $p = 0.5105$	$F = 3.857$ $p = 0.0016$	$F = 2.160$ $p = 0.0477$	$F = 6.269$ $p < 0.0001$	$F = 2.195$ $p = 0.0483$

Levels of protein analyzed by Western blot at PND 1, 3, 6, 9, 12, 15, 20 and 43 ($n = 6$ rats per group per age). Two-way ANOVA. Caspase 3, cysteinyl aspartic protease 3; Bcl-2, B-cell lymphoma 2; Bax, Bcl-2 associated X protein; ERK , extracellulr signal regulated kinase 1/2; Akt, protein kinase identified in the Akt virus or protein kinase B; Bad, Bcl-2 associated death promoter protein.
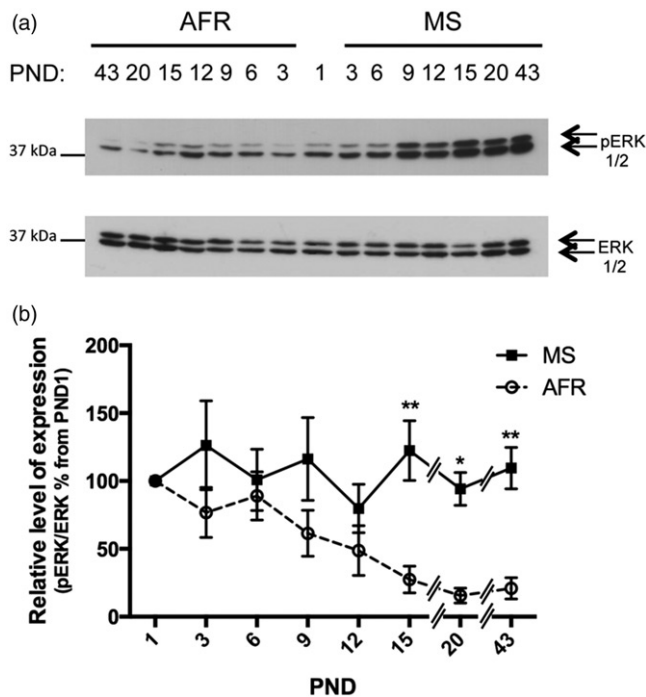
Figure 4. Effect of MS on the expression of survival active (phosphorylated) ERK1/2 kinase in early postnatal and young adult rat hypothalamus. Time course of expression of activated ERK1/2 (phosphorylated ERK1/2, pERK) levels in animal facility reared (AFR) and maternally separated (MS) rats. PND: postnatal day. (a) Representative Western blots illustrating immunoreactivity for pERK1/2 and total ERK1/2 from dissected hypothalamus. (b) Densitometric analysis of pERK1/2 immunoblots. Each age point indicates the ratio of the active protein to the total protein expressed as the relative level of expression, estimated as a percentage from PND 1. Data are mean $\pm$ SEM. Open circles correspond to AFR and black boxes to MS rats. Statistical analyses by factorial ANOVA was used to determine the effects of MS treatment, age and treatment $\times$ age on protein levels (Table 1): $*p < 0.05$ and $**p < 0.01$ versus AFR group ($n = 6$ rats per group per day).
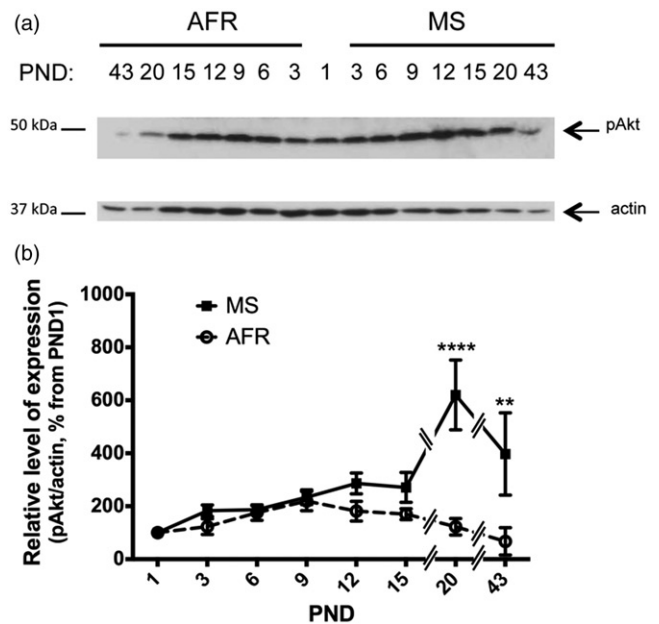

Figure 5. Effect of MS on the expression of survival active (phosphorylated) Akt kinase in early postnatal and young adult rat hypothalamus. Time course of expression of activated Akt (phosphorylated Akt, pAkt) levels in animal facility reared (AFR) and maternally separated (MS) rats. PND: postnatal day. (a) Representative Western blots illustrating immunoreactivity for pAkt and β-actin (same membrane as for caspase 3) from dissected hypothalamus. (b) Densitometric analysis of pAkt immunoblots. Each age point indicates the ratio of the active protein to the total protein expressed as the relative level of expression, estimated as a percentage from PND 1. Data are mean $\pm$ SEM. Open circles correspond to AFR and black boxes to MS rats. Statistical analyses by factorial ANOVA was used to determine the effects of MS treatment, age and treatment $\times$ age on protein levels (Table 1): $**p < 0.01$ and $****p < 0.0001$ versus AFR group ($n = 6$ per group per day).

significantly affected pBad levels, with an (*age* vs. *treatment*) interaction ($p < 0.001$, $p < 0.0001$ and $p < 0.05$, respectively; Table 1). Figure 6(b) shows higher levels of pBad during neonatal ages with a peak around PND 15 in AFR rats while this peak was reached at a later postnatal day (PND 20) with a significant 2.4-fold increase in MS rats ($p < 0.001$; Table 1). Furthermore, a significant difference in pBad levels was also observed at PND 43 ($p < 0.05$; Table 1).

Discussion

In the present study, we found that neonatal MS promotes cell survival in the rat hypothalamus and interferes with PCD, resulting in an increased density of neurons in several hypothalamic nuclei of male rat pups.

The medial preoptic nucleus (MPO), the paraventricular nucleus (PVN) and AHA from the periventricular and medial zones of the anterior region of the hypothalamus, here studied, contain neurons with projections to neuroendocrine, somatomotor and autonomic response pathways. The nuclei studied are involved in the regulation of maternal and reproductive behaviour (e.g. MPO) and hormone secretion (e.g. PVN, PePO and SChDL) (Simerly, 1995). The increased neuron number in these hypothalamic regions may explain the hyperreactivity of the stress axis in the MS adult rats

as reported in several studies (Veenema et al., 2006; Zhang et al., 2012).

Implications of PCD/survival modulation by MS

PCD is mediated by caspases and pro- and anti-apoptotic members of the Bcl-2 family. Activated (i.e. cleaved) caspase 3 is considered an apoptotic marker in the nervous system (Hengartner, 2000; Kuida et al., 1996; Porter & Janicke, 1999), as it promotes the irreversible proteolysis of critical cellular components (Bredesen, 2000). Moreover, vulnerability to PCD has been proposed to be determined also by the Bcl-2/Bax ratio (Oltvai et al., 1993). The highest levels of PCD have been reported at early postnatal ages (Ahern et al., 2013; White & Barone, 2001): in rodents, 60–70% of newly produced neuronal cells during the first postnatal week undergo PCD during the second postnatal week (Bandeira et al., 2009). In our study, the levels of expression of activated caspase 3 seen from PND 1 to PND 15 and the reduced Bcl-2/Bax ratio from PND 6 to PND 20 in AFR rats corresponds with the reported timing of neuronal death (Bandeira et al., 2009; Clarke, 1985). A similar pattern of expression of these proteins was observed in several rat brain regions (Mooney & Miller, 2000; Shimohama et al., 1998). Expression of the Bcl-2/Bax ratio does not completely coincide with the decrease in
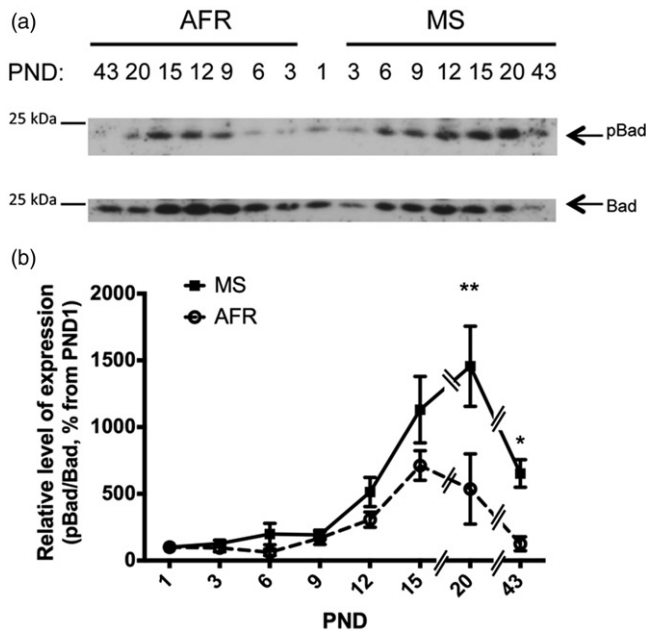
Figure 6. Effect of MS on the expression of anti-apoptotic inactive (phosphorylated) Bad kinase in early postnatal and young adult rat hypothalamus. Time course of expression of inactivated Bad (phosphorylated Bad at Ser[112], pBad) levels in animal facility reared (AFR) and maternally separated (MS) rats. PND: postnatal day. (a) Representative Western blots illustrating immunoreactivity for pBad and Bad from dissected hypothalamus. (b) Densitometric analysis of pBad immunoblots. Each age point indicates the ratio of the inactive protein to the total protein expressed as the relative level of expression, estimated as a percentage from PND 1. Data are mean $\pm$ SEM. Open circles correspond to AFR and black boxes to MS rats. Statistical analyses by factorial ANOVA was used to determine the effects of MS treatment, age and treatment $\times$ age on protein levels (Table 1): *$p < 0.05$ and **$p < 0.01$ versus AFR group ($n = 6$ rats per group per day).

active caspase 3 expression; thus, even if Bcl-2 and Bax proteins are directly involved in caspase 3 activation, other factors may also be modulating its activity.

The time course of active caspase-3-expression in the MS groups was reduced earlier (between PND 12 and PND 15) in MS rats compared to AFR rats (between PND 15 and PND 20), and by PND 20 the process was largely abated in both treatment-groups. The Bcl-2/Bax ratio was found to be significantly increased after PND 15 in MS rats indicating that the pattern of change in this ratio might be another factor for the reduction of PCD in the hypothalamus of MS offspring. Diminished caspase 3 expression is key to terminate the period of PCD (Mooney & Miller, 2000); thus, the finding here that MS decreases caspase 3 expression at an earlier PND, could precipitate the end of PCD in the hypothalamus.

Together, these results imply that MS is altering normal postnatal development of the hypothalamus by a combination of a different temporal pattern of activated caspase 3 expression with increased Bcl-2 family anti-apoptotic protein expression. Consistent with our results, a 24 h maternal deprivation (Chocyk et al., 2011) or artificially rearing of rats (Chatterjee et al., 2007; Chatterjee-Chakraborty & Chatterjee, 2010) has shown decreased levels of PCD at a particular PND and brain area, such as the substantia nigra (Chocyk et al., 2011) and some sexually dimorphic areas of the

hypothalamus (Chatterjee et al., 2007; Chatterjee-Chakraborty & Chatterjee, 2010). However, in a study using maternal deprivation for 24 h at PND 12, increased levels of PCD in hippocampus or cerebral cortex, but not hypothalamus, were observed (Zhang et al., 2002). However, the experimental model used in the present study is fundamentally different from the last mentioned one (Zhang et al., 2002). For instance, maternal deprivation for 24 h severely alters hydroelectrolyte balance in the newborn, whereas MS for 3 h has no significant effects (unpublished data). Variations in maternal behavior after the pups were handled have been reported in the literature and the long-term consequences, from beneficial to detrimental, of these manipulations have been proposed (Champagne, 2013; Chatterjee et al., 2007). In this light, it would be expected that different MS schemes yield different modifications and a trans-model comparison should be carefully considered.

We also measured expression of activated ERK1/2 and Akt, as well as inactivated Bad (by phosphorylation at Ser[112]), given the role of these proteins in signaling pathways implicated in neuronal survival and proliferation (Brunet et al., 2001; Davies, 2003; Hetman & Gozdz, 2004; Oppenheim et al., 2010); they are also important in neurogenesis, both in early development and in repair processes of the CNS (Faedo et al., 2008; Shioda et al., 2009). Around PND 15–20, MS rats showed increased phosphorylation of ERK1/2 and Akt, together with increased phosphorylation of Bad. ERK1/2 and Akt pro-survival kinases are responsible for Bad inactivation by phosphorylation (del Peso et al., 1997) leading to inhibition of caspase 3 activation and promoting cell survival (Zha et al., 1996). Thus, our results indicate that survival pathways are enhanced in MS rats.

Molecular targets of MS action

The mechanism of MS-induced ERK1/2 and Akt activation is complex and might involve neurotrophic factors, neuropeptides and/or neurotransmitters. Neurotrophic factors, like brain derived neurotrophic factor (BDNF) and epidermal growth factor activate the Ras–Raf–MEK (mitogen-activated protein kinase/ERK) pathway resulting in cellular neurotrophic actions, including neurite growth, regeneration and neurogenesis (Fishwick et al., 2010; Kaplan & Miller, 2000). Moreover, the survival-promoting effects of BDNF are also associated with inactivated/phosphorylated Bad by MAPK/ERK1/2 (Bonni et al., 1999; Downward, 1999) or Akt (del Peso et al., 1997). Therefore, neurotrophic factors could be involved in the increase of pro-survival factors during MS. In support of this, MS has been found to increase the expression of nerve growth factor and BDNF in rat hypothalamus and hippocampus (Cirulli et al., 2003).

Another possible mechanism by which MS may induce an enhanced hypothalamic cell survival is through the up-regulated vasopressin (AVP) system promoted by MS (Zhang et al., 2012). This may lead to an amplified ligand-presence of AVP in hypothalamic regions expressing vasopressin receptors, V1$_a$ and V1$_b$. AVP has been found to stimulate cellular proliferation/growth in several cell types such as fibroblasts, endothelial, muscle, kidney and other

cells, through V1$_a$, V1$_b$ and V2 receptors (Hoffert et al., 2012; Koshimizu et al., 2012) and is evidently an anti-apoptotic molecule for hypothalamic neurons (Chen et al., 2008, 2009; Koshimizu et al., 2012) and kidney cells (Hoffert et al., 2012) through vasopressin receptors. More importantly, AVP promotes cell survival through the activation of the MAPK/ERK1/2, PI3K/Akt pathways and Bad inactivation, blocking caspase 3 activation thus leading to apoptotic cell death inhibition in hypothalamic neurons (Chen et al., 2008, 2009; Koshimizu et al., 2012). It is thus possible to speculate that increased release of AVP in the hypothalamus of MS rats could act as another important pro-survival/anti-apoptotic molecule through the activation of survival pathways such as ERK1/2 and Akt inhibiting PCD during the postnatal developmental period.

The ability to inhibit PCD and promote sustained activation of survival pathways around PND 15–20, at the end or 5 d after the last separation manipulation, is not yet clear. However, other studies have shown different levels of protein expression occurring after MS has finished. Indeed, BDNF expression has been found to be increased on PND 17 or PND 16–20 (in a PND 2–14 or 10–15 MS paradigm, respectively) (Lee et al., 2012; Roceri et al., 2004). Thus, it is possible to hypothesize that prolonged and abnormal expression of some proteins, such as ERK1/2, Akt, Bcl-2 and pBad, may result from repetitive MS, which in turn is an adaptive consequence of each preceding MS event.

The results from this study provide a novel temporal description of expression changes for some key pro-/anti-apoptotic factors following MS, which may serve as a basis for further understanding the molecular mechanisms of MS consequences on development of the hypothalamus.

In summary, our present data show that the fine balance between the expression and activities of cell survival and death proteins, and their temporal pattern, are disturbed by MS. The perturbation of these profiles of PCD during this critical period of development by MS, may represent an additional correlate of vulnerability involved in aberrant cell number and plasticity of the hypothalamus. Dysregulation of the signaling pathways involving ERK1/2, Akt, Bad, Bcl-2, Bax and caspase 3 may be a key mechanism by which MS induces changes in survival of susceptible neural cells.

Acknowledgements

Declaration of interest

References

Ahern TH, Krug S, Carr AV, Murray EK, Fitzpatrick E, Bengston L, McCutcheon J, et al. (2013). Cell death atlas of the postnatal mouse ventral forebrain and hypothalamus: effects of age and sex. J Comp Neurol 521:2551–69.

Bandeira F, Lent R, Herculano-Houzel S. (2009). Changing numbers of neuronal and non-neuronal cells underlie postnatal brain growth in the rat. Proc Natl Acad Sci USA 106:14108–13.

Bonni A, Brunet A, West AE, Datta SR, Takasu MA, Greenberg ME. (1999). Cell survival promoted by the Ras-MAPK signaling pathway by transcription-dependent and -independent mechanisms. Science 286:1358–62.

Bredesen DE. (2000). Apoptosis: overview and signal transduction pathways. J Neurotrauma 17:801–10.

Brunet A, Datta SR, Greenberg ME. (2001). Transcription-dependent and -independent control of neuronal survival by the PI3K-Akt signaling pathway. Curr Opin Neurobiol 11:297–305.

Buss RR, Sun W, Oppenheim RW. (2006). Adaptive roles of programmed cell death during nervous system development. Annu Rev Neurosci 29:1–35.

Champagne FA. (2013). Early environments, glucocorticoid receptors, and behavioral epigenetics. Behav Neurosci 127:628–36.

Chatterjee D, Chatterjee-Chakraborty M, Rees S, Cauchi J, de Medeiros CB, Fleming AS. (2007). Maternal isolation alters the expression of neural proteins during development: 'stroking' stimulation reverses these effects. Brain Res 1158:11–27.

Chatterjee-Chakraborty M, Chatterjee D. (2010). Artificial rearing inhibits apoptotic cell death through action on pro-apoptotic signaling molecules during brain development: replacement licking partially reverses these effects. Brain Res 1348:10–20.

Chen J, Liu Y, Soh JW, Aguilera G. (2009). Antiapoptotic effects of vasopressin in the neuronal cell line H32 involve protein kinase Calpha and beta. J Neurochem 110:1310–20.

Chen J, Volpi S, Aguilera G. (2008). Anti-apoptotic actions of vasopressin in H32 neurons involve MAP kinase transactivation and Bad phosphorylation. Exp Neurol 211:529–38.

Chocyk A, Dudys D, Przyborowska A, Majcher I, Mackowiak M, Wedzony K. (2011). Maternal separation affects the number, proliferation and apoptosis of glia cells in the substantia nigra and ventral tegmental area of juvenile rats. Neuroscience 173:1–18.

Cirulli F, Berry A, Alleva E. (2003). Early disruption of the mother–infant relationship: effects on brain plasticity and implications for psychopathology. Neurosci Biobehav Rev 27:73–82.

Clarke PG. (1985). Neuronal death during development in the isthmo-optic nucleus of the chick: sustaining role of afferents from the tectum. J Comp Neurol 234:365–79.

Davies AM. (2003). Regulation of neuronal survival and death by extracellular signals during development. EMBO J 22:2537–45.

del Peso L, Gonzalez-Garcia M, Page C, Herrera R, Nunez G. (1997). Interleukin-3-induced phosphorylation of BAD through the protein kinase Akt. Science 278:687–9.

Downward J. (1999). How BAD phosphorylation is good for survival. Nat Cell Biol 1:E33–5.

Estrada FS, Hernandez VS, Lopez-Hernandez E, Corona-Morales AA, Solis H, Escobar A, Zhang L. (2012). Glial activation in a pilocarpine rat model for epileptogenesis: a morphometric and quantitative analysis. Neurosci Lett 514:51–6.

Estrada FS, Hernandez VS, Medina MP, Corona-Morales AA, Gonzalez-Perez O, Vega-Gonzalez A, Zhang L. (2009). Astrogliosis is temporally correlated with enhanced neurogenesis in adult rat hippocampus following a glucoprivic insult. Neurosci Lett 459: 109–14.

Fado R, Moubarak RS, Minano-Molina AJ, Barneda-Zahonero B, Valero J, Saura CA, Moran J, et al. (2013). X-linked inhibitor of apoptosis protein negatively regulates neuronal differentiation through interaction with cRAF and Trk. Sci Rep 3(2397):1–11.

Faedo A, Tomassy GS, Ruan Y, Teichmann H, Krauss S, Pleasure SJ, Tsai SY, et al. (2008). COUP-TFI coordinates cortical patterning, neurogenesis, and laminar fate and modulates MAPK/ERK, AKT, and beta-catenin signaling. Cereb Cortex 18:2117–31.

Fang X, Yu S, Eder A, Mao M, Bast RC Jr., Boyd D, Mills GB. (1999). Regulation of BAD phosphorylation at serine 112 by the Ras-mitogen-activated protein kinase pathway. Oncogene 18:6635–40.

RIGHTSLINK()

Fishwick KJ, Li RA, Halley P, Deng P, Storey KG. (2010). Initiation of neuronal differentiation requires PI3-kinase/TOR signalling in the vertebrate neural tube. Dev Biol 338:215–25.

Gonzalez-Perez G, Segovia NC, Rivas-Carvalho A, Reyes DP, Torres-Aguilar H, Aguilar-Ruiz SR, Irles C, et al. (2013). Human CD4(+) effector T lymphocytes generated upon TCR engagement with self-peptides respond defectively to IL-7 in their transition to memory cells. Cell Mol Immunol 10(3):261–74.

Hengartner MO. (2000). The biochemistry of apoptosis. Nature 407:770–6.

Hernandez VS, Ruiz-Velazco S, Zhang L. (2012). Differential effects of osmotic and SSR149415 challenges in maternally separated and control rats: the role of vasopressin on spatial learning. Neurosci Lett 528:143–7.

Hetman M, Gozdz A. (2004). Role of extracellular signal regulated kinases 1 and 2 in neuronal survival. Eur J Biochem 271:2050–5.

Hoffert JD, Pisitkun T, Saeed F, Song JH, Chou CL, Knepper MA. (2012). Dynamics of the G protein-coupled vasopressin V2 receptor signaling network revealed by quantitative phosphoproteomics. Mol Cell Proteomics 11(2):M111 014613.

Kaplan DR and Miller FD. (2000). Neurotrophin signal transduction in the nervous system. Curr Opin Neurobiol 10:381–91.

Koshimizu TA, Nakamura K, Egashira N, Hiroyama M, Nonoguchi H, Tanoue A. (2012). Vasopressin V1a and V1b receptors: from molecules to physiological systems. Physiol Rev 92:1813–64.

Kuida K, Zheng TS, Na S, Kuan C, Yang D, Karasuyama H, Rakic P, Flavell RA. (1996). Decreased apoptosis in the brain and premature lethality in CPP32-deficient mice. Nature 384:368–72.

Ladd CO, Huot RL, Thrivikraman KV, Nemeroff CB, Meaney MJ, Plotsky PM. (2000). Long-term behavioral and neuroendocrine adaptations to adverse early experience. Prog Brain Res 122:81–103.

Lee KY, Miki T, Yokoyama T, Ueki M, Warita K, Suzuki S, Ohta K, et al. (2012). Neonatal repetitive maternal separation causes long-lasting alterations in various neurotrophic factor expression in the cerebral cortex of rats. Life Sci 90:578–84.

Levine S. (1994). The ontogeny of the hypothalamic-pituitary-adrenal axis. The influence of maternal factors. Ann NY Acad Sci 746:275–88; discussion 289–93.

McLendon RE, Bigner DD. (1994). Immunohistochemistry of the glial fibrillary acidic protein: basic and applied considerations. Brain Pathol 4:221–8.

Meaney MJ, Aitken DH, Bodnoff SR, Iny LJ, Sapolsky RM. (1985). The effects of postnatal handling on the development of the glucocorticoid receptor systems and stress recovery in the rat. Prog Neuropsychopharmacol Biol Psychiatry 9:731–4.

Montes-Rodríguez CJ, Alavez S, Soria-Gómez E, Rueda-Orozco PE, Guzman K, Morán J, Prospéro-García O. (2009). BCL-2 and BAX proteins expression throughout the light-dark cycle and modifications induced by sleep deprivation and rebound in adult rat brain. J Neurosci Res 87(7):1602–9.

Mooney SM, Miller MW. (2000). Expression of bcl-2, bax, and caspase-3 in the brain of the developing rat. Brain Res Dev Brain Res 123:103–17.

Murgatroyd C, Patchev AV, Wu Y, Micale V, Bockmuhl Y, Fischer D, Holsboer F, et al. (2009). Dynamic DNA methylation programs persistent adverse effects of early-life stress. Nat Neurosci 12:1559–66.

Oltvai ZN, Milliman CL, Korsmeyer SJ. (1993). Bcl-2 heterodimerizes *in vivo* with a conserved homolog, Bax, that accelerates programmed cell death. Cell 74:609–19.

Oppenheim RW. (1991). Cell death during development of the nervous system. Annu Rev Neurosci 14:453–501.

Oppenheim RW, Milligan C, Sun W. (2010). Chapter 5: Programmed cell death during nervous system development: mechanisms, regulation, functions and implications for neurobehavioral ontogeny. In: Blumberg MS, Freeman JH, Robinson SR, editors. Oxford handbook of developmental behavioral neuroscience. New York: Oxford University Press. p 76–107.

Paxinos G, Watson C. (2009). The rat brain. 6th ed. San Diego: Elsevier.

Plotsky PM, Meaney MJ. (1993). Early, postnatal experience alters hypothalamic corticotropin-releasing factor (CRF) mRNA, median eminence CRF content and stress-induced release in adult rats. Brain Res Mol Brain Res 18:195–200.

Porter AG, Janicke RU. (1999). Emerging roles of caspase-3 in apoptosis. Cell Death Differ 6:99–104.

Roceri M, Cirulli F, Pessina C, Peretto P, Racagni G, Riva MA. (2004). Postnatal repeated maternal deprivation produces age-dependent changes of brain-derived neurotrophic factor expression in selected rat brain regions. Biol Psychiatry 55:708–14.

Sammeta N, McClintock TS. (2010). Chemical stress induces the unfolded protein response in olfactory sensory neurons. J Comp Neurol 518:1825–36.

Shimohama S, Fujimoto S, Sumida Y, Tanino H. (1998). Differential expression of rat brain bcl-2 family proteins in development and aging. Biochem Biophys Res Commun 252:92–6.

Shioda N, Han F, Fukunaga K. (2009). Role of Akt and ERK signaling in the neurogenesis following brain ischemia. Int Rev Neurobiol 85:375–87.

Simerly RB. (1995). Chapter 17: Anatomical substrates of hypothalamic integration. In: Paxinos G, editor. The rat nervous system. 2nd ed. Sydney: Academic Press. p 353–76.

Veenema AH. (2009). Early life stress, the development of aggression and neuroendocrine and neurobiological correlates: what can we learn from animal models? Front Neuroendocrinol 30:497–518.

Veenema AH, Blume A, Niederle D, Buwalda B, Neumann ID. (2006). Effects of early life stress on adult male aggression and hypothalamic vasopressin and serotonin. Eur J Neurosci 24:1711–20.

Verma SP, Cruz-Huicochea R, Díaz-González L. (2013). Univariate data analysis system: deciphering mean compositions of island and continental arc magmas, and influence of the underlying crust. Int Geol Rev 55:1922–40.

White LD, Barone Jr S. (2001). Qualitative and quantitative estimates of apoptosis from birth to senescence in the rat brain. Cell Death Differ 8:345–56.

Zha J, Harada H, Yang E, Jockel J, Korsmeyer SJ. (1996). Serine phosphorylation of death agonist BAD in response to survival factor results in binding to 14-3-3 not BCL-X(L). Cell 87:619–28.

Zhang L, Hernandez VS, Liu B, Medina MP, Nava-Kopp AT, Irles C, Morales M. (2012). Hypothalamic vasopressin system regulation by maternal separation: its impact on anxiety in rats. Neuroscience 215:135–48.

Zhang L, Hernandez VS, Medina-Pizarro M, Valle-Leija P, Vega-Gonzalez A, Morales T. (2008). Maternal hyperthyroidism in rats impairs stress coping of adult offspring. J Neurosci Res 86:1306–15.

Zhang L, Medina MP, Hernandez VS, Estrada FS, Vega-Gonzalez A. (2010). Vasopressinergic network abnormalities potentiate conditioned anxious state of rats subjected to maternal hyperthyroidism. Neuroscience 168:416–28.

Zhang LX, Levine S, Dent G, Zhan Y, Xing G, Okimoto D, Kathleen Gordon M, et al. (2002). Maternal deprivation increases cell death in the infant rat brain. Brain Res Dev Brain Res 133:1–11.

A Synaptically Connected Hypothalamic Magnocellular Vasopressin-Locus Coeruleus Neuronal Circuit and Its Plasticity in Response to Emotional and Physiological Stress

Oscar R. Hernéndez-Perez*, Vito S. Hernandez*, **Alicia Nava-Kopp***, Rafael A. Barrio, Mohsen Seifi, Jerome D. Swinny, Lee E. Eiden and Limei Zhang

*Shared first authorship

Mis contribuciones:
- Concepción del estudio: +++
- Participación en los experimentos:
    - Superación materna   +++
    - Inmunohistoquímica   ++
    - ISH RNAscope   ++
    - Análisis estadístico   ++
- Discusión de los resultados y comentarios al manuscrito: +++
- Escritura del artículo: +

(-): Ninguna contribución; (+): Contribución menor; (++): Contribución importante; (+++); Contribución crucial

A Synaptically Connected Hypothalamic Magnocellular Vasopressin-Locus Coeruleus Neuronal Circuit and Its Plasticity in Response to Emotional and Physiological Stress

Oscar R. Hernández-Pérez[1†], Vito S. Hernández[1†], Alicia T. Nava-Kopp[1†], Rafael A. Barrio[2], Mohsen Seifi[3], Jerome D. Swinny[3], Lee E. Eiden[4] and Limei Zhang[1*]

[1] Departamento de Fisiología, Facultad de Medicina, Universidad Nacional Autónoma de México, Mexico City, Mexico,
[2] Instituto de Física, Universidad Nacional Autónoma de México, Mexico City, Mexico, [3] School of Pharmacy and Biomedical Sciences, Institute for Biomedical and Biomolecular Science, University of Portsmouth, Portsmouth, United Kingdom,
[4] Section on Molecular Neuroscience, National Institute of Mental Health-IRP, Bethesda, MD, United States

The locus coeruleus (LC)-norepinephrine (NE) system modulates a range of salient brain functions, including memory and response to stress. The LC-NE system is regulated by neurochemically diverse inputs, including a range of neuropeptides such as arginine-vasopressin (AVP). Whilst the origins of many of these LC inputs, their synaptic connectivity with LC neurons, and their contribution to LC-mediated brain functions, have been well characterized, this is not the case for the AVP-LC system. Therefore, our aims were to define the types of synapses formed by AVP+ fibers with LC neurons using immunohistochemistry together with confocal and transmission electron microscopy (TEM), the origins of such inputs, using retrograde tracers, and the plasticity of the LC AVP system in response to stress and spatial learning, using the maternal separation (MS) and Morris water maze (MWM) paradigms, respectively, in rat. Confocal microscopy revealed that AVP+ fibers contacting tyrosine hydroxylase (TH)+ LC neurons were also immunopositive for vesicular glutamate transporter 2, a marker of presynaptic glutamatergic axons. TEM confirmed that AVP+ axons formed Gray type I (asymmetric) synapses with TH+ dendrites thus confirming excitatory synaptic connections between these systems. Retrograde tracing revealed that these LC AVP+ fibers originate from hypothalamic vasopressinergic magnocellular neurosecretory neurons (AVPMNNs). MS induced a significant increase in the density of LC AVP+ fibers. Finally, AVPMNN circuit upregulation by water-deprivation improved MWM performance while increased Fos expression was found in LC and efferent regions such as hippocampus and prefrontal cortex, suggesting that AVPMMN projections to LC could integrate homeostatic responses modifying neuroplasticity.

Keywords: arginine vasopressin, RNAscope, Fluoro-Gold, Morris water maze, electron microscopy

INTRODUCTION

Converging pharmacological, physiological and behavioral data indicate that the neurohormone arginine vasopressin (AVP) system is principally linked to the homeostatic regulation of fluid balance (Armstrong, 2004), yet ascending vasopressinergic projections that connect the physiology of water regulation with emotional context and adaptive behaviors have been reported (de Wied et al., 1993; Hernandez et al., 2012; Zhang et al., 2012, 2016, 2018; Zhang and Eiden, 2018). Historically, the actions of AVP within the brain were considered to primarily occur in a paracrine manner, for example, via dendritic release from hypothalamic neurons and further diffusion to target brain regions via the cerebrospinal or interstitial fluids (Leng et al., 1992; Landgraf and Neumann, 2004; Ludwig and Leng, 2006). However, we and others have since demonstrated direct synaptic connections between vasopressinergic magnocellular neurosecretory neurons (AVPMNNs) of the hypothalamus and other brain regions including hippocampus (Cui et al., 2013; Zhang and Hernandez, 2013), amygdala (Hernandez et al., 2016), and lateral habenula (Zhang et al., 2016, 2018) via dual AVPMNN projections to these regions and to the neurohypophysis (Hernandez et al., 2015). This raises the possibility of direct AVPMNN projections to additional brain nuclei that participate in integrating homeostatic with behavioral regulation (Zhang and Eiden, 2018). AVP-immunopositive (AVP+) axons have indeed been identified in a myriad of brain regions involved in such functions, including the pontine nucleus *locus coeruleus* (LC) (Buijs, 1978; Rood and De Vries, 2011). However, the source of these inputs, and therefore the putative regulatory circuits in which they participate, have not been identified.

The LC (also called nucleus pigmentosus ponti) are bilateral dense groups of cells located in the pontine tegmentum, specifically in the lateral-rostral part of the floor of the 4th ventricle. LC neurons are identified by their expression of the norepinephrine synthesizing enzymes tyrosine hydroxylase (TH) and dopamine-beta-hydroxylase (DBH), but not phenylethanolamine N-methyltransferase, thereby confirming their principal neurochemical signature of norepinephrine (NE) (Kobayashi et al., 1974; Swanson, 1976; Levitt and Moore, 1979). LC neurons provide the major source of NE throughout most of the brain (Robertson et al., 2013; Schwarz and Luo, 2015). The LC-NE system modulates some of the most salient brain functions, such as arousal, learning and memory and the cognitive response to stress (Berridge and Waterhouse, 2003; Atzori et al., 2016). At the synaptic level, NE facilitates synaptic plasticity by recruiting and modifying multiple molecular elements of synaptic signaling, including specific transmitter receptors, intracellular protein kinases, and translation initiation (Maity et al., 2015; Nguyen and Gelinas, 2018). All such LC-NE functions are strongly aligned with the levels of LC neuronal activity. While LC neurons are spontaneously active, their firing rates are strongly influenced by their afferent inputs, many of which contain an array of neuropeptides (Palkovits and Brownstein, 1983), including corticotropin-releasing factor (CRF) (Swinny and Valentino, 2006; Swinny et al., 2010) and AVP (Buijs, 1978). Regarding the former, there is consensus that

CRF fibers in LC are of hypothalamic (PVN parvocellular) origin (Valentino and Van Bockstaele, 2008). While a large body of data demonstrate the origins of CRF and other LC afferents (Schwarz and Luo, 2015), the precise source of AVP+ axons in the LC has yet to be identified, even though hypothalamic paraventricular and supraoptic regions are known sources for afferents to LC (Schwarz et al., 2015). Furthermore, conclusive evidence for AVP+ fibers making synaptic contact with LC neurons has yet to be reported.

We recently reported on the molecular and physiological correlates of the AVP-receptor system in the mouse LC (Campos-Lira et al., 2018). In the current study, we expand upon these data to demonstrate that AVP+ axons make excitatory synaptic contact with TH neurons, at the ultrastructural level, and that these axons originate from discrete hypothalamic nuclei, thereby identifying specific AVP hypothalamic-LC circuits. We further demonstrate the potential engagement of these circuits in response to life experiences which require the homeostatic properties of both the LC and the hypothalamus.

MATERIALS AND METHODS

Animals

Wistar rats from a local animal breeding facility were used throughout this study. All procedures were approved by the Research and Ethics Committee of the Faculty of Medicine, Universidad Nacional Autónoma de México (CIEFM 062/2016). Animals were housed three per cage under controlled temperature (22°C) and illumination (12 h), with water and food *ad libitum*. After surgery, animals were kept warm until fully recovered from anesthesia and then kept individually under the above-mentioned conditions for 1 week and returned to the original housing conditions.

Immunohistochemistry (IHC) for Light and Transmission Electron Microscopy (LM and TEM)

Male rats of 270 ± 30 g were deeply anesthetized with an overdose of sodium pentobarbital (63 mg/kg, Sedalpharma, Mexico) and perfused transaortically with 0.9% saline followed by cold fixative containing 4% of paraformaldehyde in 0.1 M sodium phosphate buffer (PB, pH 7.4) plus 15% v/v saturated picric acid for 15 min (0.05% of glutaraldehyde was added to fixative for the samples intended for TEM). Brains were immediately removed, blocked, then thoroughly rinsed with 0.1 M PB until they were clear of fixative. The brains were then sectioned using a Leica VT 1000S vibratome, at 70 μm thickness in the horizontal plane.

For LM IHC, non-specific binding of the secondary antibodies was minimized by incubating sections containing LC with 20% normal donkey serum (NDS) in Tris-buffered (0.05 M, pH 7.4) saline (0.9%) plus 0.3% of Triton X-100 (TBST) for 1 h at room temperature (RT). The sections were then incubated with the following primary antibodies: rabbit anti-AVP antibody (kind gift of Dr. Ruud M. Buijs; Buijs et al., 1989), mouse

anti-AVP antibody (kind gift of Dr. Hal Gainer; Alstein et al., 1988), rabbit anti-AVP (Abcam, ab39363, for **Figure 1B**) sheep anti-tyrosine hydroxylase (TH) [Abcam, ab113; guinea pig anti-VGLUT2 (Frontier Institute, VGLUT2, GP-Af810)]. The next day, the sections were washed with TBST for 30 min after

which they were incubated at RT in a cocktail of an appropriate mixture of secondary antibodies, conjugated with Alexa Fluor 488, Alexa 594 and indocarbocyanine (Cy5), all provided by Jackson ImmunoResearch, for 2 h. The sections were washed in TBST and were mounted on glass slides, air dried and
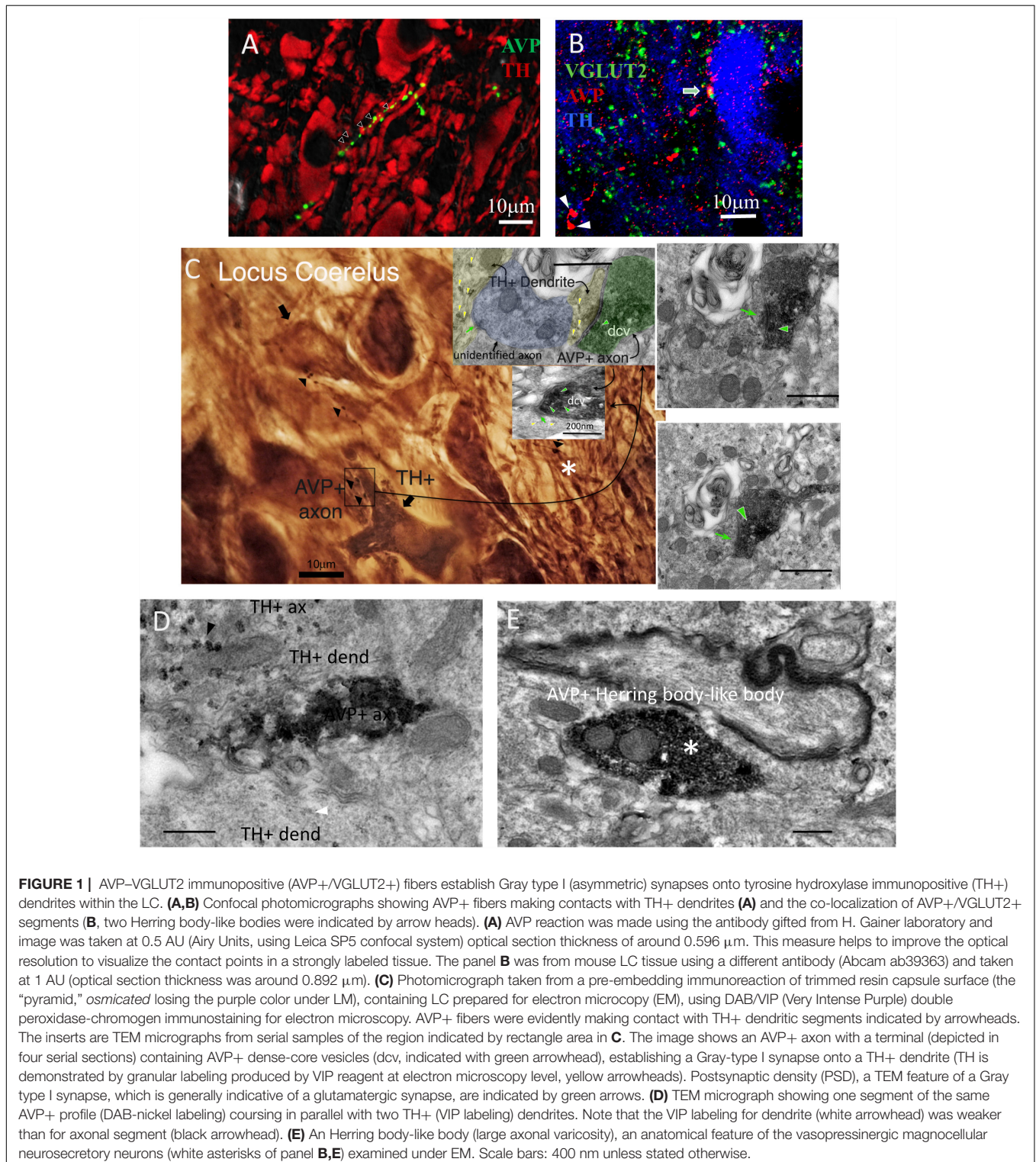

FIGURE 1 | AVP–VGLUT2 immunopositive (AVP+/VGLUT2+) fibers establish Gray type I (asymmetric) synapses onto tyrosine hydroxylase immunopositive (TH+) dendrites within the LC. **(A,B)** Confocal photomicrographs showing AVP+ fibers making contacts with TH+ dendrites **(A)** and the co-localization of AVP+/VGLUT2+ segments **(B**, two Herring body-like bodies were indicated by arrow heads). **(A)** AVP reaction was made using the antibody gifted from H. Gainer laboratory and image was taken at 0.5 AU (Airy Units, using Leica SP5 confocal system) optical section thickness of around 0.596 μm. This measure helps to improve the optical resolution to visualize the contact points in a strongly labeled tissue. The panel **B** was from mouse LC tissue using a different antibody (Abcam ab39363) and taken at 1 AU (optical section thickness was around 0.892 μm). **(C)** Photomicrograph taken from a pre-embedding immunoreaction of trimmed resin capsule surface (the "pyramid," *osmicated* losing the purple color under LM), containing LC prepared for electron microcopy (EM), using DAB/VIP (Very Intense Purple) double peroxidase-chromogen immunostaining for electron microscopy. AVP+ fibers were evidently making contact with TH+ dendritic segments indicated by arrowheads. The inserts are TEM micrographs from serial samples of the region indicated by rectangle area in **C**. The image shows an AVP+ axon with a terminal (depicted in four serial sections) containing AVP+ dense-core vesicles (dcv, indicated with green arrowhead), establishing a Gray-type I synapse onto a TH+ dendrite (TH is demonstrated by granular labeling produced by VIP reagent at electron microscopy level, yellow arrowheads). Postsynaptic density (PSD), a TEM feature of a Gray type I synapse, which is generally indicative of a glutamatergic synapse, are indicated by green arrows. **(D)** TEM micrograph showing one segment of the same AVP+ profile (DAB-nickel labeling) coursing in parallel with two TH+ (VIP labeling) dendrites. Note that the VIP labeling for dendrite (white arrowhead) was weaker than for axonal segment (black arrowhead). **(E)** An Herring body-like body (large axonal varicosity), an anatomical feature of the vasopressinergic magnocellular neurosecretory neurons (white asterisks of panel **B,E**) examined under EM. Scale bars: 400 nm unless stated otherwise.

coverslipped using Vectashield mounting medium (H-1000, Vector Laboratories Inc.).

For double peroxidase-chromogen immunostaining and electron microscopy (TEM), brain sections containing LC, were cryoprotected with 10% and then 20% sucrose in PB (under gentle agitation until the sections sank). Permeability of the tissue was then enhanced by rapidly freezing and thawing sections using liquid nitrogen. Sections were then thoroughly rinsed with PB 0.1 M and non-specific secondary antibody binding was minimized with 20% NDS in TBS for 1 h at RT. The sections were then incubated with rabbit anti-AVP and sheep anti-TH antibodies (see above) in TBS plus 1% NDS for 48 h at 4°C with gentle agitation. After rinsing in TBS, incubation was continued with first secondary antibody swine anti-rabbit IgG conjugated with horseradish peroxidase (HRP) (1:100, Dako P021702, Copenhagen, Denmark), in TBS containing 1% of NDS, overnight at 4°C. Sections were then rinsed and peroxidase enzyme reaction was carried out using the chromogen $3,3'$-diaminobenzidine (DAB, 0.05%, Electron Microscopy Sciences) and hydrogen peroxide (H_2O_2, 0.01%) as the substrate. The reaction end product in some sections was intensified with nickel. Subsequently, sections were incubated with 2nd secondary antibody, biotinylated goat anti sheep antibody (Jackson ImmunoResearch Laboratories) and then incubated with Vectastain standard ABC kit [VECTASTAIN®Elite®ABC HRP Kit (Peroxidase, Standard), Cat. No: PK-6100, Vector Laboratories, Burlingame, CA, United States]. The TH immunoreactivity was then visualized by using a Vector-VIP (*very intense purple*) peroxidase substrate kit [VECTOR®VIP Peroxidase (HRP) Substrate Kit; Vector Laboratories]. This procedure yields a reaction product that appears purple in the light microscope and granular or particulate in the electron microscope. Sections were then post-fixed with 1% osmium tetroxide in 0.1 M PB for 1 h and dehydrated through a series of graded alcohols (including 45 min of incubation in 1% uranyl acetate in 70% ethanol), then transferred to propylene oxide, followed by Durcupan ACM epoxy resin (Cat. No. 100503-434, Electron Microscopy Sciences). Sections were flat embedded on glass microscope slides, and the resin was polymerized at 60°C for 2 days. After removing the coverslip, LC containing regions, identified by TH immunoreactivity, were sectioned and carefully re-embedded in capsules in Durcupan resin. Ultrathin serial sections (70 nm) were prepared with an ultramicrotome, collected on pioloform-coated single slot grids and examined with a Philips CM100 transmission electron microscope. Digital electron micrographs were obtained with a digital micrograph 3.4 camera (Gatan Inc., Pleasanton, CA, United States).

RNAscope ISH Assays

Rats were deeply anesthetized and decapitated using a small animal guillotine (Kent Scientific corp.). Brains were removed and rapidly frozen using dry-ice powder. The fresh-frozen tissue was sectioned (12 μm thick) using a cryostat (Leica CM-1520) and mounted on positively charged glass slides (Fisher Scientific, Pittsburgh, PA, United States). The RNA probes for *in situ* hybridization used in this study to identify the genes of tyrosine hydroxylase (TH), V1a (Avpr1a), and V1b (Avpr1b) receptors

were designed and provided by Advanced Cell Diagnostics (Hayward, CA, United States). All staining steps were performed following RNAscope®2.5 HD Duplex Assay protocol for fresh frozen sections.

Fluoro-Gold Retrograde Tracing

The FG retrograde injection method was according to previously described protocols (Schmued and Fallon, 1986; Morales and Wang, 2002; Yamaguchi et al., 2011; Zhang and Hernandez, 2013). A total of twenty 300g Wistar male rats were used in this experiment. Rats were anesthetized with xylazine (Procin, Mexico) (20 mg/ml) and ketamine (Inoketam, Virbac, Mexico) (100 mg/ml) in a 1:1 volume ratio and administered intraperitoneally (*i.p.*) at a dose of 1 ml/kg of body weight. Deeply anesthetized rats were placed in a stereotaxic apparatus and the retrograde tracer Fluoro-Gold (FG, Fluorochrome, LLC, Denver, Colorado 80218, United States), dissolved 1% in 0.1 M cacodylate buffer (pH 7.5), was delivered iontophoretically (Value Kation Sci VAB-500) at the following coordinates: Bregma −9.48 mm, lateral 1.20 mm, and dorso-ventral 7.30 mm, via a glass micropipette (inner tip diameter of approximately 20 μm, current pulses of 0.1 μA, at 0.2 Hz, with a 50% duty cycle) for 20 min. The micropipette was left in place for an additional 10 min to prevent backflow of the tracer up the injection track after each injection. Upon recovery, the rats were administered 0.4 mg/kg *i.p.* Ketorolac (Apotex, Mexico) and 50 mg/kg *i.p.* ceftriaxone (Kendric, Mexico) as analgesic/anti-inflammatory and antibiotic agents, respectively. One week after the FG injections, the rats were perfused and brains sectioned in the coronal plane. Injection sites were evaluated and the inclusion criteria include: (1) the center of the injection was within the 300 μm of the core of LC and (2) there was no visible cerebro-spinal-fluid (CSF) leaking of FG, evidenced by diffused and bilateral signals. The selected cases were further processed for IHC against TH in the brain stem and AVP in the anterior hypothalamus sections.

Maternal Separation (MS) Protocol

The MS (3 h daily, MS 3 h) procedure is described in detail elsewhere (Zhang et al., 2012). Briefly, female and male adult rats were mated for 2 days. During the last week of gestation, female rats were single-housed in standard rat Plexiglas cages and maintained under standard laboratory conditions. On the day after parturition, postnatal day (PND) 2, each litter was culled to 7–8 pups, of which 5–6 were males. During the period from PND 2–PND 16, the pups were separated daily from their dams, and placed into an incubator at 29°C ± 1°C, between 09:00 and 12:00 h. After this period rats were returned to their home cages. After ending the MS protocol, animals were left undisturbed until the weaning at PND 28, when male and female rats were separated. Bedding was changed twice a week, with minimum disturbance. At PND 75, male rats of 270 ± 30 g were not allowed access to water for 24 h (WD24h) before perfusion-fixation, according to the above-mentioned protocols, in order to minimize variability in basal AVP immunoreactivity, as demonstrated previously (Verney, 1947; Fitzsimons and O'Connor, 1976; Robertson et al., 1976; Zhang et al., 2010),

thereby enhancing comparability of subjects. Following fixation, tissue sections were prepared and immunoreactivity for AVP within the LC was carried out as above described.

Optical Density Analysis

For optical density analysis of IHC, the area occupied by the signal was calculated in 10 fields in control and MS animals using a modification of the protocol described elsewhere (Ying et al., 2017). Briefly, all images were acquired under identical conditions. Using ImageJ, images were converted to grayscale. Thresholds were manually set until the majority of the area occupied by the labeled fibers was highlighted and maximally separated from the background noise. Images were converted to binary format and the threshold areas were measured. The results were expressed as mean ± SEM percentage of control and compared with a Student t-test.

Morris Water Maze Test

The Morris water maze (MWM) (Morris, 1984) assesses spatial learning and memory retention. The experimental design we used consisted of a black circular pool (diameter: 156 cm; height: 80 cm) filled with water to a height of 30 cm and temperature of 25 ± 1°C, with visual cues placed on the wall of the pool. Four virtual quadrants were named I, II, III, IV (see **Figure 5,** panes C and D for a graphical description). A circular black escape platform (diameter 12 cm) was submerged 1 cm below the water surface to serve as an escape platform. The tests were video recorded under dim red light. This setting has proved to be useful for spatial learning and memory retention assessments as previously described (Zhang et al., 2008; Hernandez et al., 2012).

Ten rats participated in this test. Animals were kept in a light-dark cycle 12:12, with light on at 7:00 am of solar time, which is denominated as the *zeitgeber* time 0, *i.e.,* circadian time 0 (CT0) and were separated in two groups: control with food and water *ad libitum* and water deprivation 24 h group (WD24h). The test was performed during rat inactivity period aiming to avoid the spontaneous high Fos expression in LC during the early activity period. Two assessments were made sequentially: the "morning" test (MT: performed between CT3–CT5) and the "afternoon" test (AT: performed between CT8–CT10). Before the MT, a pre-test habituation was done, which consisted in placing subjects from one group into the pool for 2 min to allow them to habituate the water. Rats are natural swimmers. Hence, this procedure reduces the possible stress of being immersed into water during the tests as well as to activate the innate swimming ability while making them acquainted to the environment.

The MT of MWM started by placing the escape platform in the quadrant II. Each subject was carefully introduced into the pool starting at quadrant I. Time elapsed between this event and subject arrival at the escape platform was recorded. In the first trial, subjects were allowed to explore the entire pool for 60 s, then the experimenter guided them to the platform, allowing them to climb onto the platform and to observe the location and environment for 5 s (see **Figure 5,** panels C and D, symbolized with dashed lines for a graphical description).

Six trials were completed for each subject, with intervals of 5 min between each of them. The rats were returned to the resting room with water and food *ad libitum* for 3 h. Then the AT started

at CT8 repeating the same procedure modifying the location of the escape platform to the quadrant I and the starting point to the quadrant III.

Fos IHC and Assessment

To evaluate the neuronal activity of LC, hippocampus and prefrontal cortex, the protein product of the proto-oncogene Fos was used. Since Fos is best detected in the interval between 60 and 120 min after a neuron is activated (Kovacs, 1998, 2008), we perfused the rats 90 min post-AT (MWM). For IHC, every third section containing the brain nuclei was blocked with 10% NDS in Tris-buffered (0.05M, pH 7.4) saline (0.9%) plus 0.3% of Triton X-100 (TBST) for 1 h at RT and then immunoreacted overnight with rabbit anti-Fos primary antibody (SC52, 1:1000, Santa Cruz Biotechnology, Santa Cruz, CA, United States) in TBST + 1% NDS at 4°C with gentle shaking. Afterward, sections were rinsed three times for 10 min with TBST and then incubated for 2 h at RT with biotinylated goat anti-rabbit secondary antibody (1:200; Vector Labs, Burlingame, CA, United States). Finally, sections were incubated in avidin-biotin-peroxidase complex (Elite ABC Kit, Vector Labs) for 1 h at RT. Peroxidase was detected using diaminobenzidine 0.05% as chromogen. Sections were rinsed and permanently mounted with Permount mounting medium (Electron Microscopy Sciences, Hatfield, PA, United States). Fos immunoreactive nuclei per 0.0346 mm^2 (area of a visual field: VF through the 100× objective) were counted using a Nikon Eclipse 50i microscope. The results were expressed as mean ± SEM nuclei/VF and compared with a Student t-test.

RESULTS

Synaptic Connectivity Between AVP+ Axons and LC Neurons

In mouse, sparse AVP+ axons have been reported in the region occupied by LC, using single labeling light microscopy (Rood and De Vries, 2011). We recently expanded upon these data to demonstrate that AVP+ axons in the mouse LC are located in close apposition to inhibitory and excitatory synaptic marker proteins (Campos-Lira et al., 2018). However, it is unclear whether the same association of AVP with synaptic molecular machinery exists in other species such as the rat, and whether the signal is located within synaptic junctions, or on neighboring compartments. We therefore began by examining the association of AVP+ profiles with such molecular signatures of synaptic transmission, in rat LC at the light microscopical level.

Using widely validated AVP antibodies (rabbit and mouse anti AVP), generous gifts from Ruud Buijs and Harold Gainer, respectively, we detected sparse AVP+ fibers in the LC which were closely apposed to tyrosine hydrolase (TH) immunoreactive dendrites (**Figure 1A**) and somata (**Figure 1B**). In contrast to previously reported (Aston-Jones and Waterhouse, 2016), no AVP+ cell bodies were detected in the LC. This suggests that there was no local source of AVP within the LC and these AVP+ axons originate from other brain regions. AVP+ varicosities were also immunopositive for the vesicular glutamate transporter 2 (VGLUT2) (**Figure 1B**), a protein expressed exclusively in

glutamatergic axon terminals. This suggests that AVP+ axons could form excitatory synapses with LC neurons.

To confirm this, we performed double peroxidase-chromogen immunostaining and TEM, using V – VIP (VECTOR®VIP Peroxidase (HRP) Substrate Kit; Vector Laboratories) and DAB as chromogens (see the "Materials and Methods" Section for details). It is worth noting that in EM preparations, the VIP reaction product was granular in appearance and easily distinguishable from the diffuse reaction product of DAB (Zhou and Grofova, 1995; Smiley et al., 1997; Muller et al., 2006, 2011). Visualization of the DAB reaction product at the light microscopical level revealed several AVP+ profiles (**Figure 1C** arrowheads and **Figure 1D** labeled as "AVP+ ax"). An AVP+ Herring body-like large varicose (**Figure 1B** white arrow and asterisk in **Figures 1C,E**), which is an anatomical feature of AVP-containing magnocell's axons, was also evident (**Figure 1C**, asterisk). Within this field of view, two AVP+ bouton closely apposed to a TH+ dendrite (**Figure 1C**, boxed area). Examination of serial EM sections taken from the boxed area revealed that one of these AVP+ boutons formed an asymmetric (Gray type I) synapse with a TH+ dendrite (**Figure 1C**, insert). The presynaptic button contained abundant DAB precipitate and labeled dense core vesicles (dcv, AVP+, green arrowhead), characteristic of neuropeptide-containing axon terminals. Collectively, this demonstrates that AVP is contained in a set of LC afferents, which make excitatory synaptic connections with noradrenergic profiles of the LC.

LC-NE Neurons Co-express mRNA for AVP V1a and V1b Receptors

We recently demonstrated, using immunohistochemistry, that in the mouse, V1a and V1b, but not V2 receptors are expressed in the LC (Campos-Lira et al., 2018). Whilst the V1b was expressed by both noradrenergic and non-noradrenergic LC neurons, the V1a was exclusively expressed by LC noradrenergic neurons. We used a high resolution double *in situ* hybridization technique (RNAscope®2.5 HD Duplex Assay) to assess the comparative AVP receptor expression profile in rat LC. LC noradrenergic neurons, identified by mRNA signal for TH (**Figure 2D**) co-expressed signal for both the V1a (**Figure 2A**) and V1b (**Figure 2B**) receptors. This indicates that AVP, released at excitatory synapses, uses both V1a and V1b receptors for postsynaptic signaling within LC neurons. **Figures 2C,D** shows neurons located in the dorsal raphe nucleus and LC, respectively, which expressed either V1b mRNA but not TH mRNA (**Figure 2C**) or TH mRNA but not V1b mRNA (**Figure 2D**), from the same samples as experimental controls.

AVP+ Axons in the LC Originate From the Magnocellular Neurosecretory Neurons of the PVN and SON

Our LM analysis revealed that the rat LC is devoid of AVP+ somata. This indicates that all AVP+ axons originate from regions beyond the LC. The presentation of LC AVP+ axons as large diameter profiles, with frequent-varicosities and Herring body-like structures which co-expressed the glutamatergic synaptic marker protein VGLUT2 is typical of hypothalamic

AVPMNNs (Ziegler et al., 2002; Hrabovszky and Liposits, 2007), thus making this brain region the likely source of these afferents.

To assess this hypothesis, the retrograde tracer FG was stereotaxically injected in LC, and the transported signal then evaluated in target regions. A total of four animals were confirmed to have FG injections within the core of the LC, confirmed with TH IHC (see the "Materials and Methods" Section for detailed description) (**Figure 3A**). Inspection of AVP immunofluorescence in conjunction with FG signal, in regions of the anterior hypothalamus confirmed the co-expression of AVP-FG in the hypothalamic paraventricular (PVN) and supraoptic (SON) nuclei (**Figure 3,** panels C–H). This confirms that AVPMNNs provide AVP-immunopositive innervation of LC-NE neurons. Further interpretations and discussion of this finding are developed in the Section of "Technical Considerations" at the end of this paper.

Table 1 describes the semi-quantitative analysis of the four cases matching the inclusion criteria. Interestingly, AVP/FG double labeled neurons were not found inside the suprachiasmatic nucleus.

Early Life Stress (ELS) Increases the Expression of AVP in the LC in Adulthood

We recently reported in mouse that acute stress significantly alters the expression of AVP terminals and AVP receptor expression in the mouse LC (Campos-Lira et al., 2018). The question therefore arises whether such stress-induced plasticity in the LC AVP system is enduring following exposure to chronic stress. One type of stress which induces long lasting molecular, physiological and structural plasticity in different brain regions (Caldji et al., 2003) including the LC (Swinny et al., 2010) is early life stress (ELS). Given the above data which indicate that LC AVP axons originate from, in part, the same center that integrates the stress response, i.e., the PVN, we assessed whether prior ELS alters the expression profile of AVP+ axons in the LC, using maternal separation as a model of ELS. As previously reported for other brain regions (Zhang et al., 2012; Hernandez et al., 2016), MS resulted in a noticeable increase in the intensity of AVP immunoreactivity in the LC, in adulthood (**Figures 4A,B**). Quantification of AVP immunofluorescence intensity revealed a significant increase in MS samples (**Figure 4C**), $p < 0.001$, unpaired Student's t-test; $n = 5$ animals.

Water Deprivation 24 h (WD24h) Subtly Enhances Improvement in Spatial Learning and Memory Retention, Accompanied by a Significant Increase in Fos Expression in LC, Hippocampus and Prefrontal Cortex, After MWM Assessment

To answer our question whether the hypothalamic AVPMNN system's sub-chronic upregulation exerts modulatory effects on the LC-NE neurons activation and subsequent projection regions, which could be reflected in their behavioral modifications, we devised an experiment to assess the spatial learning and memory retention in water-maze-naive rats using water deprivation (WD)
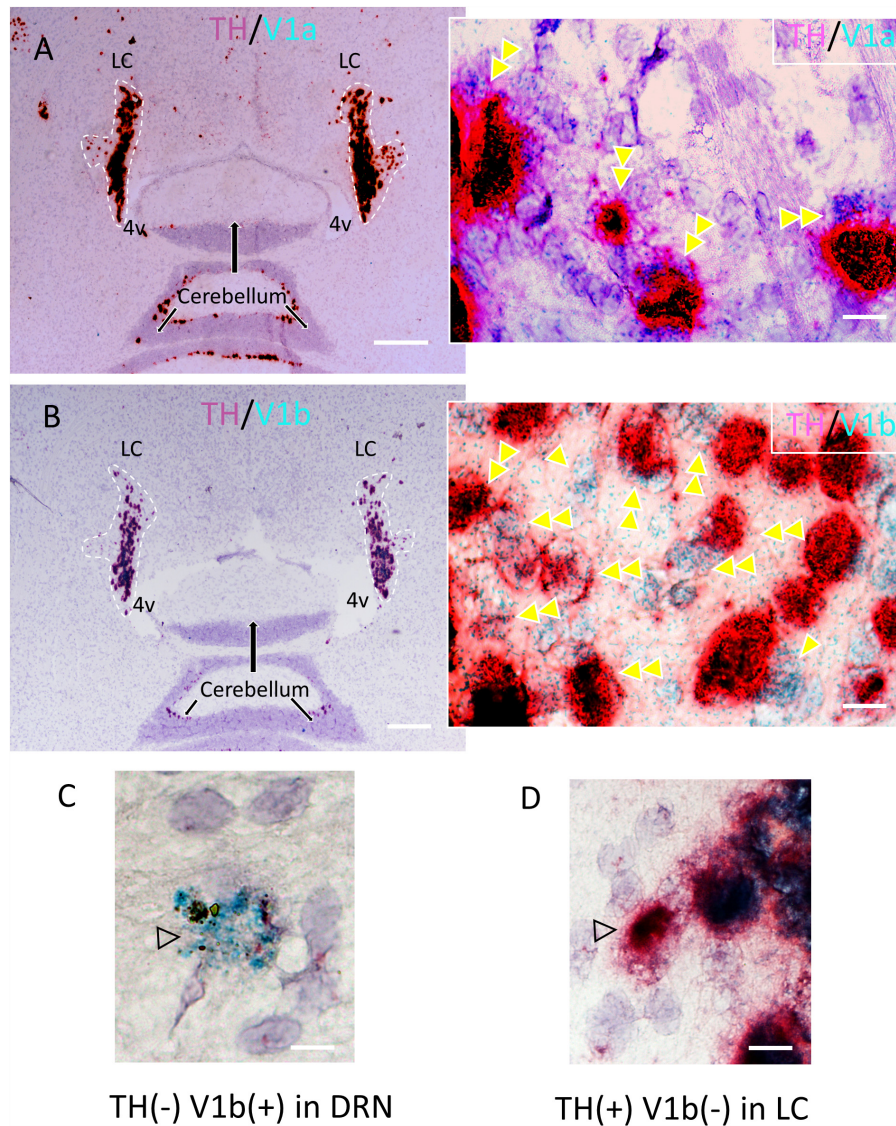
FIGURE 2 | Confirmation of the expression of V1a and V1b receptor mRNA in noradrenergic LC neurons using a high resolution *in situ* hybridization method (RNAscope®2.5 HD Duplex Assay). **(A,B)** Horizontal sections of rat LC with inserts showing the co-localization (double arrowheads) of V1a/TH **(A)** and V1b/TH **(B)**. The TH mRNA signal was amplified using RNAscope channel 2 related probes and alkaline phosphatase (AP) – based Fast Red chromogen to result in a strongly detectable red signal and either V1a and V1b signals were amplified using RNAscope channel 1 related probes and horseradish peroxidase (HRP) – based green chromogen (the green punctuated signal). This newly developed technology allows a same-day ISH for two mRNAs detection with cellular resolution and being permanently mounted and examined under conventional light micrococpy. Panels **(C,D)** are controls showing the labeling with V1b only, in the dorsal raphe nucleus and TH only in LC respectively. Scale bars: **A,B**: 0.5 mm; rest, 10 μm.

as our experimental variable. From 12 h of water deprivation, the plasma AVP concentration in rat reaches to its maximum level and continues for the next 12 h (Zhang et al., 2010). Hence, this physiological model could up-regulate the AVP afference to LC.

As shown in **Figure 5A**, in the morning test, the WD group already showed a subtle improvement of spatial learning with a smoother learning course and a significant reduction of time to reach the escape-platform in the 2nd trial compared to control. This improvement is further confirmed in the afternoon session with significant reduction of time to reach the escape-platform

in the 2nd and 3rd trials compared to control (**Figure 5B**). An interesting phenomenon was observed in the first trial of the afternoon test, in which the WD subjects spent more time swimming in the quadrant II where the escape-platform was located in the morning test, while the control rats did not show this preference (**Figures 5C,D**).

The expression of c-Fos, a marker of neuronal plasticity, assessed 90 min after the end point of MWM, revealed significant increase in the LC, as well as in the granule cell layer (gcl) of the dentate gyrus (DG) of dorsal hippocampus and prefrontal
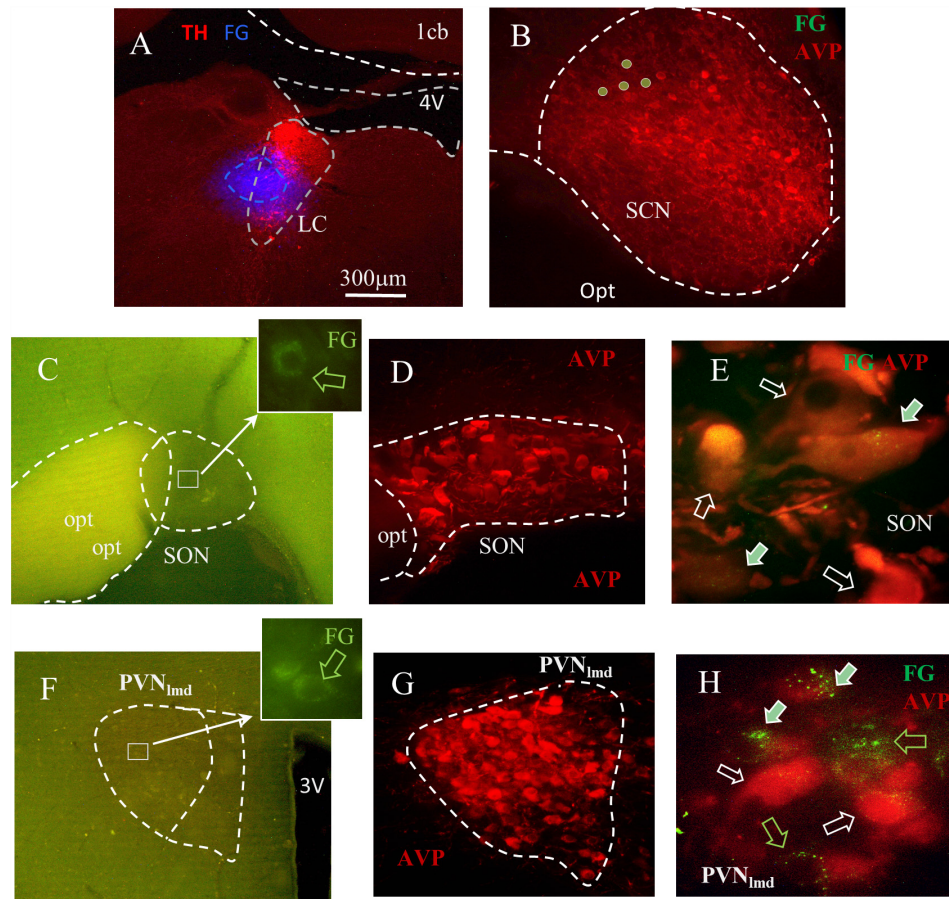
FIGURE 3 | Fluoro-Gold (FG) retrograde tracing identifies the SON and PVN nuclei as the sources of LC AVP afferents. **(A)** Coronal section of pontine tegmentum, Bregma −9.84 mm; red TH+ IHC showing LC and blue FG labeling site of about 300 μm of diameter. **(B)** Within the suprachiasmatic nucleus (SCN), the FG labeled cells were found immuno-negative for AVP. In both SON **(C–E)** and the lateral magnocellular division of PVN (PVN$_{lmd}$, **F–H**), around 20–60% of AVP+ neurons were positively labeled. **(C,F)** Photomicrographs from freshly vibratome sectioned coronal hypothalamic slices indicate the sparse FG labeled magnocellular neurons (perinuclear lysosome labeling pattern). FG and AVP immunohistochemistry were co-localized (filled arrows) in a population of the magnocellular neurons in SON **(D,E)** and PVN$_{lmd}$ **(G,H)**. White hollow arrows indicate AVP+ cells without FG and green hollow arrows show the FG+ cells without AVP. See "Technical Considerations" Section in the "Discussion" for further considerations. Scale bars: 20 μm for **E,H**; rest 300 μm.

cortex. The panel E of **Figure 5** shows a higher number of Fos+ nuclei in all regions evaluated comparing control vs. WD24h rats, i.e., LC: 9.62 ± 0.9 vs. 13.14 ± 1.2, $p < 0.05$; DG: 6.0 ± 0.7 vs. 11.62 ± 1.3, $p < 0.001$; and PFC: 12.45 ± 0.5 vs. 19.73 ± 1.5, $p < 0.001$. It is worth noting that both of the latter regions receive abundant NE innervations from LC (Schwarz et al., 2015) but no AVP direct innervations have been reported (Rood and De Vries, 2011; Zhang and Hernandez, 2013). Hence, it is coherent to interpret that these c-Fos expression increases are secondary to the potentiation of LC-NE afference to those regions.

DISCUSSION

In the current study, we provide the first demonstration that AVP-containing axons make synaptic connections with LC neurons. Furthermore, we provide evidence that these AVP afferents originate from magnocellular neurosecretory neurons (AVPMNNs) of the hypothalamic PVN and SON. Finally, our data suggest the recruitment of this AVPMNN circuit during periods of psychological and physiological challenges. Collectively, the study identifies the anatomical substrates linking two different neural systems with a common responsibility for ensuring homeostasis in complex environments.

The Molecular and Structural Components of AVP-LC Communication

In contrast to its well-characterized role as a hormone in the periphery, within the brain, AVP has been shown to also exhibit the features of a neuromodulator by directly altering neuronal excitability (Zhang and Eiden, 2018). Axons containing such neuropeptide modulators generally adopt a range of release mechanisms, thereby increasing the versatility of their communication patterns. For example, volume transmission (VT) is a key feature of such hypothalamic neuropeptide

TABLE 1 | Fluoro-Gold (FG) retrograde labeling experimental survey and anatomical description*.

Subject's Pons at Breg. −9.84 mm	Main hypoth. AVP+ Regions	Ipsi-lateral	Contra-lateral	Observation	Subject's Pons at Breg. −9.84 mm	Main hypoth. AVP+ Regions	Ipsi-lateral	Contra-lateral	Observation
VH07	PVN	+	+		OH02	PVN	+++	+++	
	SON	++	++	++ in AVP- cell in dorso-lateral portion		SON	+++	+++	++ in AVP- cell in dorso-lateral portion
	SCN	-	-			SCN	-	-	
VH09	PVN	+	+		OH05	PVN	+++	++	
	SON	++	++	++ in AVP- cell in dorso-lateral portion		SON	++	++	++ in AVP- cell in dorso-lateral portion
	SCN	-	-			SCN	-	-	

*Twenty young male rats were used in this experiment. Sixteen rat's injection sites did not meet the criteria for inclusion (see "Materials and Methods" Section), hence they were not included here. FG+/AVP+ cell number per 0.229 mm²: +, 1–5; ++, 6–10; +++, > 10. "VH" and "OH" are the initials of the two experimenters and the number followed indicate the subject sequential number.

neurotransmitters and facilitates the modulation of large ensembles of neurons (Alpar et al., 2018). The sparsity of AVP+ axons throughout the LC, in comparison to the vast expression of AVP receptors in virtually all LC neurons, suggests that the LC AVP system relies heavily on VT as a means of influencing LC neuronal excitability. However, our ultrastructural data indicate that AVP+ axons also employ the wired form of transmission in terms of forming conventional synapses with LC profiles. This suggests that AVP afferents impart highly directed, synaptic modulation of a sub-population of LC neurons, whilst maintaining a more general influence over the entire nucleus via VT. Since synaptic connectivity imparts speed and precision in neuronal network signaling, this raises the question whether the synaptically connected AVP-LC neurons represent a group of cells essential for mediating specific aspects of AVP-mediated brain functions, in a strict temporally constrained manner. This could result in the parcellation of the LC into different populations of neurons within AVP-LC pathways. Evidence for this heterogeneity of the LC AVP system stems from our recent report which demonstrated that the pharmacological activation of LC neurons resulted in contrasting effects on spontaneous firing rates (Campos-Lira et al., 2018). If so, identifying the anatomical and molecular signatures of this sub-populations of LC neurons, together with the source/s of such synapse innervating AVP+ axons, will be the crucial in furthering our understanding of the contribution of neurochemical systems to overall LC function.

The Source of LC AVP+ Afferents

There are at least five major brain AVP centers, and therefore likely sources of the AVP+ axons innervating LC neurons, namely, the PVN, suprachiasmatic nucleus, supraoptic nucleus, bed nucleus of the stria terminalis (BNST), and medial amygdala (Goodson and Bass, 2001). AVP+ inputs to the LC have been reported since the late 1970s in both the core and pericoeruleus sub-regions (Buijs, 1978). These axons were considered to originate from parvocellular vasopressinergic neurons located within the caudal paraventricular nucleus and the BNST (Urban et al., 1999). However, the retrograde tracing data in this current studies point to magnocellular neurons of the PVN (AVPMNNs) being the major source. Our ancillary molecular data, in the form of VGLUT2-AVP co-expression, a signature of AVPMNNs, further supports the notion that these axons originate from this region of the brain. Further arguments to support the notion that these axons most likely arise from the hypothalamus rather than from extra-hypothalamic AVP-positive neurons include (i) AVPMNNs are known to be glutamatergic (Ziegler et al., 2002; Hrabovszky and Liposits, 2007); (ii) most, if not all, of the AVP-parvocellular populations, in hypothalamic suprachiasmatic nucleus (SCN), central (CeA) and medial (MeA) amygdala, bed nucleus of stria terminalis, intra-amygdala (BNSTIA) and medial posterior internal (BNSTmpi) divisions have been found to express VGAT hence to be GABAergic (Zhang and Eiden, unpublished; Zhang and Eiden, 2018). As such, the data reveal a synaptically connected circuit between PVN AVP+ neurons and the LC. Future studies focused on dissecting the roles of other PVN-LC pathways, such as those using CRF as a
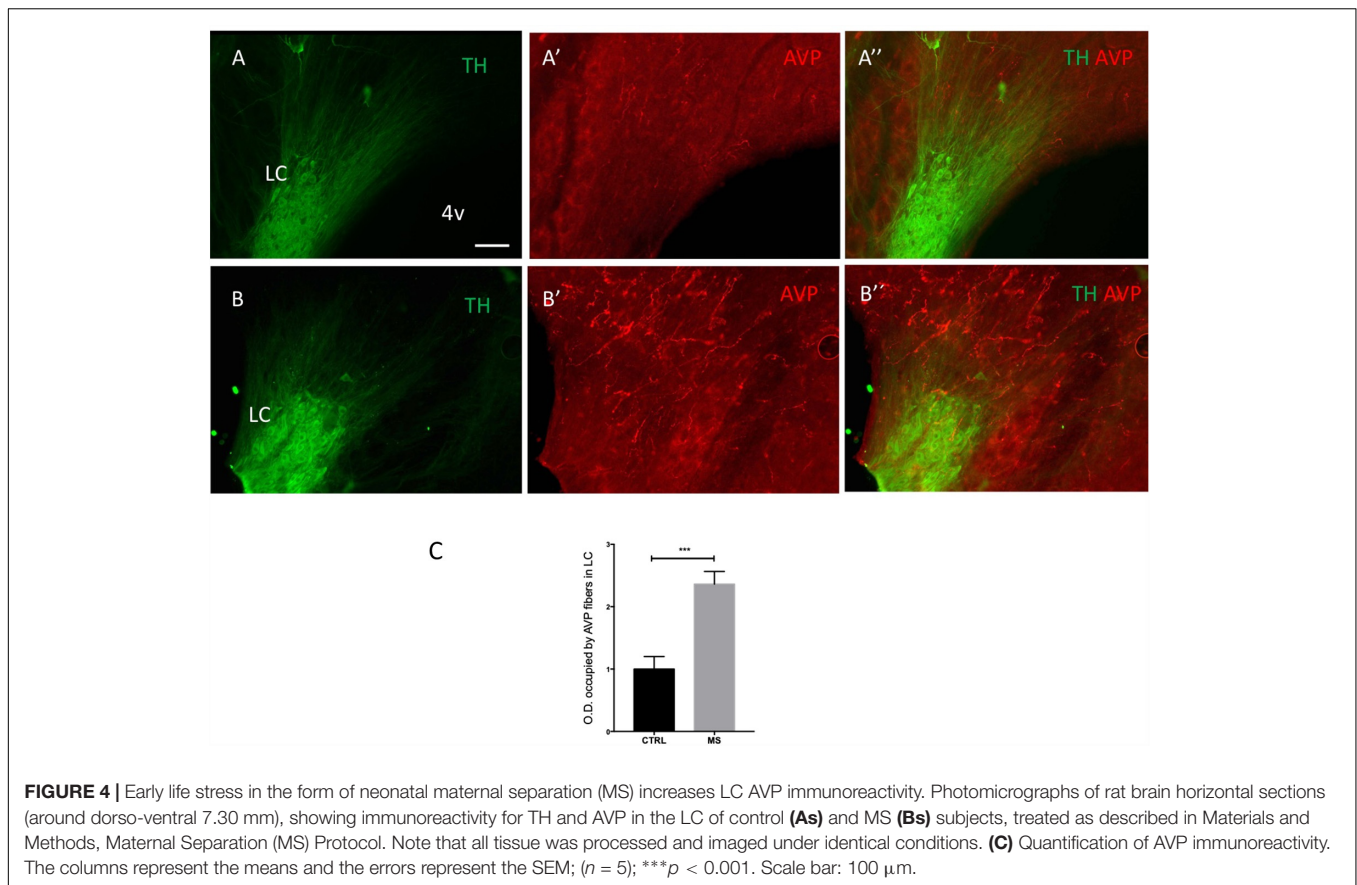
FIGURE 4 | Early life stress in the form of neonatal maternal separation (MS) increases LC AVP immunoreactivity. Photomicrographs of rat brain horizontal sections (around dorso-ventral 7.30 mm), showing immunoreactivity for TH and AVP in the LC of control **(As)** and MS **(Bs)** subjects, treated as described in Materials and Methods, Maternal Separation (MS) Protocol. Note that all tissue was processed and imaged under identical conditions. **(C)** Quantification of AVP immunoreactivity. The columns represent the means and the errors represent the SEM; (n = 5); ***$p < 0.001$. Scale bar: 100 μm.

neuromodulator, are crucial in gaining a composite view of the contributions of such circuits to brain functions mediated by these respective centers.

The LC-AVP System and Its Role in the Stress Response

A common feature of the LC and the PVN nuclei are their involvement in ensuring that the individual is capable of mediating a coordinated response to a variety of psychological and physiological stressors (Atzori et al., 2016). CRF has historically been considered the messenger of choice for both brain regions (Swinny and Valentino, 2006; Swinny et al., 2010). The current study, as well as our previous report, identifies AVP, within the LC, as an additional molecule in the arsenal of mediators used by these brain regions in times of stress. Our recent report showed that acute stress, in the form of restraint for 1 h, significantly increased the density of V1b receptors, while decreasing the density of AVP immunoreactivity. V1a receptors were unaffected (Campos-Lira et al., 2018). In the current study, we show that a more severe form of stress, namely MS, has the opposite effect on AVP expression, by significantly increasing the density of immunoreactive axons in the LC. Furthermore, a mild stress which is known to engage the PVN-AVP system, namely WD, together with novelty of being subjected to the MWM test, also appeared to engage the LC (in addition to other brain regions), based on the expression of the early gene marker Fos

(**Figure 5**). Therefore, different life experiences have contrasting effects on LC-AVP plasticity. This stress-induced plasticity of the AVP in the brain has been replicated in other brain regions. For example, MS has been shown to potentiate the hypothalamic AVPMNN system as well as increase the fiber density in amygdala resulting in stress hyper-responsivity such as hyper-anxiety tested by Vogel-conflict test and elevated plus maze (Zhang et al., 2012; Hernandez et al., 2016). Remarkably, post-mortem analysis of the brains of suicide victims has indicated an increase in the immunoreactivity for AVP in the LC, in addition to other brain regions important in regulating emotions (Merali et al., 2006). Therefore, targeting the AVPMNNs system and the LC, in mental illnesses could unearth novel therapeutic strategies for debilitating stress-induced mental illnesses which remain poorly treated with currently available drug options.

Does the Activation of This Pathway by 24 h Water Deprivation Lead to Enhancement of Memory and/or Learning?

Using MWM, we assessed spatial learning in rats after undergoing 24 h water-deprivation (WD), during which time the AVPMNNs are physiologically hyper-activated with only minimal changes in blood osmolality (Dunn et al., 1973; Zhang et al., 2010). We found here the memory retention and learning course were both
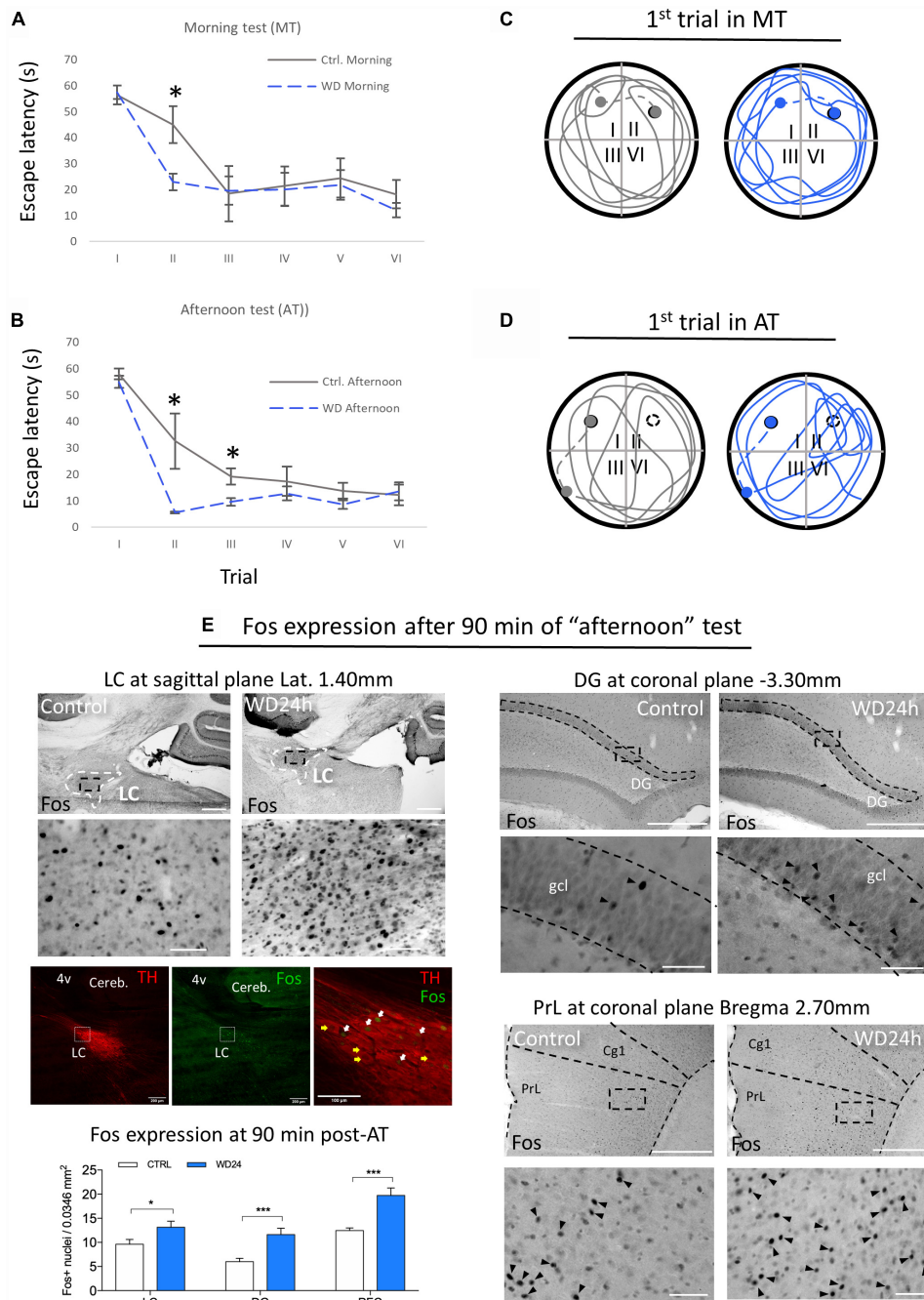
FIGURE 5 | Morris water maze (MWM) test showed that WD24h improved spatial learning and memory retention as well as increasing neuronal activity in LC, hippocampus (assessed at suprapyramidal branch of granule cell layer (gcl) of dorsal dentate gyrus (DG) and prefrontal cortex [assessed at the layer 5 of prelimbic cortex (PrL), regions relevant for working memory]. **(A)** "Morning testing" (MT, see the "Materials and Methods" Section) showed that WD24h rats learned to locate the hidden platform (quadrant II) faster than control rats, as shown by a reduction in the latency to reach the platform in the second trial. **(B)** "Afternoon testing" (AT, see the "Materials and Methods" Section) confirmed the previous observation with a significant reduction of time to reach the escape-platform (quadrant I) in the second and third trials compared to control. **(C)** No apparent differences in the swimming strategy were seen as shown in a tracing of the swimming path of the first trial of MT. **(D)** A different swimming strategy was observed in the AT, with WD24h rats spending more time swimming in the quadrant where the platform was located (quadrant I) before finding the new location (quadrant I). In panels **(C,D)** filled circles symbolize the escape platform; hollow circles symbolize the old platform location; dots symbolize the rat location when 60 s exploration lapse ends; dashed lines symbolize the route that the experimenter guided the subject to the platform. **(E)** Photomicrographs and bar graphs show an increase in the number of Fos+ nuclei in the LC, granule cell layer (gcl) of dorsal dentate gyrus (DG), and prefrontal cortex assessed at the prelimbic cortex (PrL, layer 5), 90 min post the AT. Immuno-fluorescence images from WD subject's LC (sagittal section) depict examples of Fos activation in LC-NE neurons (white arrows) after the MWM test. Note that some LC-NE neurons are not activated (yellow arrows). Scale bars 500 μm for the low amplifications photomicrographs and 50 μm for the high amplification; $*p < 0.05$; $***p < 0.001$.

improved in WD subject, while Fos-expression in LC, as well as in LC-NE projecting regions relevant for working memory, dorsal hippocampus and prefrontal cortex, were significantly increased. NE facilitates synaptic plasticity by recruiting and modifying multiple molecular elements of synaptic signaling, including specific transmitter receptors, intracellular protein kinases, and translation initiation have been extensively reported (Maity et al., 2015; Nguyen and Gelinas, 2018).

These results, adding to our previous studies, suggest that the AVPMNN system, a water homeostasis regulator, works centrally modulating the adaptive responses.

The postulated function of AVP as a modulator of LC principal neuron activity in response to osmotic stress is further supported by the finding of V1a receptors on TH+ (principal) LC neurons. Consistent with a role for AVP in linking osmotic stress to LC function, is enhancement of Fos up-regulation in LC neurons during a learning/orientation task (the MWM) after 24 h of water deprivation (WD) a reliable maneuver for enhancing AVPMNN tone in the PVN, SON and their vasopressinergic projections. In fact, performance during the MWM is also enhanced by WD. Since Fos activity is also up-regulated during MWM learning in LC target areas of the brain, some of which also receive AVPMNN inputs, it is not possible to know at this time if the effects of WD on MWM performance, though likely mediated through AVPMNN activity, are indirect (via action at the LC) or direct (via AVP release directly in these LC projection areas). Nevertheless, our findings reveal a novel neuroanatomical substrate for AVPMNN direct influence over LC neuronal function, and a new avenue for exploration of both homeostatic as well as allostatic modulation of behavior via the LC.

We take the data as a whole as indicating that the AVPMNN projections to LC likely act to potentiate a pattern of LC neuronal activity consistent with increased learning or enhanced attention under conditions of physiological stress (WD24h). This suggests that physiological need/motivation/stress enhances attention and learning under conditions in which acquisition of new information is especially critical to survival (Glennon et al., 2018).

Technical Considerations: Limitations for Quantitative Conclusions

This study describes for the first time that the hypothalamic AVPMNNs innervate the LC using FG neurotracing, immunohistochemical, and neuroanatomical methods. FG injection into the LC revealed retrogradely labeled AVP-positive cells in hypothalamic supraoptic (SON) and paraventricular nuclei (PVN). There are several technical issues concerning this observation that we considered important to discuss here. The LC are bilateral dense groups of cells located in the pontine tegmentum, specifically in the lateral-rostral part of the floor of the 4th ventricle. Here, there are two technical challenges for neuro-circuit tracing. First, the rat LC is a relatively small nucleus (for instance, dimensions measured from confocal microcopy images from one rat were rostro-caudal 566 μm, dorso-ventral 306 μm, medio-lateral 320 μm). Second, it is located just below the 4th ventricle, thus it is extremely easy to have the tracer leaking into the cerebro-spinal fluid (CSF).

Due the AVPMNNs neuro-secretion functional capacity, any leakage of FG can result in variable degree of magnocellular labeling, bilaterally. To avoid this leaking risk, we aimed to inject the tracer into the latero-ventral site of the LC as well as to use the method described in "Materials and Methods" which should yield a labeling region of less than 300 μm of diameter. In 20 attempts (20 rats used), only 4 resulted matching our inclusion criteria (20% of success rate). Although the stereotaxic coordinates and the rat body weights were kept identical, to the best of our knowledge, the first anatomical assessments for each rat yielded rather variable labeling sites. A more than 30 μm deviation, >10% of LC's diameter, resulted in other structure's labeling, which did not provide valid data for this study's aims and were excluded for further analysis. The four successful cases were analyzed and reported in the **Table 1** where we aimed to be rigorous and quantitative providing objective description of those four cases. We are fully aware that each injection only cover a small fraction of the LC's dendritic field, in a variable degree. Hence, not global quantitative conclusion should be generated from those individual descriptions of the 4 rats. The value of this discovery is that only a small portion of the AVPMNNs were labeled resulting from a given local-injection of one region of LC, and we showed AVPMNNs without FG labeling but adjacent to the double labeled cells, which suggests that the labeling was not likely, at least part of them, to be through the humoral leakage. Hence, it demonstrates the existence of a monosynaptic pathway from AVNMNN to LC.

In summary, establishment of a linkage between the AVPMNN system and the LC adds a significant component to the already-established communication to the LC from the hypothalamus, via CRF projections from the PVN. That thirst enhances performance in the MWM concomitantly with enhanced activation of LC neurons during the conduct of the MWM test may indicate either enhancement of innate learning, or increased attention to cues presented during this test, and this too is an important new avenue that we intend to develop in the future. The resolution of this question will be helpful in determining the relative functional impact of increased vasopressinergic tone in LC compared to other brain regions which are supplied with AVPMNN afferents from the PVN and SON.

AUTHOR CONTRIBUTIONS

LZ conceived and led the study. VH, AN-K, OH-P, and LZ designed the experiments. OH-P, VH, AN-K, MS, and LZ performed the experiments. All authors analyzed the data. LZ, JS, RB, and LE contributed experimental reagents and resources. LZ wrote the manuscript with contribution of JS and LE, and feedback from the remaining authors.

FUNDING

ACKNOWLEDGMENTS

REFERENCES

Alpar, A., Benevento, M., Romanov, R. A., Hokfelt, T., and Harkany, T. (2018). Hypothalamic cell diversity: non-neuronal codes for long-distance volume transmission by neuropeptides. *Curr. Opin. Neurobiol.* 56, 16–23. doi: 10.1016/j.conb.2018.10.012

Alstein, M., Whitnall, M. H., House, S., Key, S., and Gainer, H. (1988). An immunochemical analysis of oxytocin and vasopressin prohormone processing in vivo. *Peptides* 9, 87–105. doi: 10.1016/0196-9781(88)90014-9

Armstrong, W. (2004). "Hypothalamic supraoptic and paraventricular nuclei," in *The Rat Nervous System*, ed. G. Paxinos (Amsterdam: Elsevier), 369–388. doi: 10.1016/B978-012547638-6/50016-X

Aston-Jones, G., and Waterhouse, B. (2016). Locus coeruleus: from global projection system to adaptive regulation of behavior. *Brain Res.* 1645, 75–78. doi: 10.1016/j.brainres.2016.03.001

Atzori, M., Cuevas-Olguin, R., Esquivel-Rendon, E., Garcia-Oscos, F., Salgado-Delgado, R., Saderi, C., et al. (2016). Locus ceruleus norepinephrine release: a central regulator of CNS spatio-temporal activation? *Front. Synaptic Neurosci.* 8:25. doi: 10.3389/fnsyn.2016.00025

Berridge, C. W., and Waterhouse, B. D. (2003). The locus coeruleus-noradrenergic system: modulation of behavioral state and state-dependent cognitive processes. *Brain Res. Brain Res. Rev.* 42, 33–84. doi: 10.1016/S0165-0173(03)00143-7

Buijs, R. M. (1978). Intra- and extrahypothalamic vasopressin and oxytocin pathways in the rat. Pathways to the limbic system, medulla oblongata and spinal cord. *Cell Tissue Res.* 192, 423–435. doi: 10.1007/BF00224932

Buijs, R. M., Pool, C. W., Van Heerikhuize, J. J., Sluiter, A. A., Van der Sluis, P. J., Ramkema, M., et al. (1989). Antibodies to small transmitter molecules and peptides: production and application of antibodies to dopamine, serotonin, GABA, vasopressin, vasoactive intestinal peptide, neuropeptide y, somatostatin and substance P. *Biomed. Res.* 10(Suppl. 3), 213–221.

Caldji, C., Diorio, J., and Meaney, M. J. (2003). Variations in maternal care alter GABA(A) receptor subunit expression in brain regions associated with fear. *Neuropsychopharmacology* 28, 1950–1959. doi: 10.1038/sj.npp.1300237

Campos-Lira, E., Kelly, L., Seifi, M., Jackson, T., Giesecke, T., Mutig, K., et al. (2018). Dynamic modulation of mouse locus coeruleus neurons by vasopressin 1a and 1b receptors. *Front. Neurosci.* 12:919. doi: 10.3389/fnins.2018.00919

Cui, Z., Gerfen, C. R., and Young, W. S. III (2013). Hypothalamic and other connections with dorsal CA2 area of the mouse hippocampus. *J. Comp. Neurol.* 521, 1844–1866. doi: 10.1002/cne.23263

de Wied, D., Diamant, M., and Fodor, M. (1993). Central nervous system effects of the neurohypophyseal hormones and related peptides. *Front. Neuroendocrinol.* 14, 251–302. doi: 10.1006/frne.1993.1009

Dunn, F. L., Brennan, T. J., Nelson, A. E., and Robertson, G. L. (1973). The role of blood osmolality and volume in regulating vasopressin secretion in the rat. *J. Clin. Invest.* 52, 3212–3219. doi: 10.1172/JCI107521

Fitzsimons, J. T., and O'Connor, W. J. (1976). E. B. Verney's demonstration of 'The antidiuretic hormone and the factors which determine its release' [proceedings]. *J. Physiol.* 263, 92–93.

Glennon, E., Carcea, I., Martins, A. R. O., Multani, J., Shehu, I., Svirsky, M. A., et al. (2018). Locus coeruleus activation accelerates perceptual learning. *Brain Res.* doi: 10.1016/j.brainres.2018.05.048 [Epub ahead of print].

Goodson, J. L., and Bass, A. H. (2001). Social behavior functions and related neuroanatomical characteristics of vasotocin/vasopressin systems in vertebrates. *Brain Res. Brain Res. Rev.* 35, 246–265. doi: 10.1016/S0165-0173(01)00043-1

Hernandez, V. S., Hernandez, O. R., Perez de la Mora, M., Gomora, M. J., Fuxe, K., Eiden, L. E., et al. (2016). Hypothalamic vasopressinergic projections innervate central amygdala GABAergic neurons: implications for anxiety and stress coping. *Front. Neural Circuits* 10:92. doi: 10.3389/fncir.2016.00092

Hernandez, V. S., Ruiz-Velazco, S., and Zhang, L. (2012). Differential effects of osmotic and SSR149415 challenges in maternally separated and control rats: the role of vasopressin on spatial learning. *Neurosci. Lett.* 528, 143–147. doi: 10.1016/j.neulet.2012.09.002

Hernandez, V. S., Vazquez-Juarez, H., Marquez, E., Jauregui, M. M., Huerta, F., Barrio, R. A., et al. (2015). Extra-neurohypophyseal axonal projections from individual vasopressin-containing magnocellular neurons in rat hypothalamus. *Front. Neuroanat.* 9:130. doi: 10.3389/fnana.2015.00130

Hrabovszky, E., and Liposits, Z. (2007). Glutamatergic phenotype of hypothalamic neurosecretory systems: a novel aspect of central neuroendocrine regulation. *Ideggyogy. Sz.* 60, 182–186.

Kobayashi, R. M., Palkovits, M., Kopin, I. J., and Jacobowitz, D. M. (1974). Biochemical mapping of noradrenergic nerves arising from the rat locus coeruleus. *Brain Res.* 77, 269–279. doi: 10.1016/0006-8993(74)90790-2

Kovacs, K. J. (1998). c-Fos as a transcription factor: a stressful (re)view from a functional map. *Neurochem. Int.* 33, 287–297. doi: 10.1016/S0197-0186(98)00023-0

Kovacs, K. J. (2008). Measurement of immediate-early gene activation-c-fos and beyond. *J. Neuroendocrinol.* 20, 665–672. doi: 10.1111/j.1365-2826.2008.01734.x

Landgraf, R., and Neumann, I. D. (2004). Vasopressin and oxytocin release within the brain: a dynamic concept of multiple and variable modes of neuropeptide communication. *Front. Neuroendocrinol.* 25, 150–176. doi: 10.1016/j.yfrne.2004.05.001

Leng, G., Dyball, R. E., and Luckman, S. M. (1992). Mechanisms of vasopressin secretion. *Horm. Res.* 37, 33–38. doi: 10.1159/000182278

Levitt, P., and Moore, R. Y. (1979). Origin and organization of brainstem catecholamine innervation in the rat. *J. Comp. Neurol.* 186, 505–528. doi: 10.1002/cne.901860402

Ludwig, M., and Leng, G. (2006). Dendritic peptide release and peptide-dependent behaviours. *Nat. Rev. Neurosci.* 7, 126–136. doi: 10.1038/nrn1845

Maity, S., Rah, S., Sonenberg, N., Gkogkas, C. G., and Nguyen, P. V. (2015). Norepinephrine triggers metaplasticity of LTP by increasing translation of specific mRNAs. *Learn. Mem.* 22, 499–508. doi: 10.1101/lm.039222.115

Merali, Z., Kent, P., Du, L., Hrdina, P., Palkovits, M., Faludi, G., et al. (2006). Corticotropin-releasing hormone, arginine vasopressin, gastrin-releasing peptide, and neuromedin B alterations in stress-relevant brain regions of suicides and control subjects. *Biol. Psychiatry* 59, 594–602. doi: 10.1016/j.biopsych.2005.08.008

Morales, M., and Wang, S. D. (2002). Differential composition of 5-hydroxytryptamine3 receptors synthesized in the rat CNS and peripheral nervous system. *J. Neurosci.* 22, 6732–6741. doi: 10.1523/JNEUROSCI.22-15-06732.2002

Morris, R. (1984). Developments of a water-maze procedure for studying spatial learning in the rat. *J. Neurosci. Methods* 11, 47–60. doi: 10.1016/0165-0270(84)90007-4

Muller, J. F., Mascagni, F., and McDonald, A. J. (2006). Pyramidal cells of the rat basolateral amygdala: synaptology and innervation by parvalbumin-immunoreactive interneurons. *J. Comp. Neurol.* 494, 635–650. doi: 10.1002/cne.20832

Muller, J. F., Mascagni, F., and McDonald, A. J. (2011). Cholinergic innervation of pyramidal cells and parvalbumin-immunoreactive interneurons in the rat basolateral amygdala. *J. Comp. Neurol.* 519, 790–805. doi: 10.1002/cne.22550
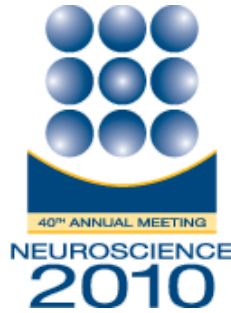
Nguyen, P. V., and Gelinas, J. N. (2018). Noradrenergic gating of long-lasting synaptic potentiation in the hippocampus: from neurobiology to translational biomedicine. *J. Neurogenet.* 32, 171–182. doi: 10.1080/01677063.2018.1497630

Palkovits, M., and Brownstein, M. J. (1983). "Locus coeruleus," in *Advances in Cellular Neurobiology*, Vol. 4, eds S. Fedoroff and L. Hertz (Amsterdam: Elsevier), 81–103. doi: 10.1016/B978-0-12-008304-6.50008-7

Robertson, G. L., Shelton, R. L., and Athar, S. (1976). The osmoregulation of vasopressin. *Kidney Int.* 10, 25–37. doi: 10.1038/ki.1976.76

Robertson, S. D., Plummer, N. W., de Marchena, J., and Jensen, P. (2013). Developmental origins of central norepinephrine neuron diversity. *Nat. Neurosci.* 16, 1016–1023. doi: 10.1038/nn.3458

Rood, B. D., and De Vries, G. J. (2011). Vasopressin innervation of the mouse (*Mus musculus*) brain and spinal cord. *J. Comp. Neurol.* 519, 2434–2474. doi: 10.1002/cne.22635

Schmued, L. C., and Fallon, J. H. (1986). Fluoro-Gold: a new fluorescent retrograde axonal tracer with numerous unique properties. *Brain Res.* 377, 147–154. doi: 10.1016/0006-8993(86)91199-6

Schwarz, L. A., and Luo, L. (2015). Organization of the locus coeruleus-norepinephrine system. *Curr. Biol.* 25, R1051–R1056. doi: 10.1016/j.cub.2015.09.039

Schwarz, L. A., Miyamichi, K., Gao, X. J., Beier, K. T., Weissbourd, B., DeLoach, K. E., et al. (2015). Viral-genetic tracing of the input-output organization of a central noradrenaline circuit. *Nature* 524, 88–92. doi: 10.1038/nature14600

Smiley, J. F., Morrell, F., and Mesulam, M. M. (1997). Cholinergic synapses in human cerebral cortex: an ultrastructural study in serial sections. *Exp. Neurol.* 144, 361–368. doi: 10.1006/exnr.1997.6413

Swanson, L. W. (1976). The locus coeruleus: a cytoarchitectonic, Golgi and immunohistochemical study in the albino rat. *Brain Res.* 110, 39–56. doi: 10.1016/0006-8993(76)90207-9

Swinny, J. D., O'Farrell, E., Bingham, B. C., Piel, D. A., Valentino, R. J., and Beck, S. G. (2010). Neonatal rearing conditions distinctly shape locus coeruleus neuronal activity, dendritic arborization, and sensitivity to corticotrophin-releasing factor. *Int. J. Neuropsychopharmacol.* 13, 515–525. doi: 10.1017/S146114570999037X

Swinny, J. D., and Valentino, R. J. (2006). Corticotropin-releasing factor promotes growth of brain norepinephrine neuronal processes through Rho GTPase regulators of the actin cytoskeleton in rat. *Eur. J. Neurosci.* 24, 2481–2490. doi: 10.1111/j.1460-9568.2006.05129.x

Urban, I. J. A., Burbach, J. P. H., and De Wied, D. (1999). *Advances in Brain Vasopressin*. Amsterdam: Elsevier.

Valentino, R. J., and Van Bockstaele, E. (2008). Convergent regulation of locus coeruleus activity as an adaptive response to stress. *Eur. J. Pharmacol.* 583, 194–203. doi: 10.1016/j.ejphar.2007.11.062

Verney, E. B. (1947). The antidiuretic hormone and the factors which determine its release. *Proc. R. Soc. Lond. B Biol. Sci.* 135, 25–106. doi: 10.1098/rspb.1947.0037

Yamaguchi, T., Wang, H. L., Li, X., Ng, T. H., and Morales, M. (2011). Mesocorticolimbic glutamatergic pathway. *J. Neurosci.* 31, 8476–8490. doi: 10.1523/JNEUROSCI.1598-11.2011

Ying, C., Qi, Y., and Cang-Bao, X. (2017). A convenient method for quantifying collagen fibers in atherosclerotic lesions by ImageJ software. *Int. J. Clin. Exp. Med.* 10, 14904–14910.

Zhang, L., and Eiden, L. E. (2018). Two ancient neuropeptides, PACAP and AVP, modulate motivated behavior at synapses in the extrahypothalamic brain: a study in contrast. *Cell Tissue Res.* 375, 103–122. doi: 10.1007/s00441-018-2958-z

Zhang, L., and Hernandez, V. S. (2013). Synaptic innervation to rat hippocampus by vasopressin-immuno-positive fibres from the hypothalamic supraoptic and paraventricular nuclei. *Neuroscience* 228, 139–162. doi: 10.1016/j.neuroscience.2012.10.010

Zhang, L., Hernandez, V. S., Liu, B., Medina, M. P., Nava-Kopp, A. T., Irles, C., et al. (2012). Hypothalamic vasopressin system regulation by maternal separation: its impact on anxiety in rats. *Neuroscience* 215, 135–148. doi: 10.1016/j.neuroscience.2012.03.046

Zhang, L., Hernández, V. S., Medina-Pizarro, M., Valle-Leija, P., Vega-González, A., and Morales, T. (2008). Maternal hyperthyroidism in rats impairs stress coping of adult offspring. *J. Neurosci. Res.* 86, 1306–1315. doi: 10.1002/jnr.21580

Zhang, L., Hernandez, V. S., Swinny, J. D., Verma, A. K., Giesecke, T., Emery, A. C., et al. (2018). A GABAergic cell type in the lateral habenula links hypothalamic homeostatic and midbrain motivation circuits with sex steroid signaling. *Transl. Psychiatry* 8:50. doi: 10.1038/s41398-018-0099-5

Zhang, L., Hernandez, V. S., Vazquez-Juarez, E., Chay, F. K., and Barrio, R. A. (2016). Thirst is associated with suppression of habenula output and active stress coping: is there a role for a non-canonical vasopressin-glutamate pathway? *Front. Neural Circuits* 10:13. doi: 10.3389/fncir.2016.00013

Zhang, L., Medina, M. P., Hernandez, V. S., Estrada, F. S., and Vega-Gonzalez, A. (2010). Vasopressinergic network abnormalities potentiate conditioned anxious state of rats subjected to maternal hyperthyroidism. *Neuroscience* 168, 416–428. doi: 10.1016/j.neuroscience.2010.03.059

Zhou, M., and Grofova, I. (1995). The use of peroxidase substrate Vector VIP in electron microscopic single and double antigen localization. *J. Neurosci. Methods* 62, 149–158. doi: 10.1016/0165-0270(95)00069-0

Ziegler, D. R., Cullinan, W. E., and Herman, J. P. (2002). Distribution of vesicular glutamate transporter mRNA in rat hypothalamus. *J. Comp. Neurol.* 448, 217–229. doi: 10.1002/cne.10257

Presentaciones en congresos internacionales

derivadas de mis estudios de doctorado

NEUROSCIENCE 2010
40TH ANNUAL MEETING

Presentation Abstract

Program#/Poster#: 612.4/MMM71

Title: A 17ß-aminoestrogen (prolame) ameliorates dendritic spine loss in hippocampal pyramidal neurons of young ovariectomized rats

Location: Halls B-H

Presentation Time: Tuesday, Nov 16, 2010, 11:00 AM -12:00 PM

Authors: *I. NISSEN[1], A. NAVA-KOPP[1], A. VEGA-GONZÁLEZ[1], A. DE LA PEÑA[2], J. M. FERNANDEZ-G[3], L. ZHANG[1];

[1]Physiol., [2]Farmacology, [3]Chem. Inst., Natl. Autonomus Univ. of Mexico, Mexico City, Mexico

Abstract: Cognitive impairment in menopausal females has been related to reduced levels of estrogens. Hormone replacement therapy (HRT) is being used to treat this and other symptoms caused by menopause. Nevertheless there are side effects of this treatment such as increased thromboembolic events and breast cancer, based on which new options of treatment are needed. In this study, we assessed the effect of N-(3-hydroxy-1,3,5(10)estratrien-17 beta-yl)-3-hydroxypropylamine (prolame) - a synthetic aminoestrogen with prolonged anticoagulant and brief estrogenic effects - on the spine density of hippocampal projection neurons of ovariectomized rats. Ninty-day-old female Wistar rats were assigned to one of the following groups: control (Ctrl), ovariectomized (Ovx), ovariectomized plus estradiol treatment (OvxET) and ovariectomized plus prolame treatment (OvxPT). At day 28 post surgery, OvxET and OvxPT rats started receiving a daily subcutaneous injection of 17β-estradiol (50 μg/kg) and prolame (60 μg/kg) respectively, whereas Ctrl and Ovx groups were injected with vehicle (glycerol) only. After 2 days of treatment, Golgi-Cox stain protocol was used to observe dendritic processes and arborization of CA1 and CA3 pyramidal neurons and dentate gyrus granular neurons. Spine density was calculated for a segment of dendrite (10μm long) at X100 for left and right primary basilar branch, primary apical branch, secondary apical branch and tertiary apical branch. There was no difference between groups for the granular cells. There were differences between groups in the CA1 and CA3 regions. The Ovx group clearly showed, in most cases, a decrease in the spine density compared to all groups, about a 35%-40% reduction in CA1 and 20%-40% in CA3. OvxEt and OvxPT groups showed comparable spine density which in most cases, when compared with the Ctrl group

showed no significant difference. These results suggest that prolame could represent an improved option of HRT ameliorating cognitive and emotional impairments produced by estrogen deficiency.

Disclosures: **I. Nissen:** None. **A. Nava-Kopp:** None. **A. Vega-González:** None. **A. De la Peña:** None. **J.M. Fernandez-G:** None. **L. Zhang:** None.

Keyword(s): Hormone Replacement Therapy

Estradiol

dendritic spine density

Support: DGAPA-UNAM IN210406

DGAPA-UNAM IN224407

CONACYT-Mexico 46141

CONACYT-Mexico 49740

CONACYT-Mexico 79641

[Authors]. [Abstract Title]. Program No. XXX.XX. 2010 Neuroscience Meeting Planner. San Diego, CA: Society for Neuroscience, 2010. Online.

118: Epigenetic Factors (contd.)

Abstract Code - Date - Time of Attendance - Poster Board No - Abstract Number

118.19　TUES 17/07/12, 13:30 - A19 - 3355
POST-TRANSCRIPTIONAL AND POST-TRANSLATIONAL REGULATION OF LSD1 EPIGENETIC ACTIVITY MODULATES MORPHOGENESIS IN NEURONS
F.S. Rusconi, L. Paganini, E. Toffolo, C. Verpelli, C. Sala, E. Battaglioli, *Milan, Italy*

118.20　TUES 17/07/12, 14:30 - A20 - 2151
CHRONIC ETHANOL INTAKE-INDUCED EPIGENETIC MODIFICATIONS AT *BDNF* GENE LEVEL IN THE MOUSE HIPPOCAMPUS
E. Stragier, R. Massart, M. Hamon, L. Lanfumey, *Paris, France*

118.21　TUES 17/07/12, 13:30 - A21 - 10
IN UTERO ANDROGEN ADMINISTRATION INDUCES CHANGES IN GENE EXPRESSION IN THE CEREBELLUM
L.M. Wilson, C.L.P. Garden, *Edinburgh, UK*

118.22　TUES 17/07/12, 14:30 - A22 - 4269
EARLY LIFE STRESS INDUCES HISTONE MODIFICATIONS OF THE SYNAPTIC PLASTICITY GENES ARC AND EGR1 IN THE PREFRONTAL CORTEX AND HIPPOCAMPUS
L. Xie, J. Bock, K. Braun, *Magdeburg, Germany*

118.23　TUES 17/07/12, 13:30 - A23 - 4024
INHERITANCE OF MATERNAL STRESS VIA RNA EDITING CHANGES IN RATS
H. Zaidan, Y. Golumbic, J. Schulkin[2], M. Leshem, I. Gaisler-Salomon, *Haifa, Israel,* [2]*Washington, DC, USA*

118.24　TUES 17/07/12, 14:30 - A24 - 268
MATERNAL SEPARATION UPREGULATES HYPOTHALAMIC VASOPRESSIN EXPRESSION IN RAT EARLY POSTNATAL AND YOUNG ADULT STAGES: IMPACTS ON CONDITIONED ANXIOUS STATE
L. Zhang, V.S. Hernéndez, A.T. Nava-Kopp, C. Irles, *Mexico City, Mexico*

119: Network Interactions II

Abstract Code - Date - Time of Attendance - Poster Board No - Abstract Number

119.01　TUES 17/07/12, 13:30 - B1 - 2356
THE INTERACTION BETWEEN ELK-1 AND MICROTUBULE BASED MOTOR PROTEINS
O. Ari, O. Demir[2], I. Aksan Kurnaz, *Istanbul, Turkey,* [2]*Dresden, Germany*

119.02　TUES 17/07/12, 14:30 - B2 - 2660
DIVERSITY AND PROJECTIONS OF VENTRAL HIPPOCAMPAL PYRAMIDAL NEURONS
A. Arszovszki, Z. Borhegyi, T. Klausberger[1,2], *Wien, Austria,* [2]*Oxford, UK*

All morning poster sessions on display from 8:00 to 13:15
All afternoon poster sessions on display from 13:30 to 18:45

NEUROSCIENCE 2012

Presentation Abstract

Program#/Poster#:	530.11/A61
Presentation Title:	Maternal separation modulates programmed cell death in rat hypothalamus
Location:	Hall F-J
Presentation time:	Tuesday, Oct 16, 2012, 10:00 AM -11:00 AM

Authors: ***A. T. NAVA KOPP**, L. ZHANG, C. IRLES;
Dept. of Physiology, Fac. of Medicine, Natl. Autonomous Univ. of, Mexico City, Mexico

Abstract: There is extensive literature showing that the peculiar features of early postnatal brain development increase the vulnerability toward the stressful experiences producing long-lasting effects in adult life. However, the underlying mechanisms remain unclear. During brain development, the number of neurons is controlled by a form of programmed cell death (PCD), in particular, the activation or inhibition of several signaling pathways such as PI3K/Akt, mitogen-activated protein kinases (MAPKs), the release of mitochondrial pro- and anti-apoptotic proteins and caspase 3 activation have been shown to play a key role in this process. In particular, activation of the MAPK, ERK 1/2 leads to the impaired translocation of the pro-apoptotic factor Bax to the mitochondria preventing the formation of the apoptosome and caspase 3 activation. Furthermore, substrates of ERK1/2 regulate several cellular responses such as cell proliferation and survival as well as transcription of immediate early response genes such as c-fos and c-jun. Previous studies from our group have revealed an increased cell number in the hypothamic vasopressin nuclei (i. e. paraventricular, supraoptic and suprachiasmatic nuclei) in a rat neonatal maternal separation (MS) model. Hence, in this study, we evaluated the effect of MS on the expression of Bax and phospho-ERK 1/2 proteins as well as the activity of caspase 3 in the developing rat hypothalamus, implicated in stress response. Whole hypothalamus from animal facility reared (AFR) and MS (3h/daily, PND 2 to 15) male Wistar rats at PND 3, 5, 7 and 10 were homogenized in lysis buffer. Caspase 3 activity was assayed by a fluorometric method in a luminescence spectrometer using caspase 3 substrate (Ac-DEVD-AMC). Proteins from AFR and MS samples were analyzed by SDS-PAGE and western blot against Bax, phospho-ERK 1/2 and total ERK 1/2 revealed by enhanced chemiluminescence. Differences in caspase 3 activity (expressed as the change of fluorescence per hour per protein milligram) were seen at PND 3 and 10 between MS and AFR pups. Furthermore, oligomeric Bax expression was found diminished in MS pups while a modest phopho-ERK 1/2 expression was found increased. Augmented ERK 1/2 activation as well as decreased Bax expression may lead to a diminished caspase 3 activity and apoptosis. Also, an augment in phospho-ERK 1/2 expression

could be involved in activation of immediate early response genes such as c-fos, resulting in cell proliferation and survival. These results may suggest that early life stress plays an important role in the regulation of the pattern of PCD during early postnatal development.

Keyword(s):   VASOPRESSIN

PROGRAMMED CELL DEATH

MATERNAL SEPARATION

[Authors]. [Abstract Title]. Program No. XXX.XX. 2012 Neuroscience Meeting Planner. New Orleans, LA: Society for Neuroscience, 2012. Online.

[Print this Page](#)

Neuroscience
2013

Presentation Abstract

Program#/Poster#: 84.14/AAA8

Presentation Title: Anatomical characterization for intra- and extra-hypothalamic kisspeptin projections in neonatal maternal-separated rats: A comparison between genders at different ages

Location: Halls B-H

Presentation time: Saturday, Nov 09, 2013, 2:00 PM - 3:00 PM

Topic: ++E.05.c. Early life experience

Authors: *A. T. NAVA KOPP, C. IRLES, L. ZHANG;
Dept. of Physiology, Fac. of Medicine, Natl. Autonomous Univ. of, Mexico City, Mexico

Abstract: The peptide kisspeptin (KP) is synthesized mainly in the arcuate nucleus (ARC), the preoptic area (MPOA) and the anteroventral periventricular nucleus (AVPV) in the rat. It's main function has been considered as for inducing the pulsatile GnRH secretion, and the pre-ovulatory surge of GnRH, in females. However, this peptide also plays a role in the regulation of the HPA axis; it's been found to modulate the expression of arginine-vasopressin (AVP), oxytocin (OXY) and corticotropin releasing hormone (CRH) in the paraventricular nucleus of the hypothalamus (PVN) (Rao, Mott & Pak, 2011). We have previously shown that the maternal separation (MS) procedure upregulates the vasopressinergic system (Zhang et al, 2012). In this study, we present whole rat brain reconstructions of KP expression patterns by IHC in MS and control rats, using light microscopy combined with Neurolucida. Our results show extensive KP innervations in the medial amygdala and the amydgalohippocampal cortex. MS up-regulates the expression of this peptide. This observation leads to suggest, though not fully demonstrated in this study, the involvement of this peptide in the control of emotion.

Disclosures: A.T. Nava Kopp: None. C. Irles: None. L. Zhang: None.

Keyword(s): KISSPEPTIN

EARLY LIFE STRESS

Support: PAPIIT IN218111

CONACyT 127777

CONACyT 179616

[Print this Page](#)

Presentation Abstract

Program#/Poster#:	642.03/PP24
Presentation Title:	Effect of neonatal maternal separation and adolescent ethanol exposure on adult preference for ethanol
Location:	WCC Hall A-C
Presentation time:	Tuesday, Nov 18, 2014, 3:00 PM - 4:00 PM
Presenter at Poster:	Tue, Nov. 18, 2014, 3:00 PM - 4:00 PM
Topic:	++E.03.e. Hormones and cognition
Authors:	***A. T. NAVA KOPP**[1], C. IRLES[1], H. BARRIO[2], L. ZHANG[1]; [1]Dept. of Physiology, Fac. of Medicine, Natl. Autonomous Univ. of, Mexico City, Mexico; [2]Fac. of Sciences, UNAM, Mexico City, Mexico
Abstract:	Mechanisms underlying physiological actions of ethanol are not fully understood. However, the involvement of different types of neurotransmitter systems, such as GABA and opioids is clear. For instance, alcohol is known to increase GABAa ionotropic receptor (GABAaR) activation, but its precise molecular mechanism remains unclear. On the other hand, there are evidences suggesting 1) adolescent exposure to ethanol (AEE) increases drinking in adulthood; 2) adverse environmental conditions during development, such as neonatal maternal separation (MS) potentiate ethanol preference. A down-regulation of GABAergic transmission via GABAaR in determined brain regions has been suggested to underlie the latter phenomenon. The potentiation of the intracerebral vasopressinergic (AVP) transmission has been associated to elevated ethanol consumption, since administration of V1bR specific antagonist has been demonstrated to decrease anxious- and depressive-like behaviors, as well as ethanol consumption in alcohol preferring rats. We have previously demonstrated that MS up-regulates the AVP hypothalamic system. Hence, it is interesting to test whether the exposition to alcohol in the MS subjects can cause permanent adaptational modifications inducing up-regulation or down regulation of V1bR in the brain. The objective of the present study is to evaluate the possible role of MS and AEE in the development of alcohol preference during adult life, and to elucidate if one of the underlying mechanisms involves AVP transmission. For this

purpose, alcohol intake of male Wistar rats exposed to 4 different developmental environments was quantified, experimental groups comprised (i) different rearing conditions: animal facility reared (AFR) vs. MS, and (ii) differences in ethanol exposure during adolescence: naïve (n) vs. experienced (e). Alcohol preference was measured during adulthood using a 2-bottle free choice paradigm. MS and AEE increased ethanol intake, observed in AFRe and MSn groups; however, rats from the MSe group had a significant higher average alcohol intake compared to all other groups. These results suggest that MS and AEE provoke a higher preference for ethanol in adults. Protein signaling pathways underlying this phenomenon is being carried out.

Disclosures:	**A.T. Nava Kopp:** None. **C. Irles:** None. **H. Barrio:** None. **L. Zhang:** None.
Keyword (s):	MATERNAL SEPARATION
	V1B RECEPTOR
	ADOLESCENT ETHANOL EXPOSURE
Support:	CONACyT Grant 127777
	CONACyT Grant 179616
	PAPIIT DGAPA-UNAM IN218111
	PAPIIT DGAPA-UNAM IN216214
	PAPIIT DGAPA-UNAM IA202314